UILU-ENG-77-2007

CIVIL ENGINEERING STUDIES

STRUCTURAL RESEARCH SERIES NO. 439
Illinois Cooperative Highway and Transportation Research
Program Series No. 167

TESTS OF A PRECAST POST-TENSIONED COMPOSITE BRIDGE GIRDER HAVING TWO SPANS OF 124 FEET

By
A. I. FADL
W. L. GAMBLE
B. MOHRAZ

Issued as a Documentation Report on an
Investigation of Field-Made Joints in
Prestressed Reinforced Concrete
Highway Bridge Girders

Project IHR-303
Phase 2

Illinois Cooperative Highway and Transportation Research Program

Conducted by
THE STRUCTURAL RESEARCH LABORATORY
DEPARTMENT OF CIVIL ENGINEERING
ENGINEERING EXPERIMENT STATION
UNIVERSITY OF ILLINOIS AT URBANA-CHAMPAIGN

in cooperation with the
STATE OF ILLINOIS
DEPARTMENT OF TRANSPORTATION
and the
U.S. DEPARTMENT OF TRANSPORTATION
FEDERAL HIGHWAY ADMINISTRATION

UNIVERSITY OF ILLINOIS
AT URBANA-CHAMPAIGN
URBANA, ILLINOIS
APRIL 1977

TECHNICAL REPORT STANDARD TITLE PAGE

1. Report No.	2. Government Accession No.	3. Recipient's Catalog No.
FHWA-IL-UI-167		

4. Title and Subtitle	5. Report Date
Tests of a Precast Post-Tensioned Composite Bridge Girder Having Two Spans of 124 Feet	April 1977
	6. Performing Organization Code
7. Author(s)	8. Performing Organization Report No.
A. I. Fadl, W. L. Gamble, and B. Mohraz	UILU-ENG-77-2007
9. Performing Organization Name and Address	10. Work Unit No.
Department of Civil Engineering University of Illinois at Urbana-Champaign Urbana, IL. 61801	11. Contract or Grant No. IHR-303
	13. Type of Report and Period Covered
12. Sponsoring Agency Name and Address Illinois Department of Transportation Bureau of Materials & Physical Research 126 East Ash Street Springfield, IL. 62706	Interim: April 1972 - Sept. 1976
	14. Sponsoring Agency Code

15. Supplementary Notes

Prepared in Cooperation with the U. S. Department of Transportation, Federal Highway Administration. Project Title "Field Made Joints in Prestressed Reinforced Concrete Highway Bridge Girders."

16. Abstract

A prototype bridge girder was designed, built, and tested. The 250 ft long two-span girder was made of 3 precast segments about 88, 74, and 88 ft in length. The segments were supported on 3 final and 2 temporary supports. The joints were of cast-in-place concrete, as was the composite deck. After the site-cast concrete was cured, the structure was post-tensioned to establish continuity and the temporary supports were removed. The two longer segments were pretensioned to resist the girder and deck dead loads, while the shorter segment was reinforced with deformed bars for the same loads.

The structure was subjected to a series of loadings, during which deflections, reactions, and concrete strains were measured. The loads approximated AASHTO HS-20 vehicles. The first 4 tests were to service loads, with total applied loads of 73.6 kips. The structure remained elastic and crack free during these tests. Two tests were to the design ultimate load, 198.7 kips. A load of 328.2 kips was applied in the final test without causing failure. The final loading was applied to produce maximum shear in one splice, and a shear failure, complicated by large flexural deformations, appeared to be developing when the test ended. The final test produced a maximum deflection of 10.8 in., and a residual of about 1.0 in.

The joint details used in the prototype structure were adequate, and the presence of the joint had no influence on the behavior of the structure until extremely large overloads were reached.

17. Key Words	18. Distribution Statement
Prestressed concrete, Post-tensioned concrete, Highway Bridges, Analysis, Structural testing, Cracking, Deflections, Reactions, Precast Concrete	No restrictions. This document is available to the public through the National Technical Information Service, Springfield, Virginia 22161

19. Security Classif. (of this report)	20. Security Classif. (of this page)	21. No. of Pages	22. Price
Unclassified	Unclassified	180	

Form DOT F 1700.7 (8-69)

TABLE OF CONTENTS

LIST OF TABLES

LIST OF FIGURES

1. INTRODUCTION

1.1 Introductory Remarks

Many of the existing interstate highway grade separation structures consist of four span I-beam girders with cast-in-place decks. The girders are simply supported on two end abutments and are continuous across a central pier and two intermediate shoulder piers. Each interior span is approximately 70 to 80 feet, while the exterior spans are each 40 to 50 feet, for cases with two 2-lane roadways and a small skew angle.

Recently however, due to more stringent safety requirements, piers are no longer permitted so close to the edge of pavement. These requirements result in an increase in the two interior spans from 70 to 80 feet to at least 90 feet. To meet these requirements, the two shoulder piers have either to be moved out toward the end abutments, resulting spans of at least 90 ft, or they have to be eliminated, resulting in spans of 100 up to 125 ft. The moving of the two shoulder piers toward the end abutments results in an inefficient structure with two long interior and two very short exterior spans. The small dead load of the two exterior spans may not be sufficient to prevent the uplift of the girder at the end abutments. In addition such a structure is not aesthetically appealing.

If the two shoulder piers were to be eliminated, the resulting two span structures will have spans of 90 to 125 feet. Such span lengths prohibit the transportation of precast concrete members. The cost and the lower quality of cast-in-place girders prohibits the use of such girders, at least within the cost structure currently existing.

One possible solution to the problem is to construct a two span girder in three segments and join them end to end by means of field splicing. The behavior and performance of the splices under various loading conditions is an important consideration in the design and construction of such a structure.

A cooperative research program between the State of Illinois Department of Transportation and the Department of Civil Engineering at the University of Illinois at Urbana-Champaign is currently being carried out to study the feasibility of various types of field splicing and the performance of field splices. The investigation consists of the design of a number of prototype structures with field splices, the fabrication and testing of one prototype test structure, and the design, fabrication, and testing of a series of small scale specimens approximately one-third in size.

As one phase of the project, a prototype test structure consisting of one two-span girder plus deck has already been built and has been subjected to a series of loadings. This report describes the design, fabrication, and testing, and the results obtained from the tests of the prototype structure.

1.2 Brief Description of Construction Procedure

A schematic drawing of a two-span continuous grade separation structures is shown in Fig. 1.1. The structure consists of a girder and a bridge deck supported on two end abutments and a center pier. Such a structure may be constructed using three precast segments for each girder. The precast girders are placed on three permanent and two temporary supports as shown in Fig. 1.2. The steel reinforcement in the joints is spliced and the joints and the deck are cast, Fig. 1.3. After the joints and the deck are cured, the entire structure is post-tensioned, Fig. 1.4, and the temporary supports are removed, Fig. 1.5. This procedure was employed in the design and construction of the prototype test structure. The end segments were pretensioned, and the central segment was precast reinforced concrete.

The feasibility of other construction procedures such as one similar to the above, but without post-tensioning, is being investigated.

1.3 Acknowledgements

This work was conducted as part of the Illinois Cooperative Highway Research Program, Project IHR-303, "Field-Made Joints in Prestressed Reinforced Concrete Highway Bridge Girders," by the Department of Civil Engineering, in the Engineering Experiment Station, University of Illinois at Urbana-Champaign, in cooperation with the Illinois Department of Transportation and the U. S. Department of Transportation, Federal Highway Administration.

The prototype girder test specimen, the testing site, and the rock anchors which provided the means of applying the loads were provided by Midwest Prestressed Concrete Co., now Blakslee-Midwest, of Rochelle, Illinois. The many contributions by Mr. J. O. Whitlock and Mr. E. L. Peck to the program are acknowledged.

The contents of this report reflect the views of the authors who are responsible for the facts and the accuracy of the data presented herein. The contents do not necessarily reflect the official views or policies of the Illinois Department of Transportation or of the Federal Highway Administration. This report does not constitute a standard, specification or regulation.

2. DESIGN OF TEST SPECIMEN

2.1 Design Criteria

The design was prepared in accordance with the 1969 AASHO (1)* Standard Specifications for Highway Bridges. Preliminary designs for a typical interior beam was carried out to determine the following:

(1) Suitable locations of the splices,

(2) An acceptable precast girder size (a modified Illinois Department of Transportation 54 in. deep girder)

(3) The cable-profile, the areas of pre-tensioned and post-tensioned steel, and the possibility of using partial post-tensioning to help carry the weight of the deck slab.

The design was controlled by service load stress conditions; the ultimate capacity was checked at several critical sections.

Because of symmetry of the structure, all computations except for effects of loadings were carried out for one span only.

The 1973 AASHO Specifications (2) reduced the load factors slightly, but this would have had no effect on this structure.

2.2 Dimensions and Section Properties

The following dimensions and section properties were used in the design:

Span lengths = 125 ft center to center of bearings

Cross-section -- Modified Illinois Department of Transportation 54 in. girder; the dimensions are shown in Fig. 2.1.

Girder spacing = 7 ft, center to center

Deck thickness = 7.5 in.

Depth to span ratio = 0.0423 (girder plus deck height)

* Number in parentheses refers to entry in List of References.

The net transformed concrete section properties given below, rather than the gross section properties, were used in the design stress computations.

Precast non-composite girder section

depth = 56.0 in.
cross-sectional area = 695 in.^{2}
moment of inertia = 258,185 in.^{4}
distance from centroid of the girder to bottom of the girder = 27.0 in.
distance from centroid of the girder to top of the girder = 29.0 in.
weight = 0.725 kips/ft.

Composite section (Transformed section, $E_{deck}/E_{girder} = 0.764$)

depth = 63.5 in.
cross-sectional area = 1176 in.^{2}
moment of inertia = 565,440 in.^{4}
distance from centroid of the composite section to bottom of the girder = 40.5 in.
distance from centroid of the composite section to top of the precast girder = 15.5 in.
distance from centroid of the composite section to top of the deck = 23.0 in.
weight of composite section = 1.381 kips/ft.

2.3 Material Properties

The following material properties were used for concrete and steel. The allowable stresses are also listed.

Concrete	Precast Girder (psi)	Deck (psi)
Twenty eight day compressive strength, f'_c	6,000	3,500
Concrete, compressive strength at release of pretension, f'_{ci}	5,000	
Concrete, compressive strength at post-tensioning, f'_{ci}	5,000	3,500
Allowable temporary stresses before long-term losses have occurred		
compressive stress in pre-tensioned segments, $0.60\ f'_{ci}$	3,000	-
compressive stress in post-tensioned beam, $0.55\ f'_{ci}$	2,750	1,925
maximum tensile stress, $7.5\sqrt{f'_{ci}}$	530	443
Allowable stresses at service load after all losses have occurred:		
Compression, $0.40\ f'_c$	2,400	1,400
Tension, $6\sqrt{f'_c}$	465	355
Principal tensile stress, $f_t = 4\sqrt{f'_c}$	310	236
Modulus of rupture, $f_r = 6\sqrt{f'_c}$	465	355
Modulus of elasticity = $60{,}000\sqrt{f'_c}$	4.7×10^6	3.59×10^6

Ratio of moduli of elasticity, $E_{deck}/E_{girder} = 0.764$

Unit weight of concrete including reinforcement = 150 pcf

The stress-strain relationships used in ultimate strength calculations are shown in Fig. 2.2.

Prestressing steel

The prestressing steel used in both the pretensioning and post-tensioning was 1/2 in. diameter 270 ksi 7-wire stress-relieved strands with the following design properties:

Ultimate strength, f'_s = 270 ksi
Yield strength, f_{sy} = 230 ksi = 0.85 f'_s
Modulus of elasticity, $E_s = 28 \times 10^3$ ksi
Cross-sectional area of strand, A_s = 0.153 in.^{2}

The stress-strain relationship used in ultimate strength calculations is shown in Fig. 2.3. Strand and other steel samples were obtained, but apparently were lost during transportation to the laboratory.

Pretensioned steel

Initial stress before release, f_{si} = 0.70 f'_s = 189 ksi
Total long-term losses = 35 ksi (does not include loss due to subsequent post-tensioning)
Maximum effective working stress after all losses have occurred, 0.60 f'_s = 162 ksi
Steel area, A_s = 14 (0.153) = 2.14 in.^{2}

Post-tensioned steel

Maximum allowable jacking stress, 0.8 f'_s = 216 ksi
Maximum allowable initial stress (immediately after transfer), 0.7 f'_s = 189 ksi < f_{sy}
Maximum allowable effective working stress after all losses have occurred, 0.60 f'_s = 162 ksi
Jacking stress assumed in design, f_{sj} = 189 ksi
Total long-term losses = 30 ksi
Tendon area, A_{sp} = 42(0.153) = 6.43 in.^{2}
Curvature friction coefficient, for 7-wire strands in steel conduits, μ = 0.15
Wobble coefficient, K = 0.0005 per ft.

The initial effective stress at transfer was computed using

$$f_{sxo} = f_{sj}\, e^{-(kx + \mu\alpha)} = \beta f_{sj}$$

where K and μ are as defined above; α is the absolute total angular change of slope of the tendon profile in radians from the jacking end to any point x, in feet.

Non-prestressed steel

The reinforcing bars in both the precast girder and the deck were ASTM A615 grade 40 deformed bars with the assumed stress-strain relationship shown in Fig. 2.4, except that grade 60 deformed bars were used for stirrups.

2.4 Eccentricity and Cable Profile

A constant eccentricity of 24.14 in. was used for the pre-tensioned steel in the two end segmental girders. The 14 strands were located as shown in Fig. 2.14.

The cable profile for the post-tensioned steel, symmetric about the central support, consists of two fourth-degree curves AB and BC as shown in Fig. 2.5. Forty-two strands, divided between three ducts, were used for post-tensioning.

2.5 Sign Convention

A positive eccentricity indicates that the center of gravity of the prestressing steel is located above the centroid of the cross-section. The designer's sign convention (positive moment causing tension in the bottom fiber) is used for moments. A positive stress denotes tension.

2.6 Loads

The following loading conditions, shown in Fig. 2.6, correspond to the different stages in the construction sequence. At the end of each

loading stage, all forces, moments, and stresses are summed to obtain the total values at that stage. The moment diagrams for the various stages are shown in Fig. 2.7 to 2.9.

1. Non-composite girder section under pretensioning and its own weight, before and after the long-term losses in pretensioning are included.
2. Non-composite girder section under the weight of the deck with the temporary supports still in position.
3. Composite section under post-tensioning with the temporary supports removed, before and after the long-term losses in post-tensioned steel are assumed to have taken place.
4. Composite section under the weight of an asphalt topping on the slab; at 50 lb/ft^2 or 350 lb/ft.
5. Live load corresponding to HS20-44 plus impact.

The temporary supports shown in Figs. 2.6 and 2.7 have been idealized as single supports while each actually was two supports separated by the length of the splice plus the approximately 12 in. distances from the ends of the members to the temporary reactions. Likewise, the equivalent support forces applied to the beam in one stage of the dead load analysis were idealized as single loads while they were actually two concentrated loads plus a distributed load corresponding to the weight of the splice plus the deck directly above it.

This simplification substantially reduces the arithmetic in the analysis without altering the results except in the immediate vicinity of the loads.

Load Factors for Strength Calculations

Dead load

Load factor for dead load = 1.5

Live load

Load factor for live load for one beam = 2.5 α_d (Live Load per loaded lane + I) where α_d and I are the distribution factor and the impact coefficients, respectively.

The distribution factor $\alpha_d = S/2C$

in which

S = girder spacing in feet

C = a coefficient which is a function of type of deck and girder.

The impact factor

$$I = \frac{50}{L + 125}$$

where L is the length in feet of that part of the span which, when loaded, produces the maximum stress in the member.

Using S = 7 ft and C = 5.5 (1), a value of 7/11 is obtained for α_d. The impact coefficient for negative moment and shear at the central support is 0.133, since both spans are loaded to obtain the maximum moment. The impact coefficient is 0.20 for maximum positive moment, positive and negative moments at the splice, and for shear at points where truck loadings govern since maximums are obtained with only one span loaded in each of these cases.

The total live load factor for a single beam thus becomes 1.80 standard loads for negative moment and shear at the central pier and 1.91 for the other moments and shear at most other sections.

The secondary moments are not included during the determination of the design ultimate moments.

2.7 Design Procedure

The following steps were used in the design of a typical interior beam in the girder-deck system.

1. Select a tentative girder size, girder spacing and deck thickness for a given span.
2. Calculate the section properties for the precast girder and the composite section (girder-deck system).
3. Select the locations of the field splices and the critical sections where the stresses controlling the design are to be checked at the end of each loading stage.
4. Design the precast end segments as simply supported girders and the middle segment as a two span continuous girder with or without pretensioning to carry their own weights and that of the deck.
5. Compute the available stress range at the selected critical sections under full service loads.
6. Determine the approximate cable profile and the effective tendon force after post-tensioned losses have occurred.
7. Modify the cable profile to keep the stresses at the critical sections within the allowable limits. Select tendon sizes and their locations, and check the resultant eccentricity.
8. Check the stresses at transfer.
9. Compute the ultimate strength accounting for the longitudinal deck steel and if necessary provide additional reinforcement to obtain the required strength.
10. Compute the shear strength and provide adequate shear reinforcement.

The cable profile was chosen to produce a positive secondary moment as large as possible at the interior support, because of problems in meeting the allowable compression stresses at the bottom of the section over the central pier.

2.8 Summary of Design for Working Stress

The dead loads and the corresponding moment diagrams for different stages in the construction sequence (weight of girder, weight

of deck, temporary support removal, and weight of asphalt) are shown in Fig. 2.7. In Fig. 2.8 are shown three dead load moment diagrams; one corresponding to the weight of the girder and the deck acting on the non-composite section, one corresponding to the effect of removal of the temporary supports and the weight of asphalt acting on the composite section, and the third is the sum of the two. The envelope of live load moments is presented in Fig. 2.9.

With the curvature friction coefficient, μ, and the wobble coefficient, k, defined in Section 2.3, and the fourth-degree cable profile as mentioned in Section 2.4, a computer program was used to obtain (a) the eccentricity of post-tensioned steel along the span, (b) the effective post-tensioning stress at transfer, (c) the slope of the centroid of the post-tensioned steel, and (d) the secondary moment (caused by the restraint of post-tensioning camber at the center support) with respect to the centroids of the non-composite, and the composite transformed sections. The program is described in Ref. 3.

A summary of stresses, forces, and moments resulting from pretensioning and post-tensioning is presented in Table 2.1. A summary of the stresses at three sections (midspan, splice, and the center support) at different loading stages is given in Tables 2.2 through 2.4.

2.9 Flexural Strength Analysis

Using the load factors given in Section 2.5, the moments corresponding to the design ultimate load at various sections (midspan, splice, and the center support) were computed and are summarized in Table 2.5. A summary of the flexural strength capacities at the same sections is also presented in Table 2.5. As can be noted, the ultimate design moments are smaller than the flexural strength capacities at the corresponding sections.

Dead load moments including the effects of the very large secondary moments are shown in Table 2.6, and may be compared with the moments listed in Table 2.5.

2.10 Shear Strength Analysis

The design ultimate shear was computed from the dead load shear and the live load shear envelope, Fig. 2.10, at service load conditions using the appropriate load factor (see Section 2.6). The web-shear capacity and the flexural-shear capacity were computed (4, 5) and compared with the design ultimate shear, Fig. 2.11, and sufficient shear reinforcement (stirrups) was provided. Only nominal stirrups were needed over most of the length of the structure. The stirrups extended out of the top of the precast beam to provide the ties with the deck which are necessary to insure composite action. The stirrups are shown in Figs. 2.13 to 2.15, and the spacings are shown in Figs. 2.12 and 2.16.

The web-shear cracking forces were computed using a principle stress analysis with a limiting tensile stress in the concrete of $4\sqrt{f'_c}$ = 310 lb/in.^{2} for the f'_c = 6,000 lb/in.^{2} concrete used. There is a discontinuity in the curve, Fig. 2.11 at the splice, since the end segments contain pretensioned reinforcement while the pier segment does not. The discontinuity in the shear diagram while the structure is on the temporary supports also contributes to this. The very large web-shear strength indicated in the region 100 ft from the abutment is the result of a large vertical component of the post-tensioning force in this area.

Shears due to secondary moments were included when analyzing the shear cracking loads, in Sec. 7.4, but not when constructing the applied load envelopes.

The discontinuity in the flexural-shear capacity curve at the splice is entirely due to the provision of pretensioned steel in the end segments but none in the pier segment. The discontinuity at 107 ft from the abutment is due to a point-of-contraflexure of sorts, in that neither positive nor negative moments cracks can be caused by flexure, considering the design ultimate loads, in this region.

2.11 Reinforcement Lay-Out

The final lay-out of the pretensioned, post-tensioned, and non-prestressed steel in the longitudinal and several transverse sections in one span of the girder-deck system are shown in Figs. 2.12 through 2.15. The reinforcement details for the two splices are shown in Figs. 2.16 through 2.18.

The pier module was designed so that it could be lifted and supported either at its ends or its midlength. The additional moment accompanying casting of the deck concrete was assumed to be the same as in a two-span continuous beam, and while the moment due to the dead load of the girder was assumed to have the same distribution in the analysis, it was recognized that it could be substantially different than this idealized distribution if the temporary supports were not placed and maintained at exactly the correct elevations.

The three ducts for tendons, each 3 in. diameter, were separated vertically by 3-1/2 in. through most of the length of the beam. This was done to insure that the radial forces from tendon curvature could not cause a tendon to break through from one duct to the next.

2.12 Additional Notes

It was found, after the load tests were completed, that incorrect live load moment and shear envelopes had been considered during part of the design of the beam. The service load flexural stresses were computed using moments which were too high, by varying amounts. The ultimate moments considered were correct for the negative moment at the central pier and slightly low for the maximum positive and splice moments. The ultimate shears were also slightly lower than the correct values, especially in the region near the central pier.

The service load positive moment used during the design corresponded approximately to that of an HS-23 truck. The negative moment corresponded approximately to an HS-28 lane loading rather than the desired HS-20 loading.

This apparently arose as a consequence of several people working independently and successively on the design, with a misinterpretation of the meaning of moment envelopes for several beam spacings, and confusion over whether impact factors had been included in the total or not.

It is clear from comparisons of the stresses listed in Tables 2.2 to 2.4 with allowable values, and comparisons of required and supplied ultimate moment capacities shown in Table 2.5, that the beam should have contained slightly less post-tensioned reinforcement. Reducing the number of post-tensioned strands to 39 instead of 42 would have reduced the negative moment capacity to about 81,700 k-in., two percent more than required. (With the Stressteel post-tensioning system, multiples of three strands are required because of the anchorage details.) A correctly done design would be controlled by stresses at the positive moment sections and strength at the negative moment sections.

With the original live load moment envelope, the limiting compression stresses were approached very closely at the bottom of the girder at the central pier and at the top of the precast, pretensioned girder at the maximum positive moment section. In no cases were the tensions limiting factors.

The number of post-tensioned strands could have been reduced to perhaps 33 before the allowable stresses governed at the bottom face of the maximum positive moment section. This would have required additional mild steel reinforcement in the deck near the central pier to provide adequate moment capacity. This redesign has not been pursued to completion so it cannot be fully evaluated.

The ultimate live load shear envelope was slightly too low, and in addition the original shear design was done using the dead load shear computed considering the effects of the secondary moment. Inclusion of the secondary moment when computing the dead load shear offset the live load error at the outer support, but compounded the situation near the central pier. The region between the splice and a section 105 ft from the abutment had somewhat less web reinforcement than required, and the five ft length of beam adjacent to the central pier needed slightly more web reinforcement. As shown in Fig. 2.11, the section located 100 ft from the abutment needed web reinforcement with 93 kips capacity, while the steel supplied was capable of only 79 kips. The critical section located d/2 from the central pier needed 169 kips capacity, while about 157 kips was supplied.

While these errors are unfortunate and tend to complicate the comparisons between the applied loads and the loads required by the AASHTO provisions, they do not invalidate the work. The basic aim was, and remains, to compare behavior of the structure, as built, with the predicted behavior of the same structure.

3. FABRICATION AND ERECTION, AS-BUILT

3.1 General Remarks

The three segmental girders, the splices, and the deck were cast at the Midwest Prestressed Concrete Company, Rochelle, Illinois. A brief description of the fabrication of various components of the girder-deck system is given in the following sections.

Some of the dimensions noted in this chapter are slightly different than those given in Chapter 2. The actual structure had two different kinds of joints, and hence the member lengths were not the same and also varied from the idealizations of the structure analyzed.

As an additional difference, the structure was fabricated 250 ft in total length, while the structure analyzed was 250 ft between centers of end bearings. The actual spans were 124.0 ft each, center to center of bearings.

The actual final dimensions are used in all comparisons of applied loads and their observed and theoretical effects.

3.2 End Girders

Because of different type of splices used, the two end girders did not have the same dimensions. The north and the south girders had lengths of 87 ft 6 in. and 85 ft 3 in., respectively. Each girder was pretensioned with 14-1/2 in. diameter 270 ksi strands. The north and the south girders were cast on June 1, 1973 and June 5, 1973, respectively. Both girders were designed for a concrete strength of 6,000 psi at 28 days, 4,000 psi at the release of the prestress, and 5,000 psi at the time of post-tensioning.

3.3 Middle Girder

The middle girder was 73 ft 0 in. long. The girder was designed for a concrete strength of 6,000 psi at 28 days and 5,000 psi at the time

of post-tensioning. No pretensioning was used for the girder. The girder was cast on May 29, 1973.

3.4 Erection of the Girders

The three girders were placed on three permanent and two temporary supports as shown in Fig. 1.2, on July 3, 1973 in the prestressing plant's yard directly south of the main building. The three girders were placed in the north-south direction. The south end of the north girder and the north end of the middle girder were placed 18 in. from each other on the north temporary support, which consisted of wood blocks set on concrete slabs. The eight #9 reinforcing bars, four each at the top and the bottom, projecting from the ends of the two girders were aligned and spliced to each other with Caldweld splices as shown in Fig. 3.1.

The north splice had originally been planned to be 12 in. long. However, after getting the final dimensions on the equipment required for the Cadweld splices, this was increased to 18 in. by shifting the north end segment 6 in. north of its original position. Adequate bar extensions had been provided, and these were trimmed to fit with an acetylene torch prior to making the splices. This lengthened the entire structure by 6 in., and resulted in a small overhang at the north abutment.

The south end of the middle girder and the north end of the south girder were placed 39 in. from each other, on the south temporary support. The eight #9 reinforcing bars, four each at the top and the bottom, which projected from the ends of the two girders overlapped for a distance of approximately 38 in.

The spacings of the girder segments and approximate locations of the temporary supports are shown in Fig. 3.2.

3.5 Splices and Deck

Before the joints were cast, post-tensioning conduits connecting the conduits at the ends of the girders were provided in the joints.

Stirrups were provided in each joint. The ends of the rebars in each stirrup were bent to form a shear key for the casting of the deck similar to those in the individual segments.

The two splices were cast on July 20, 1973, using a mix identical to that used for the three segmental girders. The deck, 250 ft long, 7 ft wide, and 7-1/2 in. thick was cast on the same day, using a different concrete mix, with a specified strength of 3500 psi at 28 days.

3.6 Post-tensioning

The entire structure was post-tensioned on July 30, 1973. Forty-two 1/2 in. diameter 270 ksi strands, twelve in the top conduit and fifteen in each of the lower two conduits, were each tensioned to 29.3 kips (189 ksi nominal stress) using a 400 ton capacity jack. All strands in one conduit were stressed at one time, and all were tensioned from both ends of the structure. Figures 3.3 to 3.6 show the post-tensioning conduits, the prestressing anchor heads, and the prestressing jack. The anchorage system was supplied by the Stressteel Corporation, and the jack was a Pine center-hole ram with accessories to adapt it to the Stressteel hardware.

The post-tensioning operation caused the girder to lift off of and free of the two temporary supports. The vertical movement was 0.63 in. at the south splice and 0.33 at the north splice. After the post-tensioning operation was completed, the temporary supports were removed, leaving the bridge supported on the center pier and the two end abutments.

3.7 Bearing Devices

The final bearing at the central pier was a 3-in. thick laminated elastomeric bearing pad. This was flexible enough to accommodate the slope changes imposed on the beam without undue restraint. The pad was grossly overloaded (D. L. reaction = 174 kips) compared to its normal

working load (about 125 kips maximum), but it behaved satisfactorily during the short term tests. The bearing was arranged as shown in Fig. 3.7a.

The ends of the beams were supported on 4-in. diam. steel rollers set between 2-in. thick plates, and on load cells. These items were arranged as shown in Fig. 3.7b.

3.8 Concrete Properties

The properties of the two concrete mixes used are listed in Table 3.1. One mix, containing 7-1/2 sacks of cement per cubic yard, was used in the girder segments and the splice. A second mix, containing 6-1/2 sacks of cement per cubic yard, was used in the deck.

All concrete was mixed in a horizontal pan mixer in the prestressing plant and transported in buckets to the prestressing bed or to the location of the test specimen.

Compressive strengths of the concrete used in the various components, as determined from tests of 6 by 12 in. cylinders, are listed in Table 3.2. Each individual test result is listed. There is a great deal of scatter, and the discrepancies between specimens tested 15 August and 28 August is particularly marked.

The 15 August tests were done at the prestressing plant, and the later tests in the Civil Engineering Department laboratories, with strain measurements being made. The later cylinders appeared to be sound and without obvious defects, and the testing rates were not greatly lower than the earlier tests. No reasonable explanation of the differences has been found.

The few cylinders remaining after the tests of 28 August were tested 8 September 1973, as spot checks, and the strengths were quite low as shown in Table 3.2.

It seems reasonable to assume that the concrete strengths at the time of the final test on 7 August were about 7,000 lb/in.^{2} for the girder elements and deck, and about 6,500 lb/in.^{2} for the splice concrete.

Young's modulus values were determined from the strain measurements made 28 August 1973. These are listed in Table 3.3. These are initial tangent modulus values. Secant modulus values at 2,000 lb/in.^{2} stress would have been about the same, as the curves were nearly linear in that stress range.

There is considerably less scatter among the modulus values than in the strength data, although in general the weaker cylinders had the lower stiffnesses. The deck concrete had the highest average modulus, and for purposes of studying the results of the applied load tests on the beam it will be assumed that all concrete has the same modulus.

3.9 Effects of Concrete Properties

The original design work was based on the deck concrete having a modulus considerably lower than the girders, as noted in Sec. 2.3. Consequently the properties of the transformed composite structure described in Sec. 2.2 and Fig. 2.1 are not valid for the test structure.

New composite section properties were computed assuming the same Young's modulus in girder and deck, and are shown in Fig. 3.8. The moment of inertia is 9 percent larger than was used in the design, and the center of gravity of the composite section is almost 2.1 in. higher. The section modulus for the bottom of the girder is increased 3.5 percent; values for the top of the girder and top of the slab are increased more than 20 percent. These changes have various effects on the computed service load stresses, but have no significant influence on the strength of the structure.

The shift in the position of the center of gravity of the composite section has a direct influence on the secondary moments, since the eccentricity of the post-tensioning steel is changed. The eccentricity is downward for most of the length of the beam, and this is increased. The upward eccentricities are limited to a region near the central pier and are, on the average, considerably smaller than the downward eccentricities.

A 2.1 in. upward shift in the composite center of gravity would be expected to significantly increase the positive secondary moment induced at the central pier as a result of post-tensioning. The structure was re-analyzed with the new eccentricities, and the computed secondary moment at the central pier was +31,630 k-in. immediately after post-tensioning rather than +27,325 k-in. as shown in Table 2.1. The overall influence of this change, which is appreciable when viewed in isolation from the other changes, is not large. The service load positive moment at the maximum positive moment section is increased slightly, but the section modulus for compression stresses is increased enormously. Increasing the secondary moment can only help the negative moment section of the central pier, since compression at the bottom of the section was most nearly critical.

4. INSTRUMENTATION

4.1 General Remarks

This chapter describes the instrumentation used for measuring the loads, reactions, strains, and deflection of the girder-deck system during the test. The locations of the mechanical strain gages and the locations at which vertical deflection measurements were made are described in this section.

4.2 Mechanical Strain Gage Measurement

A total of 84 mechanical strain gage lines were installed on the girder and the deck. Each gage line, ten in. long, was made by attaching to the beam two 1/2 by 1/2 by 3/16 in. stainless steel plates. A conical hole was countersunk with No. 1 center drill at the center of each plate. The plates were attached to the girder by first cleaning the concrete surface by sanding and then with acetone and then applying a contact cement to the concrete and an accelerator to the plates. The plates were attached to the top of the deck with a quick-setting epoxy material.

The strains were measured with a 10 in. gage length Whittemore gage. The Whittemore gage is a direct reading mechanical gage with no multiplication of movement. The minimum reading is 0.0001 in., for a minimum strain of 1×10^{-5}. The device is equipped with spherical tips (0.089 in. diameter) which fit into the conical holes drilled into the small plates. The locations and designations of the strain gage lines are shown in Fig. 4.1 and 4.2. Identical patterns were used on each side of the girder for the north and south spans. Each number was preceeded by two letters indicating span and side of beam.

Temperature compensation and standard gage readings were provided by the use of a 2 in. x 2 in. steel bar with a thermometer inserted

longitudinally in the center of the bar. The standard bar was kept on one of the piers, always in the shade. It must be noted that completely adequate temperature compensation is probably not possible in the case of a structure where some parts are in the shade and others in the direct sunlight. Nevertheless, the temperature readings were taken during the strain measurements in each load increment.

4.3 Deflection Measurements

Deflections were measured by means of a Wild N-3 precise level and a level rod. Measurements were obtained at the north abutment, 70 ft north of the center pier, 35 ft north of the center pier (north splice), north and south sides of the center pier, 35 ft from the center pier (south splice), 70 ft south of the central pier, and at the south abutment, Fig. 4.3. The deflections were measured by placing the level rod in contact with points premarked below the deck. The level rod had a small circular level attached to it for monitoring the vertical position of the level rod. The two measurements at the north and south sides of the central pier were made because two level setups were used to reduce sight distances, with one instrument station halfway between the north abutment and the center pier, and the other halfway between the center pier and the south abutment.

Level readings were made directly to 0.001 ft and estimated to 0.0001 ft.

4.4 Load and Reaction Measurements

The applied loads were measured by a series of six or ten load cells, for the design service load and the design ultimate load tests, respectively. The load cells are thick walled cylinders machined from 6061-T651 aluminum rods. Each load cell is 6 in. long with an outside diameter of 2 in. and an inside diameter of 1-1/8 in., and fit over the loading rods, between the jacks and the nuts on the rods. The four strain gages mounted on the external surface of each load cell

were wired to form a four-arm bridge measuring circuit. Each load cell has a capacity of 57 kips and was calibrated to a maximum load of 50 kips. The load cell sensitivities were about 80 $lb/10^{-5}$ strain.

A 400 kip and a 150 kip capacity load cell were used for measuring the reactions at the north and south abutments. Both were thick-walled cylinders machined from steel tubing, and were instrumented with electrical resistance strain gages wired as 4-arm bridge circuits. The 400 kip load cell had a sensitivity of 781 $lb/10^{-5}$ strain, while the value for the 150 kip cell was 300 $lb/10^{-5}$.

Since only the 400 kip load cell had enough capacity to measure the reaction in the loaded span during the design ultimate and overload tests, the two cells were switched from end to end of the structure as needed.

5. LOADINGS AND TEST PROCEDURE

5.1 General

Loads simulating the tractor and the trailer of an HS vehicle were applied by a series of jacks pulling on bars anchored to the ground. A total of 28 1-in. diameter high strength steel rods, each connected to a 2-3/4 in. diameter steel plate washer, were grouted into holes drilled in the bedrock. The bedrock is approximately 15 to 20 ft. below the ground surface.

The bars were placed on both sides of the beam at a transverse spacing of 4 ft., to the north and south of the center pier at distances of 40 ft, 44 ft, 54 ft, 58 ft, 68 ft, 72, ft, and 84 ft from the pier, as shown in Fig. 5.1.

These hole spacings were selected to allow application of loading combinations approximately the AASHTO HS vehicle axle spacings of 14 ft, without requiring excessive numbers of anchor bars to be grouted into the rock.

The bars projected about 4 ft above the ground. The ends of the bars projecting above the ground level were threaded and connected to other bars with the use of a sleeve nut. A series of 1-1/2 in. diameter holes were provided in the deck at locations directly above the embedded rods. Loads were applied by center-hole jacks placed on the deck, with 1-inch high strength steel rods passing through the jacks and deck and fastened to the sleeves connected to the bars below the deck, as shown in Figs. 5.2 and 5.3.

The rods which were anchored into the bedrock were Stressteel post-tensioning bars. The loading rods which were coupled to them were AISI 4142 heat-treated steel (similar to ASTM-A193, Grade B7 bolt material), and the 2.0 in. diameter by 4.5 in. sleeve nuts were of the same material. The sleeve nuts also provided transitions from the 14 threads/in. used on the Stressteel bars to the 8 threads/in. used on

the upper rods. The upper rods were part of the general stock of testing equipment from the University of Illinois Structural Research Laboratory, and were used with ASTM A194 Grade 2H nuts and hardened washers.

5.2 Service Load Tests

The first four loading conditions correspond to design service load for an HS20-44 truck on the bridge. The loading positions were as follows:

1. Load causing the maximum positive moment in the north span, Fig. 5.4
2. Load causing the maximum shear at the north splice, Fig. 5.5
3. Load causing the maximum positive moment in the south span, Fig. 5.6
4. Load causing the maximum shear at the south splice, Fig. 5.7

Loadings No. 2 and No. 4, in addition to causing the maximum shear at the two splices, give approximately the maximum positive moment at these two locations. According to AASHO specifications, when the girder spacing is 7 feet, the total service live load for one typical interior girder is 45.8 kips without impact, and the additional load due to impact was also applied through the jacks. Additional forces were also applied to account for the weight of the asphalt deck topping; the forces used reproduced the shear acting at the splice but the same force was used with all loading positions. Accounting for the impact and the weight of the asphalt, the total service test load is 73.6 kips. The load was applied through six 30 ton jacks, two accounting for the front axle loads and the remaining four accounting for the rear axle loads of the truck. The loads were applied in such a manner that each jack corresponding to a front wheel carried one-eighteenth (1/18) and that each jack corresponding to a rear wheel carried four-eighteenths (4/18) of the total load. The total load was applied in five equal increments.

To avoid excessive stress concentrations at the points of application of the loads, front axle jacks were placed on 8 by 8 in. by 1/2 in. steel plates, and the rear axle jacks were placed on a 9 by 15 channel sections, 3.5 ft long, as shown in Fig. 5.2.

The load applied through each jack was measured with a load cell placed directly above the jack. The pressure for the two front axle jacks was applied with a manual hydraulic pump, whereas the pressure for the four rear axle jacks was applied with an electrical pump. The force required to produce the loading in the system was monitored by two strain indicators, one connected to one of the front axle jacks and the other connected to one of the rear axle jacks. An attempt was made to coordinate the application of the pressure in the front and rear axle jacks.

5.3 Design Ultimate Loads

The remaining three loading conditions correspond to design ultimate load of 1.5 times the dead load and 2.5 times the live load plus impact. The loadings were as follows:

1. Load causing the maximum shear at the north splice, Fig. 5.8
2. Load causing the maximum positive moment in the north span, Fig. 5.9
3. Load causing the maximum shear at the south splice, Fig. 5.10

For the last loading condition the total load was eventually increased to 1.65 times the design ultimate load. The equivalent weight of the asphalt and the additional 50 percent of the dead load, as well as the 2.5 times the live load plus impact were applied through a series of ten jacks. The total load corresponding to the design ultimate load was 198.7 kips. To avoid concentration of the load on the deck and to remain within the capacity of the rock anchors, the load was applied through two jacks for the front axle loads and eight instead of four jacks for the rear axle loads of the truck. The loads were applied such that each front

axle jack carried one-eighteenth (1/18) and each rear axle jack carried two-eighteenths (2/18) of the total load. The total load was applied in six increments. The design service load was applied in the first two increments and the difference between the design ultimate and the design service loads was applied in four additional equal increments. In the last loading condition (load causing the maximum shear and moment at the south splice), the load was increased in equal increments until a total load of 1.65 times design ultimate load was reached at which the test had to be terminated mainly due to reaching the end of the threads in the loading bars, and limitations on available time. It was thought that the threaded lengths of the pull rods were more than adequate, but some of the rock anchors slipped considerably before resisting their share of the load.

A procedure similar to that used for applying, measuring, and monitoring the pressure for the design service load tests was used for the design ultimate load tests. To avoid stress concentrations at the points of application of the loads, front axle jacks were placed on the 9 in. 15 lb. double channel sections parallel to the girder, whereas the rear axle jacks were placed on 12 in. x 25 lb. double channel sections placed perpendicular to the girder, as shown in Fig. 5.3.

5.4 Testing Procedure

For each loading condition described above, before the application of the load, initial readings were obtained on all load and reaction cells, the strain gages, and the level rod for the vertical deflection measurements. To insure that no load was applied through the jacks, approximately 1/2 inch slack was provided in the jack by loosening the nut directly above the load cell. A standard bar strain reading was also taken with the Whittemore strain gage and the temperature recorded for possible temperature correction.

For the four design service load tests, the design service load of 73,600 lbs was applied in five equal increments of 820 lbs in each of the two front axle jack and of 3280 lbs in each of the four rear axle

jacks (See Tables 6.1 to 6.4). After each load increment was applied, strain indicator readings were obtained for each load and reaction cell. Concrete strains at the various locations were recorded and the level readings were taken. When the loads were removed after each loading condition, zero readings were again taken on all load cells, strains, and the level rod. The time for each complete test varied between 2-1/2 to 5 hours, depending on difficulties with the hydraulic system. The average time for the completion of each loading increment including the reading of load cells, strains, and level rod was approximately 30 minutes. For some loading increments, if no difficulty was encountered, the time was reduced to 15 minutes. A slack or slip of 1 to 1.5 in. in most of the loading rods was taken up during the application of design service loads. During the application of the third loading increment of the third test, the loading rod on the east side of the bridge 54 feet south of the center pier came loose and it was pulled up approximately one foot before it finally reseated itself and resisted additional load.

For the three design ultimate loads, the design ultimate load of 198,700 lbs was applied in six increments. For the first two loading increments, a load of 2050 pounds was applied to each of the two front axle jacks and a load of 4100 lbs was applied to each of the eight rear axle jacks. The second increment corresponded to the design service load. For the next four loading increments, additional loads of approximately 1,740 pounds were applied to each of the two front axle jacks and loads of approximately 3470 pounds were applied to each of the eight rear axle jacks. The magnitudes of the total loads for each increment are given in Tables 6.5 to 6.7.

In the last loading test, (load causing maximum shear at south splice), the load was increased in additional equal increments beyond the design ultimate load. A total load of 328,000 lbs, equivalent to 1.65 the design ultimate load, was reached at which time the test had to be terminated because the end of the threads in a loading rod had been reached, as had the end of the daylight needed for illumination.

The time for the completion of the loading increments for the design ultimate load tests was longer than that for the design service load tests, mainly due to the inspection and marking of the cracks in the girder.

At the end of each loading increment of the design ultimate load tests, the girder and the deck was examinated for cracks. The cracks were marked and identified by the load number before the next load increment was applied.

6. RESULTS OF TESTS

6.1 Introduction

The results of the tests, in terms of load-deflection, load-strain, load-reaction, and cracking response will be described in this chapter. Most of the discussion of the results will occur in Chapter 7.

The data for the successive sets of tests to service load, design ultimate, and the final overload test will be presented in successive sections. The post-tension operation was actually the first test loading, and the deformations produced will be discussed first, in Sec. 6.2.

6.2 Deformations and Reactions at Post-tensioning

The vertical deformations at post-tensioning are important, since if the structure lifts enough, it will come free of the temporary supports, facilitating their removal. The test structure deflections were not very symmetrical, but both spans came free of the supports. The upward deflections, relative to the central pier, were as shown below (inches):

S. Abutment	S.70'	S35'	Pier	N35'	N70'	N. Abutment
0.09	1.39	0.63	0	0.33	1.01	0.10

The apparent upward movement at the ends of the bridge is probably actually a downward movement at the central pier due to compression of the elastomeric bearing pad.

The south span was more flexible than the north. The Young's modulus values from Table 3.3 are lower for the south span than in the north, but the differences were not great enough the explain the differences in camber.

Reaction load cell readings were taken at each stage of post-tensioning. The measured reactions are compared with theoretical values below, immediately before post-tensioning:

	S. Abutment	N. Abutment
Measured	57.8 kips	57.3 kips
Theory, 150 lb/ft^3	58.9 kips	60.4 kips
Theory, 145 lb/ft^3	56.9 kips	58.4 kips

The agreement between measured and computed values is well within reasonable ranges of variation of the unit weight of an air-entrained concrete. The theoretical reactions for the two ends of the structure are different because of the different lengths of the end segments, as shown in Fig. 3.2.

Differences between theory and measurement can occur because the unit weight of the concrete is not known exactly and may vary along the length of the structure, and because of cross-sectional area variations. Measuring errors may also occur, especially since the minimum reading on the south load cell was about 0.8 kips.

After all tendons were stressed from both ends, the measured and computed reactions were:

	S. Abutment	N. Abutment
Measured	84.0 kips	83.4 kips
Theory, 150 lb/ft^3 and design eccentricities	88.5 kips	88.5 kips
Theory, 145 lb/ft^3 and design eccentricities	86.2 kips	86.2 kips

The final reactions are slightly smaller than anticipated. In addition to the reasons previously discussed for such differences, the secondary moments play an appreciable role in this case, with 18.2 kips of these reactions being attributed to secondary moments. Any error in the secondary moment calculation, such as may occur if friction is greater than assumed or the actual centroid of the section being slightly different than assumed will lead to proportionate changes in that component of the reaction.

The final reactions are nearly the same, and the changes accompanying post-tensioning and lifting off the temporary supports are also nearly equal, at 26.2 and 26.1 kips, for north and south, respectively. This tends to support the validity of the reaction measurements.

The concrete probably weighed about 145 $\pm$ 2 lb/ft^3, and the secondary moment was apparently slightly lower than expected. The average measured reaction, with 145 lb/ft^3 concrete, leads to a net positive moment at the central support of about 125 k-ft, and maximum positive dead load moment of about 2620 k-ft.

Tendon elongations were measured during post-tensioning, but the measurements were relatively imprecise, and tendon friction information cannot be reliably extracted from the values. In stressing, a preload force of 88.7 kips (750 lb/in.^{2} hydraulic pressure in jack) was applied, and elongations were measured from that point. The elongations from the first end stressed exceeded the jack extension capacity, so the tendons had to be anchored, the jack retracted, and a new pull made to reach the required force. This resetting greatly reduced the precision of the elongation measurement.

The tendons were all stressed from both ends. Pulling the second end produced relatively little additional elongation.

Measured and calculated elongations, in inches, are listed below, with the calculation being for zero friction, for forces in excess of the preload force, and for E_s = 28 x 10^6 lb/in.^{2}.

Tendon	Force	Measured, N	Measured, S	Total	Theory
Top	347 kips	11 9/16	2 3/4	15 5/16	15.1
Middle	434 kips	14 3/4*	1 3/4	16 1/2	16.1
Bottom	434 kips	13 1/8	1 15/16	15 13/16	16.1

* Best estimates at time of post-tensioning, known to be in error.

The top duct had been partially blocked 21 ft from the north end of the beam. The obstruction was found while pulling a 2.4 in. diameter steel "ball" through the duct with a steel cable, although the cable had been inserted with out serious problems. The obstruction was eventually cleared, but this duct must have had somewhat higher friction than the other two. The extra elongation at the south end seems to suggest that the high friction area was concentrated near the north end of the structure.

The measured elongations were all greater than the computed ones, which may be a result of measurement problems, or of E_s being lower than assumed, or both.

6.3 Service Load Tests

Four tests to service load levels were conducted with the loading positions shown in Figs. 5.4 to 5.7. The nominal applied load was 73.6 kips. Of this, 54.9 kips was from the design HS-20 vehicle load, including impact, proportioned for a 7 ft beam spacing. The remaining 18.7 kips was to compensate for the additional design dead load from the asphalt topping which was not present on the test structure. This load was specifically the additional load to cause the correct shear force at the splice when the vehicle was positioned for the maximum splice shear loading.

The 73.6 kips load was attained in 5 equal increments. The values of each of the "axle" loads at each increment are listed in Tables 6.1 to 6.4. There are no major deviations from the desired axle loading ratios during these tests. Differences between the two rear axle loads, which were applied by four jacks connected to a common pump, can result from different friction in the jacks.

Although there are small differences between the actual and desired load distributions, the data will be presented in terms of total applied loads, and interpreted as if the distributions were exactly as shown in Figs. 5.4 to 5.7, where the rear two axle loads are 4.0 times the front axle load.

The service load tests produced no cracking in the structure. The general behavior was elastic with respect to both deflections and reactions. The service load deformations were small, with maximum deflections of about 1.0 in. downward in the loaded span and about 0.4 in. upward in the other span. Superposed on these deflections were undetermined deflections caused by temperature gradient effects caused as the sun shown on the east side of the girder, then only on the top of the deck, and later on the west side of the girder. Buildings adjacent to the west side of the girder limited the late afternoon sun.

Load-deflection curves for the first four tests are shown in Figs. 6.1 to 6.4. Also shown in the same graphs are theoretical elastic load-deflection curves, computed using $I = 615{,}570$ in.^{4}, as shown in Fig. 3.8, and with $E_c = 5.5 \times 10^6$ lb/in.^{2}.

The measured curves are generally linear in nature, and there were only small residuals on unloading. The residuals are shown only when they exceed 0.02 in.

The deflections were relatively insensitive to the loading locations, as the deflections due to the splice shear loading were about the same as those due to the maximum positive moment loading. The maximum deflection in the loaded span was approximately the same as the deflection at the 70 ft point. The maximum upward deflection in the unloading span was somewhat greater than at either the 35 or 70 ft point. The structure was nearly symmetrical, with comparable loadings causing nearly identical deflections in the two spans.

Deflections were computed using $E_c = 5.5 \times 10^6$ lb/in.^{2} rather than a value between 4.8 and 5.3 x 10^6 k/in.^{2} as determined from cylinder tests. This was done to match the measured deflections. The beam deflection measurements represent a very large Young's modulus test, and more accurately represent the beam concrete quality than do the cylinder tests listed in Table 3.3.

Measured and computed elastic reactions at the two ends of the structure are plotted versus applied load in Figs. 6.5 and 6.6. The general trends of measurements and theory agree reasonably well, but there are some marked deviations. The loaded-span reactions are considerably

smaller than those computed for a simply supported beam for all cases except the second increment of the fourth test.

The causes of the deviations are not completely known, but it is believed that the difficulties were more likely to be in the precision of the measurements than in the actual forces. There were some large and unexplained zero shifts during the tests, which may be due to moisture accumulating in at least the 150 kip load cell.

The load cells were four-arm bridge measuring circuits which are relatively well self-compensated for temperature changes as long as the entire load cell changes temperature uniformly. In the bridge test the temperatures were undoubtedly nonuniform at least part of the time since the sun could shine directly on the cells early and late in the day. The extent of any reading changes produced by this effect cannot be readily assessed, but could have been significant.

Because of the uncertainties introduced into the load-cell readings, it does not appear that the reactions can safely be used in determining moment and shear distributions in the service load tests. The reaction measurements must be viewed as only indicators of trends.

As was noted earlier, no cracks were found during the service load tests. The measured strains also indicated that no cracking was likely to have occurred. The maximum strain measured was 0.000,25 tension, at the bottom gage line 70 ft north of the central pier. The precompression at that section was about 2,100 lb/in.^{2}. A strain of at least 0.000,47 would be expected at initiation of cracking, if $E_c = 5.5 \times 10^6$ lb/in.^{2}. The maximum tensile strains in the deck were about 0.000,10, at the central pier, about one-third the expected cracking strain, considering the different precompression at this section.

6.4 Design Ultimate Load Tests

Design ultimate loads of about 197 kips were applied in two different positions in the north span. The loads were positioned to give maximum shear at the splice and maximum positive moment, respectively, in the two tests.

The nominal load of 198.7 kips was determined using the 1969 AASHO load factors of 2.5 live load plus impact and 1.5 dead load. The live load component was 137.5 kips, and the remaining load was applied to reproduce the correct shear at the splice resulting from 1.5 dead loads, including the asphalt topping. The extra 61.2 kips was required with the splice shear loading position, and the same load was then applied in the positive moment loading position.

Because of the high total load required, it was applied with five "axles" rather than three. The nominal loads on the four rear loads were each twice that on the front axle. The axle loads are listed for each of the six increments of each test in Tables 6.5 and 6.6. The relative loads were in reasonable balance except on the first two increments of Test 5 and the last increment of both tests. The load positions are shown in Figs. 5.8 and 5.9. The low load at 68 ft north at increment 56 may be a result of slip of one of the anchor rods.

These two tests caused flexural and shear cracking and caused deflections in excess of three in. in the loaded span. However, there was not much damage apparent after unloading. The flexural cracks were all all tightly closed and generally not visible. The residual deflections were extremely small.

Load-deflection curves for the two tests are shown in Figs. 6.7 and 6.8, as are elastic deflections. In Test 5 there is a slight deviation from the initial linear response at loads above 100 kips, and a more marked deviation above 165 kips. The residual deflections in each case are quite small.

Load-reaction curves are given in Fig. 6.9. The reactions from the splice shear loading are in reasonable agreement with the theoretical elastic reactions. The south reaction was considerably too small during most of the positive moment loading test, but this is apparently the result of a measurement problem rather than a low reaction, since the north reaction was not significantly higher than the elastic value. The deviations of the abutment reactions from the elastic values must be equal. If, for example, the south reaction were 8.0 kips lower than expected, the north abutment reaction must be 8.0 kips higher than expected, from simple equilibrium.

Apparently there was some error made in determining the applied loads in the second increment of the sixth test, as neither the deflections nor the reaction curves go smoothly through that point. The curves would all be smooth if the load were plotted as 75 kips rather than the 86.7 kips shown in Table 6.6. The test records have been carefully examined without finding any evidence of the trouble. It would have been relatively easy to have applied 86.7 kips rather than the intended 74 kips, but the deflections should have corresponded to the higher load.

The first cracks were found at the fourth increment, 135.7 kips, in the splice shear test. One vertical crack occurred at each edge of the north splice, at the joint-beam interfaces. These cracks extended through the lower flange and about 5 in. into the web. Two horizontal cracks at midheight of the splice web were also found. These cracks were approximately along the paths of the post-tensioning ducts, and may have existed earlier.

The fifth load increment, 165.3 kips, caused a number of web-shear cracks just north of the central pier. Two cracks crossed most of the depth of the web, and the rest were short cracks near the junction of the beam web and the top flange. None penetrated into either flange. All cracks were very small.

The final increment, to 197.2 kips, caused considerable additional cracking. Eleven flexural cracks were found in the area between 48 and 68 ft north of the central pier. Six of these cracks extended about half way up the web, the others were confined to the lower flange. Additional shear cracking occurred, with most of these cracks inclined about 30° above the horizontal. One inclined crack crossed the splice.

No cracks were found in the deck, nor were any flexural cracks found in the negative moment region of the girder.

A number of negative moment and shrinkage related cracks occurred in the pier module before post-tensioning. None of these cracks reopened during this test, and shear cracks crossed them with little change in direction.

Several crack widths were measured. The flexural cracks were 0.008 to 0.010 in. wide at the lower flange. A shear crack in the north precast element, 4 in. from the splice and near the top of the beam web, was 0.014 in. wide, and was the widest crack found. Most of the shear cracks were much smaller, with 0.006 in. being a good representative width.

The maximum positive moment loading in the north span, the sixth test, was initially plagued by slipping of two of the loading rods at different stages of the test.

The structure was carefully examined to determine when cracks reopened. The fourth load increment, to 136.9 kips, produced the first reopening of flexural cracks. They were extremely small at this stage, with the greatest measured width being 0.003 in.; most widths were too small to measure.

The fifth increment, to 168 kips, caused one new flexural crack, under one of the center axles. The maximum crack widths were 0.006 to 0.007 in.

The last load increment, to 194.5 kips, caused considerably more flexural cracks, with the last cracking 80 ft north of the central pier. At least 11 new cracks opened at this load. The widths remained small, with maximum measured widths again in the range of 0.006 to 0.007 in.

Figure 6.10 shows the locations, lengths, and locations of all cracks in the north span. The drawing was prepared from photographs taken after the tests were completed. The cracks are not marked in the drawing to distinguish which test caused them. However, all cracks more than 68 ft north of the central pier occurred during the 6th test. All cracks near the central pier and those near the north splice occurred during the 5th test, which was the loading for maximum shear at the splice.

The cracks marked on the deck occurred during the loading in the south span. These cracks were not carefully marked on the sides of

the slab, and there were many more than shown here, but the northern limit of deck cracking is about right. No negative moment cracks were found during either north span test.

The loading positions are marked on the drawing.

The interpretation of the cracking loads, and discussion of tensile stresses at cracking, will be deferred until Chapter 7.

Strains are plotted versus live load moment in Figs. 6.11 and 6.12, for a number of gage lines. Moments are used rather than loads in order to facilitate comparisons between the effects of the two different loadings. In each case the strain is the average of the measurements on the two sides of the beam. Before cracking, the values were always very close to being the same. After cracking, the differences were occasionally large, exceeding 50 percent in some cases.

The moments plotted are those from an elastic analysis of the structure, using the ideal distributions of forces. Figure 6.11 has been plotted assuming the moment computed at 37.5 ft north exists at gages lines 23, 33, and 43, even though the moments are slightly different at these sections.

Cracks crossed all three gage lines near the north splice during Test 5, and the graphs are marked to indicate when the cracks were seen. There is no strong indication that these cracks reopened during Test 6, except at gage N33, located at the middle of the splice.

There is a discontinuity in most of the moment-strain curves between the second and third increment of Test 6. This is a reading error apparently caused by some accidental damage to the mechanical strain gage either while the second increment readings were being taken or between readings. There is a large change in the standard bar gage readings at this time, and the normal correction procedure followed has not removed quite all of the error.

Test 5 caused no cracks at the section 70 ft north of the central pier, as is confirmed by the strain plot for line N53 Fig. 6.12. There was a crack at 68 ft north, and this may have disturbed the trend of the graph slightly at the last load increment. Test 6 caused numerous cracks in this area, at the last increment, and this shows up clearly in the graph.

Strains are plotted in Fig. 6.12 for gages N63, located 90 ft north of the central pier and 10 ft beyond the last crack, and gage N10, located just north of the central pier. Gage N10 shows some decrease in slope after the fourth increment of Test 5. No cracks were found in the deck, but web-shear cracks were occurring in the beam web near this section during the final two load increments.

6.5 South Span Overload Test

The final test loading produced maximum shear at the south splice. A maximum load of 328.2 kips was reached, in the 11 increments listed in Table 6.7. This load did not cause failure of the structure even though the maximum deflection was nearly 11 in. Extensive cracking occurred throughout the loaded span and over much of the length of the unloaded span. There was considerable distress in the precast beam just south of the splice, but the structure apparently would have carried more load before failure.

The extent of cracking at the beginning of the test was described in Sec. 6.4. There were no cracks in the south span. The residual deflections at the beginning of the final test were small, and are listed below. The values are relative to the position of the structure at the beginning of testing.

Point	S70	S35	N35	N70
Deflection	0.06 in. up	0.05 in. up	0.09 in. down	0.10 in. down

Load-deflection curves for the four points are given in Figs. 6.13 to 6.15. The final deflection was 10.8 in., at the point 70 ft south of the central pier, and was approximately the maximum in the span. In spite of the fact that the curve started leaving the original straight line at only one-third of the final load, the residual deflection of 1.02 in. at the end of the test was relatively small.

The other curves are similar, in that quite large deflections under the maximum load have resulted in relatively small residual deflections. The upward deflections in the unloaded (north) span were always larger than the elastic deflections, and the residuals were relatively larger than in the loaded span.

The initial low stiffness in the north span may be due to cracking during Tests 5 and 6. The higher residual may be a result of very extensive cracking in the deck during this test. The precompression in the deck was lower than in the beams, and cracks would have less tendency to close completely. In addition, the steel in the deck was not prestressed so would not be very effective in closing cracks.

The deflected shape of the structure shows up clearly in Fig. 6.16. The photograph was taken from the southwest late in the test, but slightly before the final load was applied since it was too dark for normal photography by the end of the test.

The live-load reactions are plotted versus applied load in Fig. 6.17, along with theoretical values for continuous and simply supported beams. The numerical values are not entirely consistent, but there are some indications of the changes which took place in the structure.

If the north abutment reaction is viewed as a direct measure of the negative moment at the central pier, it appears that this moment was lower than the theoretical elastic moment in the early parts of the test. Since the measured deviations of the reactions from the theoretical values are not equal, the extent of the deviation cannot be fully evaluated.

At loads above 200 kips, the reaction values both indicate that the negative moment increased faster than the positive moment with increasing load, and the increase in negative moment at the central pier appears to be appreciable. There are probably two effects causing this redistribution of moments. As the loads increase, different sections loose stiffness at different rates. For this loading position, the maximum elastic live load positive moments are about 1.71 times the support negative moment. The dead load moments, including secondary moments, are entirely positive.

Thus, the ratio of applied positive to negative moments was much higher than the ratio of either design ultimate moments or the ultimate moment capacities provided, which are shown in Table 2.5. The redistribution which occurred was tending to bring the ratio of positive to negative moments toward the ratio of the section strengths.

The positive sections were most heavily loaded, and might be expected to loose stiffness at a greater rate than the negative moment sections. As the beam becomes more extensively cracked with increased load, the influence of the secondary moments must be gradually eliminated, as the moments approach the capacities of the various sections. Both effects are operating in this case, and the secondary moment is very large and consequently represents a large redistribution potential.

The changes in the moment distribution with load will be more extensively discussed in Chapter 7.

This test caused extensive cracking in both spans. The south span cracks are shown in Fig. 6.18. The first crack, a horizontal crack parallel to a duct, was found near the south splice at the third load, 106 kips. The first flexural crack was found at the south edge of the splice at load 4, to 136 kips. After load 6, 197.1 kips, was applied the crack pattern was about the same as in the north span at the end of Test 5, though there were fewer cracks. There was one long inclined crack at the central pier, and 10 short shear cracks at the junction of the web and the upper flange, all within about 10 ft of the central pier. Three cracks were found in the precast beam just north of the splice, and four just south of the splice, plus cracks at the interfaces between the splice and the precast beams. Four vertical cracks were found in the region between 56 and 64.5 ft south of the central pier. This load was left in place for about two hours, and three new short shear cracks developed near the central pier, and other cracks grew slightly in length.

Load 7, to 227.5 kips, produced additional cracking, especially inclined cracks located 40 to 44 ft south of the pier, near the rear axle loads. A second inclined crack developed in the splice. Two of the flexural cracks were 0.007 and 0.008 in. wide.

Load 8, to 261 kips, caused cracks as far as 74 ft south of the pier, slightly beyond the front axle load. Negative moment cracking also occurred in the deck, with cracks from 1 ft to 74 ft north of the pier. These cracks were either near the central pier or beyond the splice, but not between the pier and splice. These cracks were small and not well developed. Some crossed the width of the deck, and some extended through the deck thickness, but others did not. One crack was at the south edge of the north splice, and several other cracks were in the same area.

After load 9, to 290.6 kips, was applied, web-shear cracks occurred nearly continuously from the central pier for 28 ft south, as shown in Fig. 6.18. Flexure or flexure-shear cracks existed from about 30 ft to 80 ft south, with cracks at 12 in. or smaller intervals for the entire length. Some cracks from the splice to 75 ft south reached as high as the top of the beam web, but none ever penetrated the top flange.

More serious cracking occurred during application of load 10. The load step was applied in two half-steps because it was necessary to retract some jacks to gain deflection capacity. While the jacks were being retracted, a 1/8-in. wide crack was found in the lower flange, starting at 41 ft south and sloping upward to the south at about 30° above horizontal, as shown in Fig. 6.19. This width was maintained for only a foot, but a large crack continued across the sloping part of the lower flange. On the basis of the widths of cracks in the web at 43 ft south, it appears that some stirrups may have yielded at this load. The width of one of the shear cracks was about 0.02 in., near the mid-depth of the web.

This large crack was one of several which occurred earlier in the same part of the end precast segment, and there was one similar crack in the splice concrete, as also shows up in the photograph. There was quite a visible offset on the lower surface of the beam at the end of the one large crack. The crack was almost under the rear axle of the test load, at the point of maximum shear. It was close

enough to the end of the precast segment to be within the region of development of the prestressing force from the pretensioned strands, but there should not have been large anchorage bond stresses in the reinforcing bars extending into the splice.

The half step of load beyond increment 9, to about 305 kips, caused flexure-shear cracking as far as 83 ft south, and a crack at 80 ft south was 0.016 in. wide, on the lower flange.

The completion of the tenth load increment, to 320.7 kips, caused few new cracks but many extensions of old cracks and obvious growth of widths. The crack at 85 ft south was the last one found. The inclined crack in the lower flange grew in length and width.

The eleventh load, to 328.2 kips, was reached when more jacks reached the end of their travel. This small additional load produced little new cracking, or at least very few cracks were found in the fading daylight.

It was then 7:30 p.m. and rapidly growing dark. The structure was then unloaded, a process that took an hour since the deflection recovered almost 10 in. and the jacks had to be retracted and reextended under load because of their 5-in. maximum stroke. The final readings were taken in darkness with flashlights and car headlights, which is not ideal, especially for the level readings.

The structure did not fail, although it seems reasonable to assume that a failure would have occurred just south of the south splice if the loading had continued. The crack at that location was quite wide at the end of the test, and did not close very well upon unloading.

The test results will be discussed in the next chapter, with attention to initiation of cracking, changes in moment distribution, and the predicted strength of the structure.

Even though the test structure was not heavily instrumented for strain measurements, a large volume of data was gathered during the final test. Part of this data will be presented using load-strain curves. A few distributions of strains across the depth of the structure at particular cross-sections will also be presented.

The cracking near the south splice was the most important in the structure, and the concrete strains in this area are consequently of interest. The strains measured at gages lines S23, S33, and S43 are plotted versus load in Fig. 6.20. Line S23 was on the lower flange of the central segment just north of the splice. The strain response was much as expected, in that the strain increased continuously with applied load, and at a generally increasing rate. Line S33, at the center of the splice, and S43, in the south pretensioned segment show a somewhat different behavior in that the initial response was as expected but the rate of increase of strain then became much smaller and stopped or reversed as the maximum load was approached. The first cracks near the splice were found at the third load, 135.9 kips, but no cracks crossed the strain gage lines until later.

These reversals of trends are probably due to the shear damage which was occurring just south of the splice. The first inclined crack crossed gage line SE43 at load 6, 197 kips, and this is reflected in the curve for S43, the average of the strain on the two sides of the beam. At load 7, 227.5 kips, a shear crack passed outside of the end of the gage line; this crack was to become the largest in the structure after more load was applied. Another crack passed near the gage line at the next increment. These cracks show up in Fig. 6.19. The strain gage line designation is not legible, but the two 1/2 in. sq. plates forming the reference points for the gage line are visible, and line SE42 is clearly marked above this point.

Once these two shear cracks passed near gage line SE43, they tended to relieve the stress in the concrete in the area. The eventual opening of the crack outside of the gage line rather than a crack through the line may be chance, but it is more likely related to the exact position of some piece of the reinforcement, and especially to the locations of the confinement reinforcement in the bottom flange of the beam which is shown in Fig. 2.17.

The reversals may also be indications of loss of bond between the reinforcing bars in the splice and the concrete, although the cracking

that developed appeared to be related more directly to the shear forces than due to bond distress in the lap splice.

Strains measured at the three gage lines at mid-depth of the web are plotted in Fig. 6.21. The strains were generally low until high loads were reached. Line S42 was especially affected by cracking in the beam-splice interface adjacent to it, until a crack finally crossed the line.

Additional load-strain curves are plotted in Figs. 6.22 to 6.26. Line S53, Fig. 6.22, was located 70 ft south of the central pier. The discontinuity between 198 and 227 kips load is the direct result of tensile cracking about 12 in. outside the gage line during application of that load increment, and an additional crack formed nearby at the next load. The large increase in strain at 290 kips, load step 9, occurred when a crack crossed the gage line. Line S63, 90 ft south, was about 5 ft from the nearest crack.

A series of curves of load versus deck tension strain are in Figs. 6.22 and 6.23. The south span had only a few negative moment cracks in the deck, and line S10 clearly shows the occurrance of one of the cracks. There were many cracks in the deck in the north span, and line N10 was crossed by a crack. Several cracks occurred in the deck near the north splice, but apparently none crossed the deck strain gage lines on the top surface of the deck even though there was at least one crack directly below line N20 on the bottom of the deck. A crack obviously passed near gage line N50, and cracks were found as far north as 74 feet at load 8, 291 kips. A crack apparently formed at N60, 90 ft north of the central pier, but it was never seen.

Compression strains in the top of the deck in the south span and in the lower flange from the central pier north are plotted versus load in Figs. 6.24 and 6.25. The south span deck strains remained small and recovered virtually to the original readings on unloading. Line S40 was inaccessible, as it was under a loading beam. The strains were far short of those required for a compression failure.

The largest compression strains were those near the central pier, line S13 and N13, on the bottom flange. Again, these were relatively low strains which were much smaller than the expected failure strain, even when the strains due to prestress and dead load are included. The remainder of the lower flange strains in the north span were smaller. However, the residuals remaining after unloading were larger than in the deck in the south span, indicating some locked-in stresses and moments existed after unloading

The strains in the top flange of the girder were predictably small since the gage lines were not far from the neutral axis. After cracking, the neutral axis rose toward the deck in the positive moment regions of the south span, and the strains remained extremely small throughout the test.

The top flange strains in the region subjected to negative line load moments are plotted versus load in Fig. 6.26. Cracks obviously crossed gage lines S11 and N21, though the latter was not found on the structure. Cracks were found on both sides of line N11. Only three cracks penetrated from the deck to the top flange in the south central pier, and another three formed on the north side. Two of these were reopening of cracks found before post-tensioning.

Strain distributions across the depth of the section for the gage lines at and on both sides of the south splice are shown in Figs. 6.27 to 6.29. In all three cases, the strain distributions are reasonably linear until the sixth load was reached. Beyond that load, the strain distributions from the middle of the web to the top of the beam remained relatively linear, but the strains in the lower flange became extremely erratic as the shear cracking developed.

Figure 6.30 shows strain distributions at the section 70 ft south of the central pier, at several load increments. The distributions were nearly linear up to the sixth increment. Beyond that load, the distribution were erratic in the lower part of the beam. There were shear cracks at this section, though there was no obvious distress by the end of the test.

7. DISCUSSION OF TEST RESULTS

7.1 General Remarks

Figures 7.1 to 7.5 contain information that may aid in the interpretation of the results of the tests. Figure 7.1 contains three different moment diagrams for one span of the test structure. The two lower curves are the best estimates of the dead load moments existing in the test structure as it was built. These diagrams are based on the average measured reactions at the end of the structure, a span of 124 ft, and on concrete having a unit weight of 145 lb/ft^3, as was discussed in Sec. 6.2. One curve is for the conditions immediately after post-tensioning, and the other is for conditions at the beginning of testing a few days later. The third curve is that implied in the original design calculations, assuming concrete at 150 lb/ft^3, spans of 125 ft, and conditions immediately after post-tensioning and removal of the temporary supports. This curve was used for part of calculations summarized in Chapter 2.

These are not final dead load moment diagrams, as there are expected to be decreases in the secondary moment with time as the prestressing force changes. In addition, the in-service structure would have additional dead load from curbs, handrails, possibly span diaphragms, and an asphalt overlay over a waterproofing membrane, so that there would be a significant negative moment at the central support rather than the small positive moment existing immediately after post-tensioning.

Figure 7.2 gives the approximate distribution of stress along the length of one span, for the bottom of the deck and the top of the deck, as determined from the original design calculations, some of which are reflected in Tables 2.2 to 2.4. The stresses are those existing immediately after post-tensioning.

Figure 7.3 gives the same information for the test structure. Stresses were recalculated using the 124 ft span, the measured reactions, concrete at 145 lb/ft^3, and with the Young's modulus values of the girder

and deck equal. The change in the Young's modulus of the deck is a significant change, as it increases the effective area resisting the post-tensioning force, and increases the section modulus, resulting in lower stresses from the moment effects of the post-tensioning force and from the secondary moment and support removal forces. In addition, the change in the location of the center of gravity of the section (compare Figs. 2.1 and 3.8) by 2.1 in. results in a considerable change in the forces applied by the determinate part of the post-tensioning moment, and also changes the magnitude of the calculated secondary moment.

In view of the differences between the stresses shown in Figs. 7.2 and 7.3, it should be clear that there are reasonable uncertainties about the actual stresses in the structure, and that the exact stresses will never be known. The stresses at any section are the sum of several components, and the components are often of comparable magnitude but with different signs, as can be seen, for example, in the summary of stresses at the bottom of the beam over the central support, as shown in Table 2.4. The stress immediately after post-tensioning is -57 lb/in.^{2}. A 3 percent increase in the secondary moment caused by post-tensioning results in a small net tension at the section, and a 3 percent decrease in the secondary moment increases the stress to -116 lb/in.^{2}. While the actual stress increase is insignificant, the percentage change is very large and serves to illustrate the sensitivity of the final answer to the collective precisions and uncertainties of the various force components contributing to the total stress.

The areas of tensile stress in the bottom fiber near the central support are basically the result of greatly different rates of change with distance from the central support of the external dead load moment as compared to the determinate and indeterminate components of the post-tensioning moments. These tensions would be greatly diminished by the time-dependent losses and the additional dead load existing in a completed structure. The tension stresses are of no basic concern in any event, since they occurred in an area which was adequately reinforced with deformed reinforcing bars.

Figures 7.4 and 7.5 are elastic bending moment diagrams for the live load configurations used in the final three tests. Both are for total loads of 90 kips distributed to five axles, and may be scaled directly to other loads as long as the moment distributions are elastic.

Section 7.2 is concerned with the stresses at initiation of flexural cracking. The redistribution of moments that was occurring in the final test is discussed in Sec. 7.3. The strength of the structures is examined in Sec. 7.4. Sec. 7.5 contains a few recommendations for changes of details and procedures which would make construction of such a structure somewhat easier or its behavior better.

7.2 Predicted and Observed Cracking Moments

Tensile stresses at cracking can be determined only within fairly broad limits, because of both the size of load increments used and uncertainties about the precompression existing at any particular time. Instead, the emphasis in this section is on the moments causing cracking rather than the tensile stresses, which in effect compares the computed and observed values of the sum of precompression plus tensile strength rather than tensile strength alone.

Data from the two overload tests on the north span are shown in Fig. 7.6. The gross cracking moment is plotted versus position along the span, for two different assumptions about the tensile strength of the concrete. These curves were obtained by taking the precompression values shown in Fig. 7.3, adding the modulus of rupture, and multiplying the sum by the section modulus to obtain the net cracking moment in excess of dead load. The dead load moment at the time of testing, from Fig. 7.1, was then added to obtain the gross cracking moment. The dead load moment is plotted in the same graph simply to give some perspective to the drawing.

The next step was to evaluate the total moments acting at various sections when cracks occurred. Since the load steps were fairly large, the load at the beginning of cracking was not precisely known. As a consequence, the moments were evaluated for the load at which a crack was found, and for the previous load step when the crack had not been discovered, to establish bounds. These two points, for a number of cracks, have been plotted in Fig. 7.6, and connected by short vertical lines. The live load moments were taken as elastic moments for these two tests.

The first cracks were found at load 44, at the junction of the splice and the precast girders. The moments for loads 43 and 44 are plotted at 37 ft from the central pier, and show that the moment at this section corresponded to approximately 6 $\sqrt{f'_c}$ tension at initiation of cracking.

At most other locations, the two moments tend to bracket the predicted cracking moments quite satisfactorily, and in no case does the maximum possible cracking moment fall below the moment computed using 6 $\sqrt{f'_c}$, and in many cases it appears that 7.5 $\sqrt{f'_c}$ is either appropriate or low.

Some of the particular cracks deserve comment. The crack at 34 ft was the closest to the central support. The one at 48 ft was the closest to the central support that occurred in the pretensioned end element and away from the splice. The crack at 68 ft was the farthest from the central pier in the splice shear loading, and the one at 80 ft was the farthest from the pier in the maximum positive moment loading. Each of these cracks thus represents a relatively isolated condition in which there could have been influence from other cracks only on one side, and in most cases the adjacent cracks were not too close.

The crack at 51 ft was by contrast one that formed between cracks that had occurred in the previous test, and while the moment is of the right magnitude, it perhaps should not be included as the stress conditions were somewhat disturbed by the earlier cracking.

The moments at cracking during the loading of the south span are harder to determine, because there was some redistribution of moments going on during the progress of the test, with the negative moment at the central pier initially lower than the elastic value and later higher, as was noted in Sec. 6.5.

The redistribution of moments in the final test is discussed in Sec. 7.3, and there are some uncertainties which cannot be fully resolved. However, the moments based on the idealized reactions discussed in Sec. 7.3 were used in evaluating the cracking in the south span, and predicted and observed cracking moments are plotted versus position in the span in Fig. 7.7, as was done for the north span.

The agreement between computed and observed cracking moments is not as good as it was for the north span, but it is still reasonable. The first crack at the splice was predicted well enough. The moments at first cracking in the region just south of the splice, from 40 to 75 ft south of the central pier, were all somewhat higher than predicted, and those north of the splice were slightly high.

In view of the good agreement found in the north span, it is likely that the errors are largely in the determination of the applied moments rather than in the predicted cracking moment. If the negative moments existing in the structure were larger than assumed here, the applied positive moments would have been less than shown in Fig. 7.7 and the agreement between observations and computations would have been improved. If the north reaction alone (Fig. 6.17) had been taken as the only indicator of the negative moments, they would have been slightly larger throughout the test.

The north span slab had numerous cracks due to negative moments by the end of the test. Figure 7.8 contains two plots of computed cracking moment versus position in the north span. In this case, the net cracking moment in excess of the dead load moment is considered. This was obtained by taking the precompression for the top of the deck as shown in Fig. 7.3, adding the estimated modulus of rupture of the concrete, and multiplying the sum by the section modulus for stresses at the top of the deck.

The negative live load moment diagram for this span is straight line from the maximum at the central pier to zero at the abutment. Two such lines are plotted in the figure. One is for load 68, 261 kips, corresponding to the load which caused the first extensive cracking in the slab. The second is for load 71, 328 kips, the maximum load on the structure.

Load 68 caused cracking as far as 74 ft north of the central pier. No cracks were predicted, but the applied moment closely approached the minimum predicted cracking moment in the area 70 to 80 ft north of the pier. While the numerical values were not accurately predicted, the trends were in that most of the observed cracks were either near the central pier or more than about 35 ft from the pier.

Load 71 clearly should have caused cracking nearly everywhere from the central pier to about 95 ft north, except for an area from 5 to 30 ft north. Cracks were found all the way from the pier to a point about 100 ft north of the pier.

Although the computed cracking moments were higher than the observed moments, the correlation is not too unacceptable. There are a number of possible reasons for the differences. The first is that the negative moments may have been somewhat larger than those considered in Sec. 7.3. A second factor is found in the concrete itself. The section modulus for the top of the deck is extremely sensitive to the ratio of Young's modulus of deck and girder concretes. Small errors in evaluating the deck modulus can lead to large errors in stresses. This would affect the result twice, as the section modulus was used in evaluating the precompression due to dead load and post-tensioning as shown in Fig. 7.3, and also in computing the predicted cracking moment, but at least these errors tend to compensate rather than add.

A third source of error is in the effects of creep and shrinkage of the two concretes. One effect of differential creep of the older girder concrete and the much younger deck concrete is a transfer with time of some of the initial compression from the deck to the girder, as is discussed extensively in Ref. 3. While this structure is slightly outside the capability of the analysis given in that reference, it appears that as much as 200 lb/in.^{2} precompression could be lost in the few days between post-tensioning and testing. This would have a large influence on the predicted cracking moment, and has not been taken into account. A 200 lb/in.^{2} reduction in effective stress at cracking corresponds to a change in predicted cracking moment almost twice as great as that caused by the difference between $6\sqrt{f'_c}$ and $7.5\sqrt{f'_c}$ modulus of rupture, and consequently is a very large source of potential error.

The same analysis also indicates that the deck compression over the central support may eventually drop to about 1/3 of the initial precompression, and this aspect of the time-dependent behavior of the structure was not taken into account in the design of the structure. As a result of this indicated change in precompression, the expected negative moment at

cracking would be considerably less in a two-year old structure than in the test specimen.

The positive moment precompression is not strongly influenced by the differential creep and shrinkage effects, and there should be no drastic change in the positive cracking moments with time.

In spite of the problems with the prediction of the negative cracking moments, the predicted and observed cracking moments were in relatively good agreement in the test structure. The use of a modulus of rupture of $7.5\sqrt{f'_c}$ gave a good indication of the positive moment cracking potential, and $6\sqrt{f'_c}$ worked well for the negative moment cracking and cracking at the junctions between the precast girders and the cast-in-place splice concrete.

7.3 Redistribution of Moments During the Final Test

As was noted in Sec. 6.5, there appeared to be an appreciable change in the distribution of the live load moments during the overload test on the south span. It was also noted there that the exact magnitude of this redistribution could not be readily determined because of inconsistencies in the reaction measurements.

In order to obtain some additional information on this, the measured reactions were adjusted slightly to make them consistent, that is to make the deviations from the elastic reactions equal at the two abutments. This was done by simply averaging the deviations, and the results are plotted in Fig. 7.9, which may be compared with the actual measure values plotted in Fig. 6.17. The adjustments were not large, although the implications are magnified by the long lever arm effective for moment at the central support. Using these reactions, live load negative moments were then computed for the section at the central pier. These moments are plotted versus live load in Fig. 7.10, along with the straight line representing the theoretical elastic loading line.

Coefficients of the negative moment, M/P where P is the total live load, are plotted in Fig. 7.11, and the relatively steady increase in the negative moment coefficient from the beginning of the test up to

an applied load of about 260 kips is quite apparent. Above that load there were only small changes.

It must be remembered that this is only one possible interpretation of the changes in moment that occurred in the final test. Either of the measured reactions could have been correct, with all of the error in the other, and both circumstances would have led to slightly different negative moments and indications of redistribution. However, the trends would not be different, as the measured reactions were consistent to the point of both indicating the same directions of deviations.

The initial low values of the negative moment are probably due to the cracking which had occurred in the north span in the previous tests. If there were positive cracks still slightly open in that span, the span would not have been as stiff as it originally had been, and it would have been less able to restrain the section at the central pier. As the load increased, the additional negative moments were imposed on the north span, which would tend to close the positive moments cracks, making the span stiffer and resulting in larger negative moments with increased load.

By the time 200 kips load had been applied, the south span had cracked extensively, and the two spans were then in some senses of equal stiffness again. As the load was increased, there was a tremendous increase in the positive moment cracking in the south span, which would have lead to a considerable decrease in stiffness, and a consequent increase in the negative moment, assuming that the negative moment stiffness did not degrade at the same rate at the same time.

Extensive negative moment cracking started occurring at about 260 kips load and above, and it appears that little additional redistribution of moment occurred after that load was reached. This would be the expected behavior when all sections were extensively cracked. The absolute stiffnesses of the cracked sections were much lower than the original stiffnesses, as indicated by the low slope on the load-deflection curves, but the relative stiffnesses apparently were approximately the same as before cracking occurred.

The small increase in negative moment coefficient at the final load increment may either be an accident of the deviations in the readings,

or it may be a true reflection of the damage and loss of positive moment stiffness accompanying the extensive cracking which was occurring near the south splice.

A moment diagram is plotted in Fig. 7.12 to aid in the interpretation of the information on the observed redistribution. The static moment diagram, that is the moment diagram for a simply supported span subjected to the splice shear loading configuration, is plotted as the upper polygonal diagram. The negative moments are then superposed as the sloping straight line from the peak value at the left to zero at the right. The positive moment for a particular negative moment is then read off as the distance from the polygon to the sloping line. Three negative moment lines are plotted; the elastic moment, the minimum moment from the initial load, and the maximum negative moment from the final load. The moments are plotted in terms of M/P, where P is the total live load applied on the five axles, and M/P has units of inches.

There is no strong evidence of changes in the distribution of the dead load moments in the structure. The end reactions after unloading after the final test were only slightly different than at the beginning of the tests, although there were uncertainties because of problems with zero shifts in one of the load cells that tend to mask small changes in actual reactions.

7.4 Evaluation of the Strength of the Test Structure

The structure did not fail during the loading tests, and the evaluation of the possible strength becomes crucial to understanding the behavior of the structure. Since both flexure and shear were possible modes of failure, the expected strengths in both modes must be carefully compared with the applied moments and shear forces.

Figure 7.13 contains a moment diagram for the south span at maximum load, 328 kips at load 71. Both dead and applied loads are included, and the negative moment was determined from the idealized reactions discussed in Sec. 7.3. The variation of the positive moment capacity along the span is also plotted.

The moment capacity varies along the span because of the variation in the depth of the post-tensioned reinforcement and because the remainder of the steel is not continuous for the full length of the span. The end segment contains 14 pretensioned and 42 post-tensioned 1/2-in. strands. The center module contains the 42 post-tensioned strands, which get very high in the cross section and consequently contribute little to the moment capacity as the central pier is approached, and at least 4-#9 bars.

The splice contains 4-#9 bars plus the post-tensioned strands. The variation in the moment capacity in the region just south of the splice is complex because of the development length of the 14 pretensioned strands and the 4-#9 bars which were terminated 6 ft 10 in. south of the splice. The exact variation of the moment capacity in this region cannot be determined, but the variation shown as a broken line appears to be a reasonable estimate.

The development length of a pretensioned strand is highly variable, and is strongly influenced by the surface condition of the strand. However, a recent reinterpretation of some old test results (6) indicates the development length may be as much as 12 ft for a 1/2-in. strand stressed to 260 k/in.^{2} at ultimate moment.

The moment capacity for several feet just south of the splice is influenced by the bond capacity of the strand. However, the available capacity at the south edge of the splice is not affected, and that is the point where the strength and applied moment curves are closest. A shorter development length would not have increased the capacity of the structure to resist loads applied in the test positions, although it would result in somewhat smaller crack widths.

The crack patterns and widths indicated that the prestressing steel was generally in the inelastic portion of the stress-strain curve from the splice to perhaps 65 to 70 ft south of the central pier. The stress at flexural failure at the splice was expected to be about 260 k/in.^{2}, and the ratio of applied to ultimate moments at the south edge of the splice implies that the stress was about 248 k/in.^{2}. The minimum yield stress for the steel is about 230 k/in.^{2}, but it may reasonably be expected to be somewhat larger (7).

The ratio of applied to ultimate moments at the point of maximum moment, 58 ft south of the central pier, implies a stress of about 234 $k/in.^2$. This may not be larger than the actual yield stress but since it is about 80 $k/in.^2$ above the prestress level at the beginning of the test it would account for relatively large crack widths.

At the end of the test the negative moment at the central pier was only 60 percent of the ultimate value, so the redistribution of moment from positive to negative sections which was discussed in Sec. 7.3 was clearly reasonable.

The moment diagram for the north span, which was subjected to only its dead load plus the moment at the central pier, is shown in Fig. 7.14 for the final load. The negative moment capacity is also plotted for part of the span, and the shape is basically that of the post-tensioning cable profile. There were clearly no problems with the negative moment capacity during this test.

The applied negative moment is closest to the capacity in the vicinity of the north splice, and it appears that if the negative moment at the pier were increased, the section at 34 ft north, near the splice, would reach ultimate when the pier moment was about 80,800 k-in. Consequently, a fully developed flexural failure mechanism for this structure would include a positive moment hinge under one of the applied loads in the south span and a negative moment hinge near the splice in the north span rather than at the central pier.

Any additional loads in the north span would reduce the negative moment at the splice, and relatively small loads would cause the critical section to be at the central pier.

Considering only flexure and ignoring possible problems with moment-rotation capacity, the failure load under the distribution of loads used in the final test was computed to be 405 kips. A positive moment hinge would form 40 ft south of the pier, under the rear-most axle load, and a negative moment hinge would form about 34 ft north of the pier.

At the end of the test, the positive moment hinge was forming, as the applied moment was about 95 percent of the ultimate moment. Considering flexure alone, the section had considerable rotation capacity remaining

since the deck strains were small and the neutral axis was still near the top of the beam web rather than about 5.5 in. from the top of the deck as would be expected at flexural failure of the section.

The expected collapse loads for other positions of the applied loads were also investigated, considering the applied load to be a moveable vehicle with the axle spacing used in the last test, and again considering only flexure. The computed collapse load of 405 kips with the loads in the test position was a local minimum. Moving the vehicle small distances north or south resulted in higher computed loads, because of the nature of the variation in the positive moment capacity near the splice.

The lowest collapse load, 383 kips, was found when the rear axle load was 54 ft south of the central pier. The collapse mechanism included a positive moment hinge under the load located 68 ft south of the pier, and the same negative moment hinge 34 ft north of the pier.

The shear diagram for the south span in the final loading is shown in Fig. 7.15. In addition, the computed shear forces to cause shear cracking are also plotted.

There are two different initiation processes for shear cracking, and each limits the shear strength in different parts of the beam. The "Web-Shear" cracking, force, V_{cw}, is cracking due to principal tension stresses in the beam web in areas remote from any flexural cracks. The "Flexure-Shear" cracking force, V_{ci}, is closely related to flexural cracking in that the shear cracks are either extensions of or directly initiated by flexural cracks. At any section of a member, either initiation process may govern, and once a shear crack begins, the other process becomes irrelevant. Shear reinforcement is then provided for the shear force in excess of the cracking force, without consideration of which process actually started the cracking.

Both shear concepts are included in the 1971 ACI Code (4) and are extensively explained and documented by Olesen, Sozen and Siess (5). These concepts are not included in the 1973 AASHO Specifications (2), but their use is recognized in a footnote to Sec. 1.6.13. In this analysis, the under-strength factor, ϕ, was taken as 1.0.

The web-shear calculation assumes shear cracks occur when the principal tensile stress reaches $4\sqrt{f'_c}$ at the centroidal axis of the cross section, or at the top of the beam web if the centroid is in the upper flange. Starting from a Mohr's circle analysis, the following equation can be derived, following the logic of Ref. 5:

$$V_{cw} = \frac{I_c\, b_w}{Q_c}\left[f_t\sqrt{1 + f_h/f_t} - \frac{V_d\, Q_g}{I_g\, b_w}\right] + V_p + V_d$$

where I_c = Moment of inertia of composite (transformed) section,

b_w = Thickness of beam web,

Q_c = First moment of area of portion of composite section lying above composite centroidal axis about that axis (see Fig. 7.16),

f_h = Horizontal stress at centroid of composite section caused by prestressing force and all forces acting on noncomposite section,

$f_t = 4\sqrt{f'_c}$ = Tensile strength of concrete (both f'_c and f_t are in $lb/in.^2$ units in this expression, that is if $f'_c = 6000\ lb/in.^2$, then $f_t = 4\sqrt{6000} = 310\ lb/in.^2$),

V_d = Dead load shear force,

I_g = Moment of inertia of noncomposite girder,

Q_g = First moment of girder area as defined in Fig. 7.16, and

V_p = Vertical component of prestressing force.

The terms within the brackets represent the total shear stress available at cracking, less the dead load shear stress which is resisted by the girder section alone. The horizontal stress, f_h, varies substantially along the length of the member as a result of the variation in dead load stresses in the girder. It also varies in this particular structure because of friction between the post-tensioned tendons and the ducts, and because of the presence of the pretensioned strands only in the end segments.

The vertical component of the prestressing force is important in part of the region between the splice and the central pier, but is not large at other sections.

The calculations leading to Fig. 7.15 were done assuming the deck and girder had the same values of Young's Modulus, and the as-built span and dead loads were considered. The applied shear diagram was computed using the idealized negative moment at the central pier and the actual axle loads as listed in Table 6.7.

Reference 5 recommended that $f_t = 5\sqrt{f'_c}$, but the lower value of $4\sqrt{f'_c}$ was used as required by the ACI Code. The higher value is essentially an average, while the lower is a lower bound which is suitable for design.

The calculations predict web-shear cracking only in the 12 ft length of beam just south of the central pier, as can be seen in Fig. 7.15. The shear force exceeded the calculated cracking force by about 120 kips at the pier, but adequate shear reinforcement was present. As shown in Fig. 6.18, there were numerous inclined cracks in the area from 1 to 10 ft south of the pier. In the area from 10 to 20 ft south there were also numerous short cracks near the top of the beam web. These cracks were not predicted, but seem to have caused no problems as they remained short and narrow after they formed.

The flexure-shear cracking force was calculated using the equation:

$$V_{ci} = 0.6\sqrt{f'_c}\, b_w d + \frac{\text{Net } M_{cr}}{\frac{M}{V} + \frac{d}{2}} + V_d$$

where d = Effective depth to tension reinforcement, but not less than 0.8 of the total member height,

$\text{Net } M_{cr}$ = Live load moment to cause flexural cracking, or cracking moment in excess of dead load, for a tensile stress of $6\sqrt{f'_c}$,

M = Live load moment at the section considered, and

V = Live load shear at section considered.

The net cracking moment varies along the span, and was computed in the process of preparing Figs. 7.2, 7.6, 7.7, and 7.8. The ratio of M/V was taken from the elastic moment and shear diagrams, since the moment distribution was essentially elastic at the time most of the shear cracking

started. M/V is taken as positive in all cases, and has a complex variation along the span because of the abrupt changes in shear from one side to the other of each axle load.

The central term in the equation is the live load shear accompanying flexural cracking at a section d/2 away, in the direction of decreasing moment, from the section being considered. The first term then represents the additional shear force required to cause the flexural crack to bend over and become a shear crack.

The 1971 ACI version of this equation lacks the d/2 term in the denominator of the middle term, but this is a "simplification" from the original equation, and is present in the Ref. 5 derivation. Reference 5 used 1.0 in place of the 0.6 in the first term, but again this was an average value rather than a lower bound.

Figure 7.15 shows that the calculated flexure-shear cracking force was smaller than the applied shear from 22 to 80 ft south of the central pier, except for the area between 54 and 58 ft south. In the remainder of the area between 44 and 68 ft south, the applied shear exceeds the predicted shear cracking load by only small amounts.

The cracking pattern shown in Fig. 6.18 is in substantial agreement with the predictions of Fig. 7.15. The last shear crack to cross the centroidal axis is about 80 ft south. There is an inclined crack at 22 ft south, but it could not be traced across the lower flange and it is hence hard to label as a flexure-shear rather than a web-shear crack.

The failure shear force is the sum of the shear cracking force plus the contribution of the stirrups. In the regions of flexure-shear cracking, it may also be reasonably argued that the vertical component of the prestressing force can also be added to the resistance. In the web-shear cracking evaluations, this component was considered in determining the shear cracking load.

The nominal contribution of the stirrups can be expressed as

$$V' = \frac{A_v f_y d}{s}$$

where A_v = Area of one stirrup (two legs),
f_y = Yield stress of stirrups, and
s = Stirrup spacing.

This equation has been experimentally confirmed as a lower bound to the contribution of the web reinforcement (5). It can be derived on the basis of assuming a shear crack with an average slope of about 45° above the beam axis. If the cracks have a lower slope, they will intersect additional stirrups, and the force V' will be larger than indicated by the equation.

In the region near the central pier, #5 stirrups were spaced at 12 in., as shown in Fig. 2.12. With the minimum d = 0.8h = 50.8 in., V' = 157 kips. The required shear force at the critical section d/2 away from the central support was 100 kips, so the shear reinforcement was considerably in excess of the requirement for this loading. In addition, the cracks in this area had slopes considerably lower than 45°, and the real stirrup contribution would be more than the nominal calculated value.

In the region near the splice, there is a maximum requirement of about 115 kips from web reinforcement. The shear steel contribution in this region is complex because of the extra stirrups which were added at the ends of the precast beams and in the splice, as shown in Fig. 2.16. These stirrups add a great deal of capacity locally, and were ideally located to aid the beam for this particular loading position.

Part of the shear diagram, in the region from 20 to 45 ft south of the central pier, is shown in Fig. 7.17. In addition, the flexure-shear cracking force and the contribution of the web steel are shown. The actual variation in the contribution of the web steel cannot be as abrupt as it is drawn, but this is a reasonable picture. The applied shear exceeds the computed resistance only in a very short area at 30 ft south, and the vertical component of the prestress could be credited with carrying the excess, as it amounts to over 100 kips at 30 ft, but only about 40 kips at 37.5 ft.

The applied shear and the computed capacity were nearly the same for a short distance at 43 ft south. In this case, evidence of very high

stirrup stresses was found, as a crack at 43 ft at mid-depth of the girder web was 0.02 in. wide at load 70, as noted in Sec. 6.5.

From the above discussion of the basic shear strength, it appears that the damage that was occurring at about 42 ft south at the end of the test, shown in Fig. 6.19, was not a consequence of general yielding of the stirrups. The damage must be related instead to local detail problems.

The state of stress in the lower part of the end segment is complex. The 4-#9 bars which extend into the splice are anchored in this region since they extend only 6 ft 10 in. into the member. The 14 pretensioned strands terminate at the end of the segment, and they are consequently anchored by bond throughout this region. The applied moment was about 95 percent of the calculated ultimate value, so the strains in all of the tension steel would have been large. Since the shear force was also high, the cracking in the lower flange can perhaps be best described as being due to large flexural deformations, but extensively modified by shear forces and deformations.

One problem with the stirrups used in precast I-girders, as shown in Fig. 2.13, is that they do not enclose the tension steel in the way that a U-stirrup used in a rectangular or T-girder encloses the steel. A U-stirrup is able to provide definite, and important, support to the steel, so that it can either develop doweling forces or at least not let cracks form and easily propogate approximately parallel to the tension steel. The #3 bars which were placed in the lower flange as shown in Fig. 2.17 are able to do this to some extent, but their area was inadequate and there are serious problems in anchoring them firmly enough into the upper part of the beam to be fully effective. This anchorage problem is especially severe in this case, because of interference with the ducts for the post-tensioned tendons.

7.5 Recommendations for Changes in Future Structures

From the discussion in the last section, it is obvious that some different details in the non-prestressed auxiliary reinforcement near the ends of the precast segments could improve the behavior of the structure under extremely high overloads.

Some form of closed stirrups would have supported the bottom steel, and would have probably delayed the nearly-horizontal cracking that was developing at the end of the test. This is a difficult detailing problem, because the obvious closed stirrup forms would greatly interfere with the easy construction of the girders, and limit the amount of prefabrication of the reinforcement cage that could be done.

The arrangement of the lap spliced bars in the south splice was awkward in terms of construction. The bar placement is shown schematically in Fig. 7.18(a), and this effectively forced the end segment to be lowered to almost exactly its correct final elevation and then be shifted sideways into the correct longitudinal alignment. A more convenient arrangement is shown in Fig. 7.18(b), assuming that the central segment will be placed first, followed by the end segment. This arrangement allows the beam to be positioned laterally some distance above its final position, and then lowered directly to its temporary bearings. This is a more convenient sequence for most cranes, and the difference in bar placement has no structural significance.

The #9 reinforcing bars which were joined by Cadweld splices in the north joint were too close together. The equipment used for making the splices includes end-alignment fittings which are considerably larger in diameter than are the splice sleeves. At the bar spacings used (see Fig. 2.18), these fittings were installed only with great difficulty, and this added greatly to the time required for the splicing operation. This was a detailing error, and the bars should have been spaced 3.5 in. or further apart. Again, this is a detailing problem which would have had no influence on the behavior of the structure.

8. SUMMARY AND CONCLUSIONS

Chapters 2 and 3 of this report describe the design and construction of a prototype scale test structure of a specialized form of segmental precast concrete girders suitable for highway bridges with two spans of up to about 125 ft each. Three segments, 88, 74, and 88 ft long, were supported on three final and two temporary supports, and then joined end to end to form a continuous two span structure.

The two end segments were precast, pretensioned concrete and the central segment, which rests across the central pier of the completed structure, was precast, reinforced concrete. Concrete was cast in place to form the splices, and to form the composite deck. After the composite concrete was cured, the entire structure was post-tensioned to establish the required continuity. The precast segments were designed to support their own dead loads plus the additional weight of the deck concrete, while resting on the final plus temporary supports. The temporary supports are removed after post-tensioning. The basic sequence is described in Chapter 1 and illustrated in Figs. 1.1 to 1.5.

The test structure, with two spans of 124 ft each, was subjected to a series of loadings simulating truck loadings. In each test, reactions, deflections, and strains were measured at each load increment. The instrumentation, loading equipment, and test procedures are described in Chapters 4 and 5. There were four tests to service load levels, with an applied load of 73.6 kips in each test. These were followed by two tests to design ultimate load, 198.7 kips, and a final test in which a maximum load of 328.2 kips was reached without causing the structure to collapse. The extremely high capacity is primarily a result of the design process used, in that the allowable stresses controlled the proportioning of all cross sections, and the accompanying ultimate moments were considerably higher than required.

The structure was essentially elastic during the service load tests. The deflections were linear functions of load, with maximum values

of 1.05 in., and the residuals were extremely small. No cracks were found during these tests. The measured reactions also indicated elastic response.

The design ultimate load tests caused extensive flexural and shear cracking, as shown in Fig. 6.10. The flexural cracks reclosed tightly when the load was removed, while the shear cracks generally remained visible but very small. The maximum deflections were 3.5 to 3.7 in., and the residuals remaining after unloading were 0.1 to 0.25 in. Design ultimate loads were applied in positions to produce maximum shear at the north splice and maximum positive moment in the north span.

The final test was a loading to produce maximum shear at the south splice, and a total load of 328.2 kips, about 1.65 times the required design ultimate load, was reached. The maximum deflection was about 10.8 in., and the residual produced by the test was slightly over 1 in. The structure was extensively cracked by this loading, as shown in Fig. 6.18. There was some load capacity remaining when the test was ended. The remaining flexural capacity was significant, but from the appearance of the girder in the vicinity of the south splice, it appeared that a shear failure was developing. The applied moment was about 95 percent of the computed ultimate moment at the same section, and the combination of flexural and shear deformations produced severe cracking in this region.

The test demonstrated that this structural system was a practical alternate for the construction of highway bridge spans up to at least 125 ft. With the proper attention given to joint details, such a segmental structure can be expected to develop at least its required ultimate load capacity, and to behave as if there were no joints throughout the load range of interest.

9. REFERENCES

1. "Standard Specifications for Highway Bridges," American Association of State Highway Officials, Washington, D. C., Tenth Ed., 1969, 384 p.

2. "Standard Specifications for Highway Bridges," American Association of State Highway Officials, Washington, D. C., Eleventh Ed., 1973, 469 p.

3. Fadl, A. I., and W. L. Gamble, "Time-Dependent Behavior of Noncomposite and Composite Post-Tensioned Concrete Girder Bridges," Civil Engineering Studies, Structural Research Series No. 430, University of Illinois at Urbana-Champaign, Oct. 1976, 377 p.

4. "Building Code Requirements for Reinforced Concrete (ACI 318-71)," American Concrete Institute, Detroit, 1971, 78 p.

5. Olesen, S. Ø., M. A. Sozen, and C. P. Siess, "Investigation of Prestressed Reinforced Concrete for Highway Bridges, Part IV: Strength in Shear of Beams with Web Reinforcement," University of Illinois at Urbana-Champaign, Engineering Experiment Station Bulletin No. 493, 1967, 46 p. plus illustrations and tables.

6. Martin, L. D. and N. L. Scott, "Development of Prestressing Strand in Pretensioned Members," Proc. ACI, Vol. 73, No. 8, Aug. 1976, pp. 453-456.

7. Gamble, W. L. and A. I. Fadl, Discussion of "Recommendations for Estimating Prestress Losses," Journal PCI, Vol. 21, No. 2, March/April 1976, pp. 108-110.

TABLE 2.1 SUMMARY OF PRETENSIONING AND POST-TENSIONING STRESSES, FORCES, AND MOMENTS

Type of Pre-stressing	Item	Dist. from Pier " " Abutment	Max. + Mom. 75 ft 50 ft		At Splice 37 ft 88 ft		At Central Pier 0 125 ft.	
			before losses	after losses	before losses	after losses	before losses	after losses
Pre-tensioning	Eccentricity from centroid of non-composite section (in.)		-24.14		-24.14			
	Effective stress (ksi)		179	144	179	144	--	--
	Effective force (kips)		387	311	387	311		
	Pretensioning moment (k-in.)		-9,342	-7,508	-9,342	-7,508	--	--
Post-tensioning	Friction reduction factor		0.9638		0.9407		0.8952	
	Eccenticity from centroid of composite section (in.)		-30.50		-24.00		9.45	
	Effective stress (ksi)		182	152	178	148	169	139
	Effective force (kips)		1,186	991	1,157	962	1,101	906
	Post-tensioning moment (k-in.)		-36,170	-30,220	-27,770	-23,090	10,400	8,560
	Secondary moment with respect to centroid of composite section (k-in.)		10,930	9,200	19,237	16,190	27,325	23,000

Note:"before losses" refers to stresses immediately after transfer

TABLE 2.2 SUMMARY OF STRESS COMPUTATION FOR THE MAXIMUM POSITIVE MOMENT SECTION

(75 ft from central pier, 50 ft from abutment)

Stresses caused by:	Stresses in girder bottom	Stresses in girder top	Stresses in deck bottom	Stresses in deck top
	(ksi)		(ksi)	
Pretensioning force	-0.557	-0.557		
Pretensioning moment	-0.977	1.050		
Weight of girder	0.865	-0.962		
Sub-total	-0.672	-0.433		
Pretensioning losses	0.302	-0.097		
Sub-total	-0.370	-0.530		
Weight of deck	0.783	-0.840		
Sub-total	0.413	-1.370	0	0
Net post-tensioning force	-1.008	-1.008	-0.770	-0.770
Post-tensioning moment	-2.591	0.992	0.758	1.122
Secondary moment	0.783	-0.300	-0.229	-0.340
Removal of temporary supports	0.407	-0.156	-0.119	-0.177
Sub-total	-1.996	-1.842	-0.360	-0.165
Post-tensioning losses	0.469	0.050	0.038	-0.006
Sub-total	-1.527	-1.792	-0.322	-0.171
Weight of asphalt	0.329	-0.126	-0.096	-0.143
Sub-total	-1.198	-1.918	-0.418	-0.314
Live load moment + impact	+1.049	-0.401	-0.307	-0.455
Total	-0.149	-2.319	-0.725	-0.769

TABLE 2.3 SUMMARY OF STRESS COMPUTATIONS FOR THE SECTION AT THE SPLICE
(88 ft from abutment, 37 ft from central pier)

Stresses caused by:	Stresses in girder (with pretensioning) bottom (ksi)	Stresses in girder (with pretensioning) top (ksi)	Stresses in girder (without pretensioning) bottom (ksi)	Stresses in girder (without pretensioning) top (ksi)	Stresses in deck bottom (ksi)	Stresses in deck top (ksi)
Prestressing force	-0.557	-0.557				
Pretensioning moment	-0.977	1.050				
Sub-total	-1.534	0.493				
Pretensioning losses	0.302	-0.097				
Sub-total	-1.232	0.396	0	0	0	0
Net post-tensioning force	-0.984	-0.984	-0.984	-0.984	-0.751	-0.751
Post-tensioning moment	-0.990	0.762	-0.990	0.762	0.582	0.863
Secondary moment	1.378	-0.528	1.378	-0.528	-0.404	-0.598
Removal of temporary supports	0.716	-0.274	0.716	-0.274	-0.209	-0.310
Sub-total	-2.112	-0.628	-0.880	-1.024	-0.782	-0.796
Post-tensioning losses	0.283	0.129	0.283	0.129	0.099	0.077
Sub-total	-1.829	-0.499	-0.597	-0.895	-0.683	-0.719
Weight of asphalt	0.076	-0.029	0.076	-0.029	-0.022	-0.033
Sub-total	-1.753	-0.528	-0.521	-0.924	-0.705	-0.752
Live load moment						
Positive	0.682	-0.261	0.682	-0.261	-0.199	-0.296
Negative	-0.365	0.140	-0.365	0.140	0.107	0.158
Total (Positive)	-1.071	-0.789	0.161	-1.185	-0.904	-1.048
Total (Negative)	-2.118	-0.388	-0.886	-0.784	-0.598	-0.594

TABLE 2.4 SUMMARY OF STRESS COMPUTATIONS FOR THE SECTION AT CENTER SUPPORT

Stressed caused by	Stresses in girder bottom (ksi)	Stresses in girder top (ksi)	Stresses in deck bottom (ksi)	Stresses in deck top (ksi)
Weight of girder	-0.156	0.167		
Weight of deck	-0.141	0.152		
Sub-total	-0.297	0.319	0	0
Net post-tensioning force	-0.937	-0.937	-0.716	-0.716
Post-tensioning moment	0.744	-0.285	-0.218	-0.324
Secondary moment	1.957	-0.750	-0.573	-0.850
Removal of temporary supports	-1.524	0.583	0.445	0.661
Sub-total	-0.057	-1.070	-1.062	-1.229
Post-tensioning losses	-0.276	0.335	0.256	0.319
Sub-total	-0.333	-0.735	-0.806	-0.910
Weight of Asphalt	-0.588	0.225	0.172	0.255
Sub-total	-0.921	-0.510	-0.634	-0.655
Live Load moment	-0.909	0.348	0.266	0.394
Total	-1.830	-0.162	-0.368	-0.261

TABLE 2.5 SUMMARY OF DESIGN ULTIMATE MOMENTS AND SECTION CAPACITIES

	Section Location		
	Max. +M (50 ft from abutment)	Splice	Central Pier
Moments (kip-in.) caused by:			
Weight of precast element	8,270	0	- 1,490
Weight of deck	7,480	0	- 1,350
Removal of temporary support	5,680	10,000	-21,300
Weight of asphalt	4,560	1,060	- 8,200
Total dead load moments	25,990	11,060	-32,340
Ultimate dead load (1.5 dead load)	39,000	16,600	-48,500
Service live load moment for Full Standard Truck or Lane Loading, without impact			
Postive	19,250	13,000	--
Negative	--	-7,110	-17,600
Ultimate live load moments, including impact, for 7 ft beam spacing			
Positive	36,770	24,830	
Negative		-13,580	-31,680
Design Ultimate Moments			
Positive	75,770	41,430	--
Negative	--	-4,580*	-80,180
Ultimate Flexural Capacity (with Design material strengths)			
Positive	116,000	75,000	
Negative	--	-21,900	-86,500

*For no asphalt, 0.9 of dead load moment, live load and impact.

TABLE 2.6 DESIGN DEAD LOAD MOMENTS INCLUDING SECONDARY MOMENTS

Moments (kip-in.) caused by:	Section Location		
	Max. +M (50 ft from abutment)	Splice	Center Support
Weight of precast element	8,270	--	- 1,490
Weight of deck	7,480	--	- 1,350
Removal of temporary supports	5,680	10,000	-21,300
Sub-total	21,430	10,000	-24,140
Secondary moment after losses	9,200	16,190	23,000
Sub-total	30,630	26,190	- 1,140
Weight of asphalt	4,560	1,060	- 8,200
Total Moment	35,190	27,250	- 9,340

Table 3.1 CONCRETE MIXES, PER CUBIC YARD

Girder and Splice Concrete

Cement	705 lbs
Sand	965 lbs
3/4 in. crushed limestone	1,975 lbs
Added water*	250 lbs
Air Entraining Agent	12 oz.
Specified Air	4 to 7 %
Specified Slump	2 1/2 to 3 1/2 in.

Deck Concrete

Cement	611 lbs
Sand	1120 lbs
3/4 in. crushed limestone	2040 lbs
Added water*	240 lbs
Air Entraining Agent	10 oz
Specified Air	4 to 7 %
Specified Slump	1 1/2 to 2 1/2 in.

---

* Aggregates were wet, estimated w/c ratios in the range of 0.4 to 0.5.

TABLE 3.2 STRENGTH OF CONCRETE TEST SPECIMENS, LB/IN.^{2}

Component	A(North)	A1(South)	B(Pier)	Splices	Deck
Date Cast	1 June 1973	5 June 1973	29 May 1973	20 July 1973	20 July 1973
f'_c at Pretensioning or form Removal	4,420 4,530	4,170 4,210	3,010 2,760 2,900	4,500*	4,300*
30 July 1973				6,120 5,940	6,650 6,260 6,510 6,720
15 August 1973	7,360 7,000	7,070 7,140	7,220 7,070		
28 August 1973	5,410 5,860	6,580 5,300 5,660	7,110 7,640 6,030	7,180 7,620 7,180	7,640 7,320 6,150
8 September 1973	5,660	5,480			5,300

* Approximate Values from Swiss Hammer tests

TABLE 3.3 INITIAL YOUNG'S MODULUS VALUES FOR CONCRETE TESTS OF 28 AUGUST 1973

Component	A(North)	A1(South)	B(Pier)	Splices	Deck
	5.16	5.01	5.07	4.86	5.52
	5.02	4.78	5.04	5.15	5.14
		4.65	4.90	5.02	
Average	5.09	4.81	5.00	5.01	5.33

TABLE 6.1 APPLIED LOADS,
SERVICE LOAD TEST, NORTH SPAN POSITIVE MOMENT LOADING, LBS.

Load No.	Rear Axle 54 ft N	Center Axle 68 ft N	Front Axle 84 ft N	Total
1	6,260	6,550	1,470	14,280
2	12,930	13,180	2,890	29,000
3	18,790	19,580	4,630	43,000
4	26,090	26,210	6,850	59,150
5	32,200	32,600	8,350	73,150

TABLE 6.2 APPLIED LOADS
SERVICE LOAD TEST, NORTH SPAN SPLICE SHEAR LOADING, LBS.

Load No.	Rear Axle 40 ft N	Center Axle 54 ft N	Front Axle 68 ft N	Total
11	6,550	6,340	1,660	14,550
12	13,100	12,770	3,330	29,200
13	21,070	20,220	4,910	46,200
14	26,520	25,850	6,410	58,780
15	32,520	32,120	8,310	72,950

TABLE 6.3 APPLIED LOADS,
SERVICE LOAD TEST, SOUTH SPAN POSITIVE MOMENT LOADING, LBS.

Load No.	Rear Axle 54 ft S	Center Axle 68 ft S	Front Axle 84 ft S	Total
21	6,980	5,760	1,660	14,400
22	12,770	12,240	3,320	28,330
23	19,350	19,180	4,750	43,280
24	25,930	26,210	7,120	59,260
25	32,120	32,520	9,020	73,660

TABLE 6.4 APPLIED LOADS,
SERVICE LOAD TEST, SOUTH SPAN SPLICE SHEAR LOADING, LBS.

Load No.	Rear Axle 40 ft S	Center Axle 54 ft S	Front Axle 68 ft S	Total
31	6,950	6,980	1,820	15,750
32	13,180	13,400	3,170	29,750
33	19,730	19,900	4,910	44,540
34	26,210	26,490	7,040	59,740
35	32,520	32,360	9,340	74,220

TABLE 6.5 APPLIED LOADS,
DESIGN ULTIMATE LOAD TEST, NORTH SPAN SPLICE SHEAR LOADING, LBS.

	Rear Axles		Center Axles		Front Axle	Total
Load No.	40 ft	44 ft	54 ft	58 ft	68 ft N	
41	6030	4990	5440	5090	4480	26030
42	16270	14870	14860	14410	12370	72780
43	23450	22810	22740	22300	11950	103250
44	31620	30070	29780	29170	15020	135660
45	38720	37170	35810	35450	18180	165330
46	47150	44860	42940	44440	17770	197160

TABLE 6.6 APPLIED LOADS,
DESIGN ULTIMATE LOAD TEST, NORTH SPAN POSITIVE MOMENT LOADING, LBS.

	Rear Axles		Center Axles		Front Axle	Total
Load No.	54 ft	58 ft	68 ft	72 ft	84 ft N	
51	11700	11700	12470	11240	3900	51010
52	19150	18990	20400	19760	8390	86690
53	24690	24170	24850	24410	11460	109760
54	31800	31290	32620	26200	15020	136930
55	37920	37140	38470	35820	18600	167950
56	47290	47480	30400	45450	23830	194450

TABLE 6.7 APPLIED LOADS,
OVERLOAD TEST, SOUTH SPAN SPLICE SHEAR LOADING, LBS.

	Rear Axles		Center Axles		Front Axle	Total
Load No.	40 ft	44 ft	54 ft	58 ft	68 ft S	
61	8670	8190	8230	8310	4230	37630
62	17250	16390	16290	16370	8710	75010
63	24350	23320	22970	23240	12120	106000
64	31290	29740	29440	29860	15600	135930
65	38390	36500	36320	36640	19090	166940
66	45490	43250	42350	43260	22740	197090
67	53000	50600	47790	50210	25900	227500
68	60600	58040	55020	57160	30130	260950
69	66700	64710	62090	64460	32620	290580
70	75460	72150	64940	71490	36610	320650
71	76370	73160	68050	72510	38100	328190

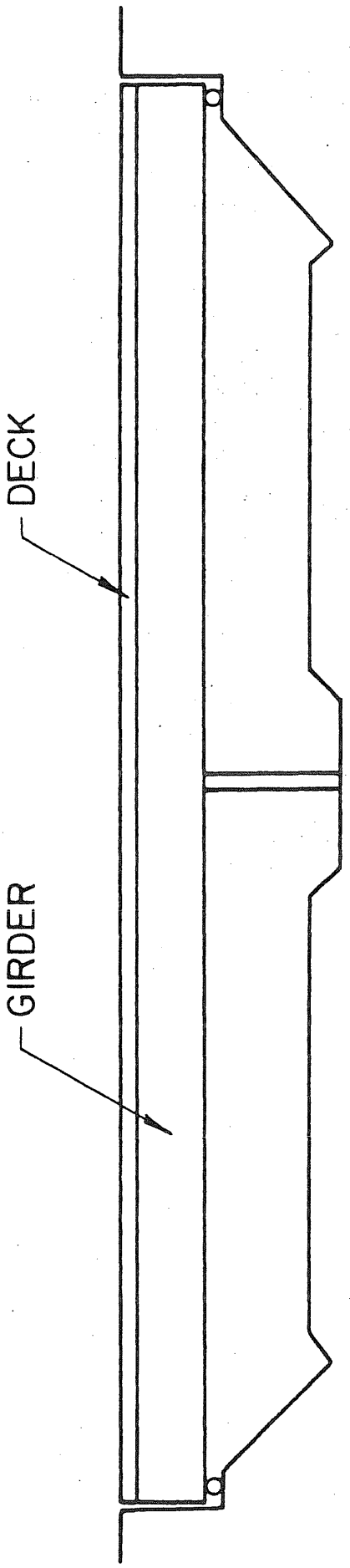

FIG. 1.1 NEW TWO-SPAN CONTINUOUS GRADE SEPARATION STRUCTURE

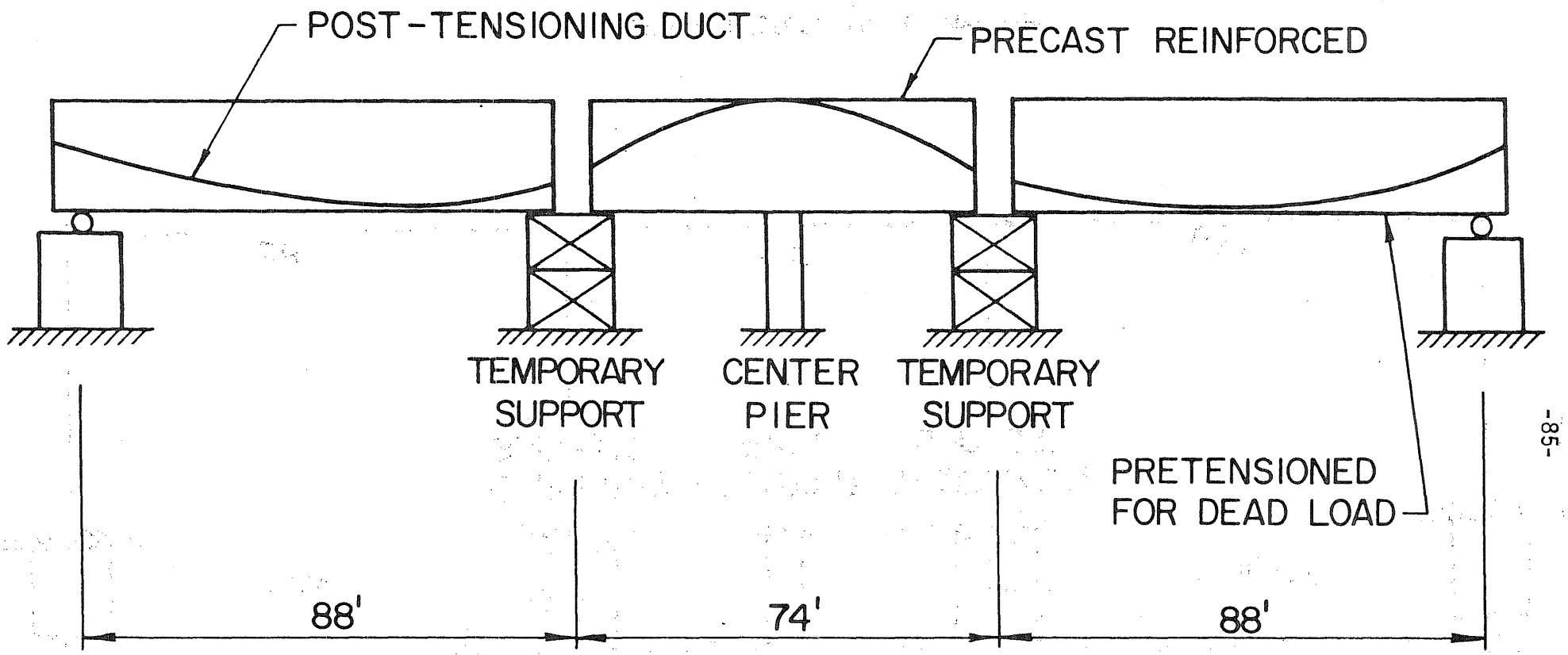

FIG. 1.2 SEGMENTAL GIRDERS PLACED ON TEMPORARY AND FINAL SUPPORTS

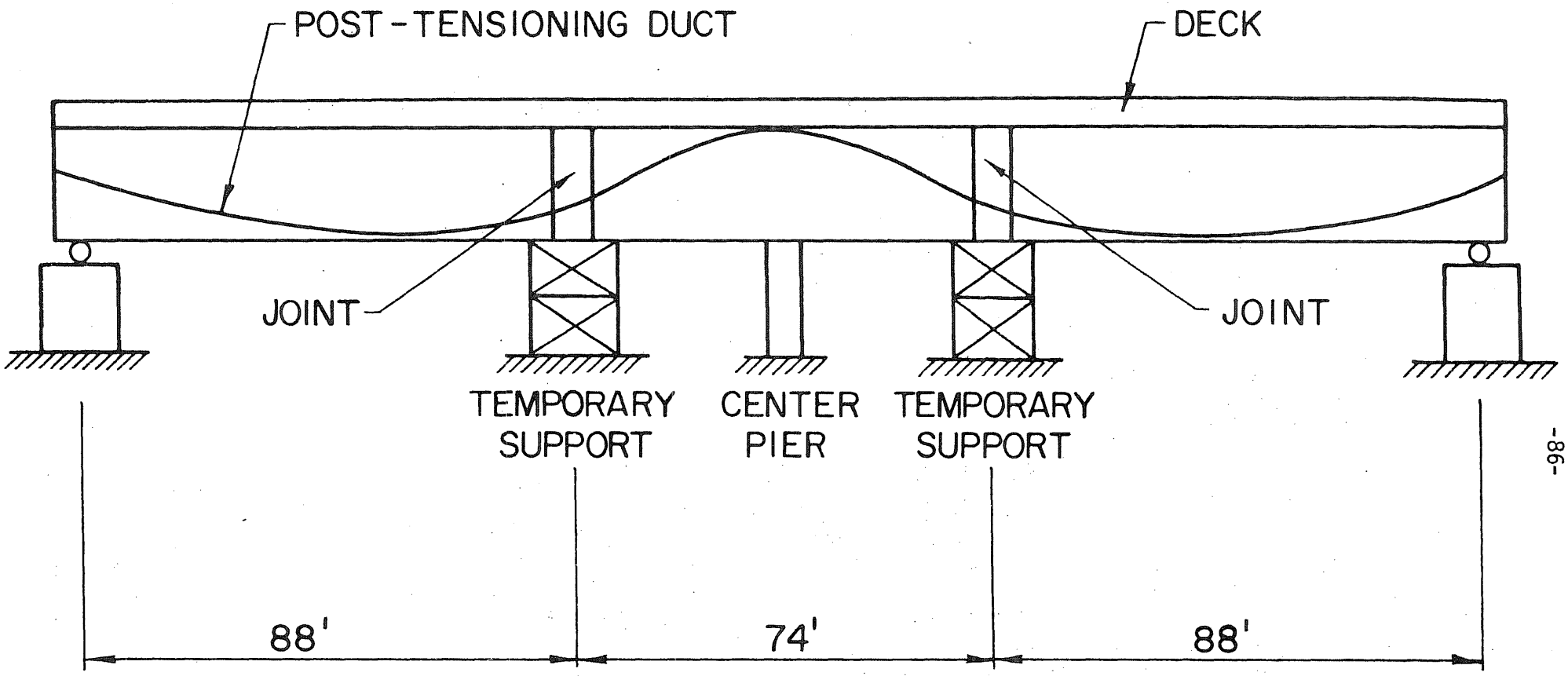

FIG. 1.3 DECK AND JOINTS CAST AT SAME TIME

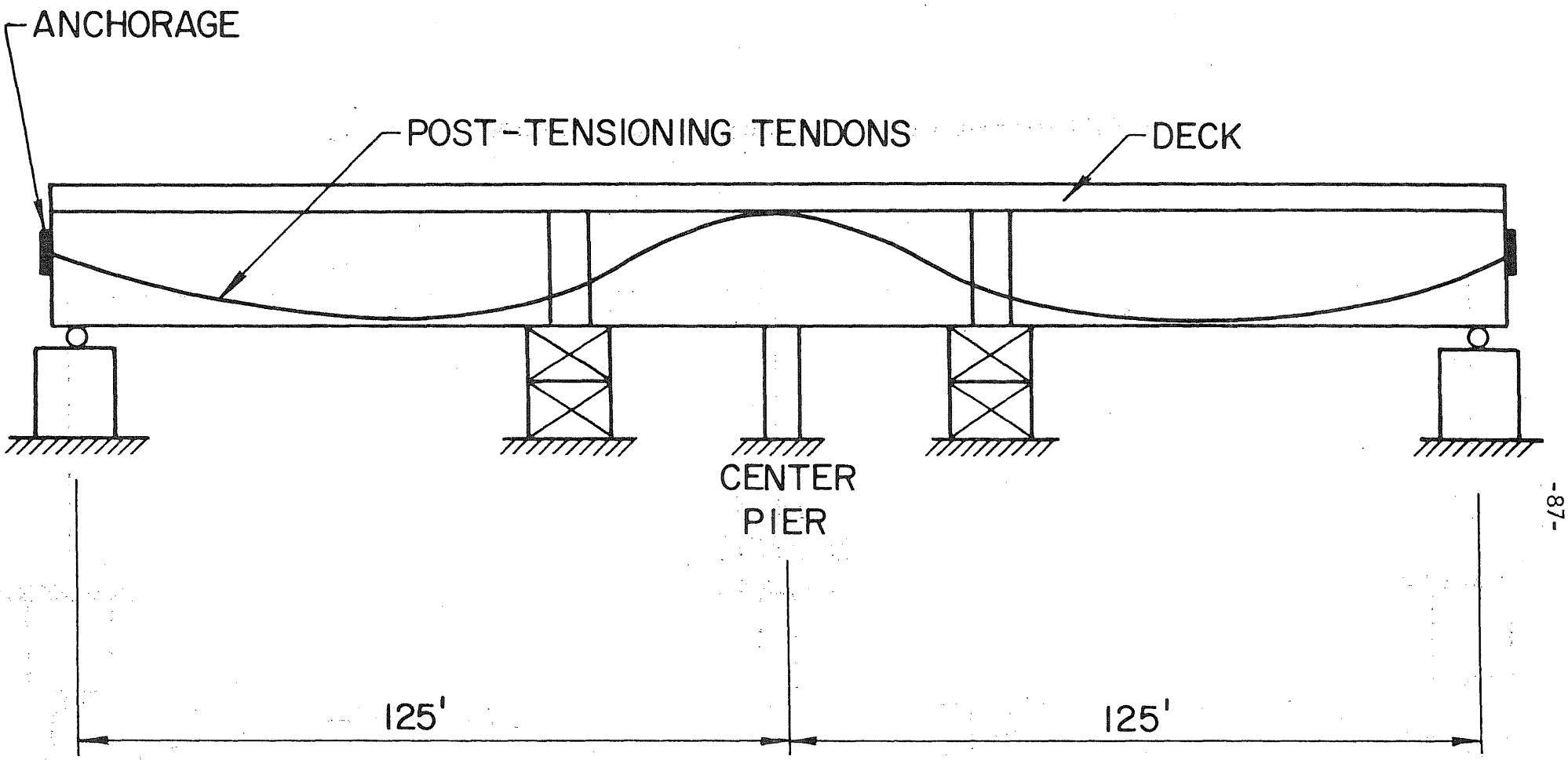

FIG. 1.4 ENTIRE STRUCTURE POST-TENSIONED TO ESTABLISH CONTINUITY

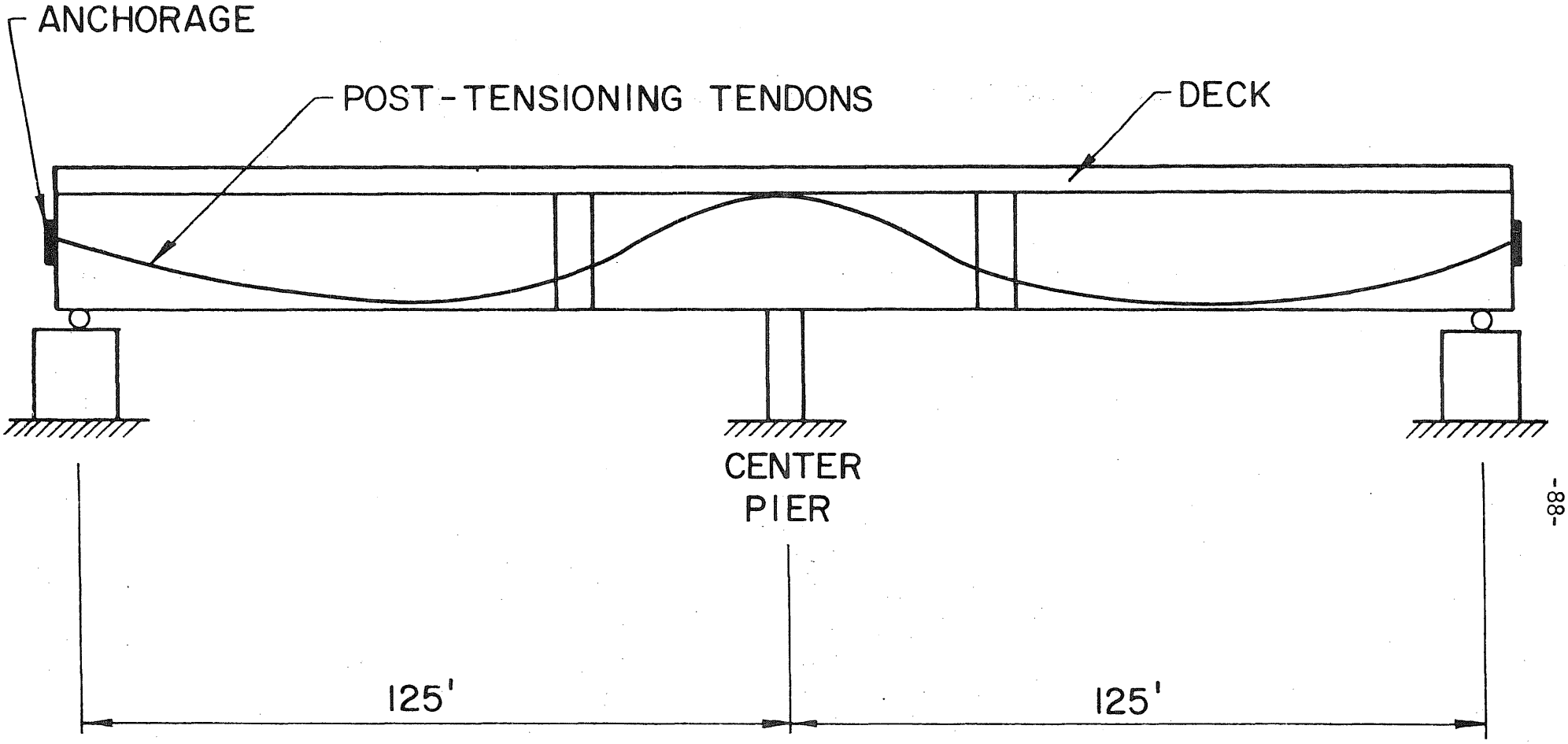

FIG. 1.5 TEMPORARY SUPPORTS REMOVED TO COMPLETE TWO-SPAN STRUCTURE

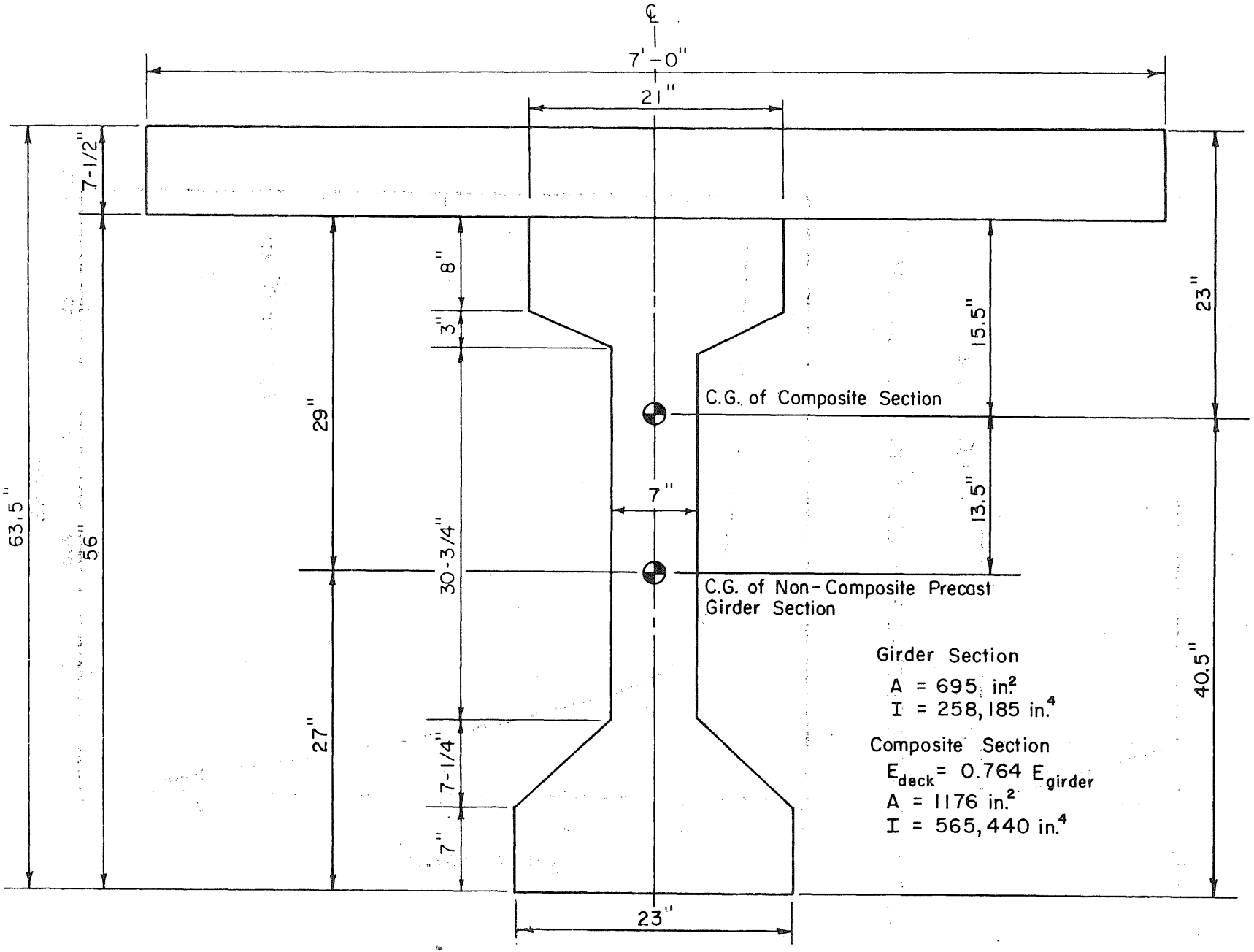

FIG. 2.1 CROSS-SECTION OF GIRDER AND DECK

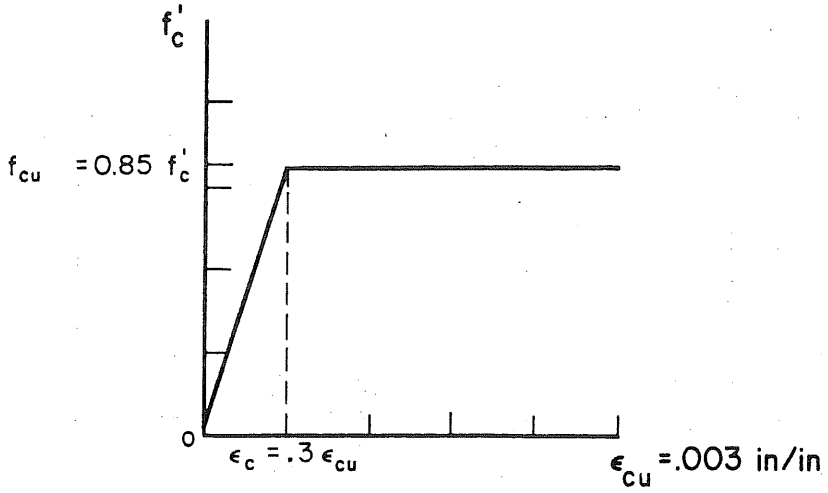

FIG. 2.2 IDEALIZED STRESS-STRAIN RELATIONSHIP FOR CONCRETE

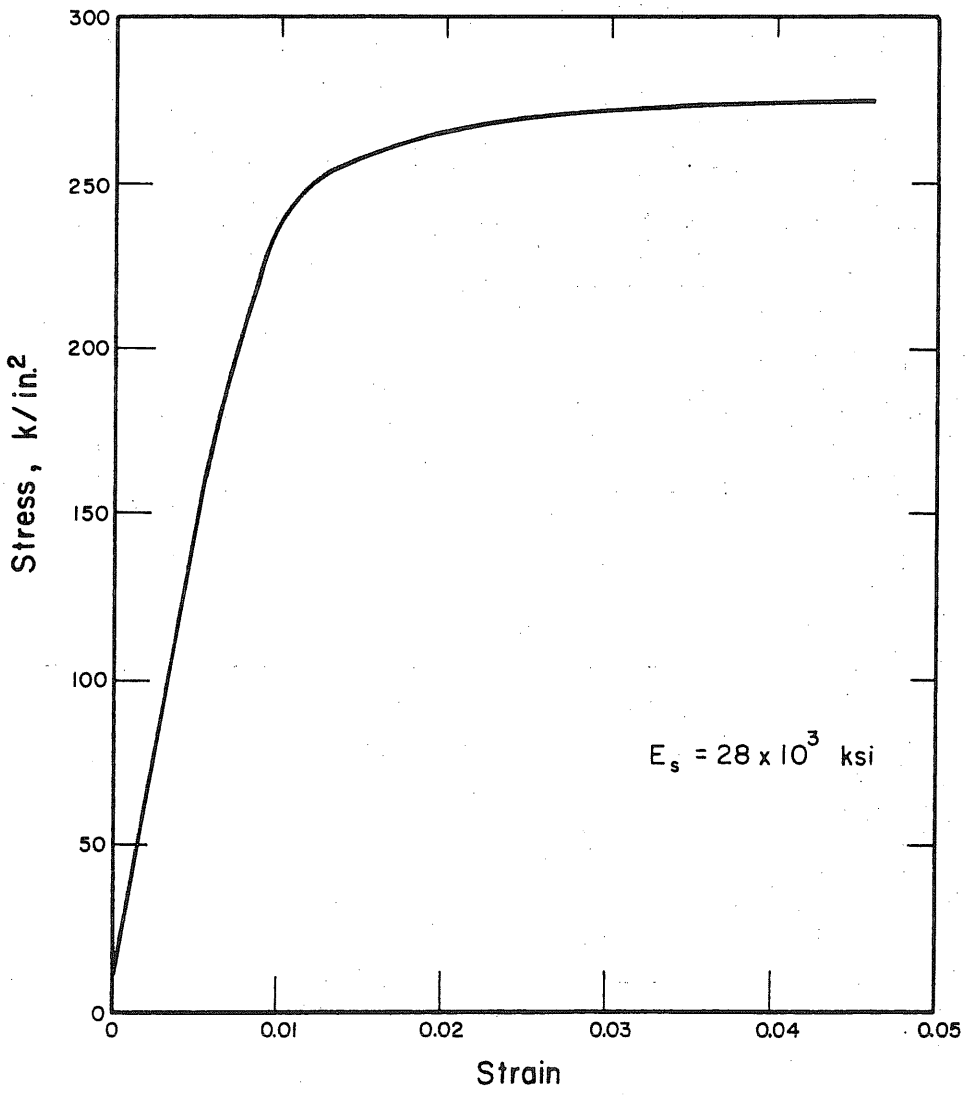

FIG. 2.3 ASSUMED STRESS-STRAIN RELATIONSHIP FOR PRESTRESSING STEEL

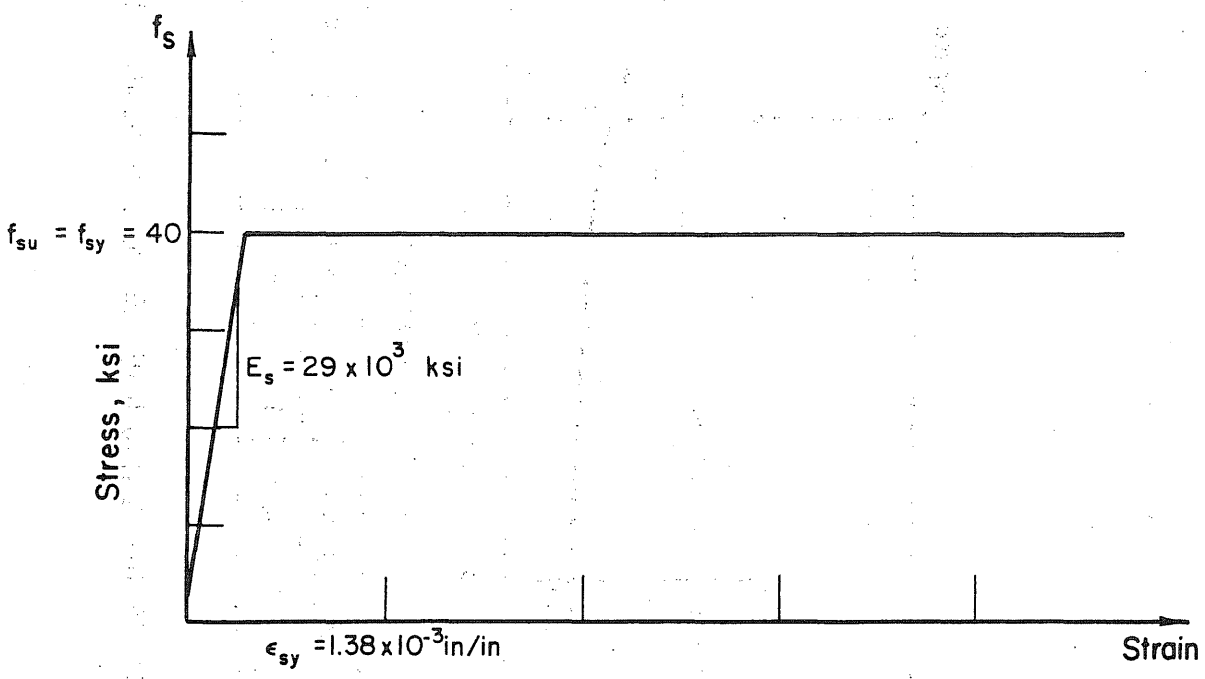

FIG. 2.4 ASSUMED STRESS-STRAIN RELATIONSHIP FOR NONPRESTRESSED DECK REINFORCEMENT

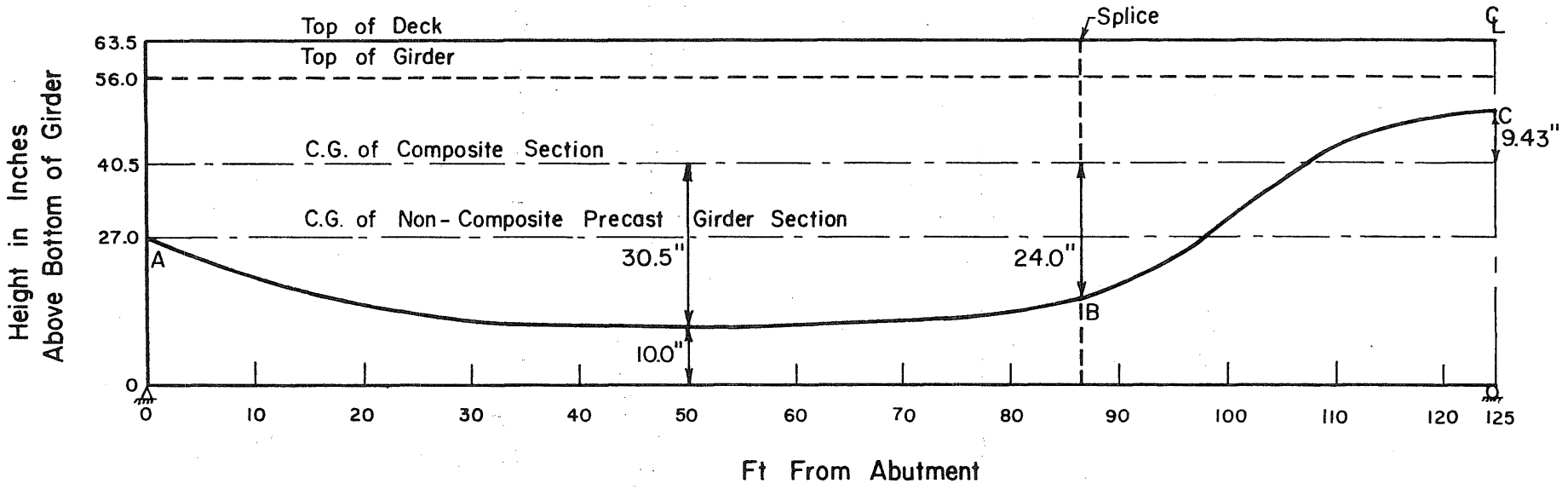

$e_{post.}$ - in.	-13.5	-21.2	-26.0	-28.7	-30.1	-30.5	-30.1	-29.0	-26.8	-22.8	-10.5	+2.5	+8.9	+9.43
C.G.S. To Bottom - in.	27.0	19.3	14.5	11.8	10.4	10.0	10.4	11.5	13.7	17.7	30.0	43.0	49.4	49.93

FIG. 2.5 PROFILE OF THE CENTROID OF THE POST-TENSIONING STEEL

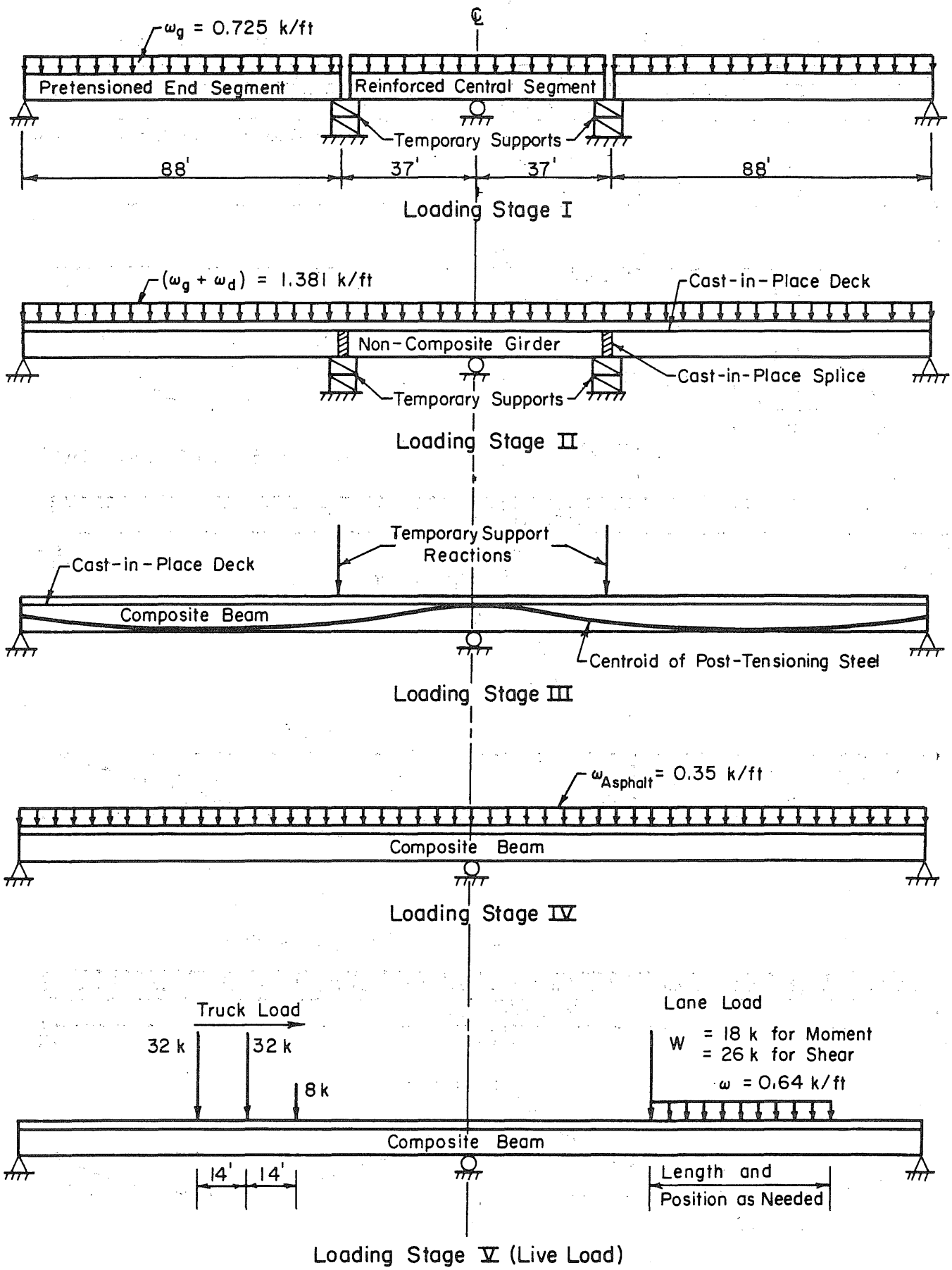

FIG. 2.6 LOADINGS DURING VARIOUS STAGES OF CONSTRUCTION

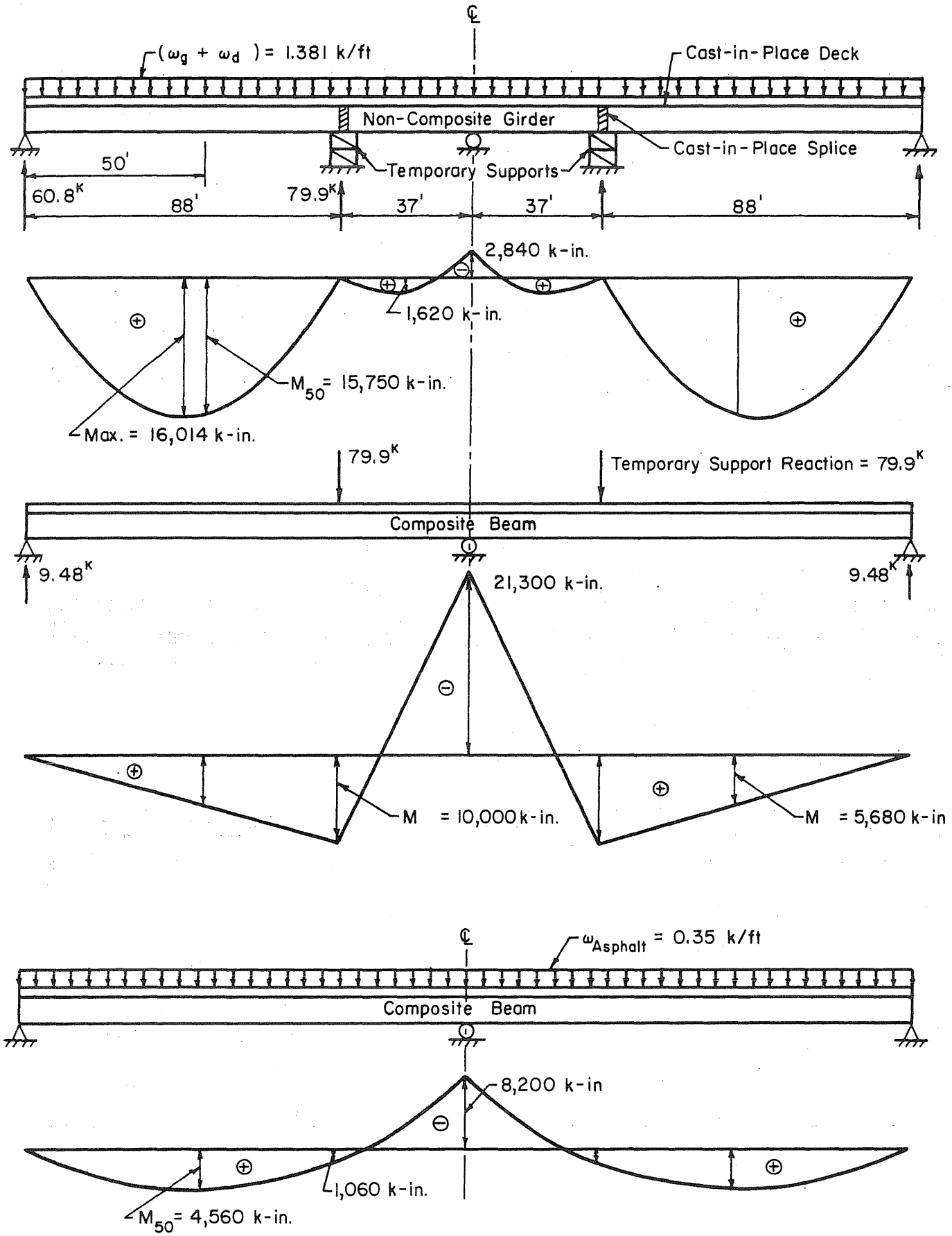

FIG. 2.7 MOMENT DIAGRAMS DUE TO DIFFERENT COMPONENTS OF DEAD LOAD

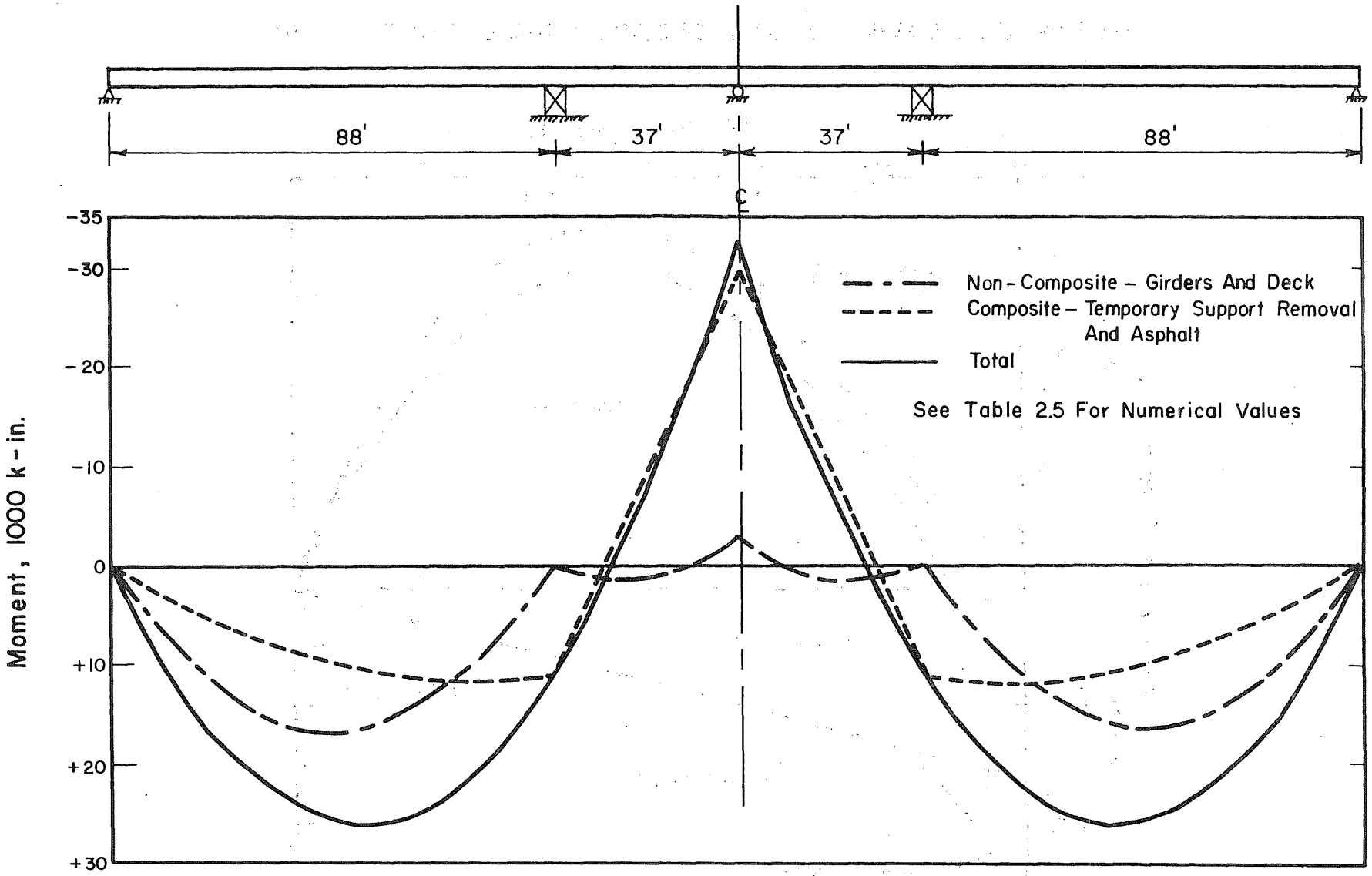

FIG. 2.8 DEAD LOAD MOMENT DIAGRAMS WITHOUT EFFECTS OF SECONDARY MOMENTS

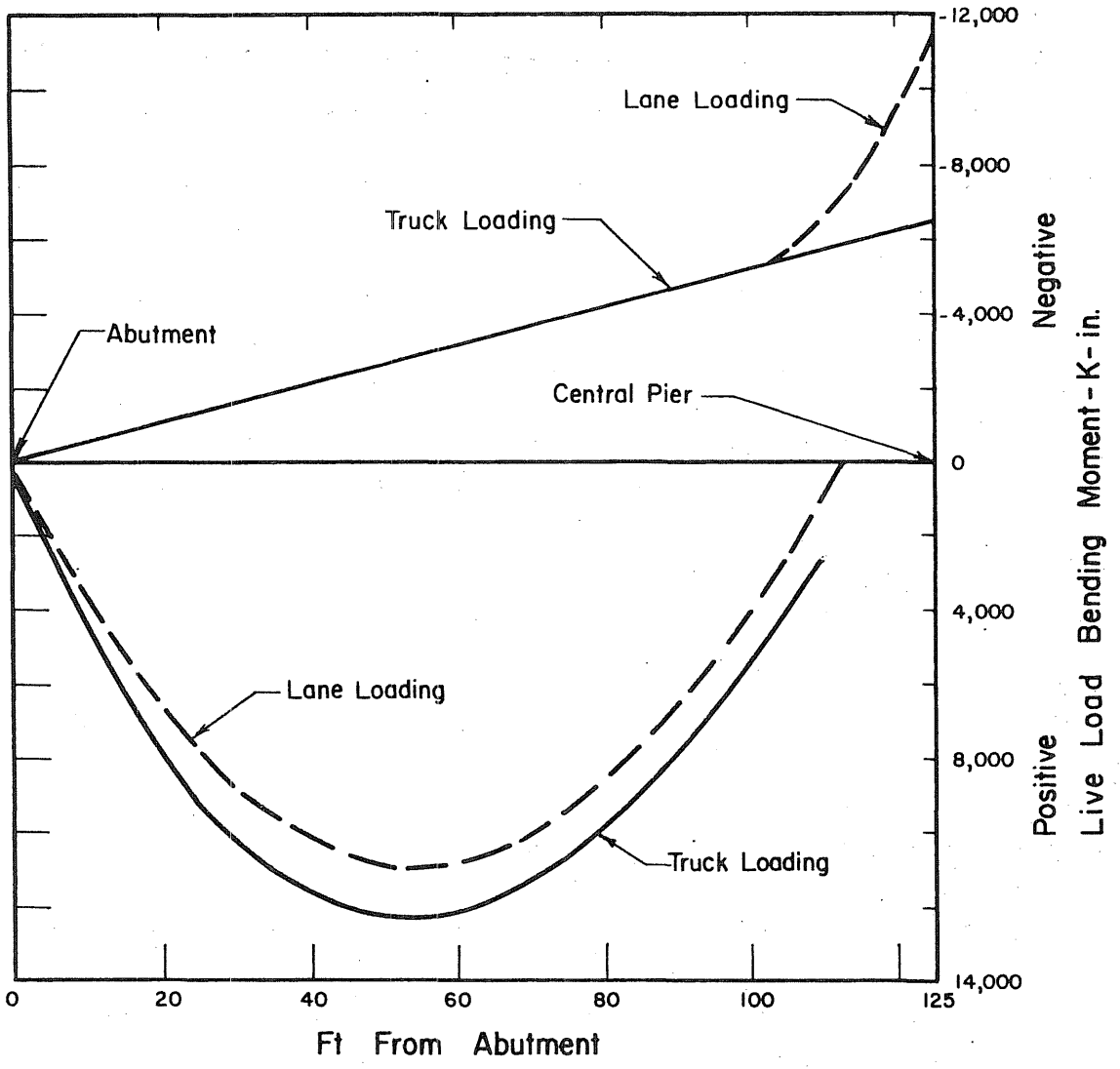

FIG. 2.9 LIVE LOAD MOMENT ENVELOPES, HS20, 7 FT BEAM SPACING, NO IMPACT

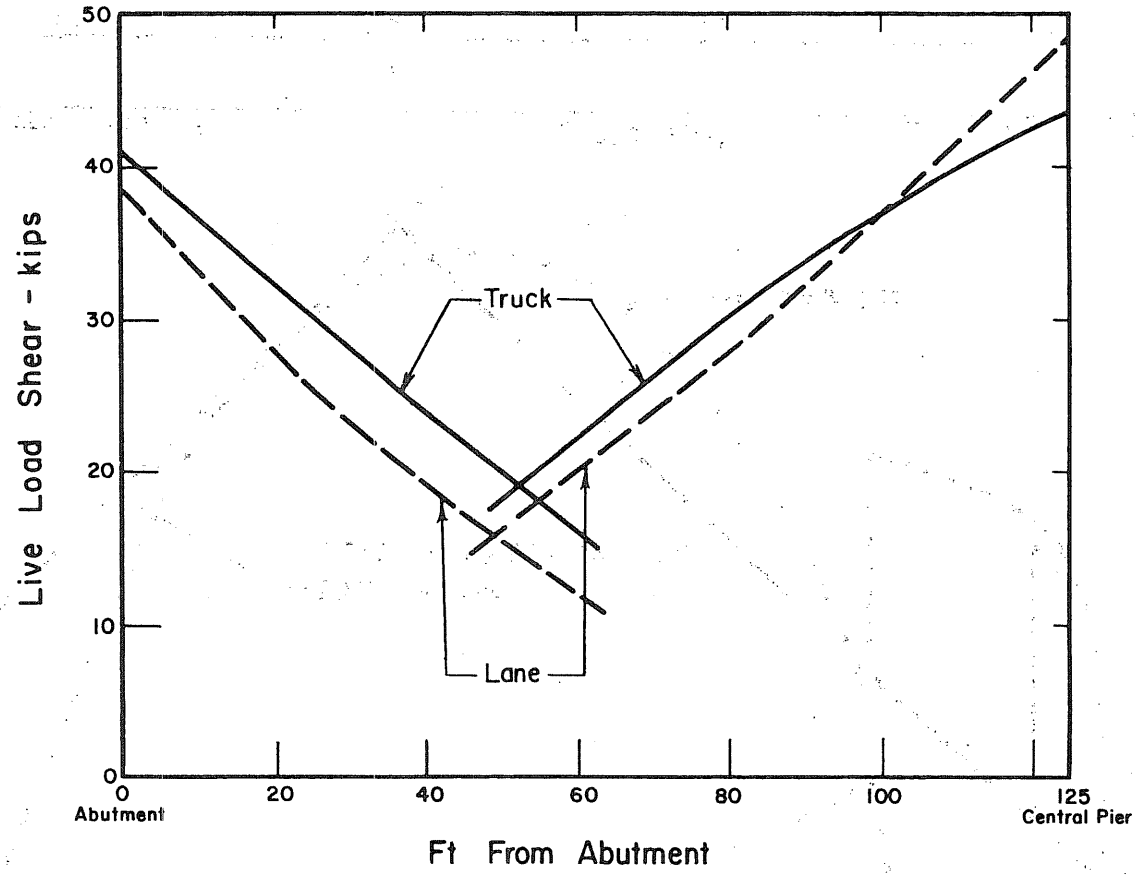

FIG. 2.10 LIVE LOAD SHEAR ENVELOPES, HS20, 7 FT BEAM SPACING, NO IMPACT

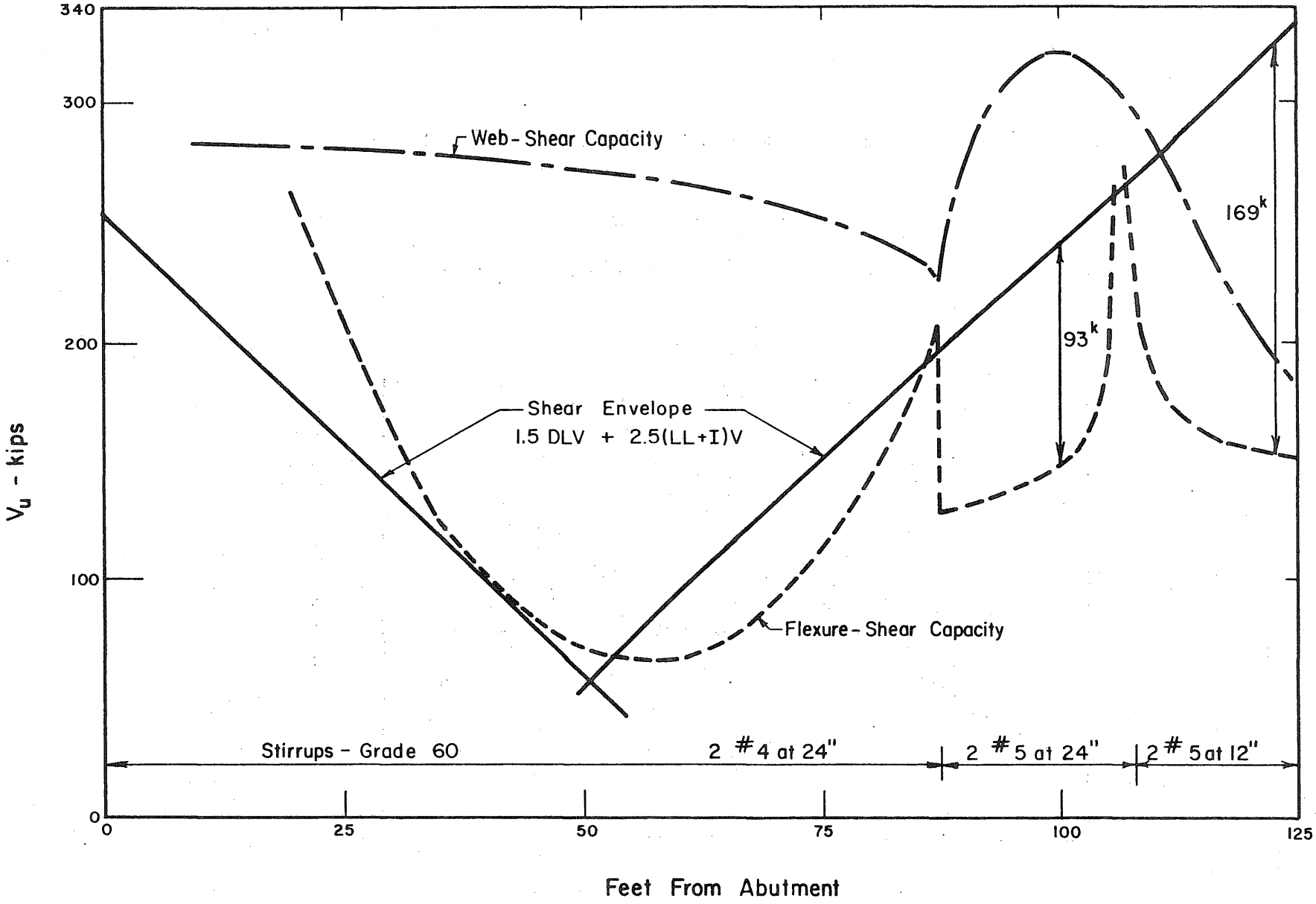

FIG. 2.11 DESIGN ULTIMATE SHEAR ENVELOPE AND SHEAR CAPACITY OF CONCRETE CROSS-SECTION

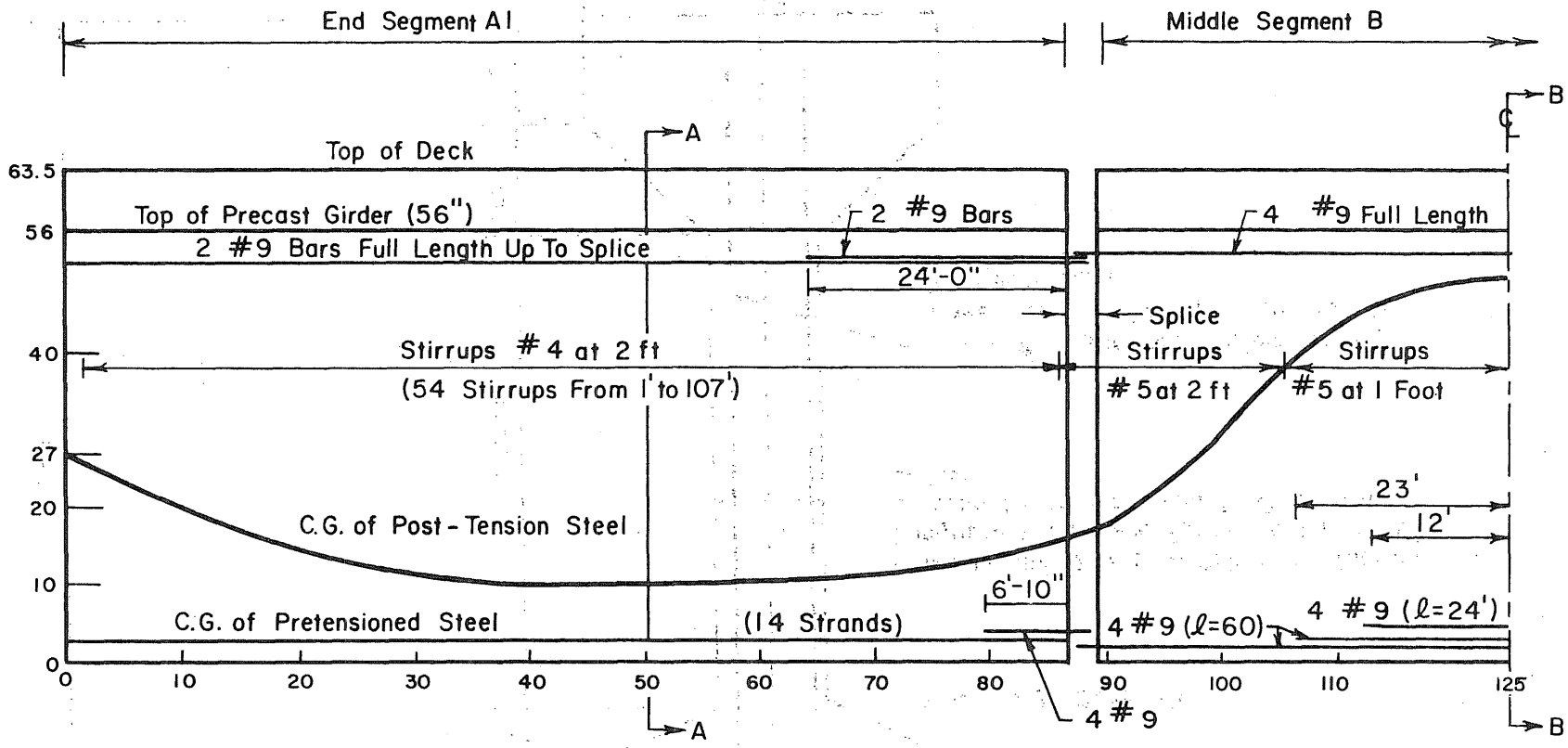

FIG. 2.12 REINFORCEMENT ARRANGEMENT ALONG HALF-LENGTH OF STRUCTURE

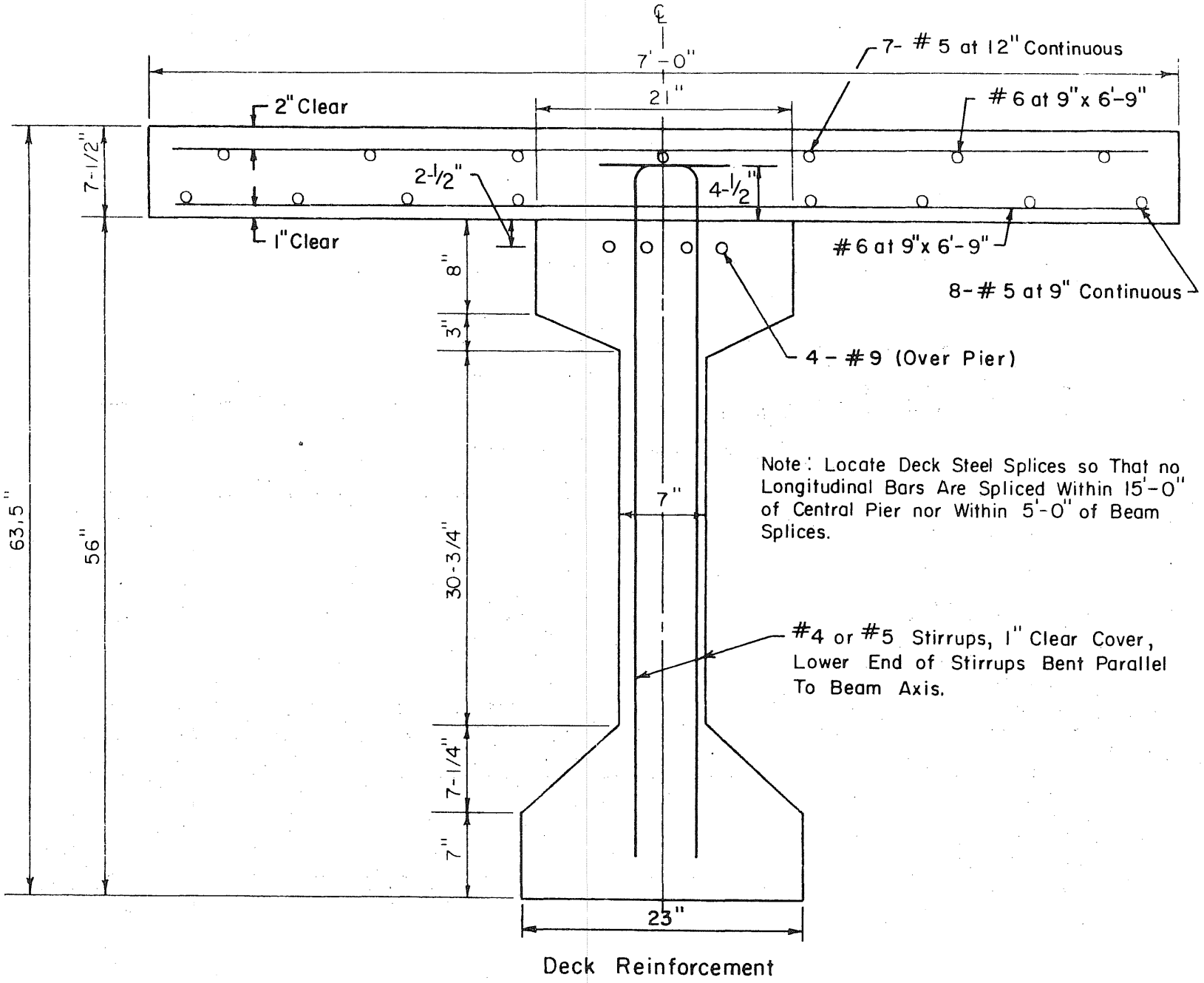

FIG. 2.13 ARRANGEMENT OF REINFORCEMENT IN DECK

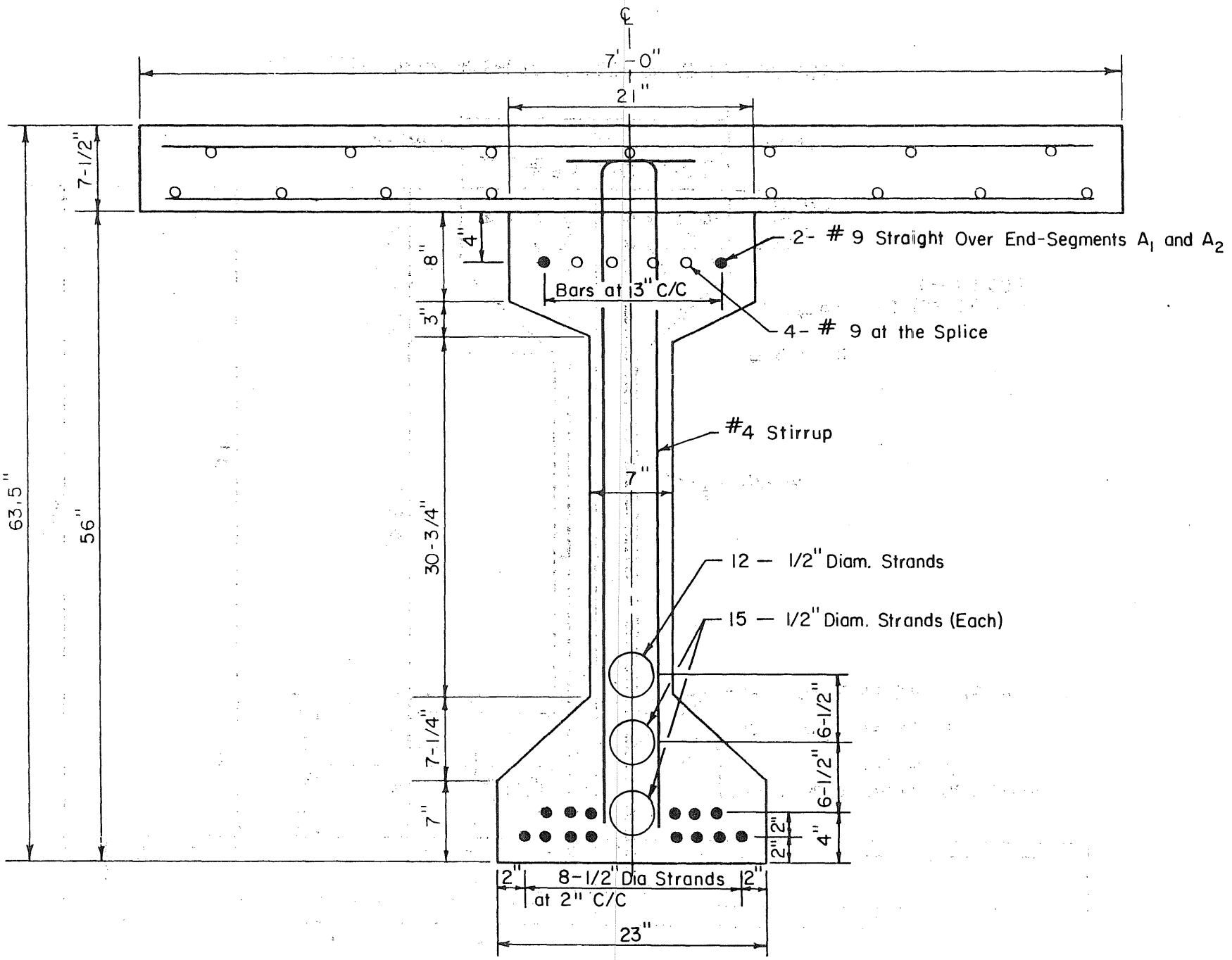

FIG. 2.14 ARRANGEMENT OF REINFORCEMENT IN END SEGMENT AT SECTION 50 FT FROM ABUTMENT

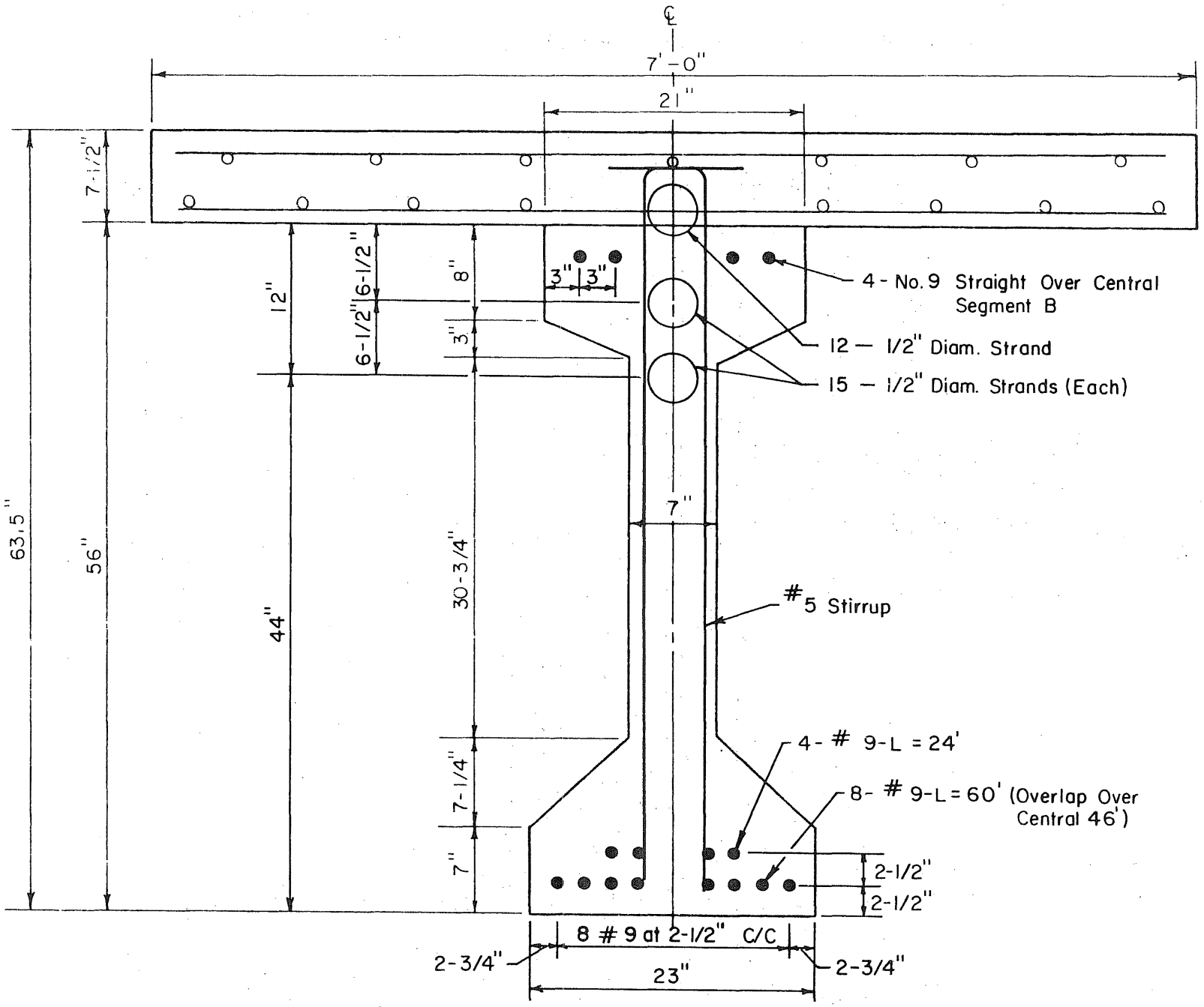

FIG. 2.15 REINFORCEMENT AT SECTION AT CENTRAL PIER

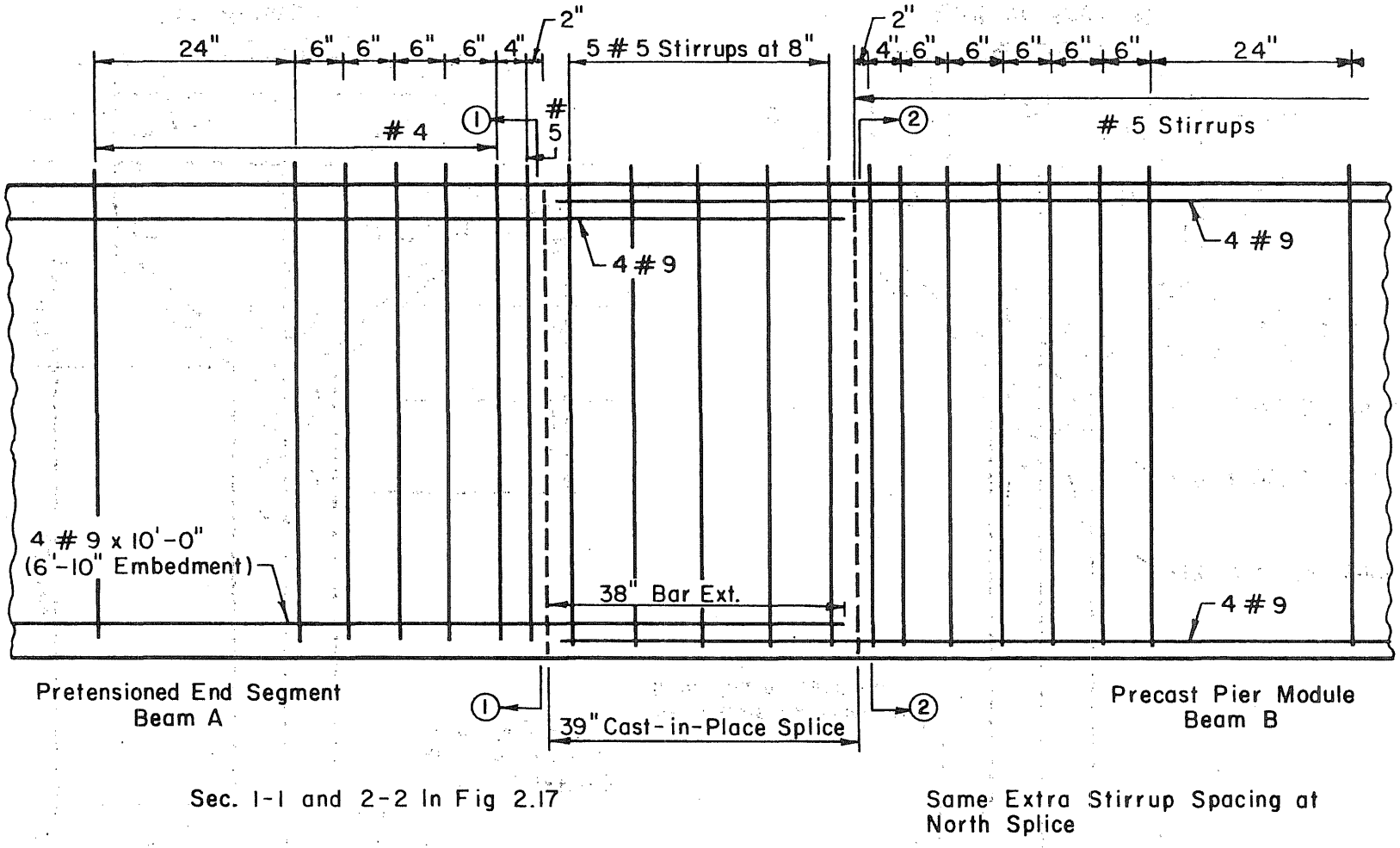

FIG. 2.16 ELEVATION OF REINFORCEMENT DETAILS AT SOUTH SPLICE

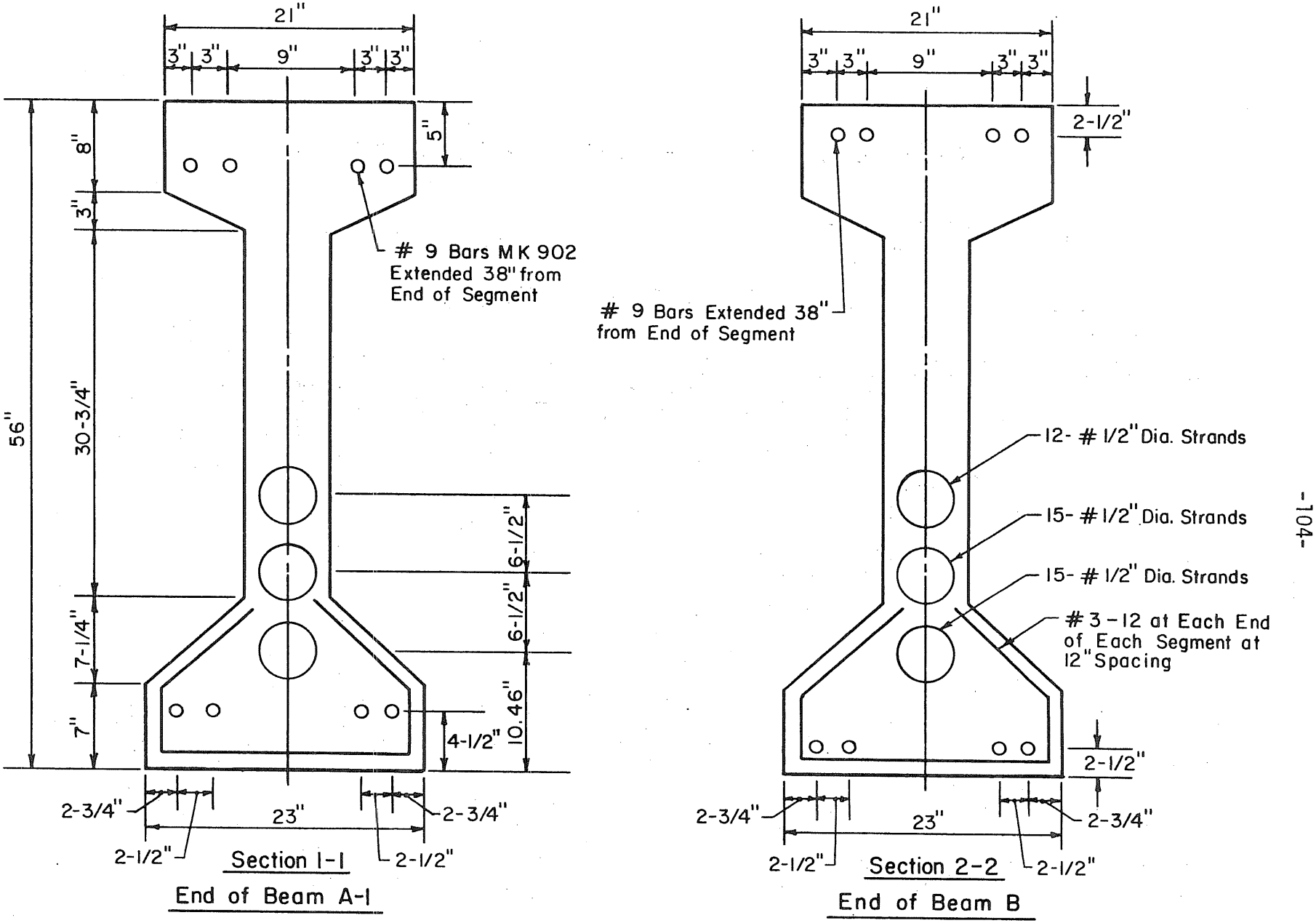

FIG. 2.17 SECTIONS SHOWING REINFORCEMENT ARRANGEMENT AT SOUTH SPLICE

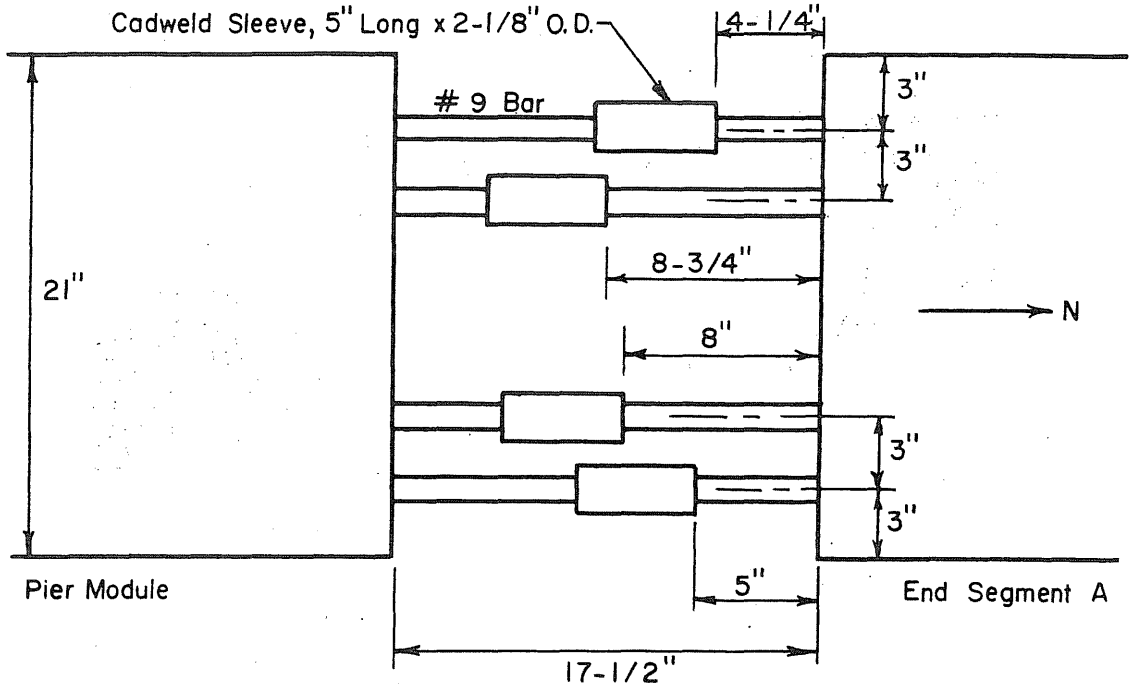

(a) Locations of Cadweld Splices In Top of North Splice, Bars In Plane 5 in. Below Top of Precast Section

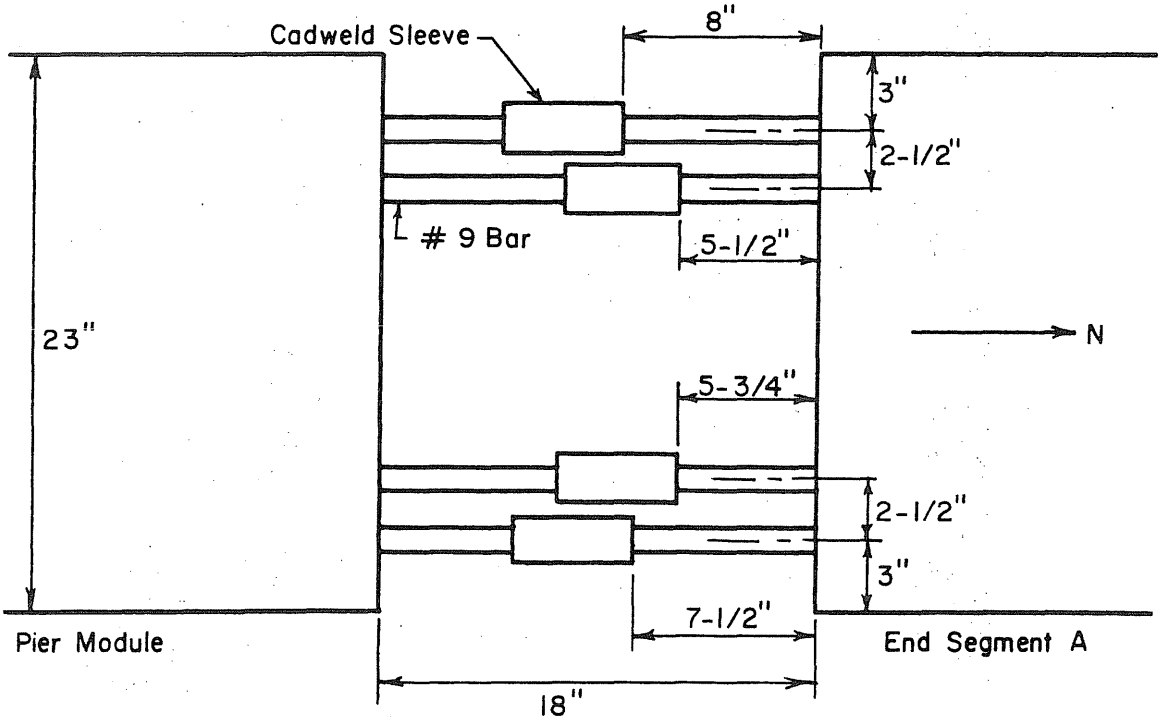

(b) Locations of Cadweld Splices In Bottom of North Splice Bars In Plane 2-3/4 in. Above Bottom of Precast Section

FIG. 2.18 LOCATIONS OF CADWELD SPLICES IN BARS IN NORTH SPLICE

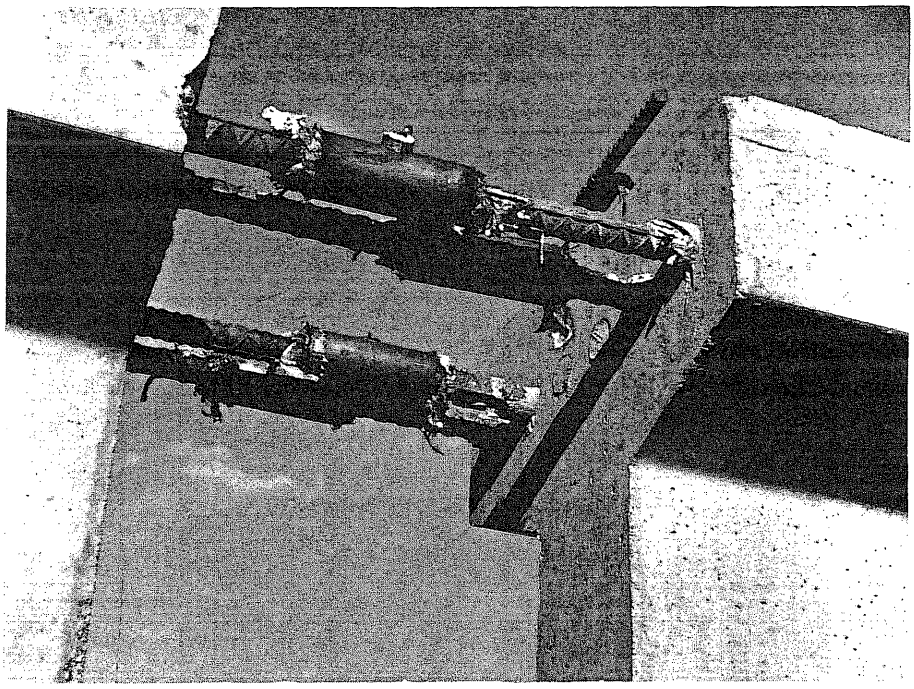

(a) Steel at Top of Beam

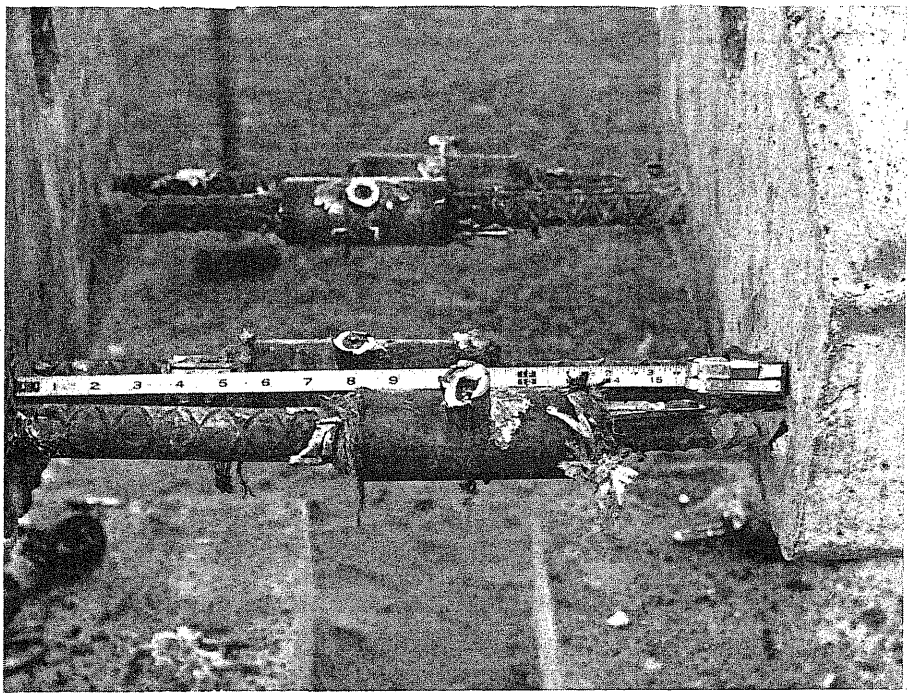

(b) Steel at Bottom of Beam

FIG. 3.1 PHOTOGRAPH SHOWING REINFORCEMENT AND CADWELD SPLICES AT NORTH SPLICE

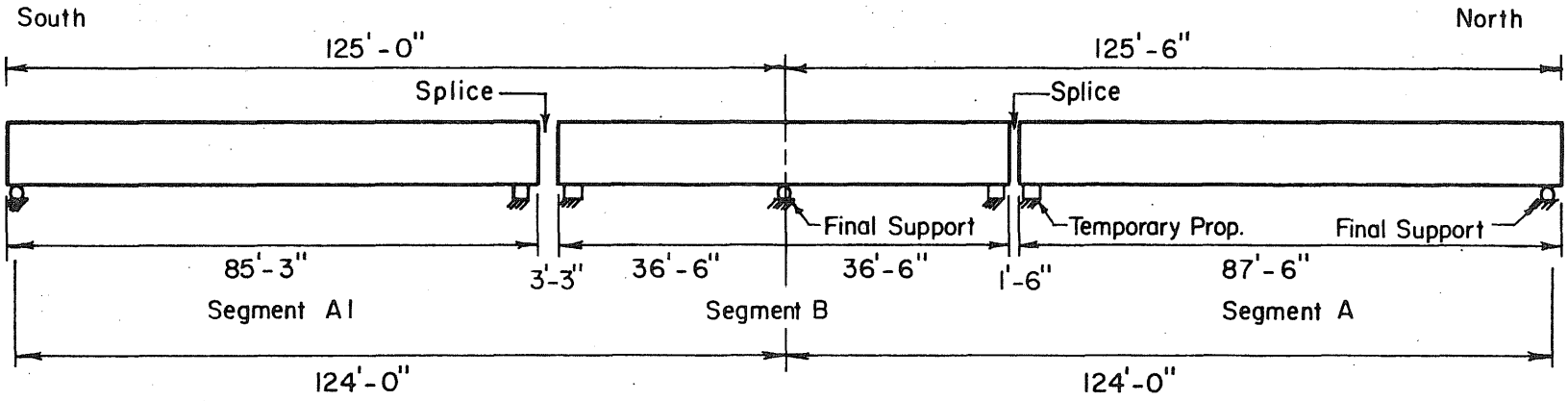

Vertical Scale = 2 x Horizontal Scale

FIG. 3.2 AS-BUILT MEMBER LENGTHS AND LOCATIONS IN TEST STRUCTURE

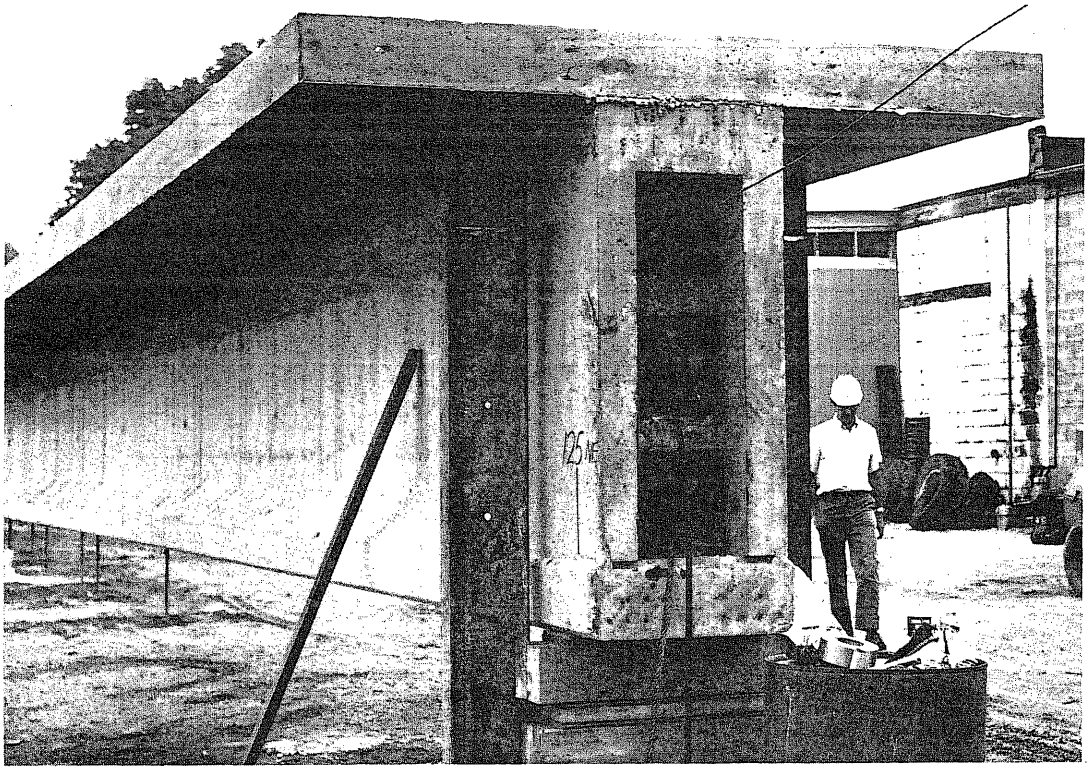

FIG. 3.3 PHOTOGRAPH OF END OF BEAM SHOWING POST-TENSIONING ANCHORAGES

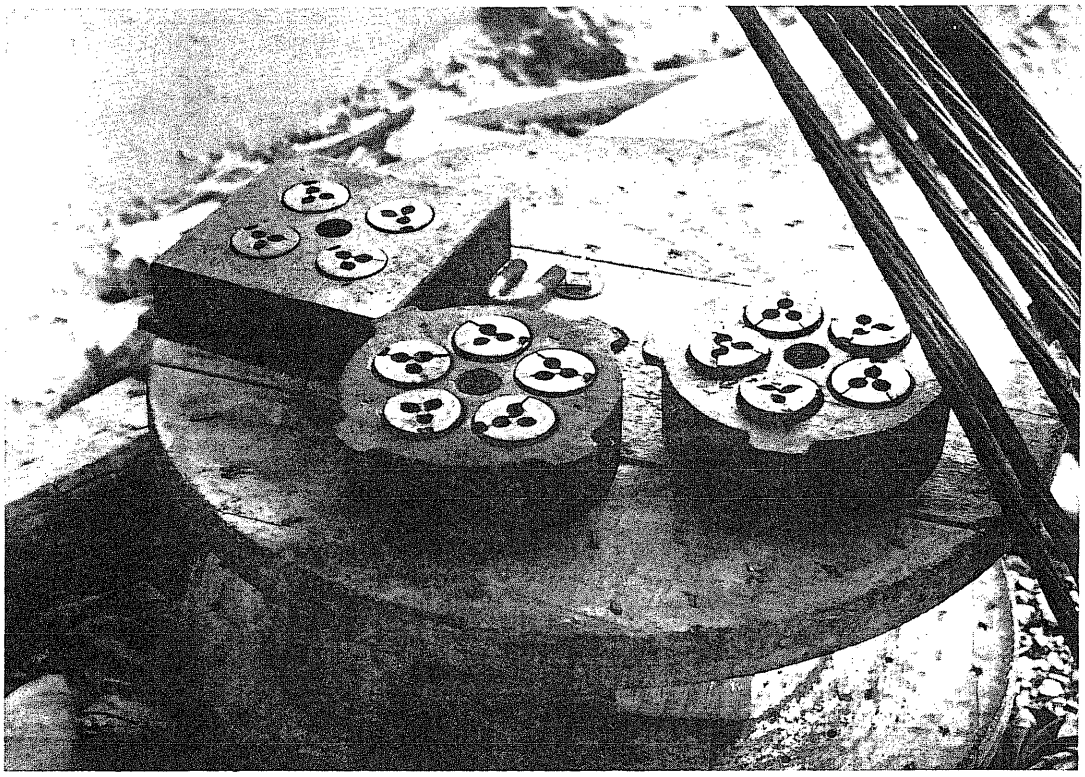

FIG. 3.4 PHOTOGRAPH OF POST-TENSIONING ANCHORAGE HEADS

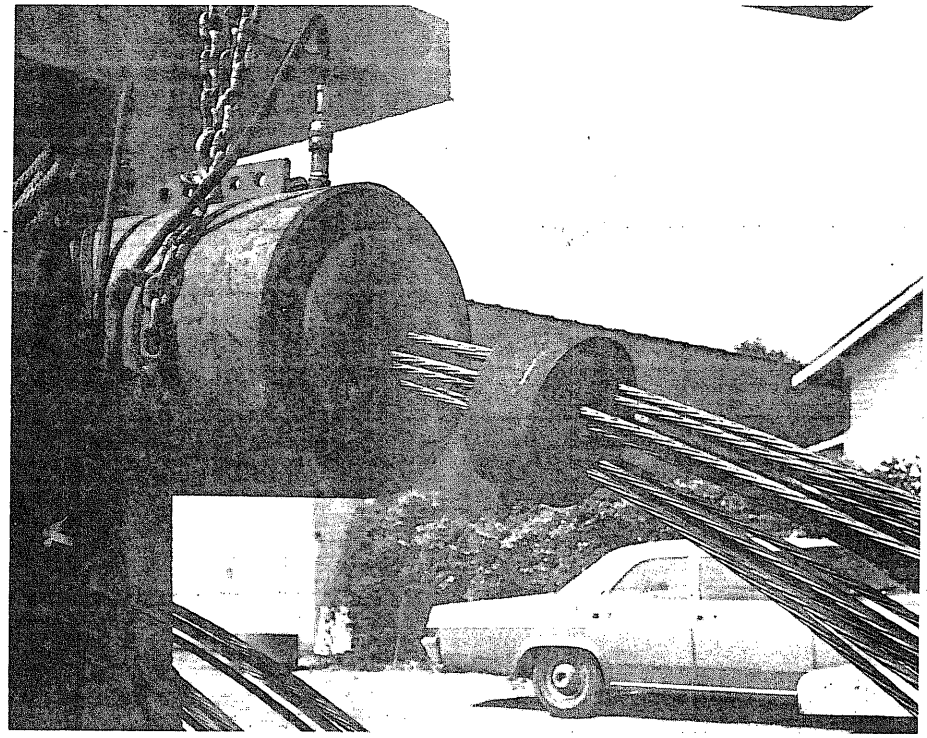

FIG. 3.5 PHOTOGRAPH OF POST-TENSIONING JACK AND STRESSING HEAD

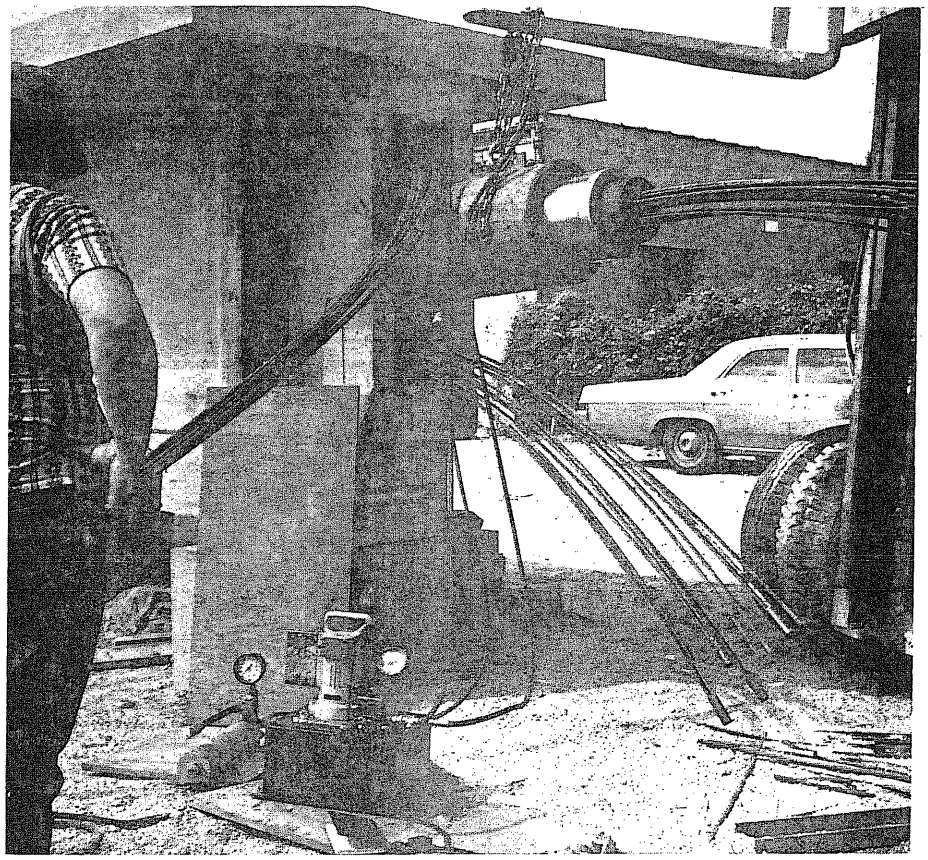

FIG. 3.6 PHOTOGRAPH OF POST-TENSIONING JACK PULLING CENTER TENDON

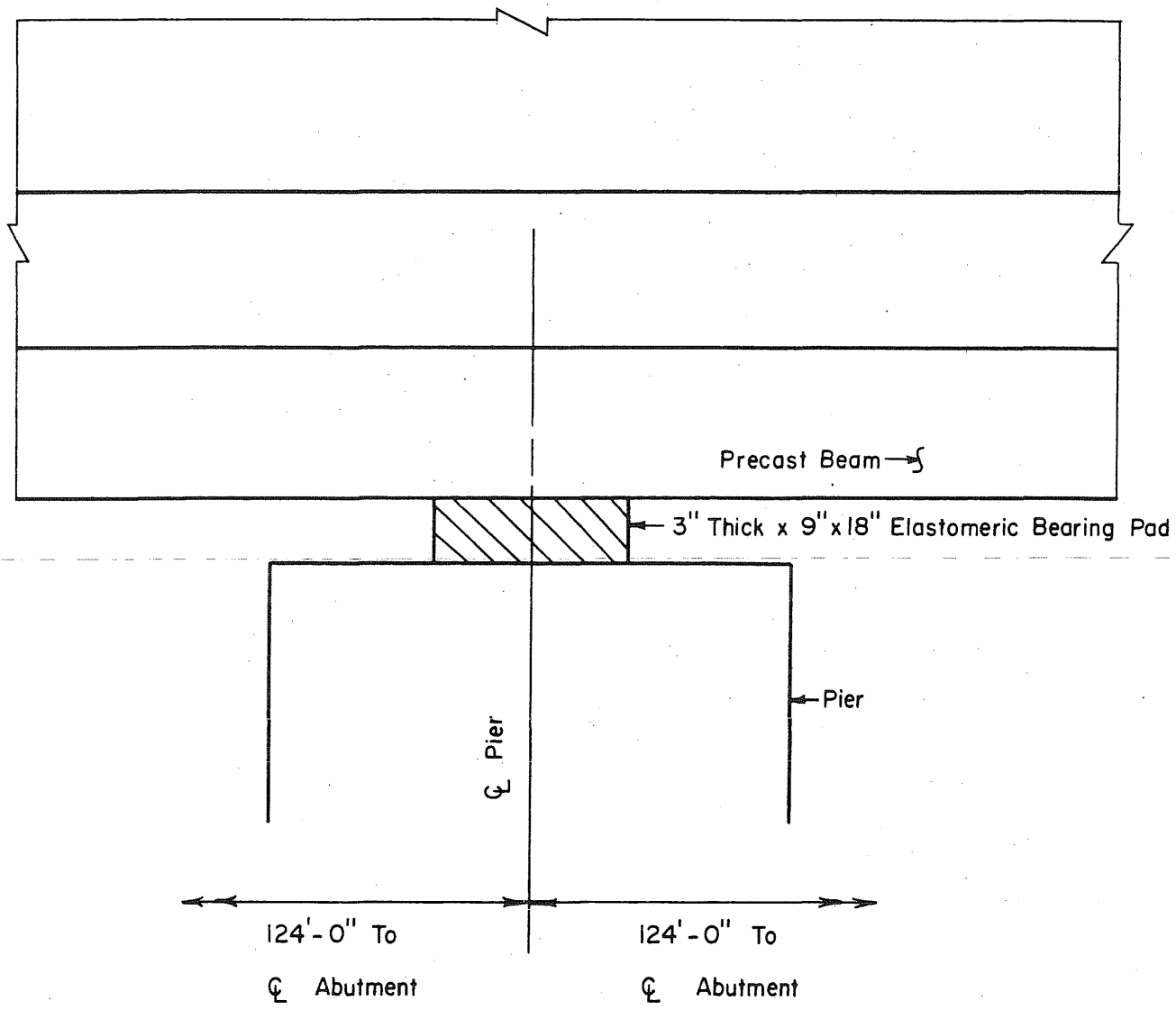

(a) Bearing At Central Pier Of Test Structure

FIG. 3.7 DETAILS OF BEARING DEVICES IN TEST STRUCTURE

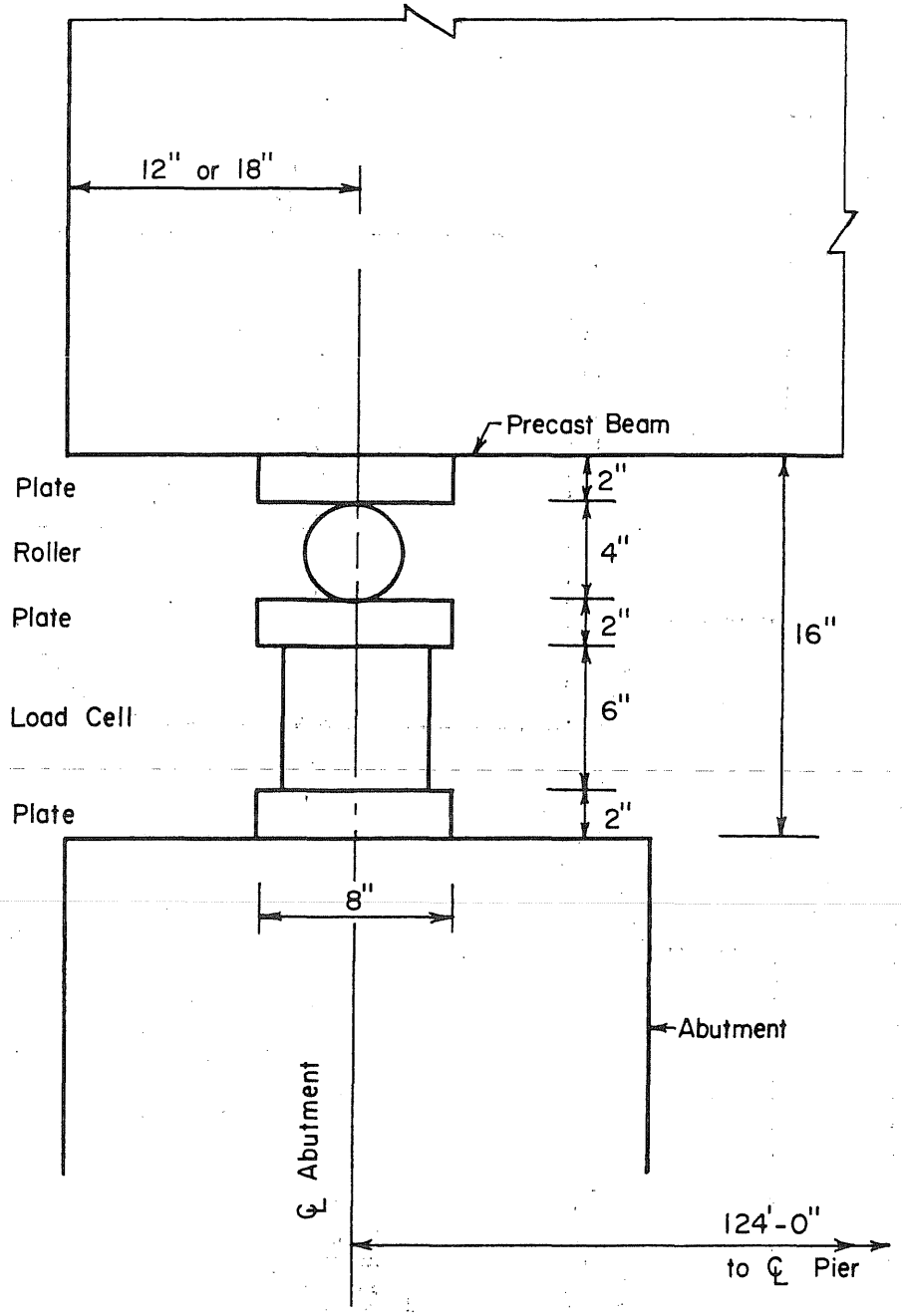

(b) Reaction Arrangement at Abutments of Test Structure

FIG. 3.7 Cont.

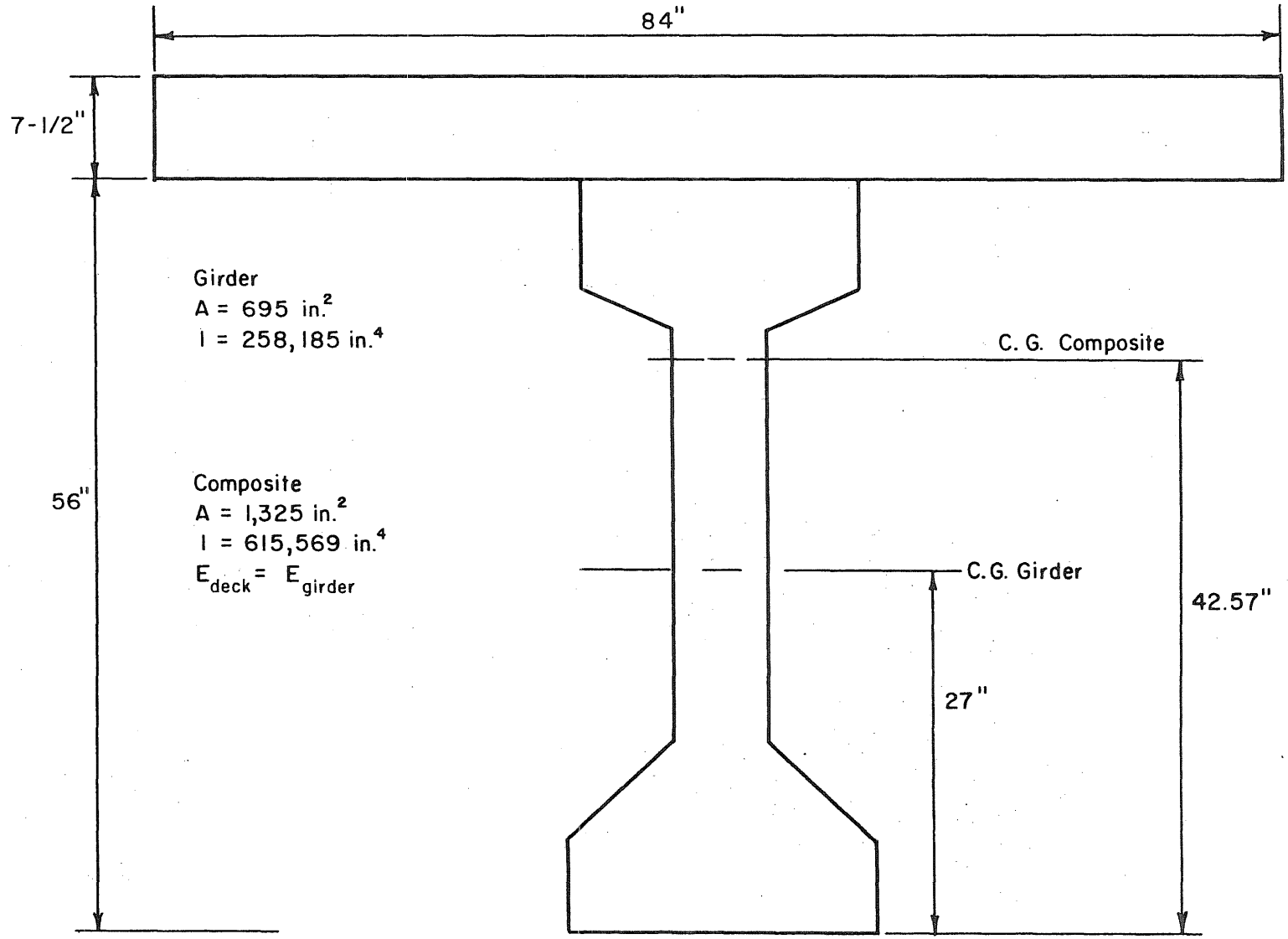

FIG. 3.8 COMPOSITE CROSS SECTION PROPERTIES WITH $E_{girder} = E_{deck}$

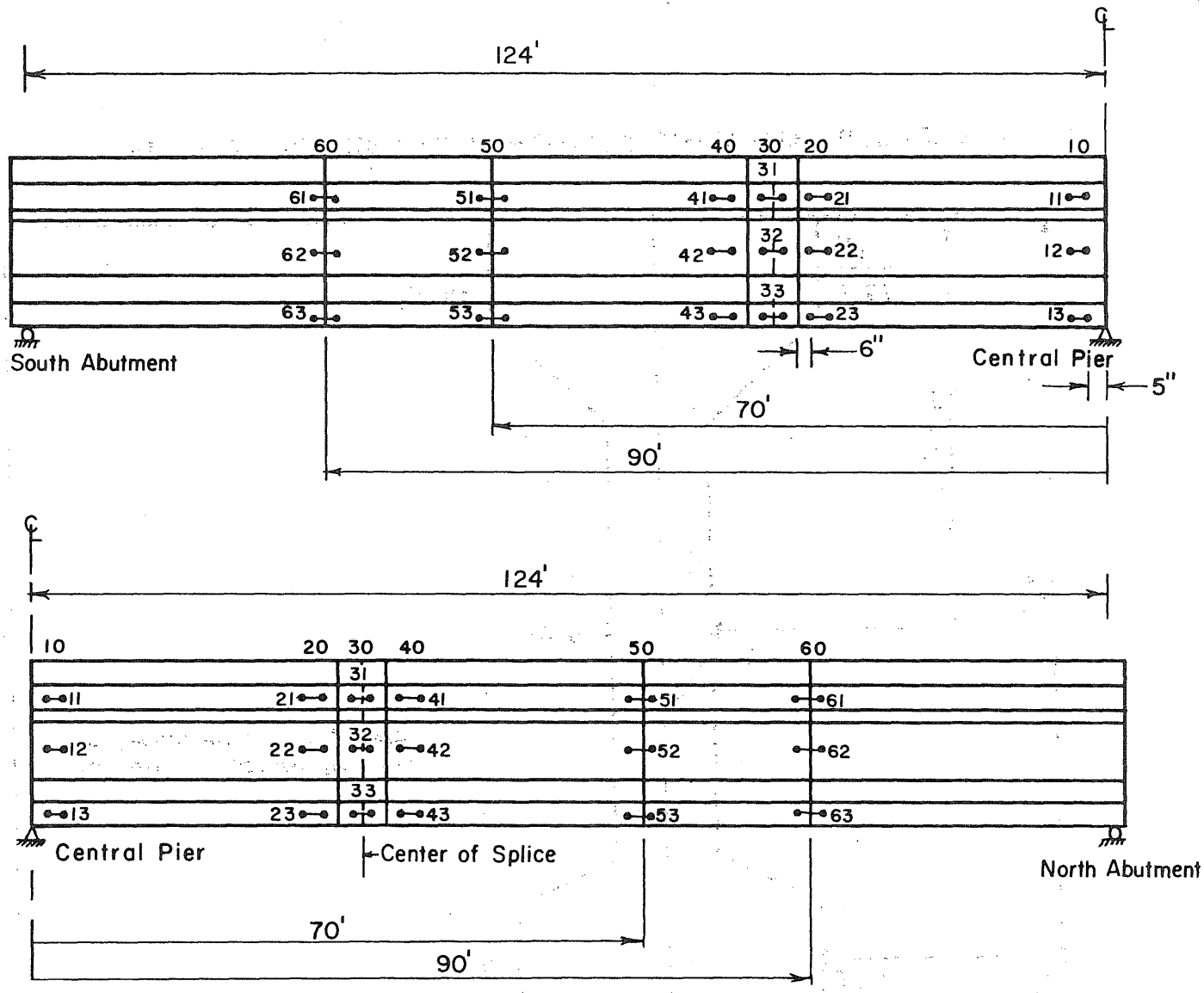

FIG. 4.1 LOCATIONS OF MECHANICAL STRAIN GAGES LINES ALONG LENGTH OF STRUCTURE

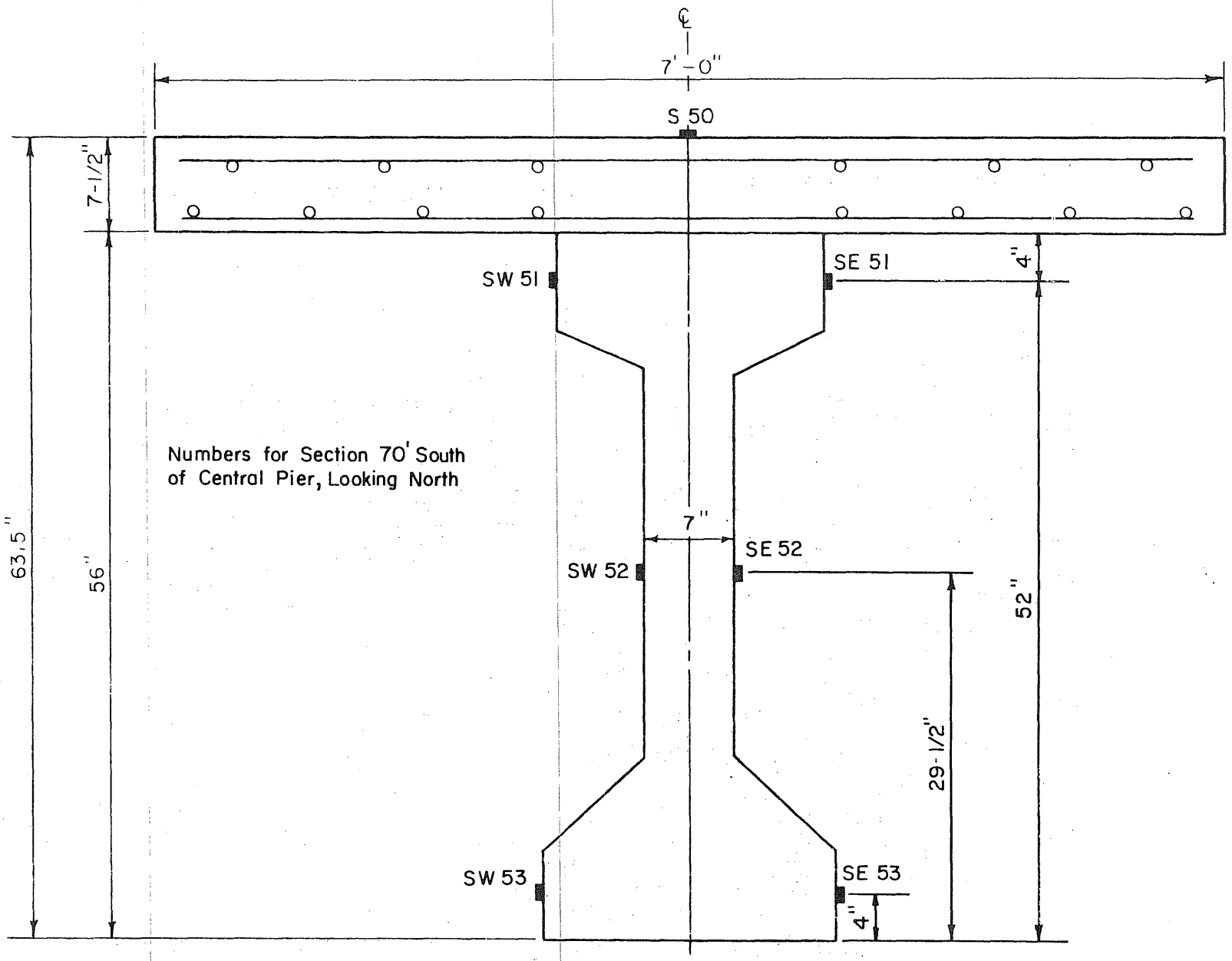

FIG. 4.2 DISTRIBUTION OF MECHANICAL STRAIN GAGE LINES ACROSS SECTION

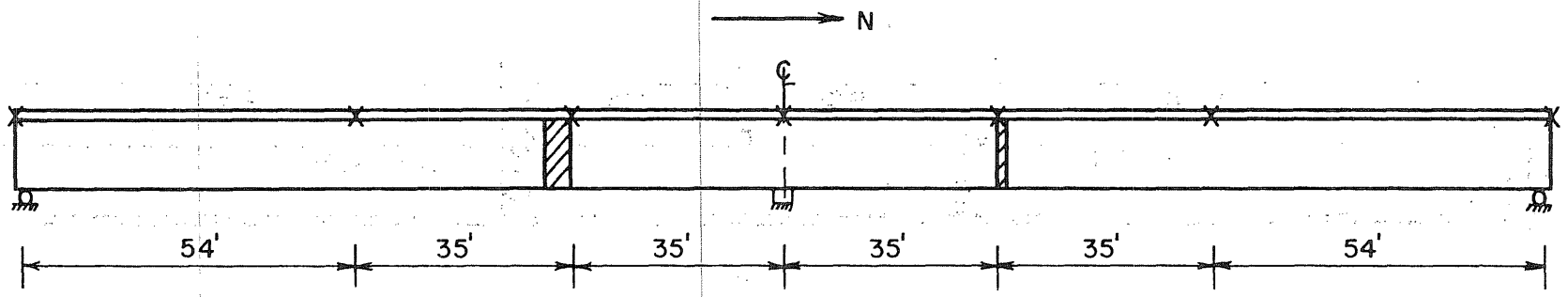

FIG. 4.3 LOCATIONS OF MEASUREMENTS OF VERTICAL DEFLECTIONS

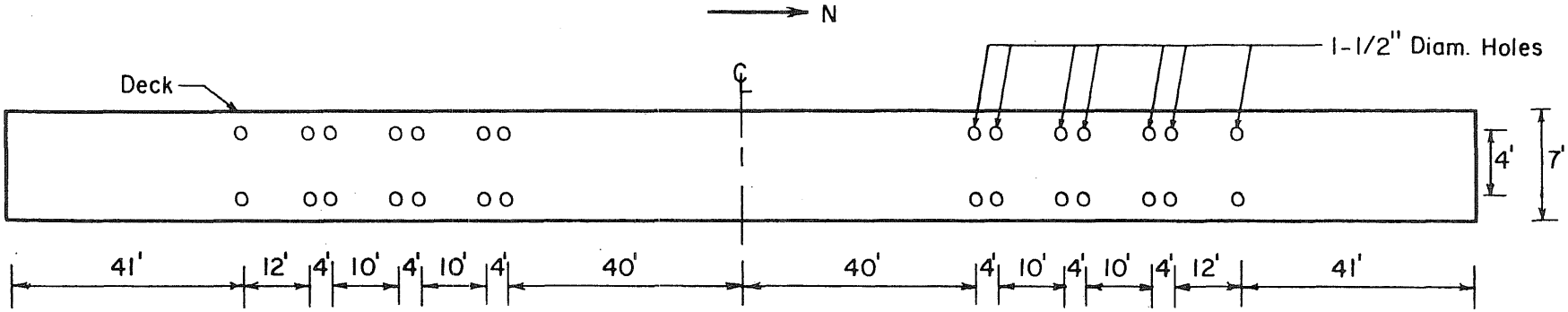

(a) Plan View Of Loading Points On Deck

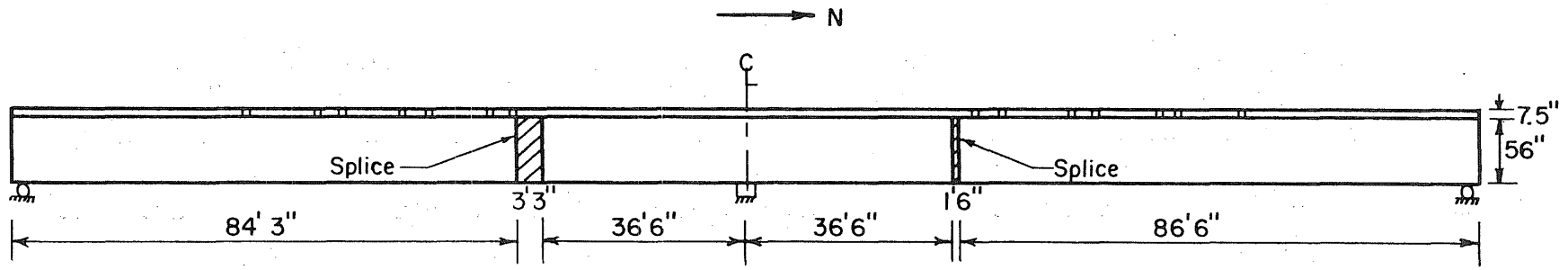

(b) Elevation Of Beam Showing Loading Positions

FIG. 5.1 LOCATIONS OF HOLES IN DECK FOR LOADING RODS

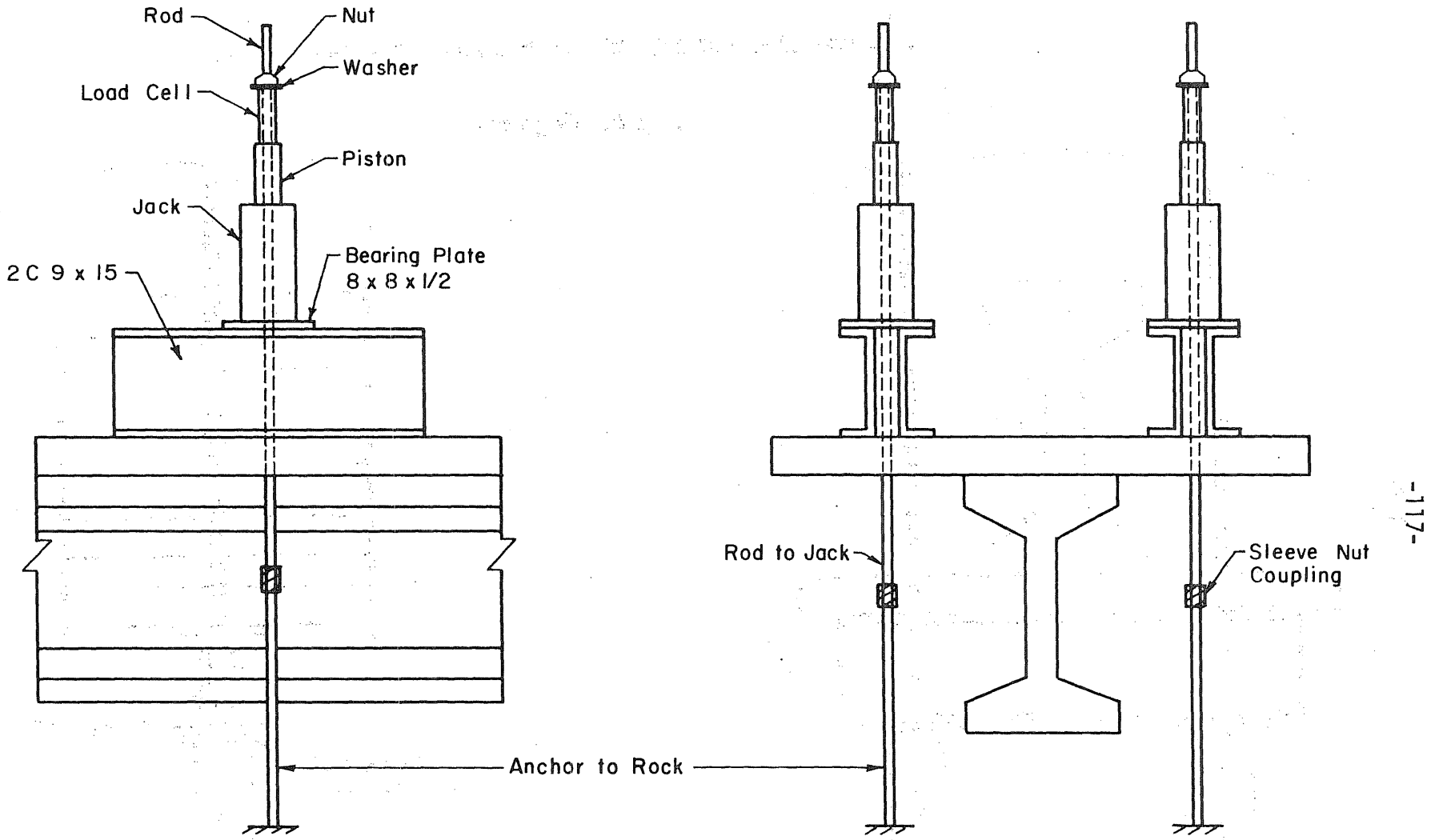

FIG. 5.2 LOADING SYSTEM USED FOR SERVICE LOAD TESTS

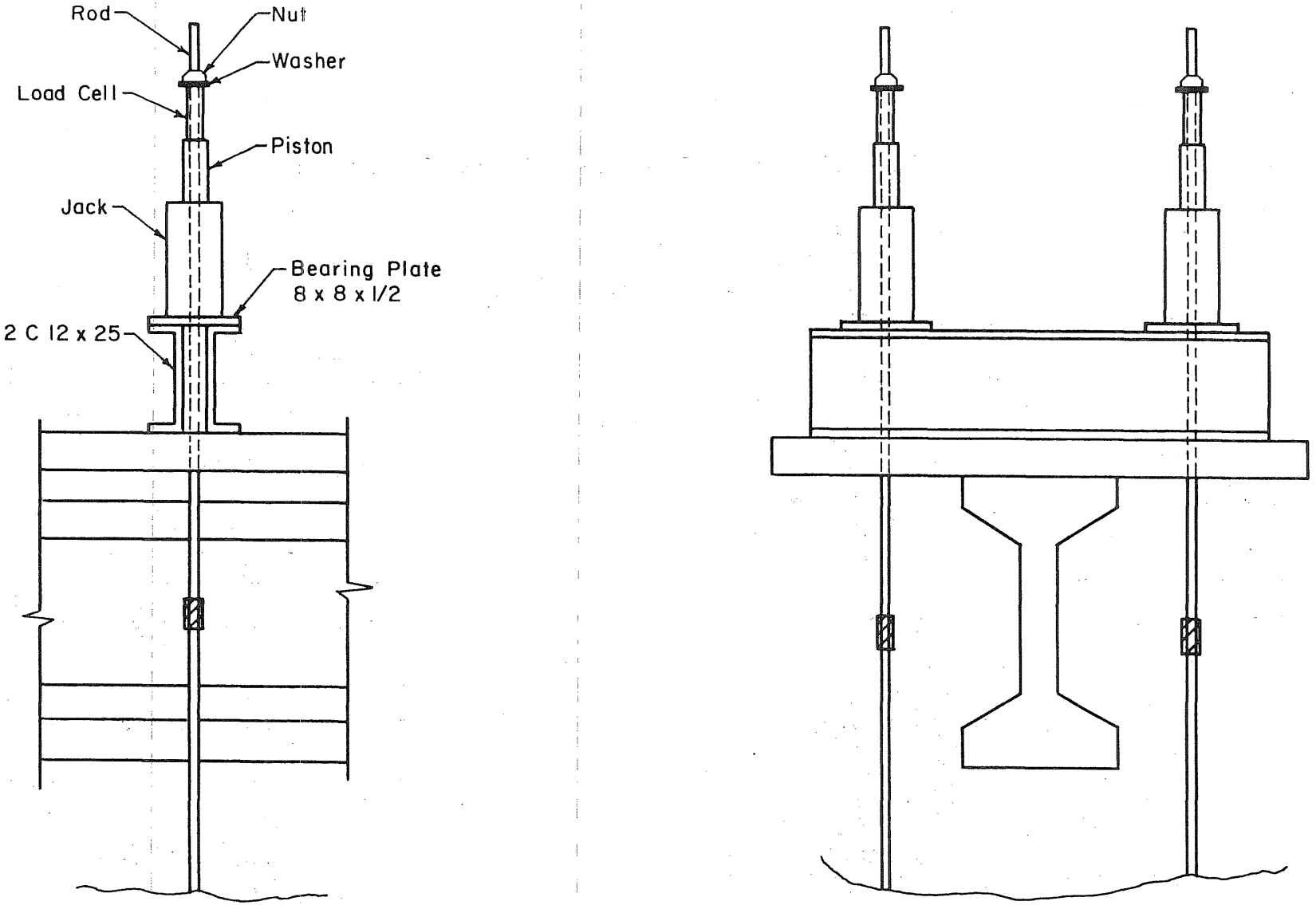

FIG. 5.3 LOADING SYSTEM USED FOR OVERLOAD TESTS

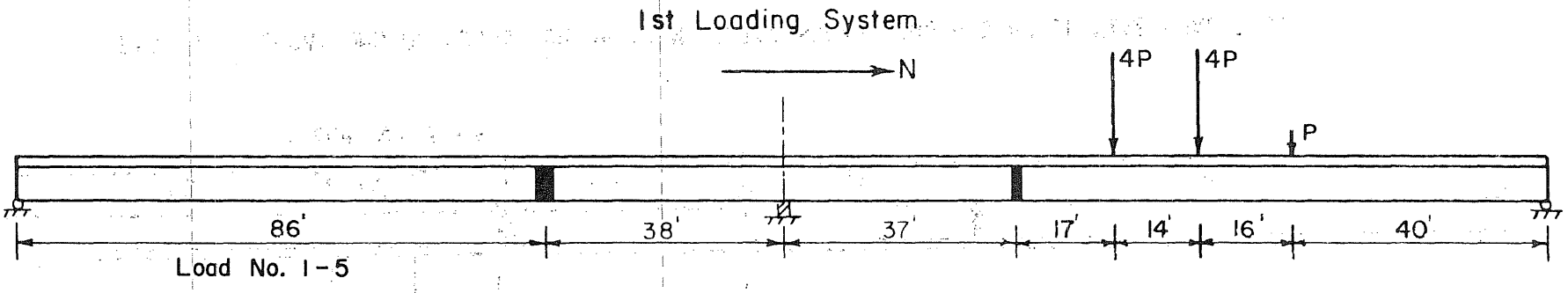

FIG. 5.4 LOCATIONS OF LOADS FOR MAXIMUM POSITIVE MOMENT, NORTH SPAN SERVICE LOAD TEST

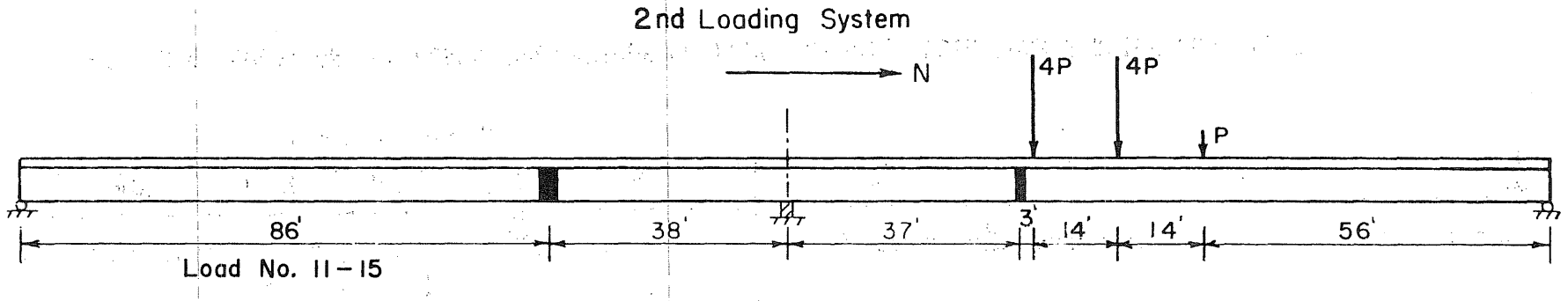

FIG. 5.5 LOCATIONS OF LOADS FOR MAXIMUM SPLICE SHEAR, NORTH SPAN SERVICE LOAD TEST

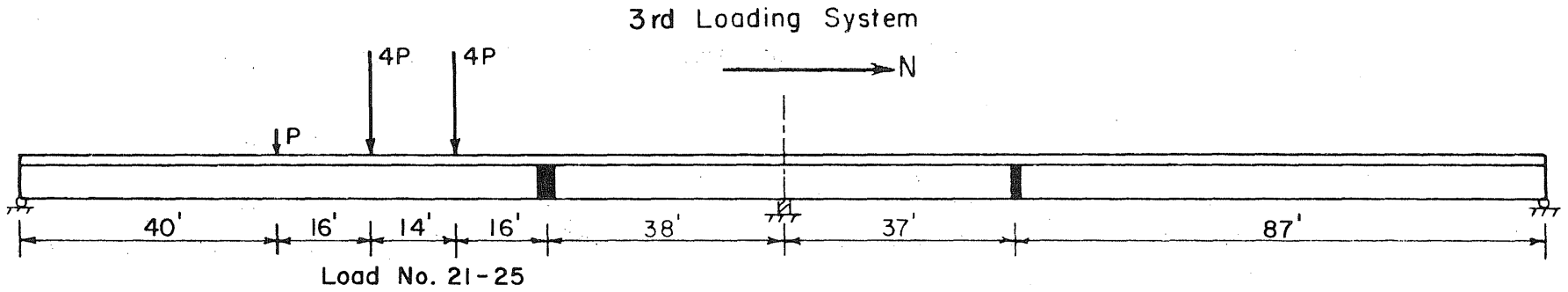

FIG. 5.6 LOCATIONS OF LOADS FOR MAXIMUM POSITIVE MOMENT, SOUTH SPAN SERVICE LOAD TEST

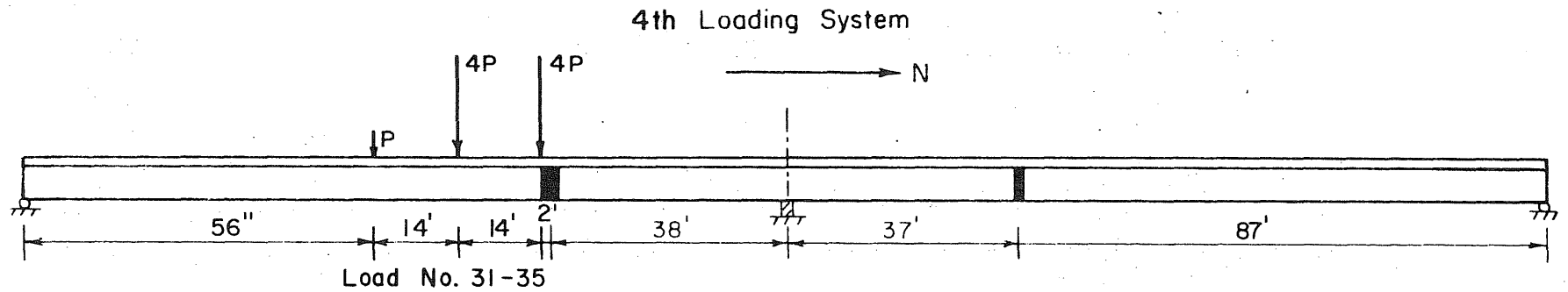

FIG. 5.7 LOCATIONS OF LOADS FOR MAXIMUM SPLICE SHEAR, SOUTH SPAN SERVICE LOAD TEST

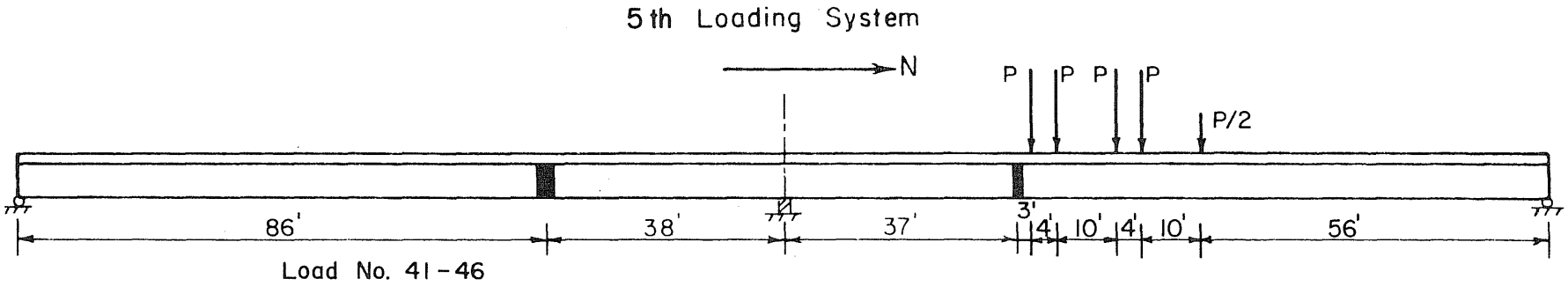

FIG. 5.8 LOCATIONS OF LOADS FOR MAXIMUM SPLICE SHEAR, NORTH SPAN DESIGN ULTIMATE LOAD TEST

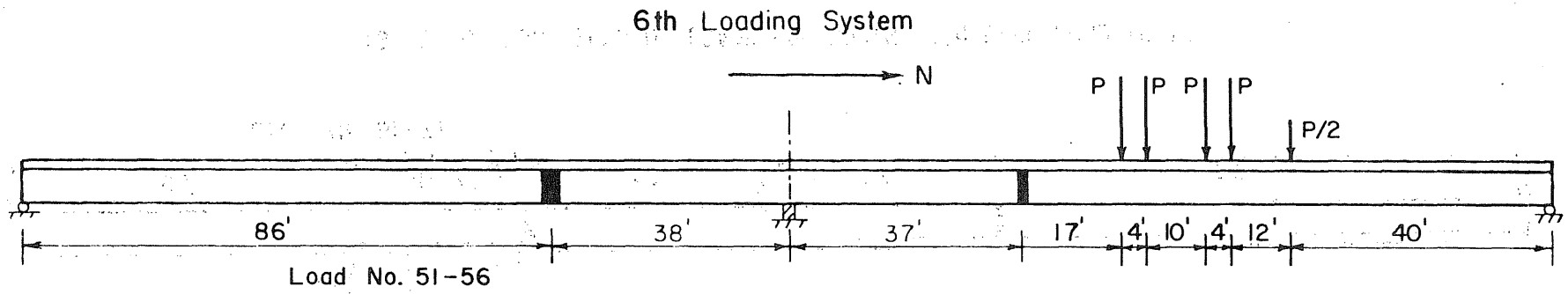

FIG. 5.9 LOCATIONS OF LOADS FOR MAXIMUM POSITIVE MOMENT, NORTH SPAN DESIGN ULTIMATE LOAD TEST

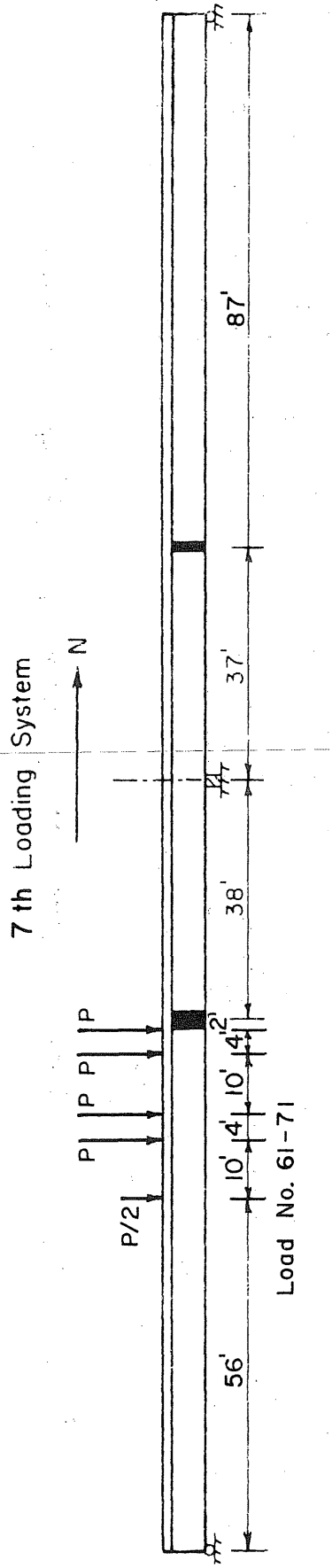

FIG. 5.10 LOCATIONS OF LOADS FOR SOUTH SPAN OVER LOAD TESTS

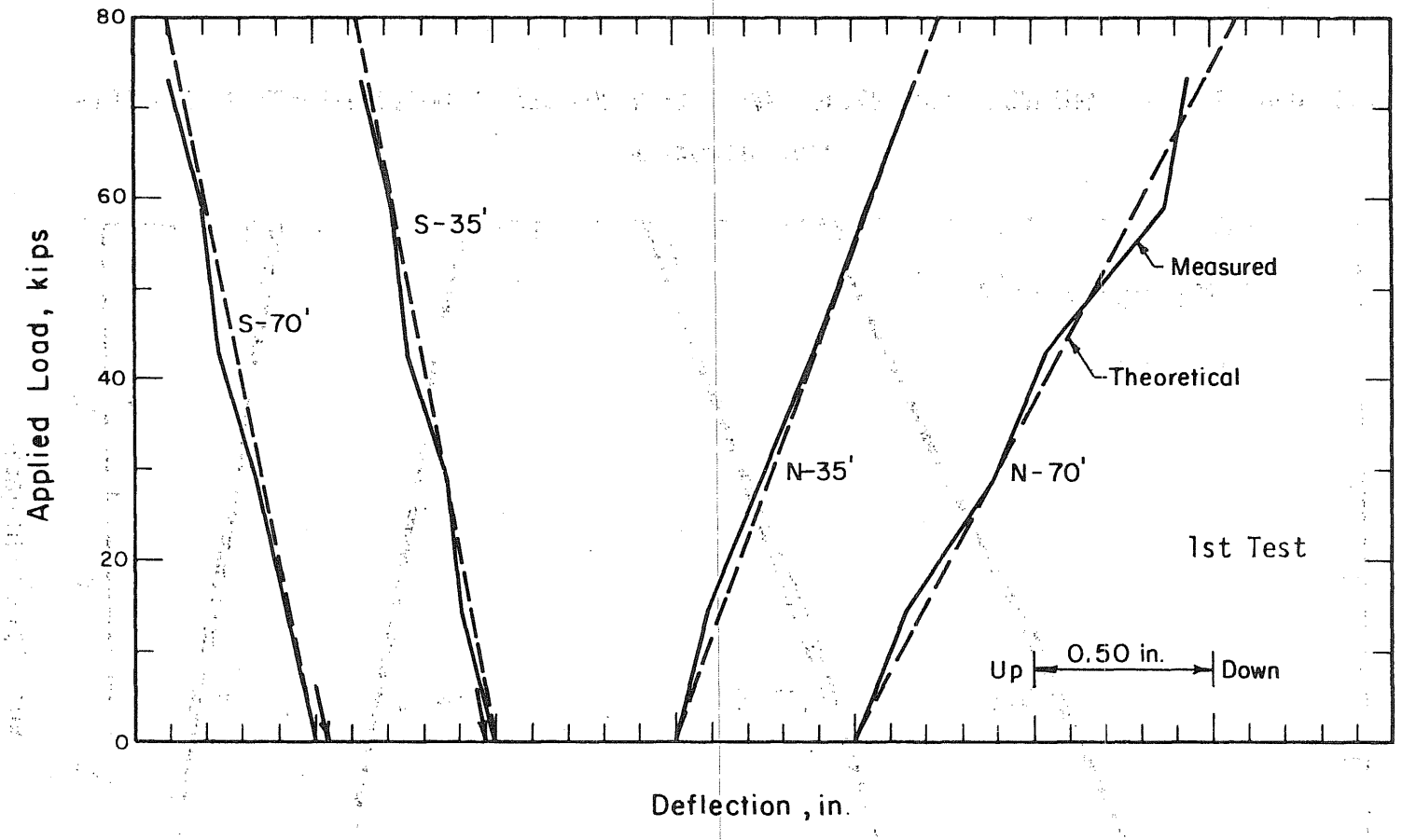

FIG. 6.1 LOAD-DEFLECTION CURVES FOR NORTH SPAN POSITIVE MOMENT LOADING, SERVICE LOAD TEST

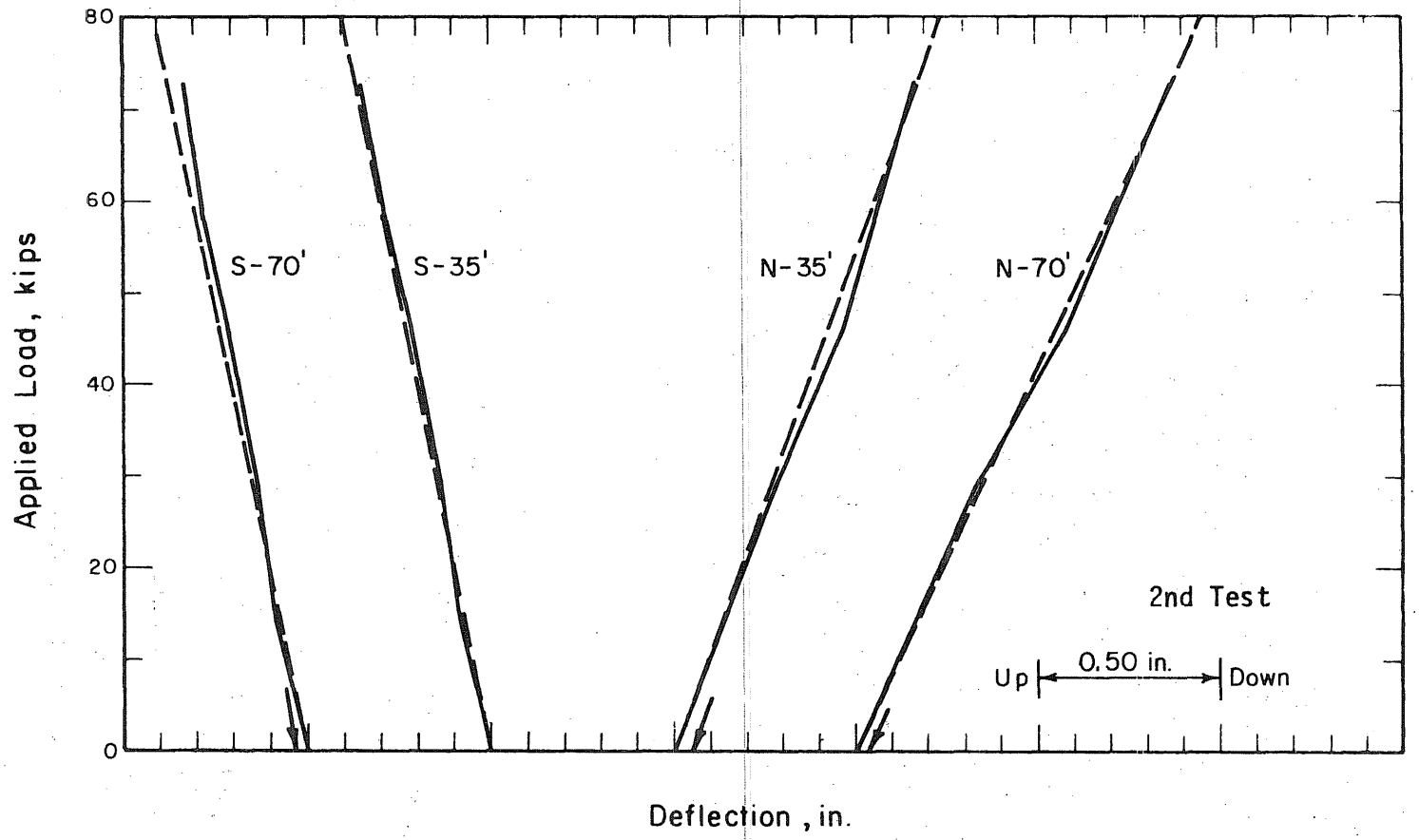

FIG. 6.2 LOAD-DEFLECTION CURVES FOR NORTH SPAN SPLICE SHEAR LOADING, SERVICE LOAD TEST

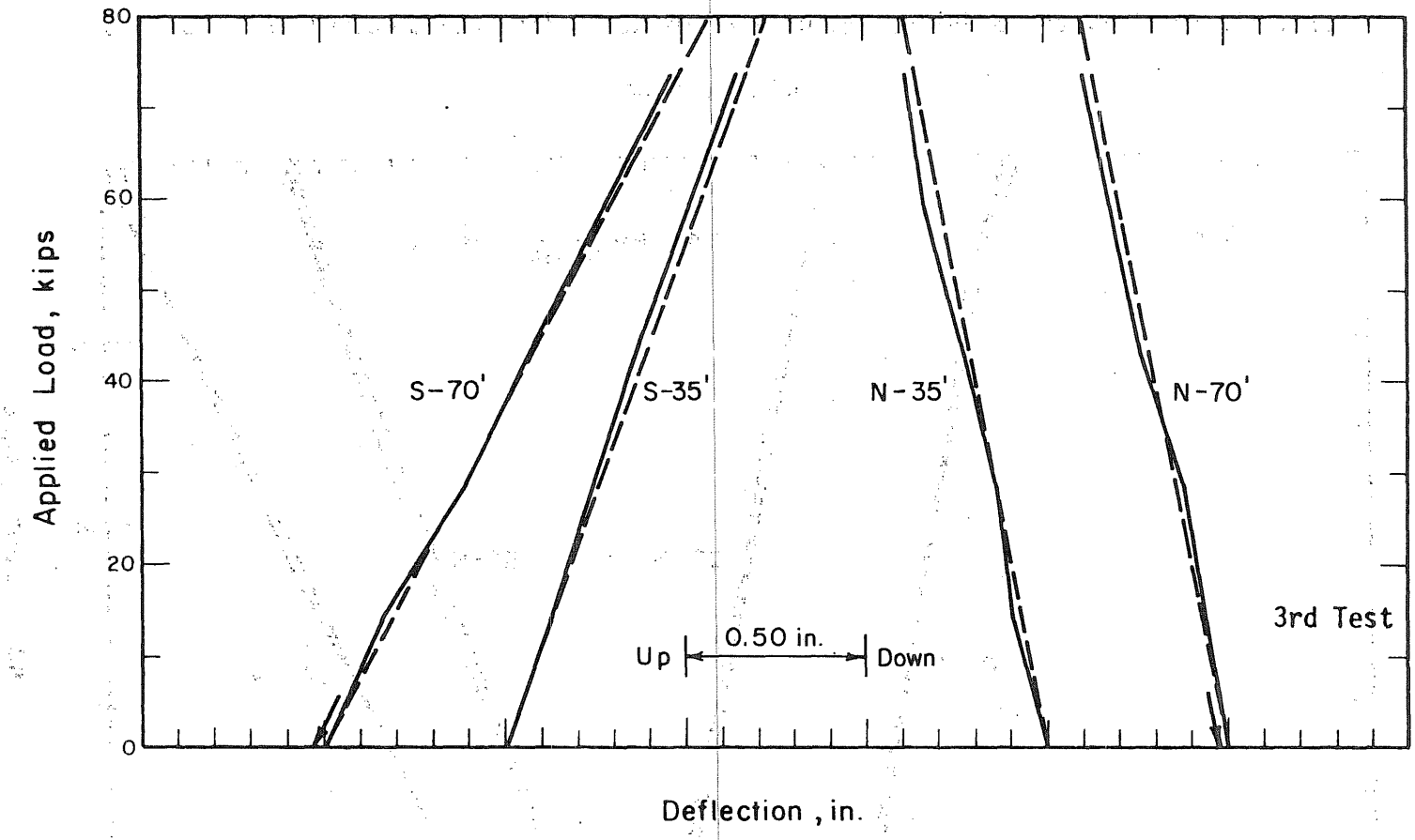

FIG. 6.3 LOAD-DEFLECTION CURVES FOR SOUTH SPAN POSITIVE MOMENT LOADING, SERVICE LOAD TEST

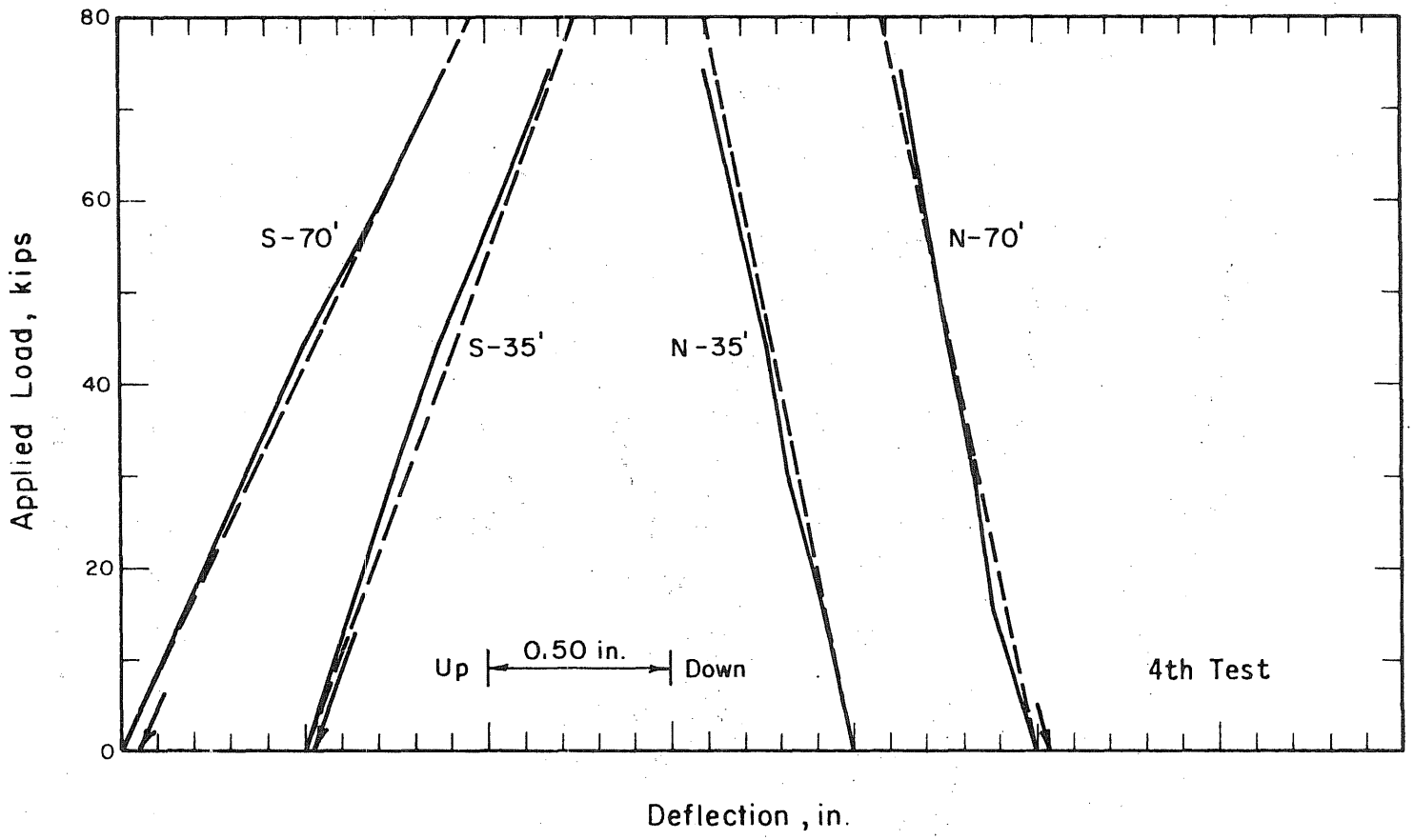

FIG. 6.4 LOAD-DEFLECTION CURVES FOR SOUTH SPAN SPLICE SHEAR LOADING, SERVICE LOAD TEST

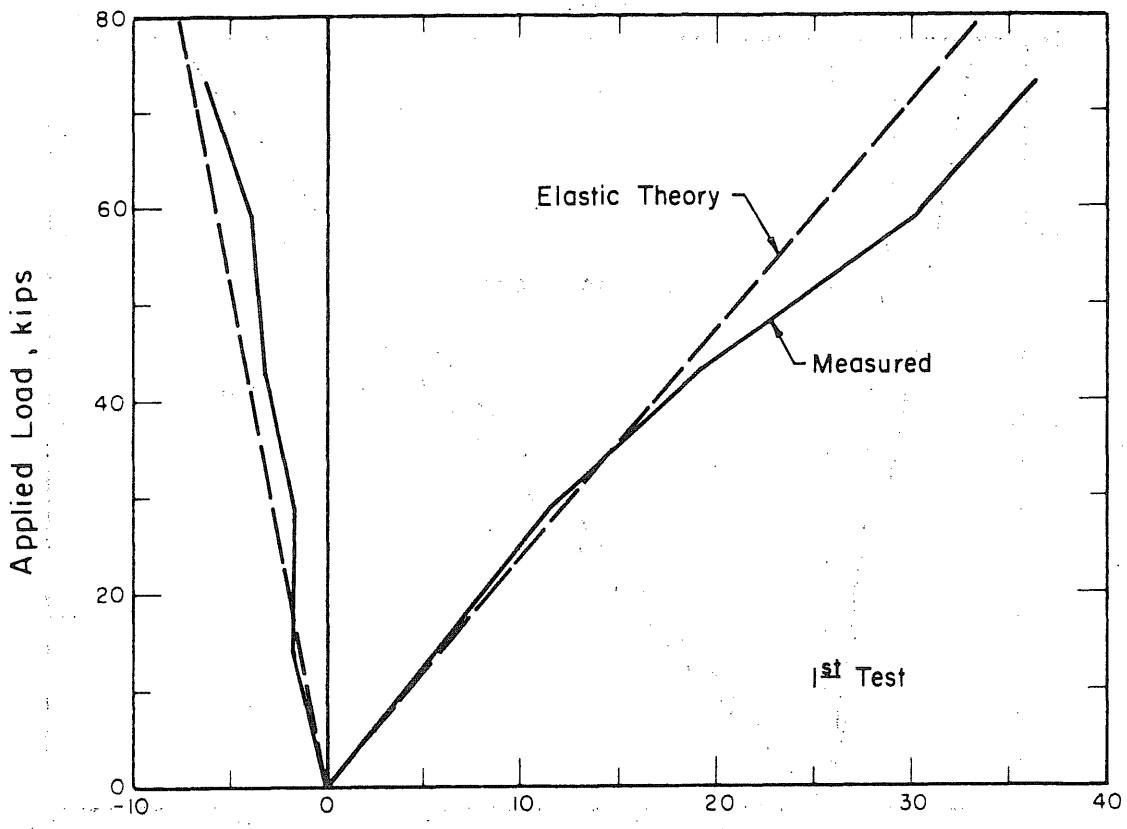

(a) Positive Moment Loading

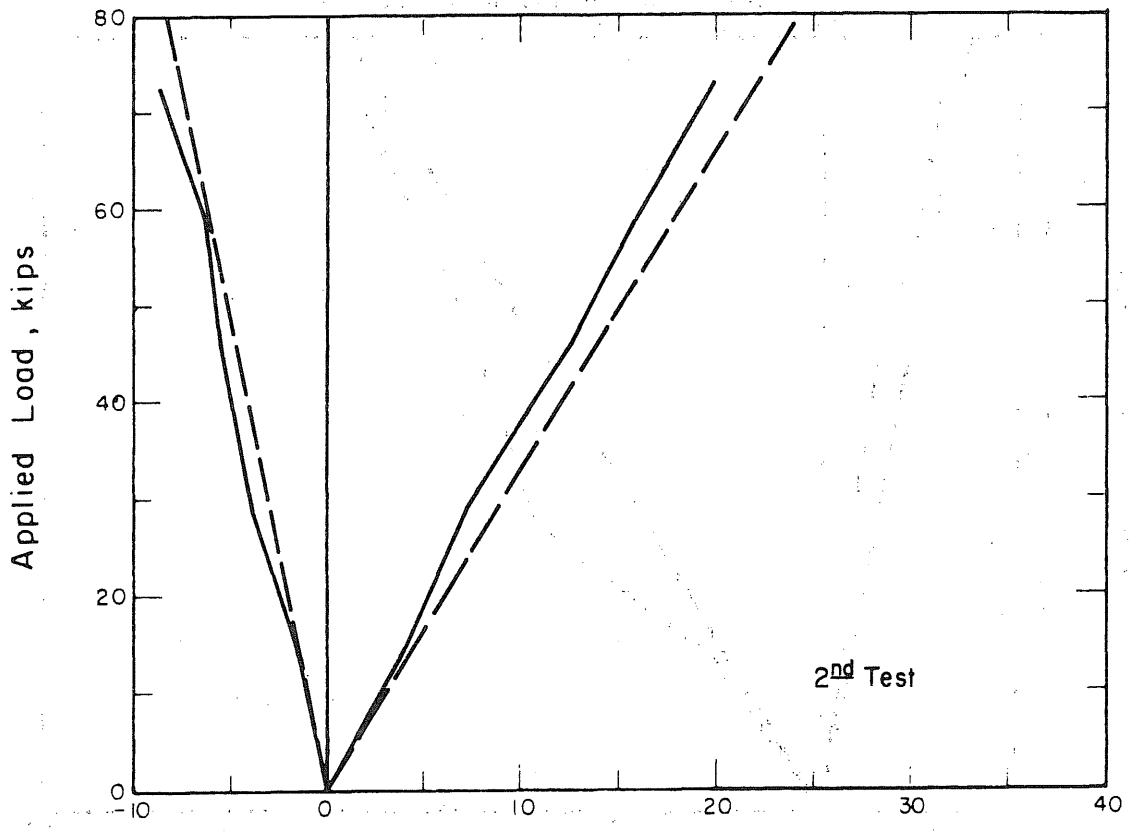

(b) Splice Shear Loading

FIG. 6.5 LOAD-REACTION CURVES FOR NORTH SPAN SERVICE LOAD TESTS

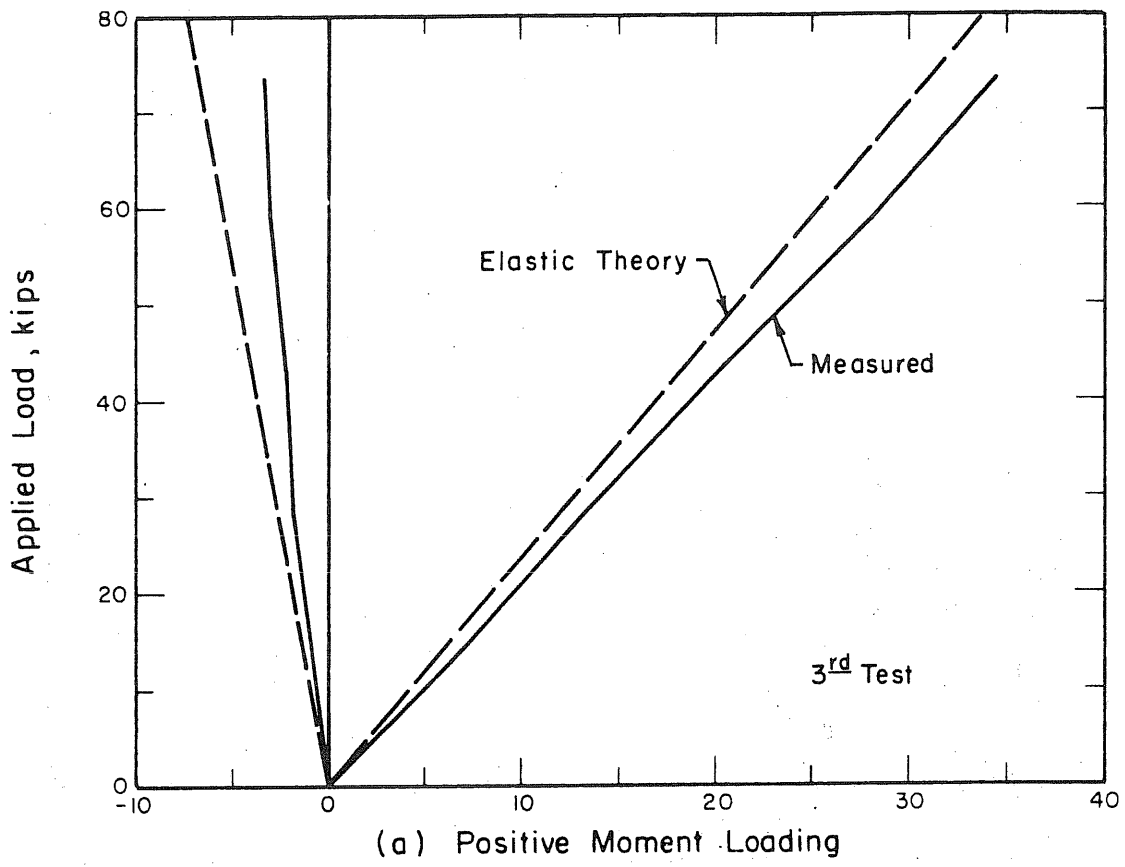

(a) Positive Moment Loading

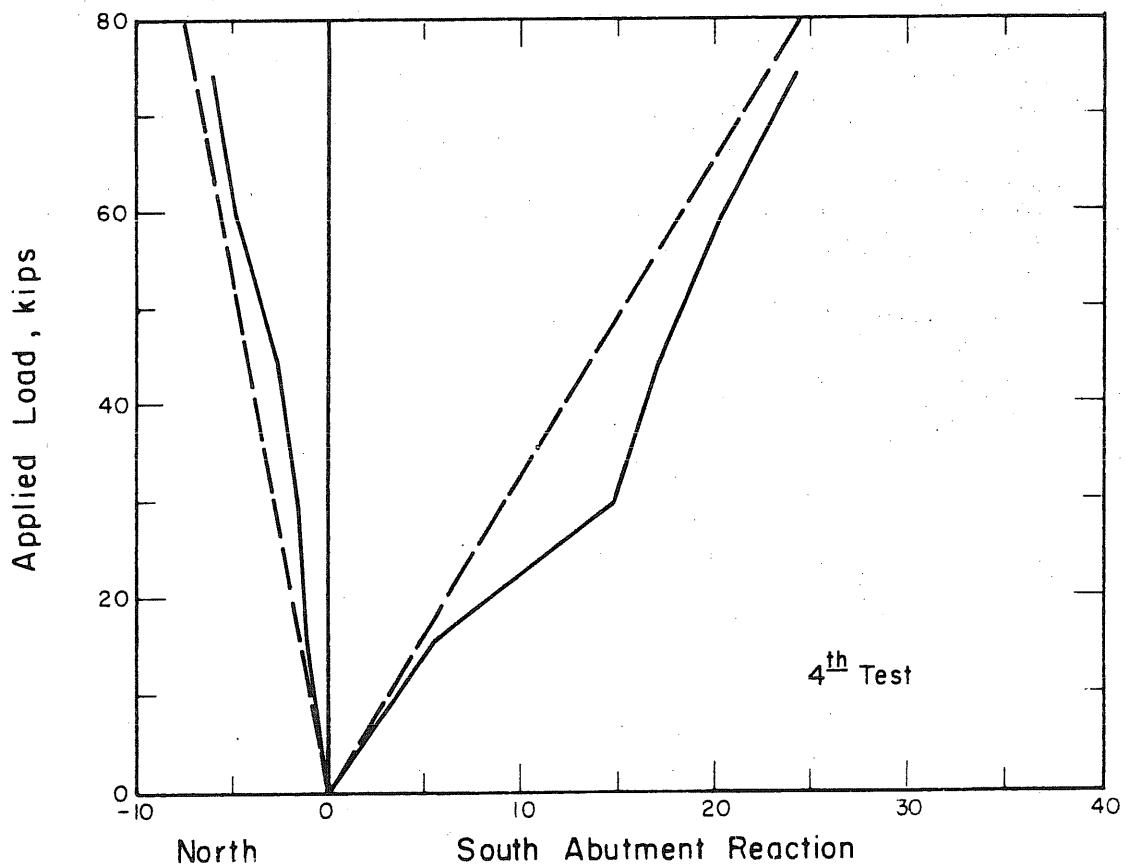

(b) Splice Shear Loading

FIG. 6.6 LOAD-REACTION CURVES FOR SOUTH SPAN SERVICE LOAD TESTS

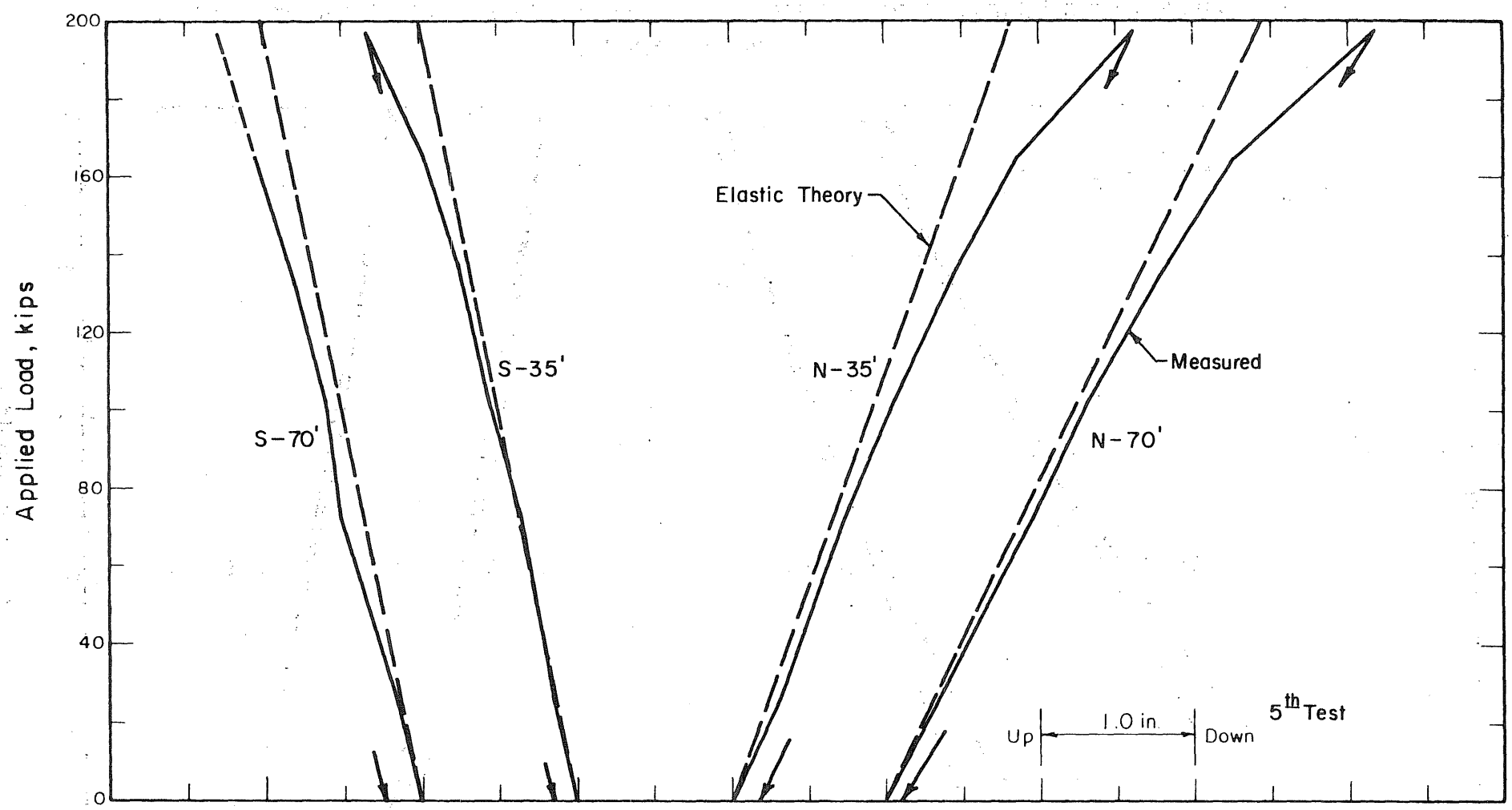

FIG. 6.7 LOAD-DEFLECTION CURVES FOR NORTH SPAN SPLICE SHEAR LOADING, DESIGN ULTIMATE TEST

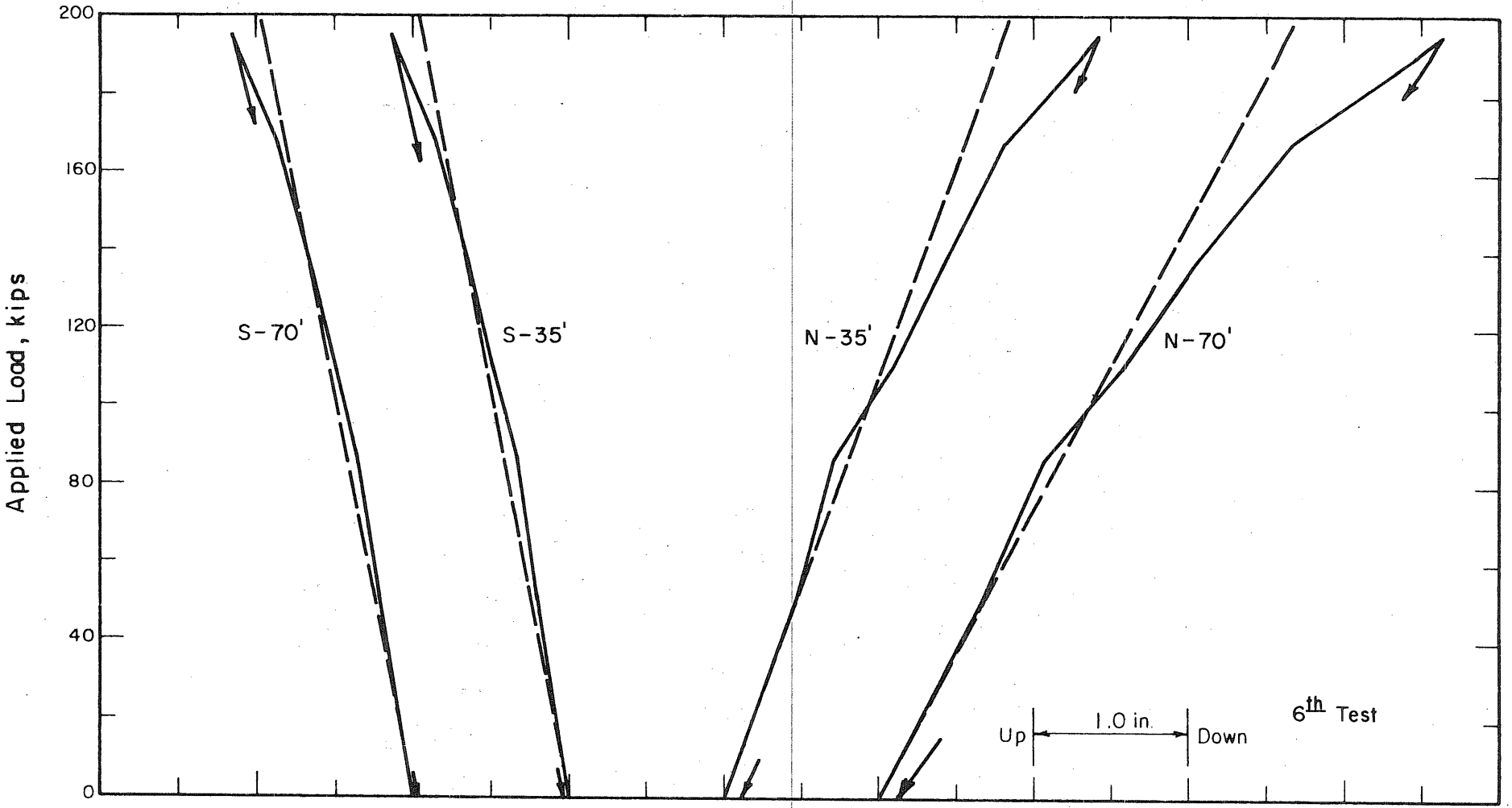

FIG. 6.8 LOAD-DEFLECTION CURVES FOR NORTH SPAN POSITIVE MOMENT LOADING, DESIGN ULTIMATE TEST

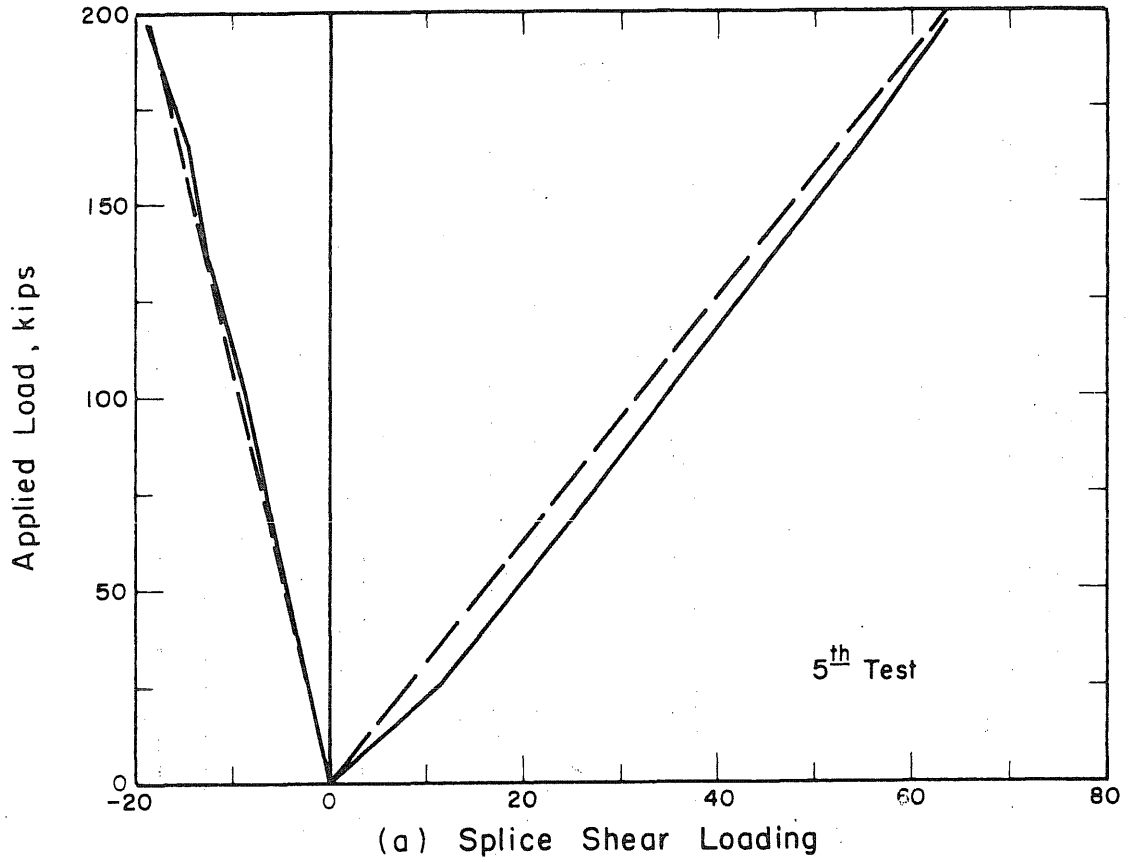

(a) Splice Shear Loading

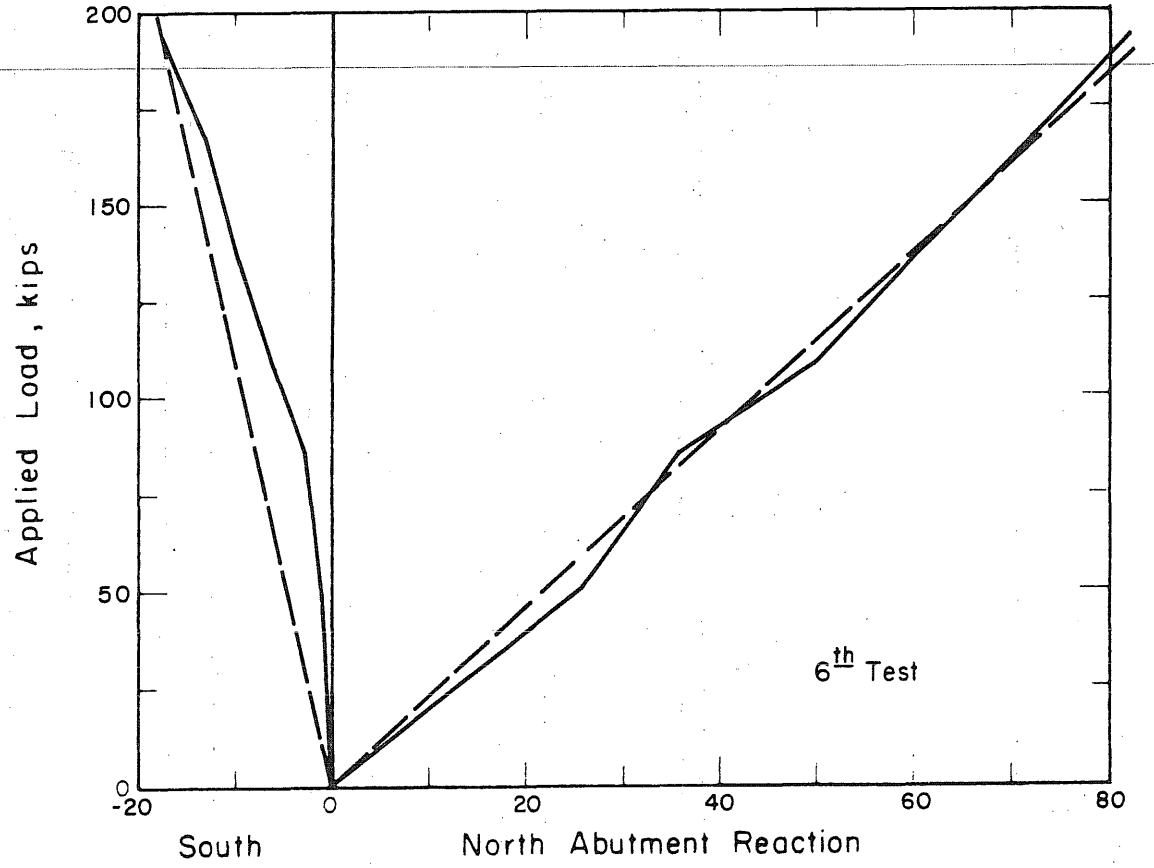

(b) Positive Moment Loading

FIG. 6.9 LOAD-REACTION CURVES FOR NORTH SPAN DESIGN ULTIMATE LOAD TESTS

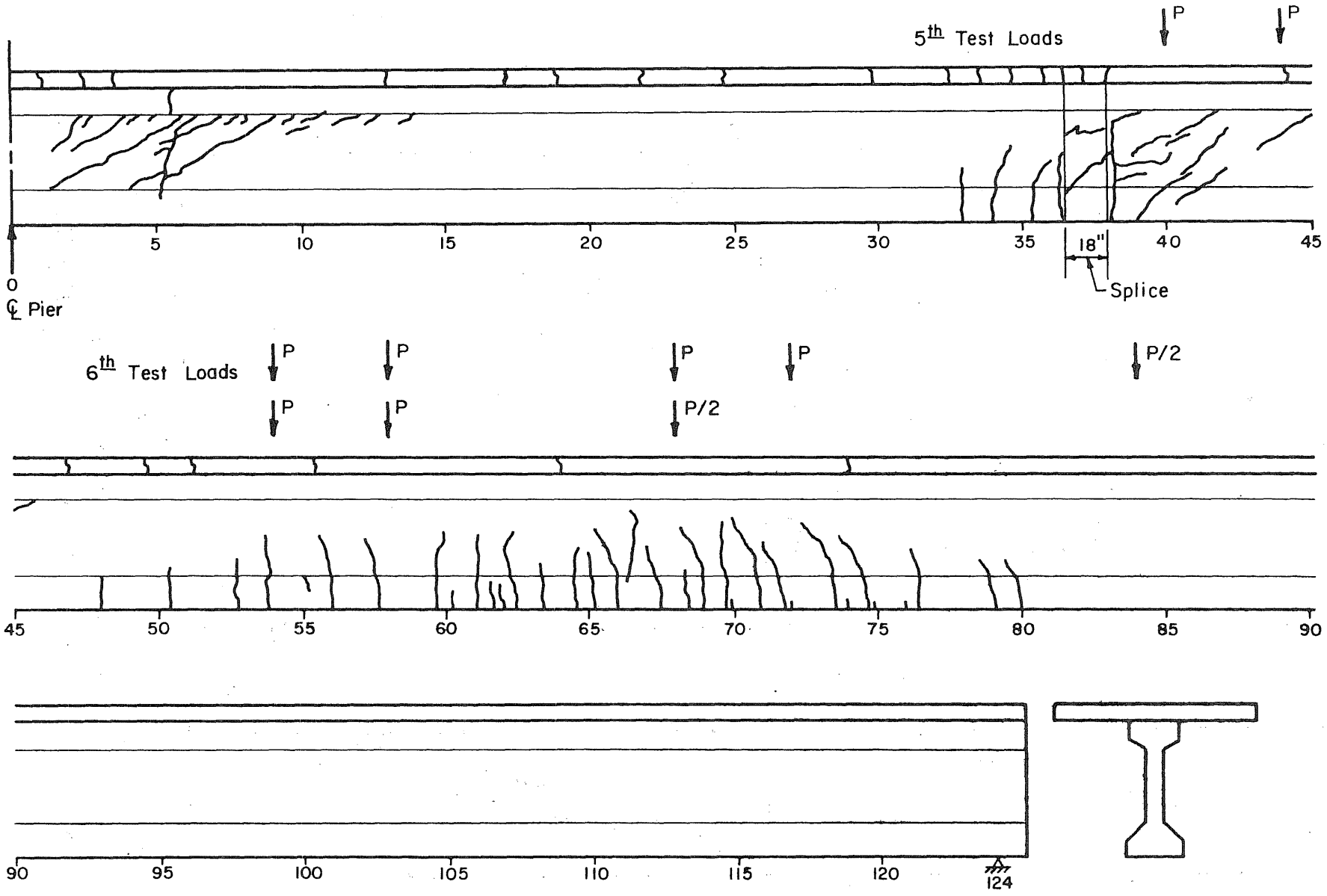

FIG. 6.10 CRACKING IN NORTH SPAN AFTER COMPLETION OF TESTING

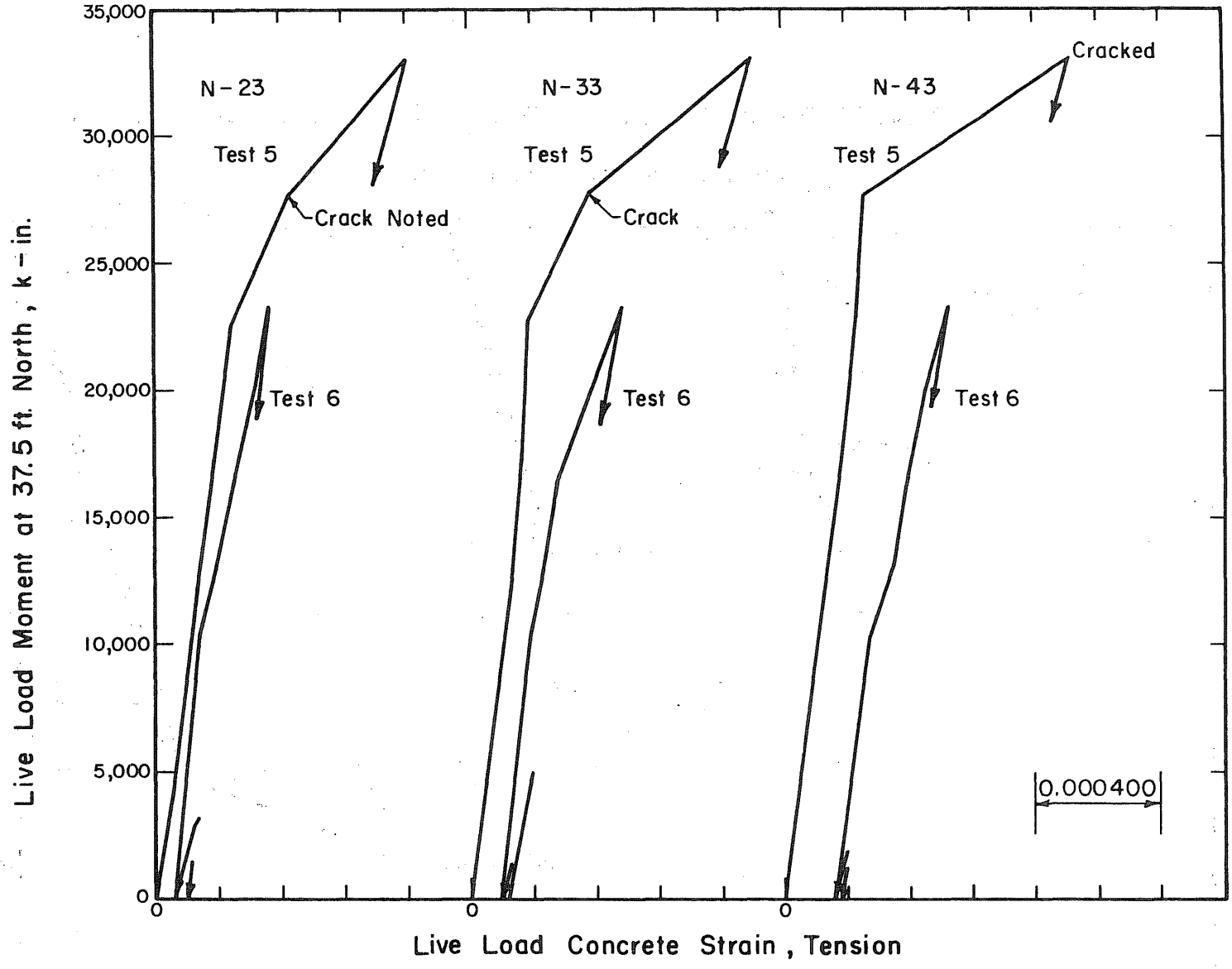

FIG. 6.11 MOMENT-CONCRETE STRAIN CURVES FOR SECTIONS NEAR SPLICE, NORTH SPAN DESIGN ULTIMATE LOAD TESTS

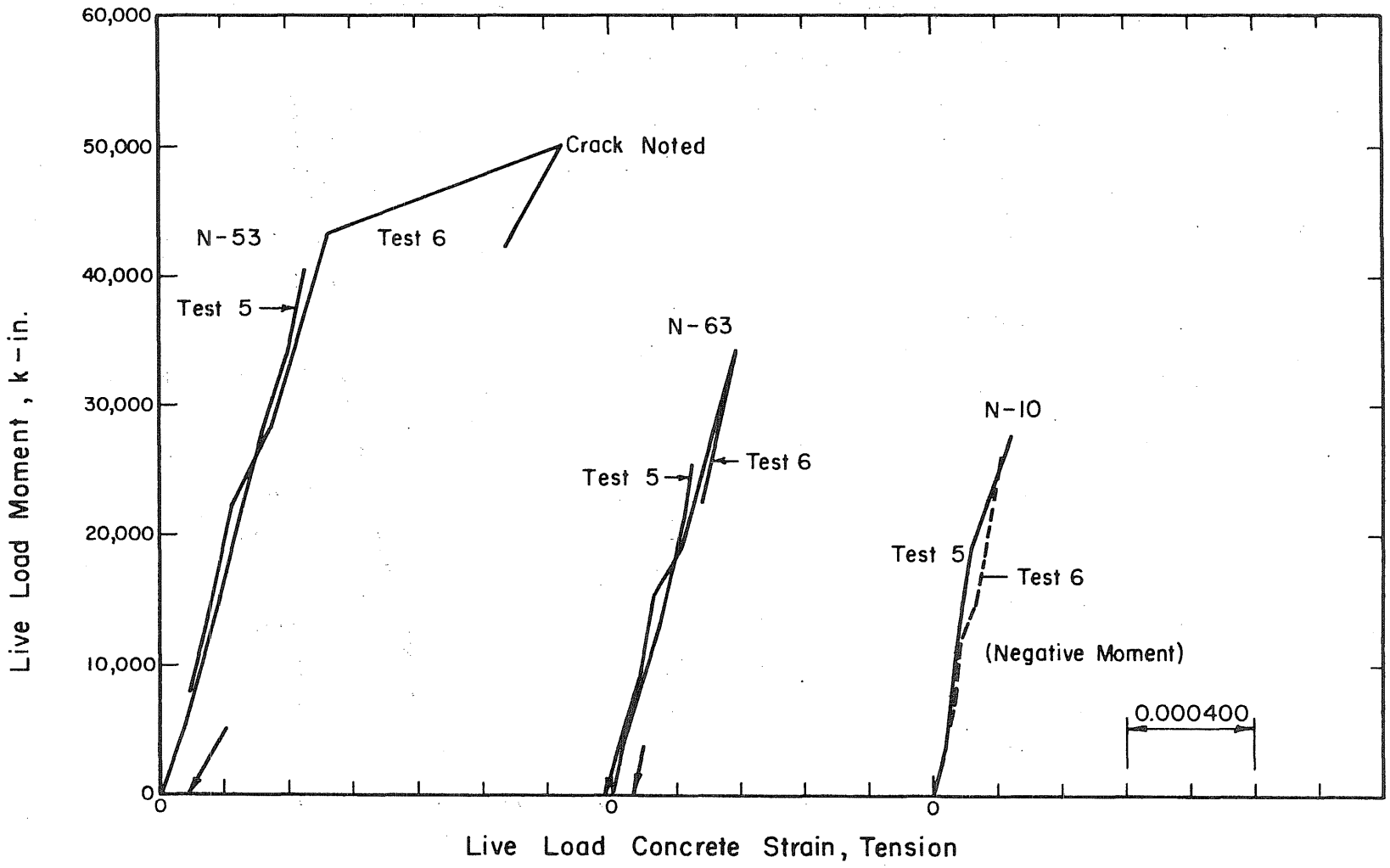

FIG. 6.12 MOMENT-CONCRETE STRAIN CURVES, NORTH SPAN DESIGN ULTIMATE LOAD TESTS

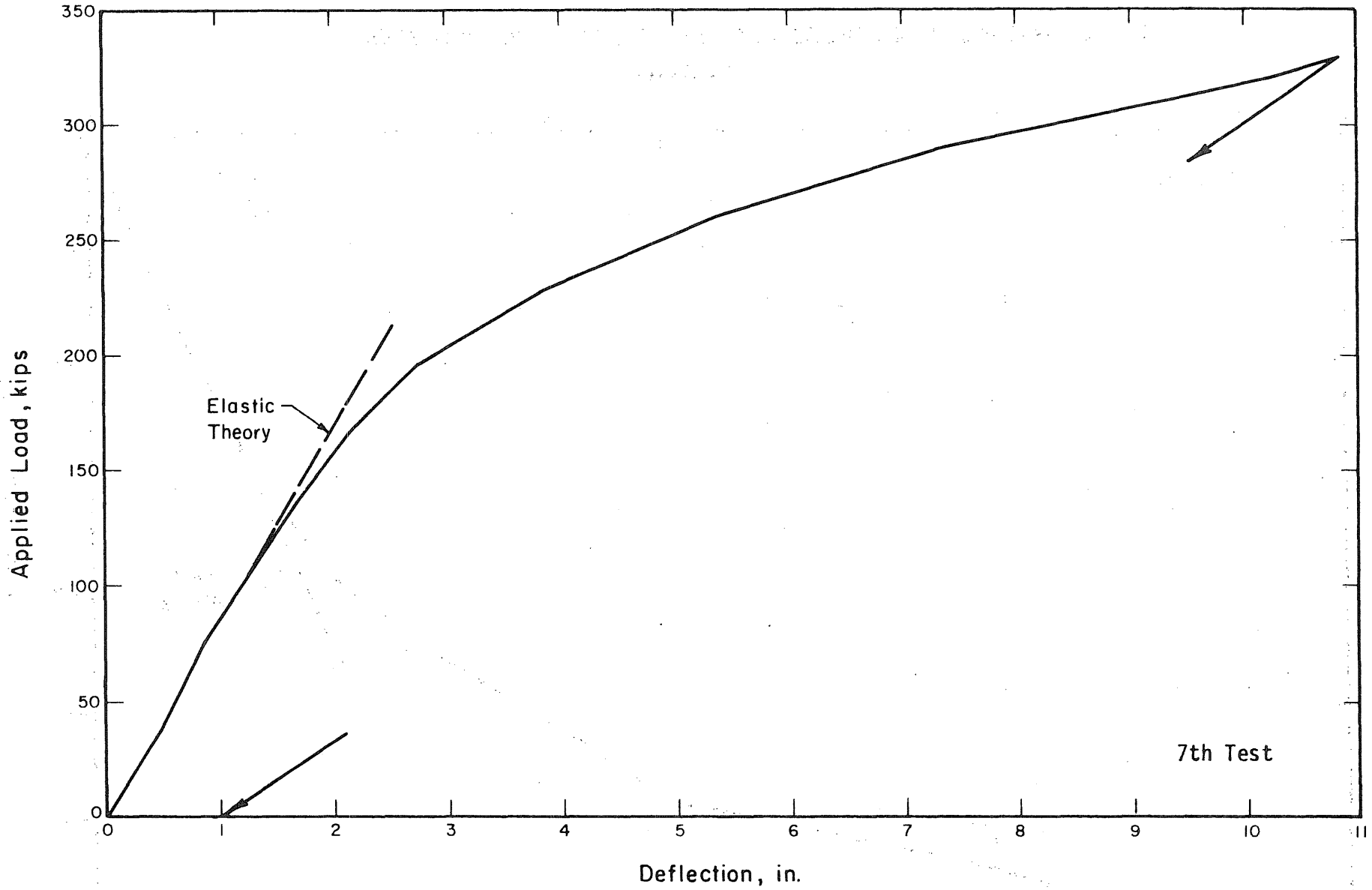

FIG. 6.13 LOAD-DEFLECTION CURVE FOR POINT AT 70 FT SOUTH, SOUTH SPAN OVERLOAD TEST

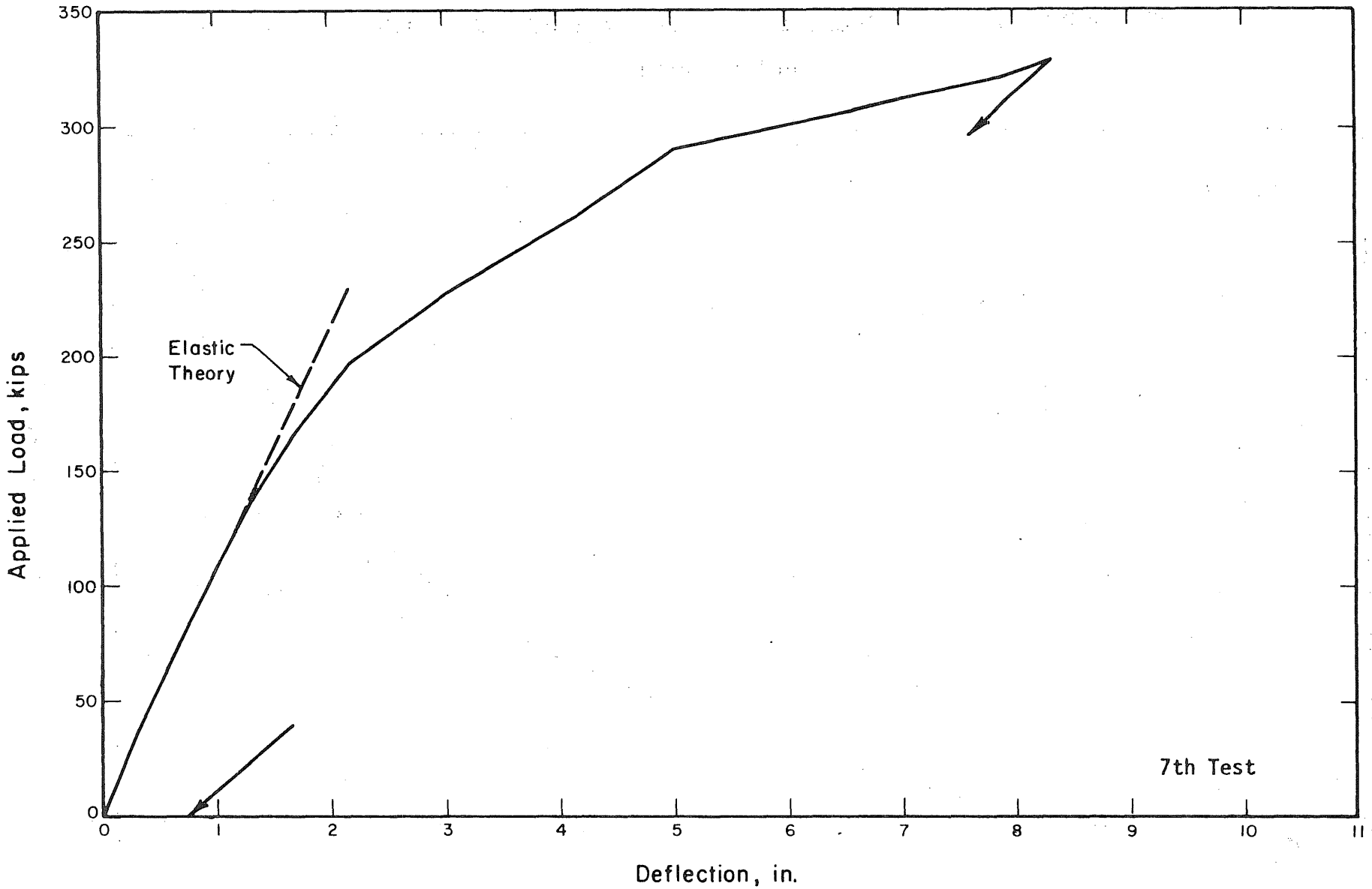

FIG. 6.14 LOAD-DEFLECTION CURVE FOR POINT AT 35 FT SOUTH, SOUTH SPAN OVERLOAD TEST

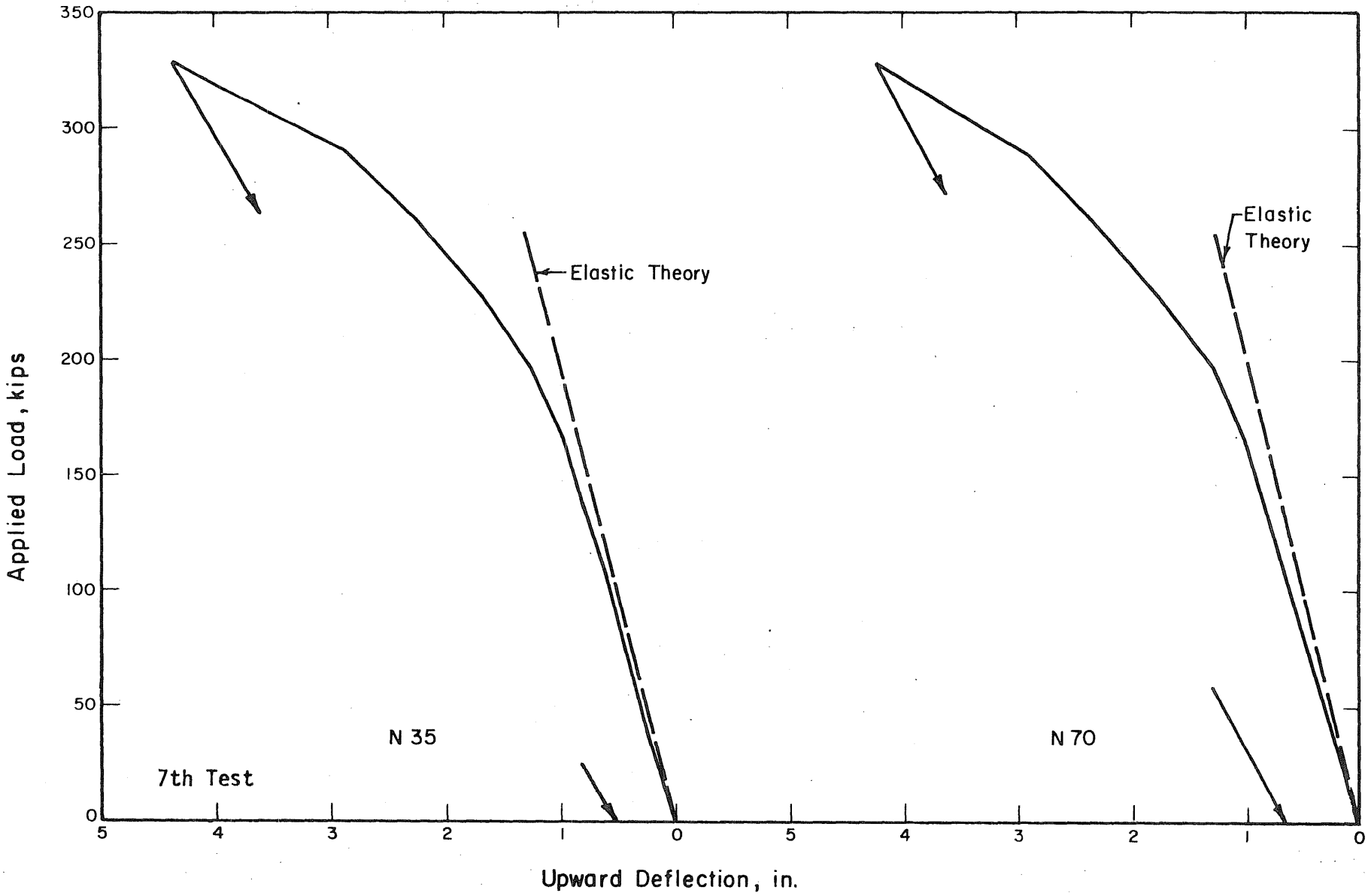

FIG. 6.15 LOAD-DEFLECTION CURVES FOR NORTH SPAN POINTS, SOUTH SPAN OVERLOAD TEST

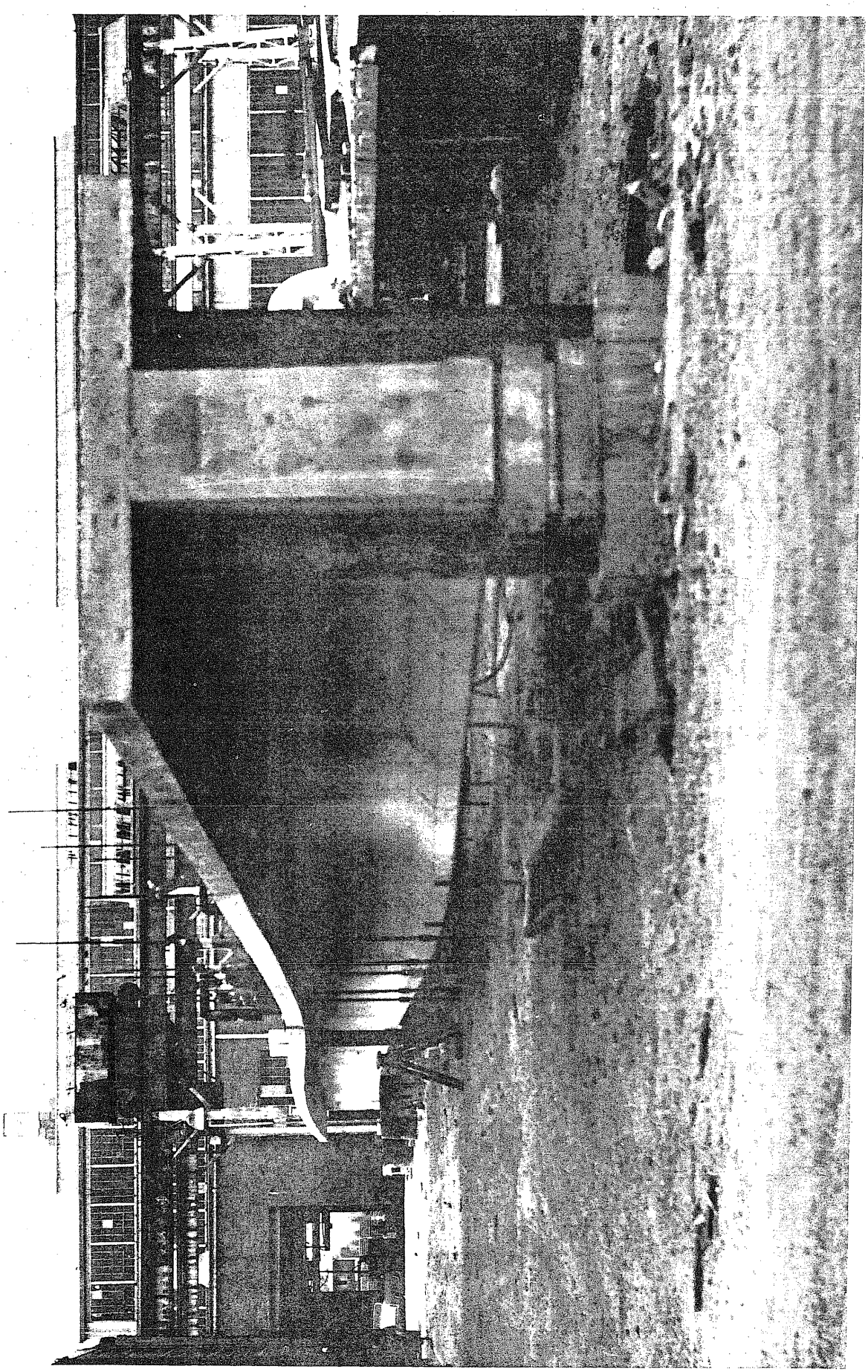

FIG. 6.16 PHOTOGRAPH OF TEST STRUCTURE NEAR END OF SOUTH SPAN OVERLOAD TEST

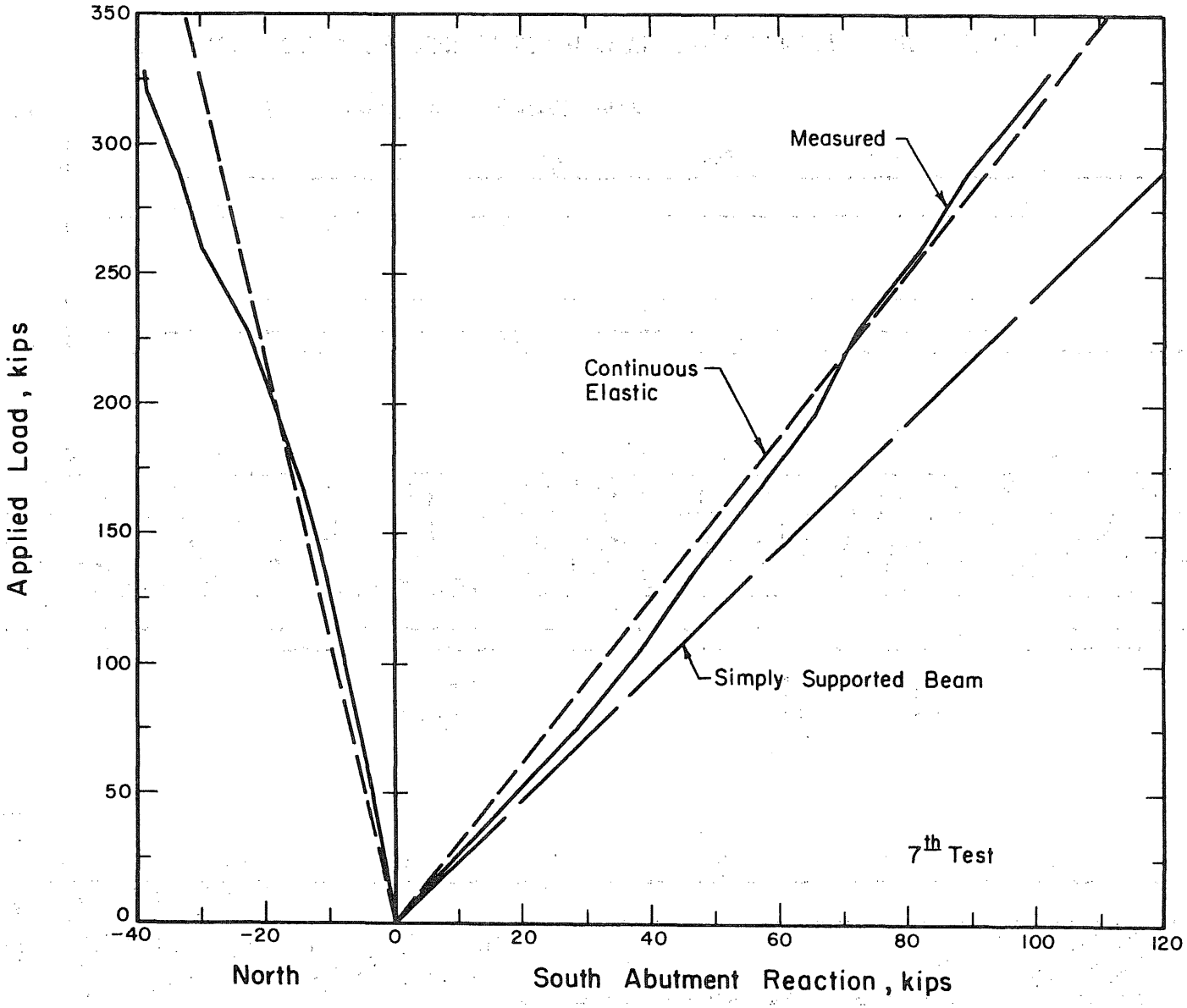

FIG. 6.17 LOAD-REACTION CURVES FOR SOUTH SPAN OVERLOAD TEST

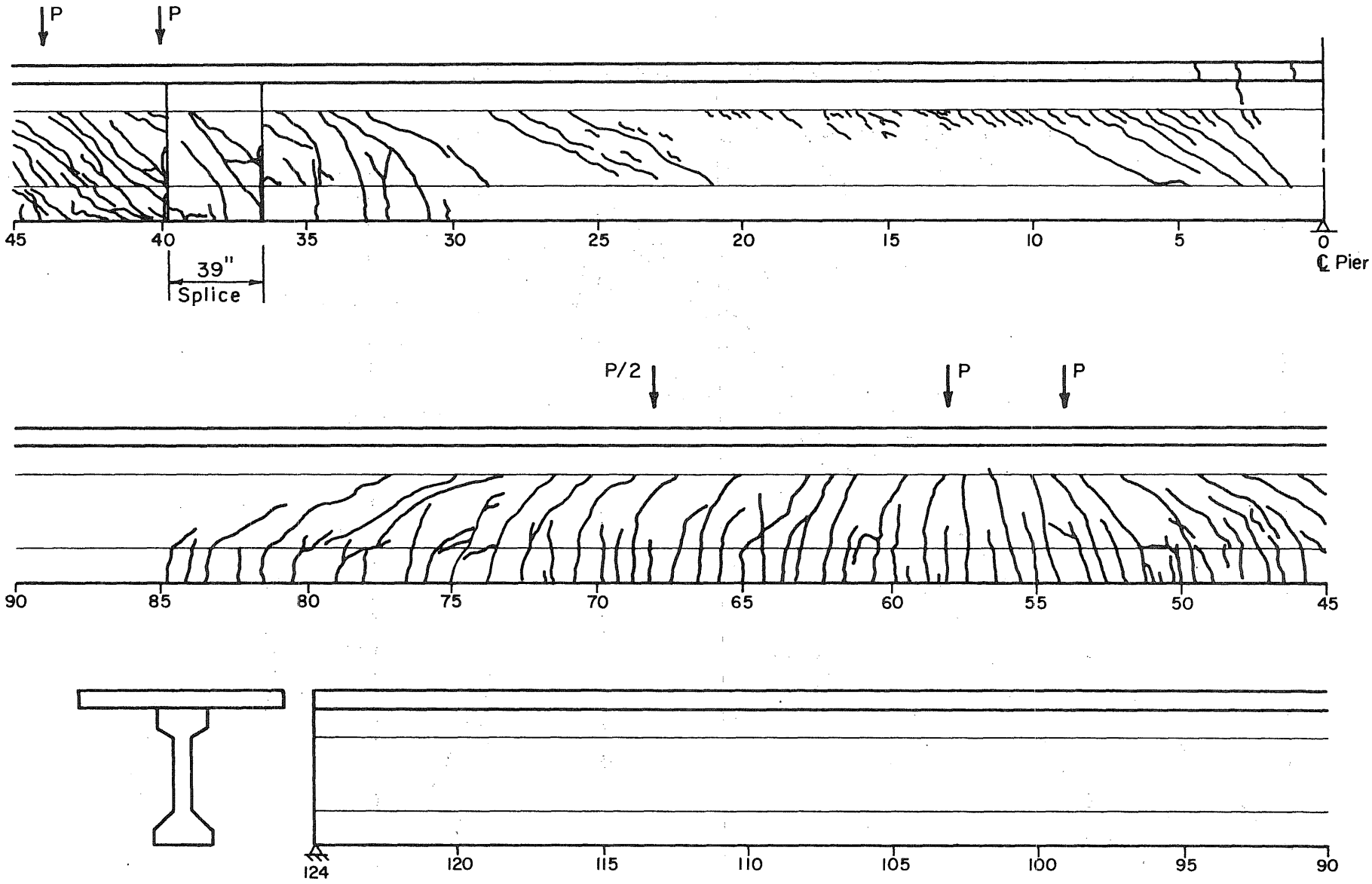

FIG. 6.18 CRACK PATTERN IN SOUTH SPAN AFTER COMPLETION OF TESTING

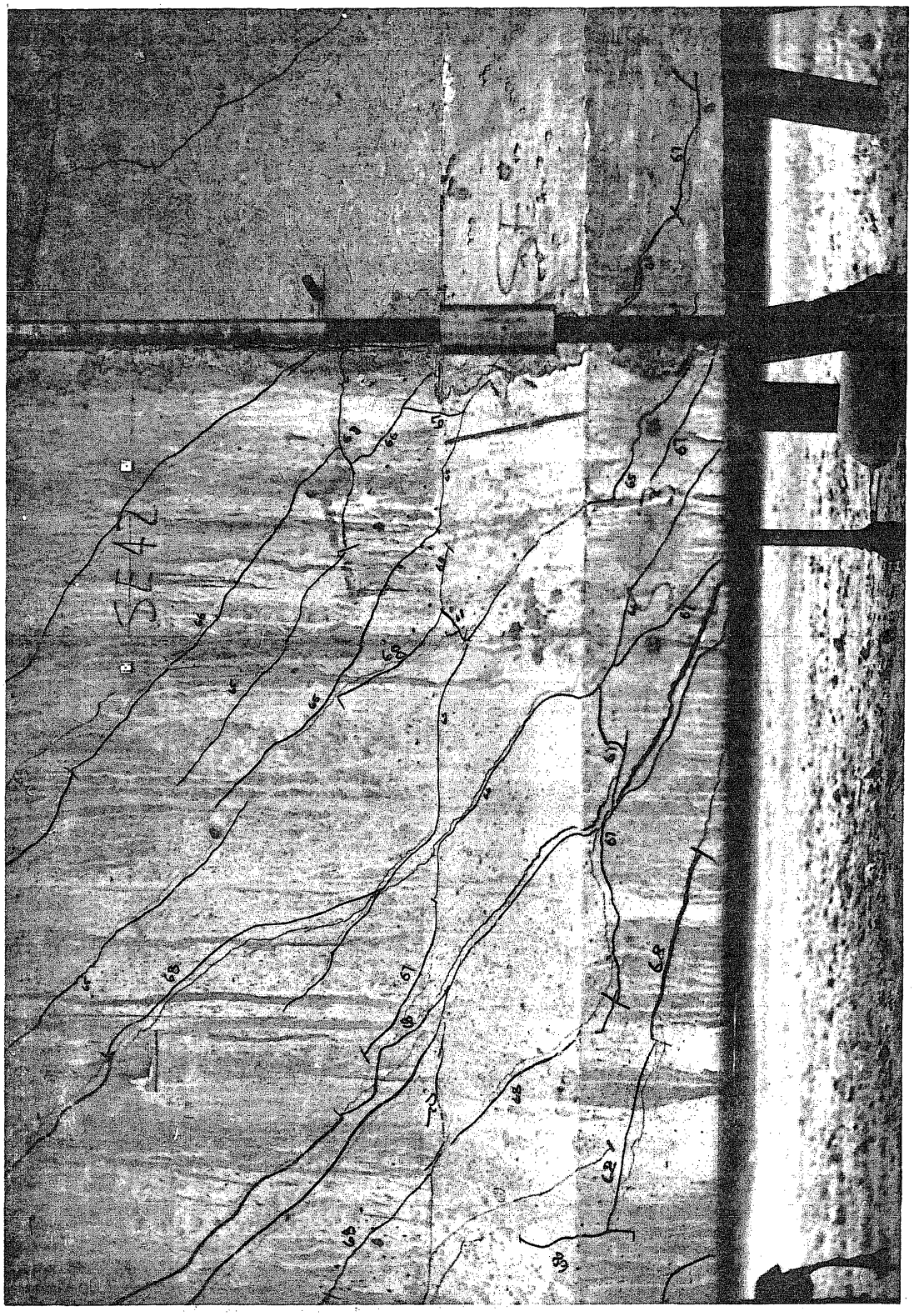

FIG. 6.19 PHOTOGRAPH OF CRACKING SOUTH OF SOUTH SPLICE, LOAD 69,
SOUTH SPAN OVERLOAD TEST

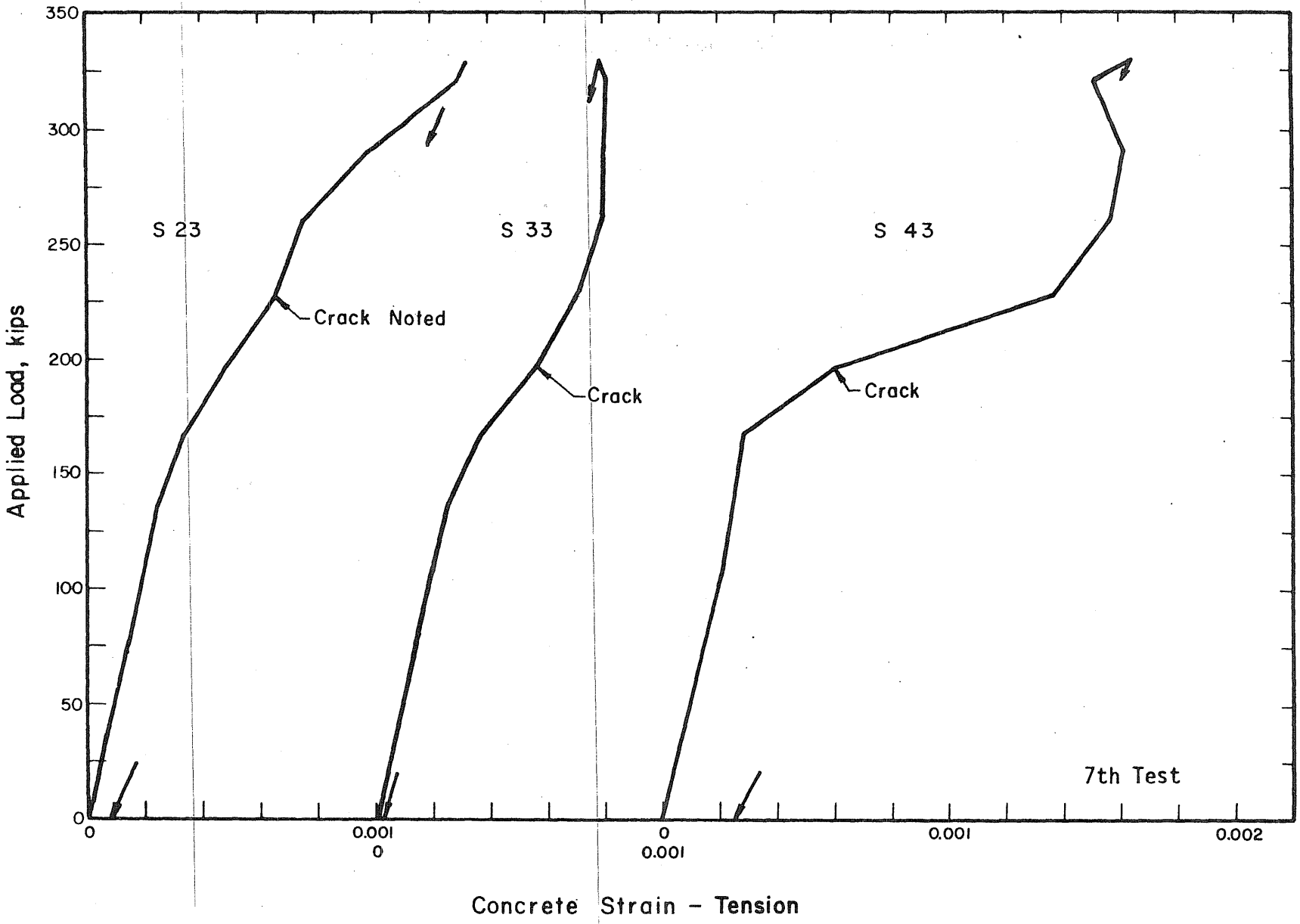

FIG. 6.20 LOAD-CONCRETE STRAIN CURVES FOR BOTTOM GAGE LINES NEAR SOUTH SPICE, SOUTH SPAN OVERLOAD TEST

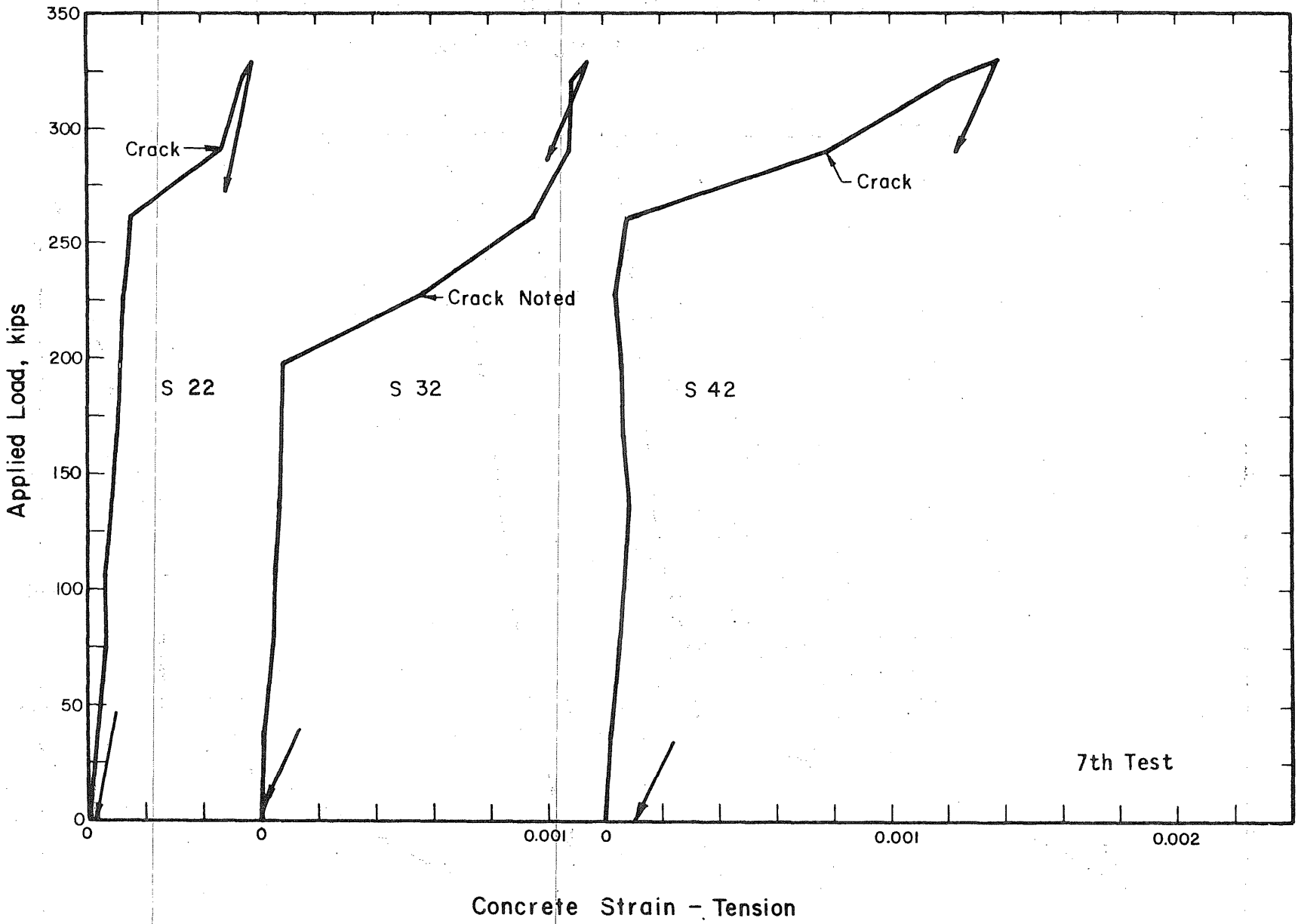

FIG. 6.21 LOAD-CONCRETE STRAIN CURVES FOR MIDDLE GAGE LINES NEAR SOUTH SPLICE, SOUTH SPAN OVERLOAD TEST

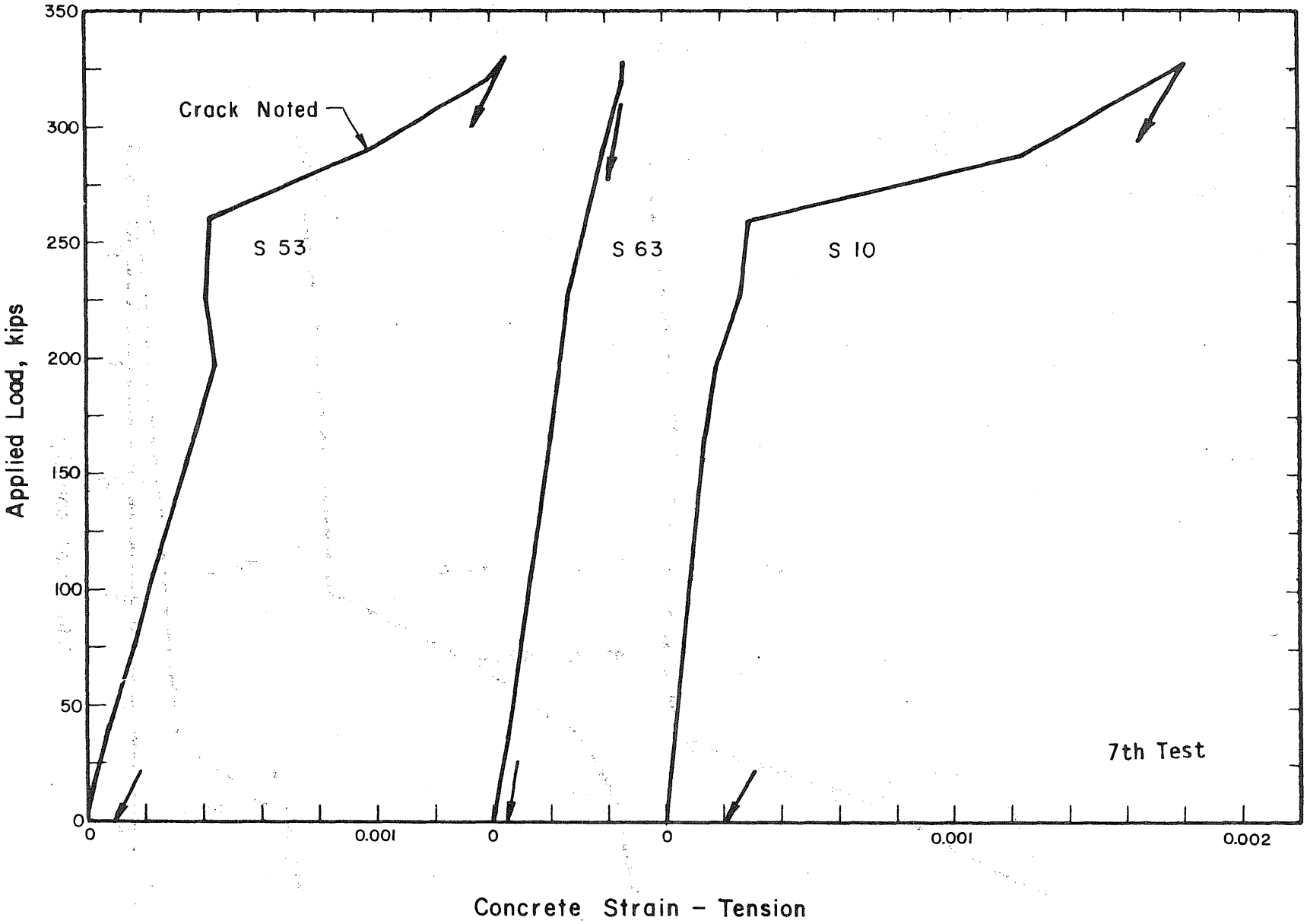

FIG. 6.22 LOAD-CONCRETE STRAIN CURVES FOR SOUTH SPAN GAGE LINES, SOUTH SPAN OVERLOAD TESTS

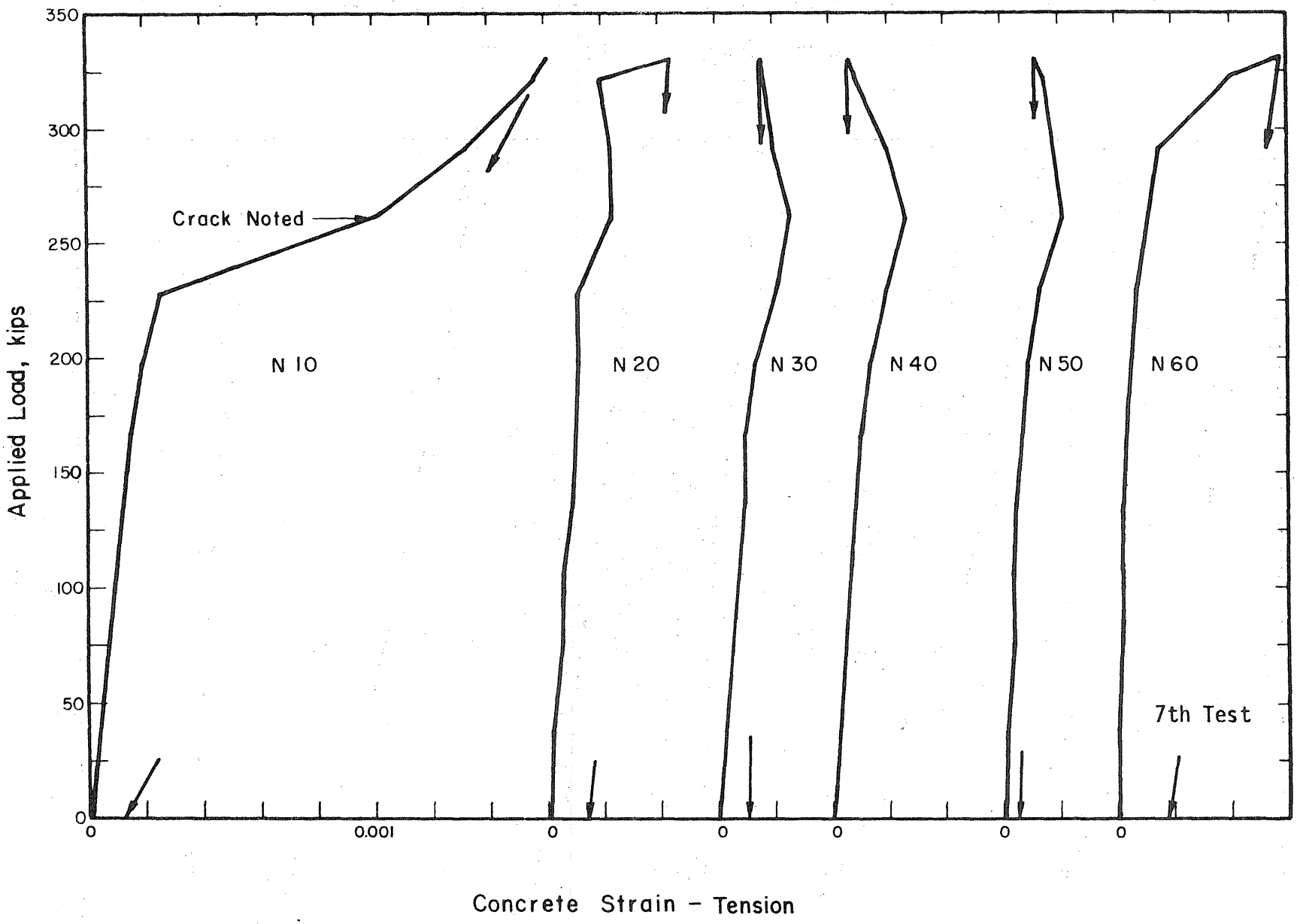

FIG. 6.23 LOAD-CONCRETE STRAIN CURVES FOR TOP OF DECK IN NORTH SPAN, SOUTH SPAN OVERLOAD TEST

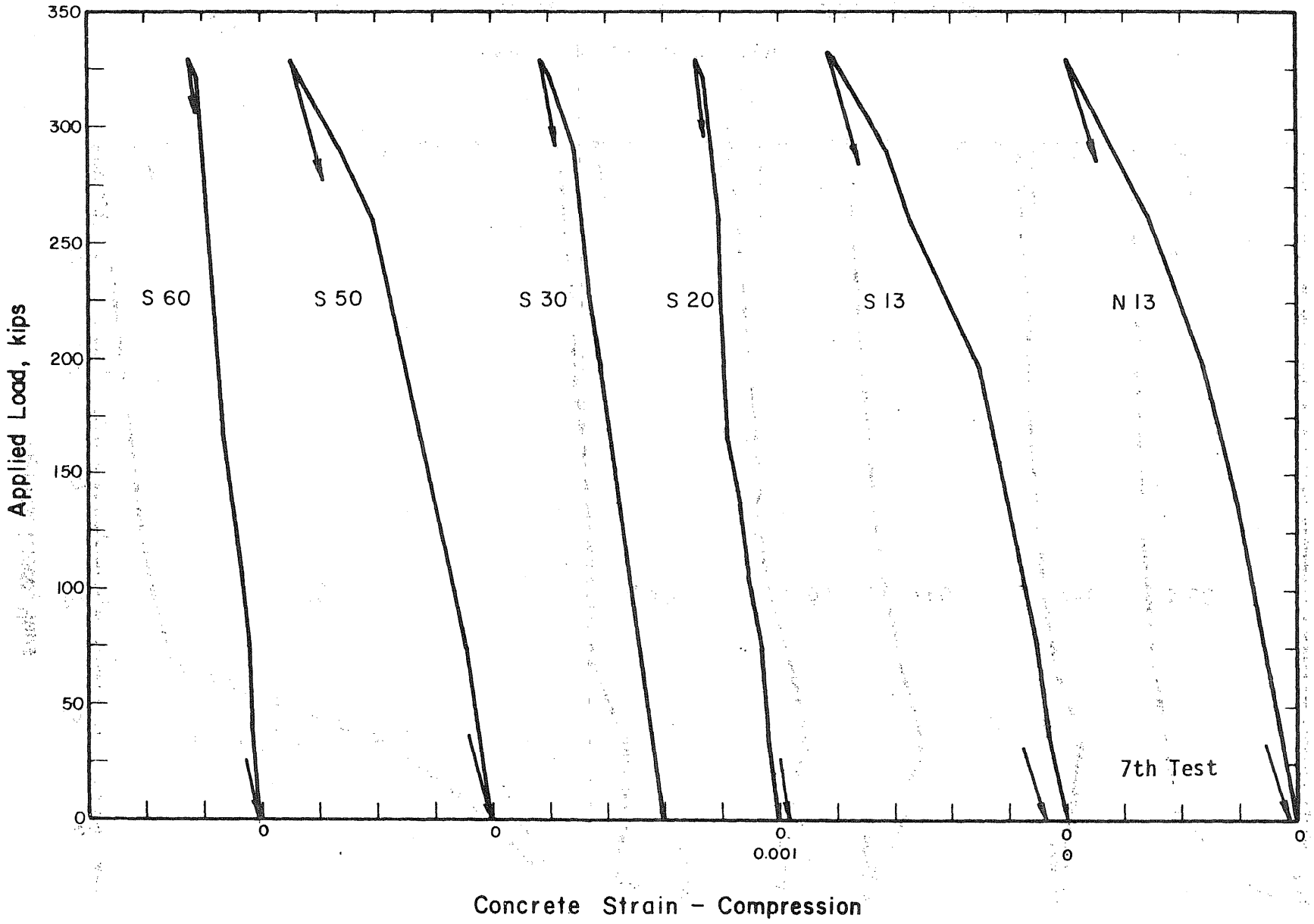

FIG. 6.24 LOAD-CONCRETE STRAIN CURVES FOR SOUTH SPAN DECK AND BOTTOM OF GIRDER AT CENTRAL PIER, SOUTH SPAN OVERLOAD TEST

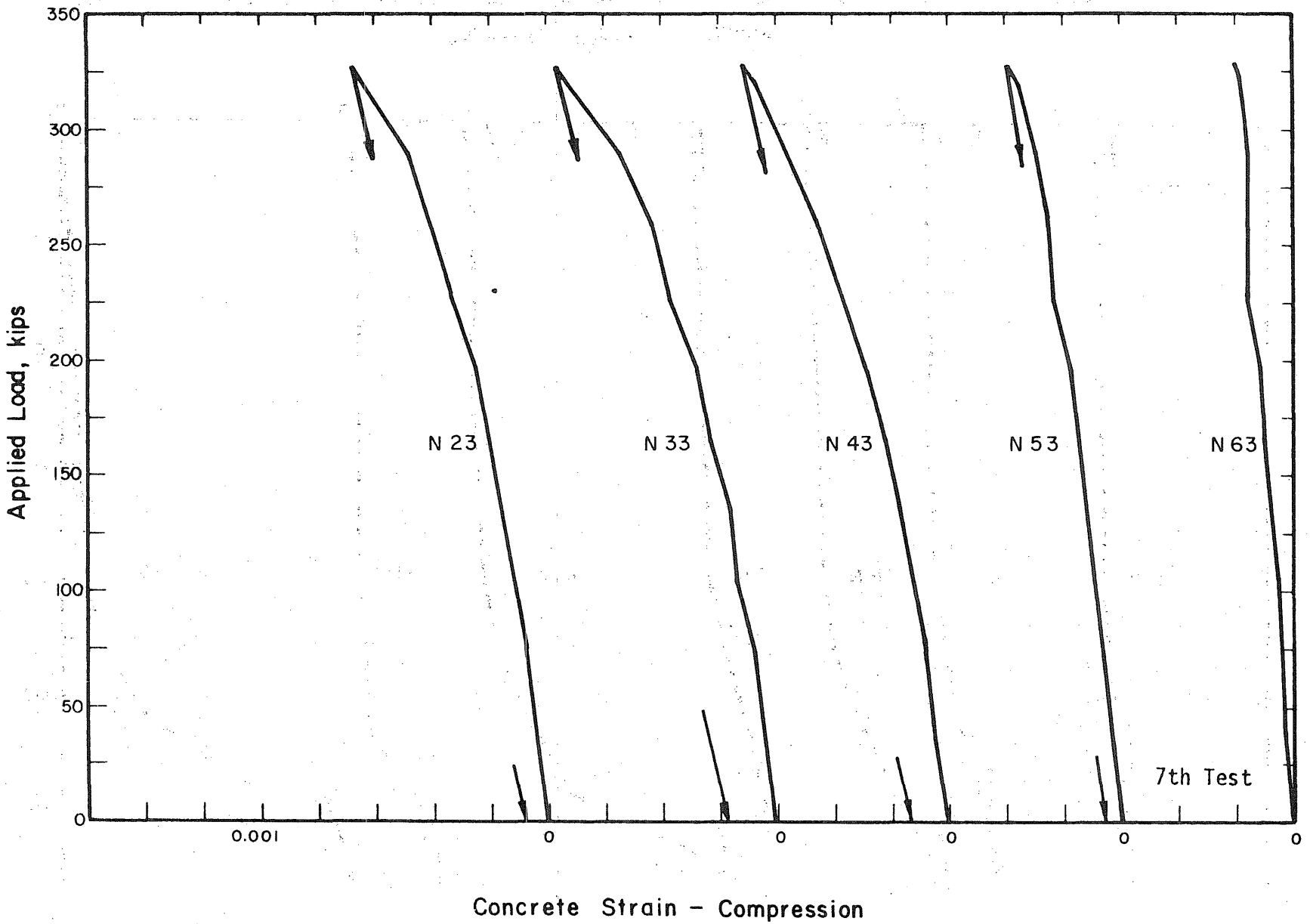

FIG. 6.25 LOAD-CONCRETE STRAIN CURVES FOR BOTTOM OF NORTH SPAN GIRDER, SOUTH SPAN OVERLOAD TEST

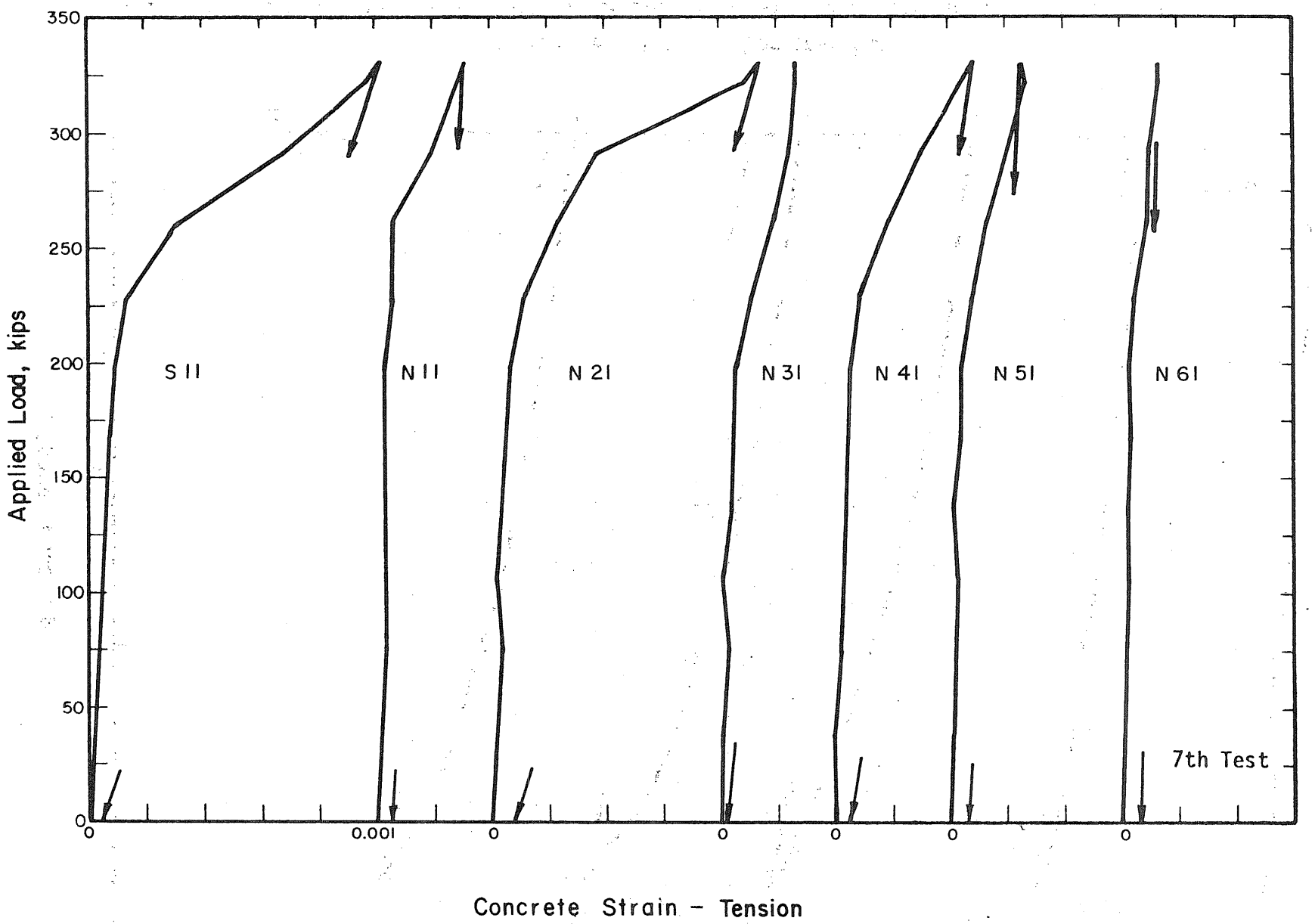

FIG. 6.26 LOAD-CONCRETE STRAIN CURVES FOR TOP OF NORTH SPAN GIRDER, SOUTH SPAN OVERLOAD TEST

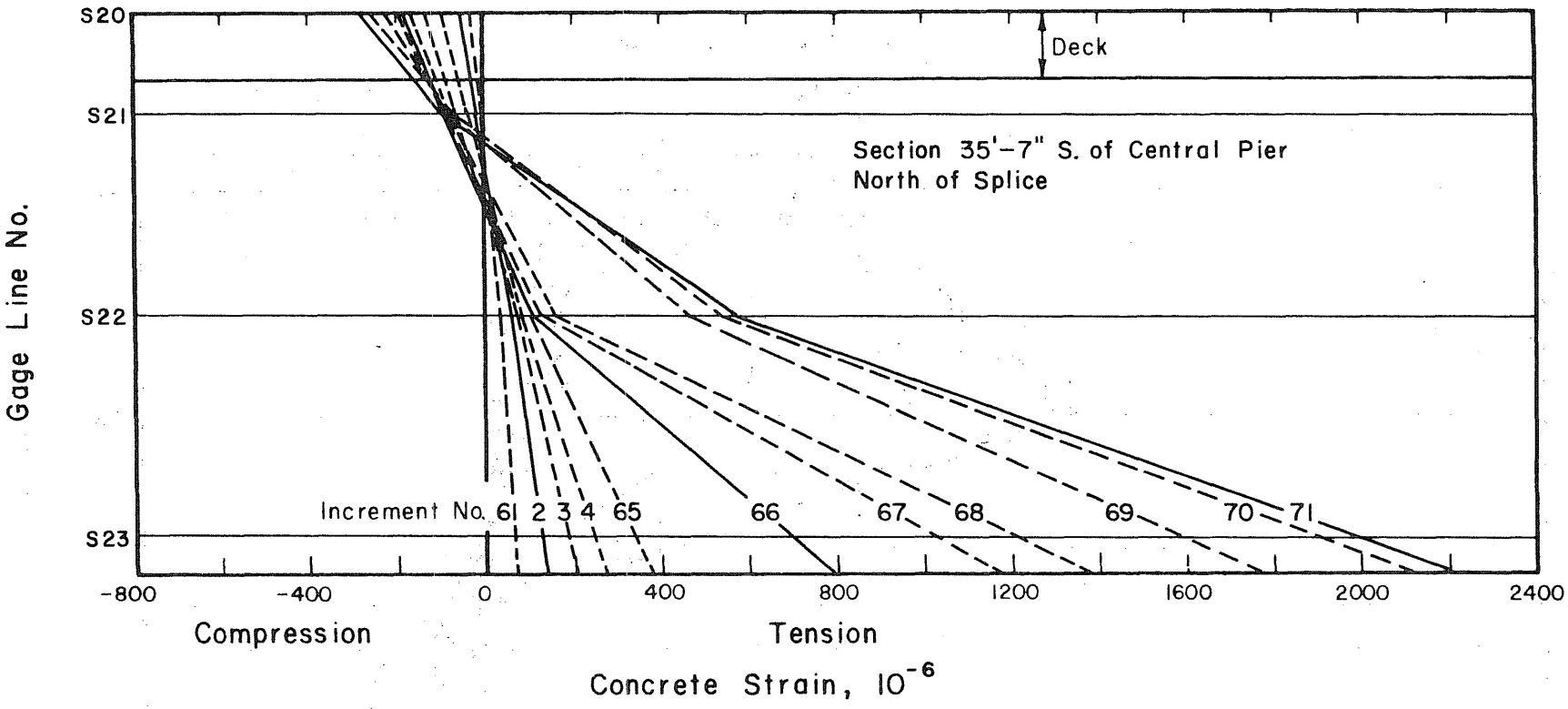

FIG. 6.27 STRAIN DISTRIBUTIONS ACROSS DEPTH OF MEMBER, SECTION NORTH OF SOUTH SPLICE

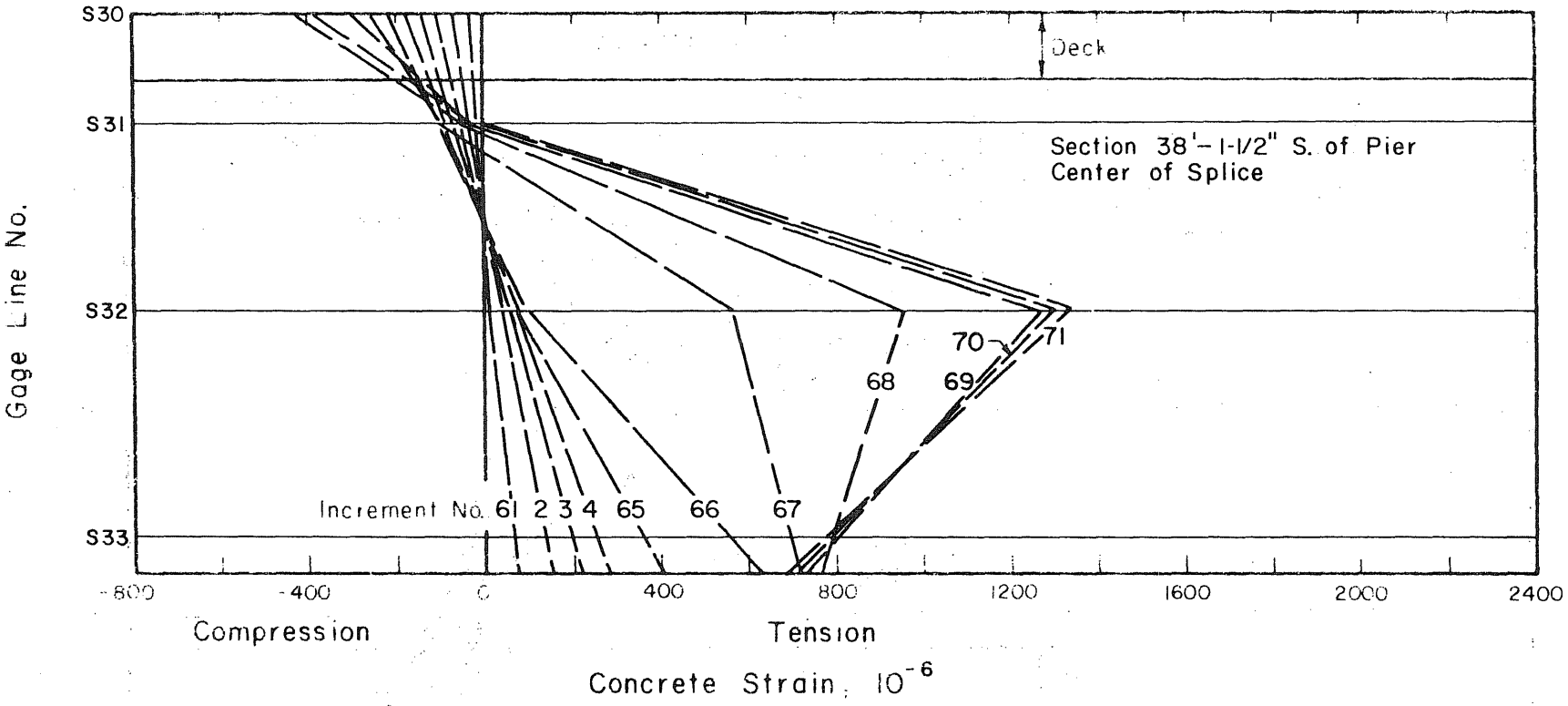

FIG. 6.28 STRAIN DISTRIBUTIONS ACROSS DEPTH OF MEMBER, SECTION IN SOUTH SPLICE

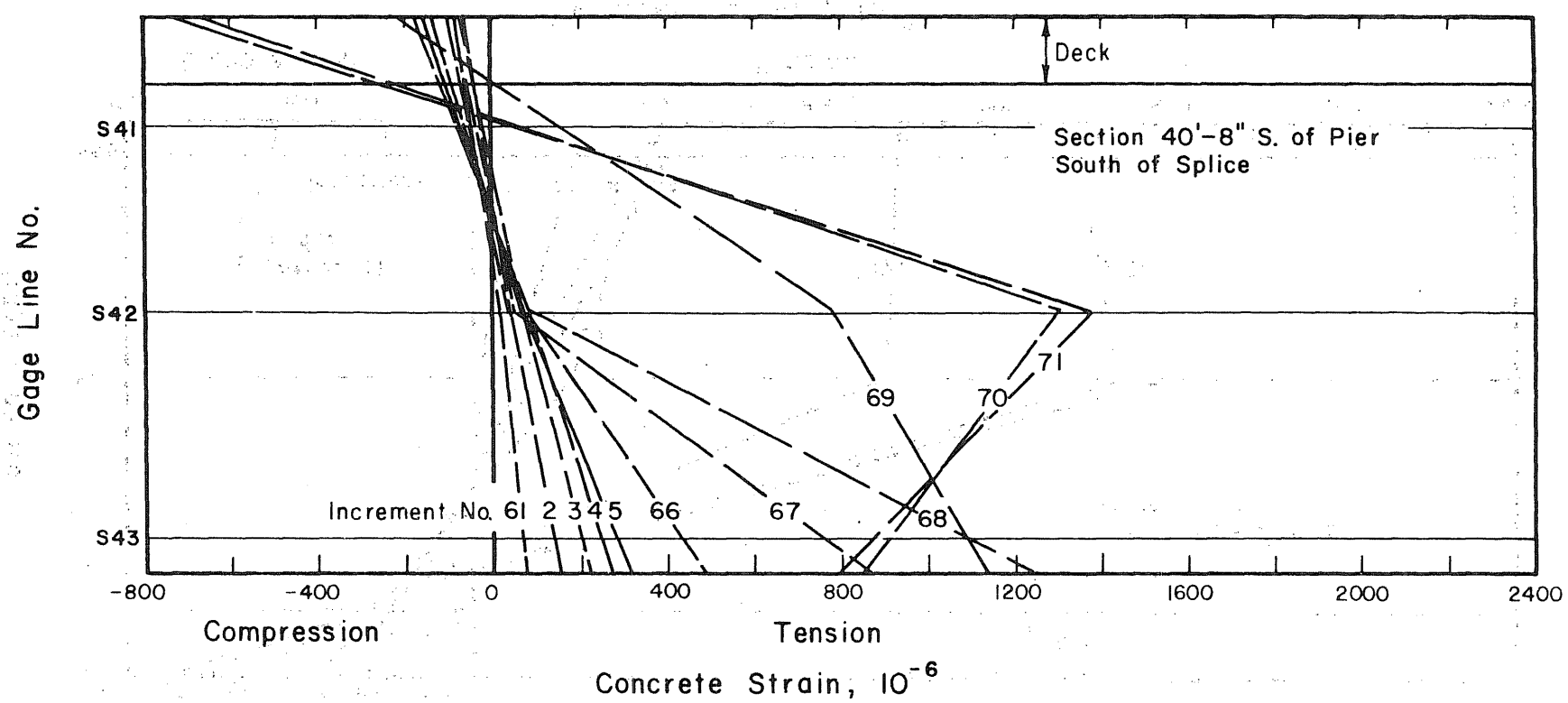

FIG. 6.29 STRAIN DISTRIBUTIONS ACROSS DEPTH OF MEMBER, SECTION SOUTH OF SOUTH SPLICE

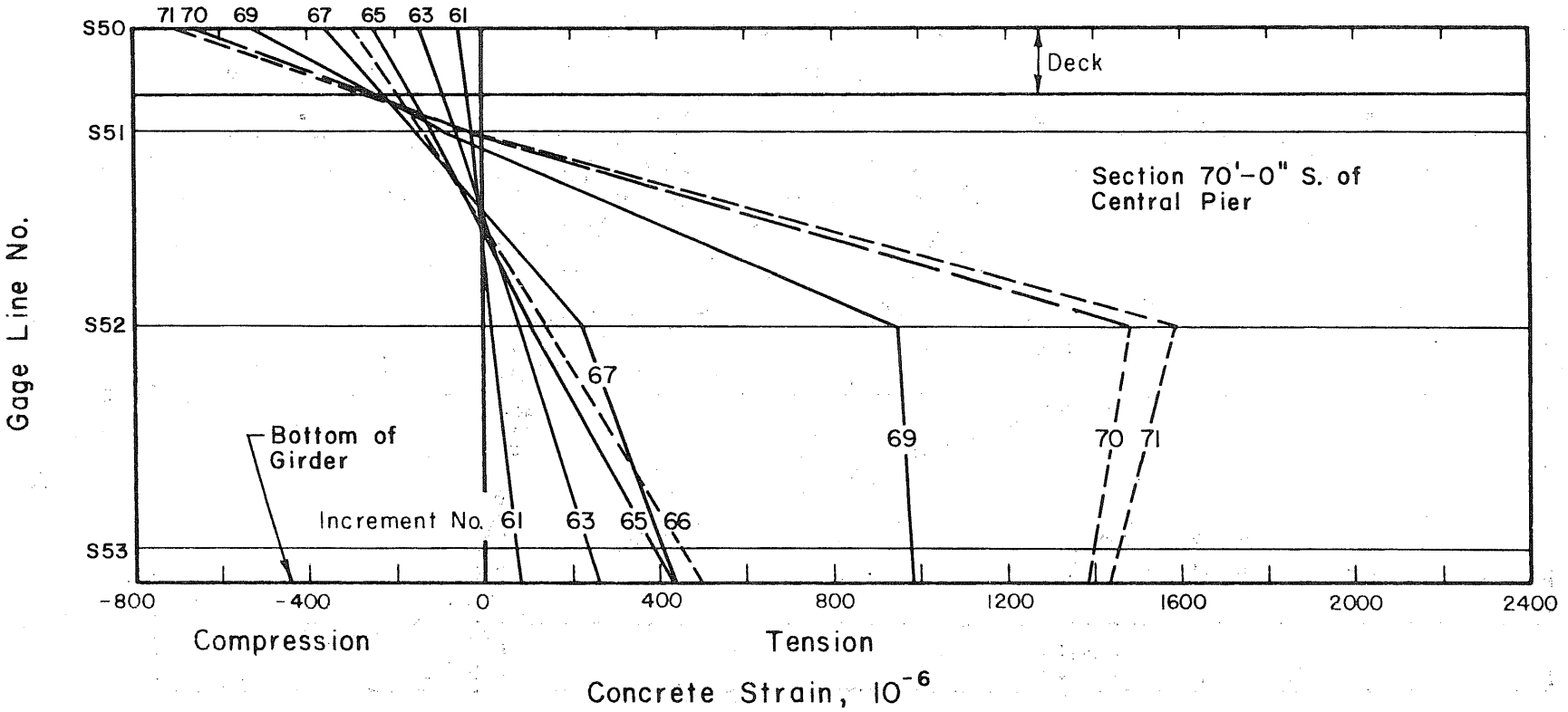

FIG. 6.30 STRAIN DISTRIBUTIONS ACROSS DEPTH OF MEMBER, SECTION 70 FT SOUTH OF CENTRAL PIER

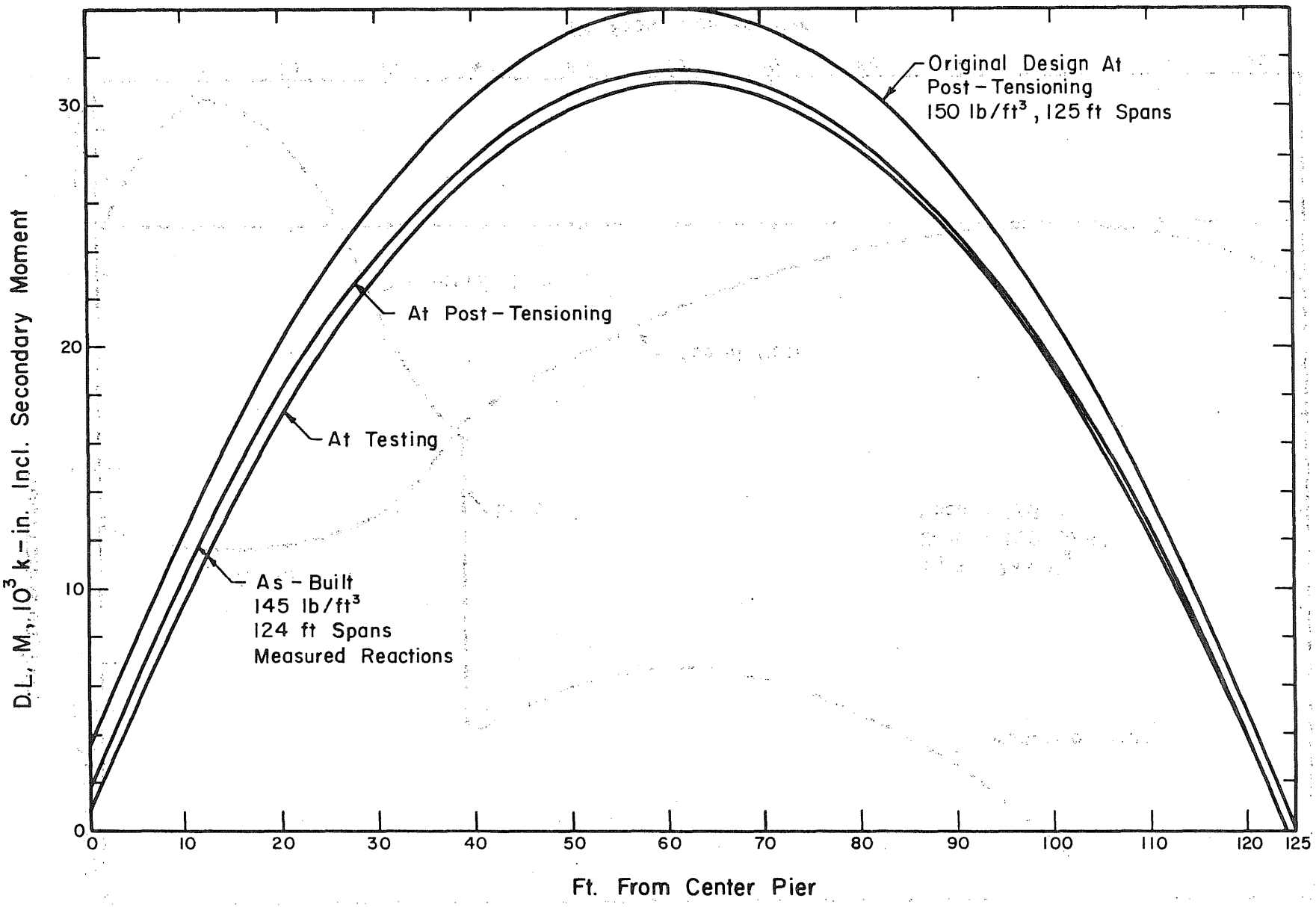

FIG. 7.1 DEAD LOAD MOMENT DIAGRAMS FOR DESIGN AND AS-BUILT CONDITIONS, INCLUDING SECONDARY MOMENTS

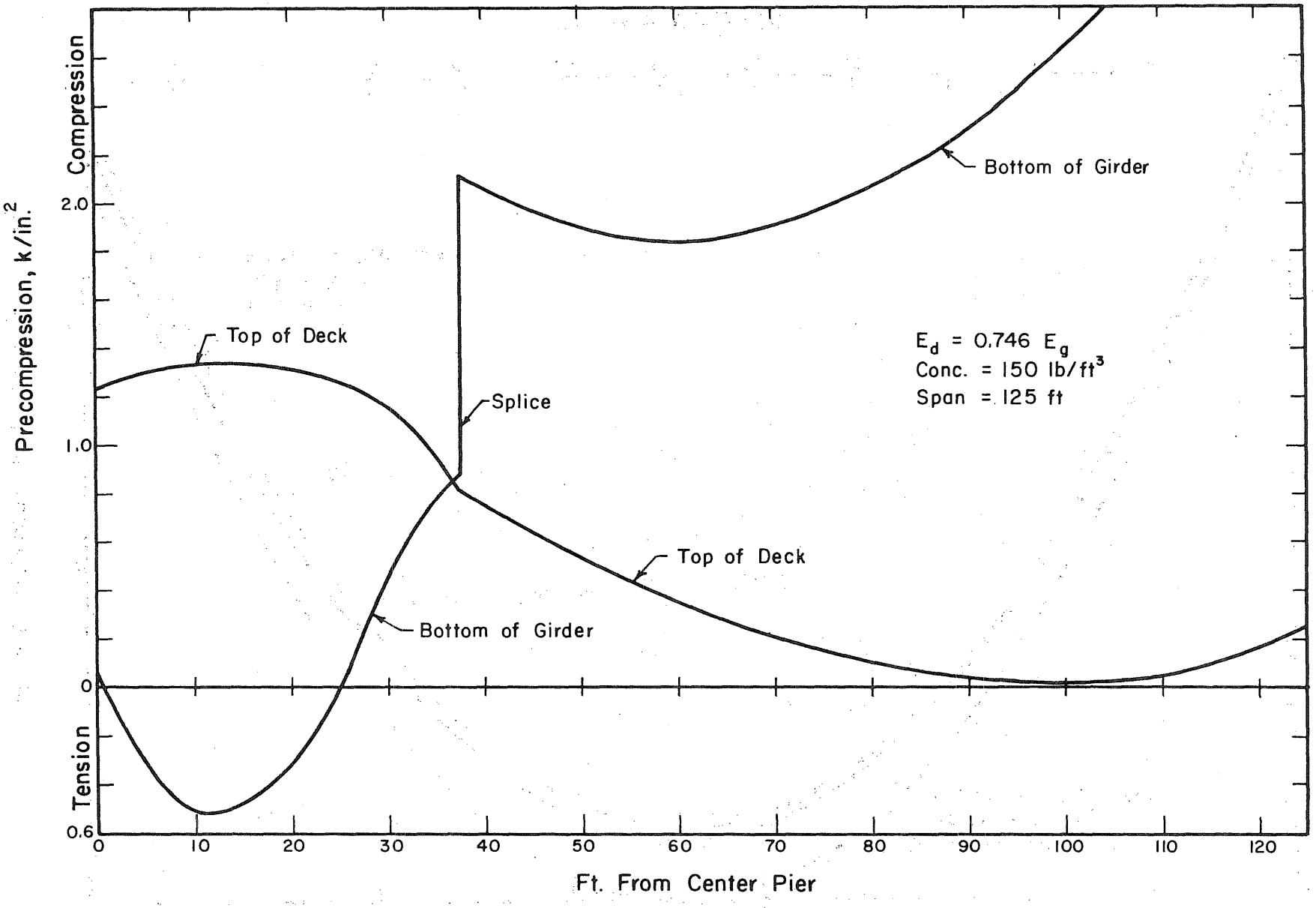

FIG. 7.2 DISTRIBUTIONS OF STRESS ALONG TOP OF DECK AND BOTTOM OF BEAM IMMEDIATELY AFTER POST-TENSIONING, AS DESIGNED

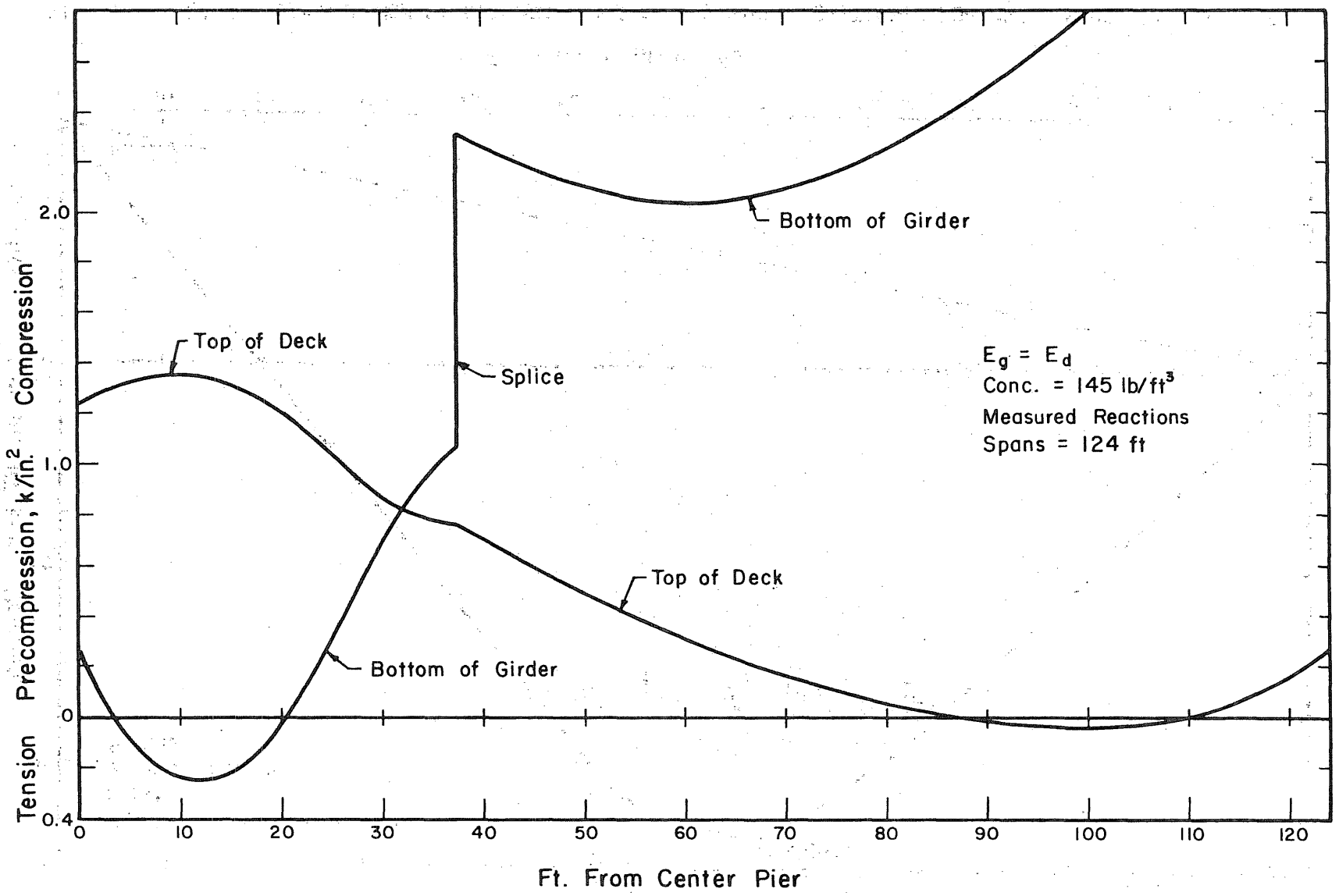

FIG. 7.3 DISTRIBUTIONS OF STRESSES ALONG TOP OF DECK AND BOTTOM OF GIRDER IMMEDIATELY AFTER POST-TENSIONING, AS-BUILT

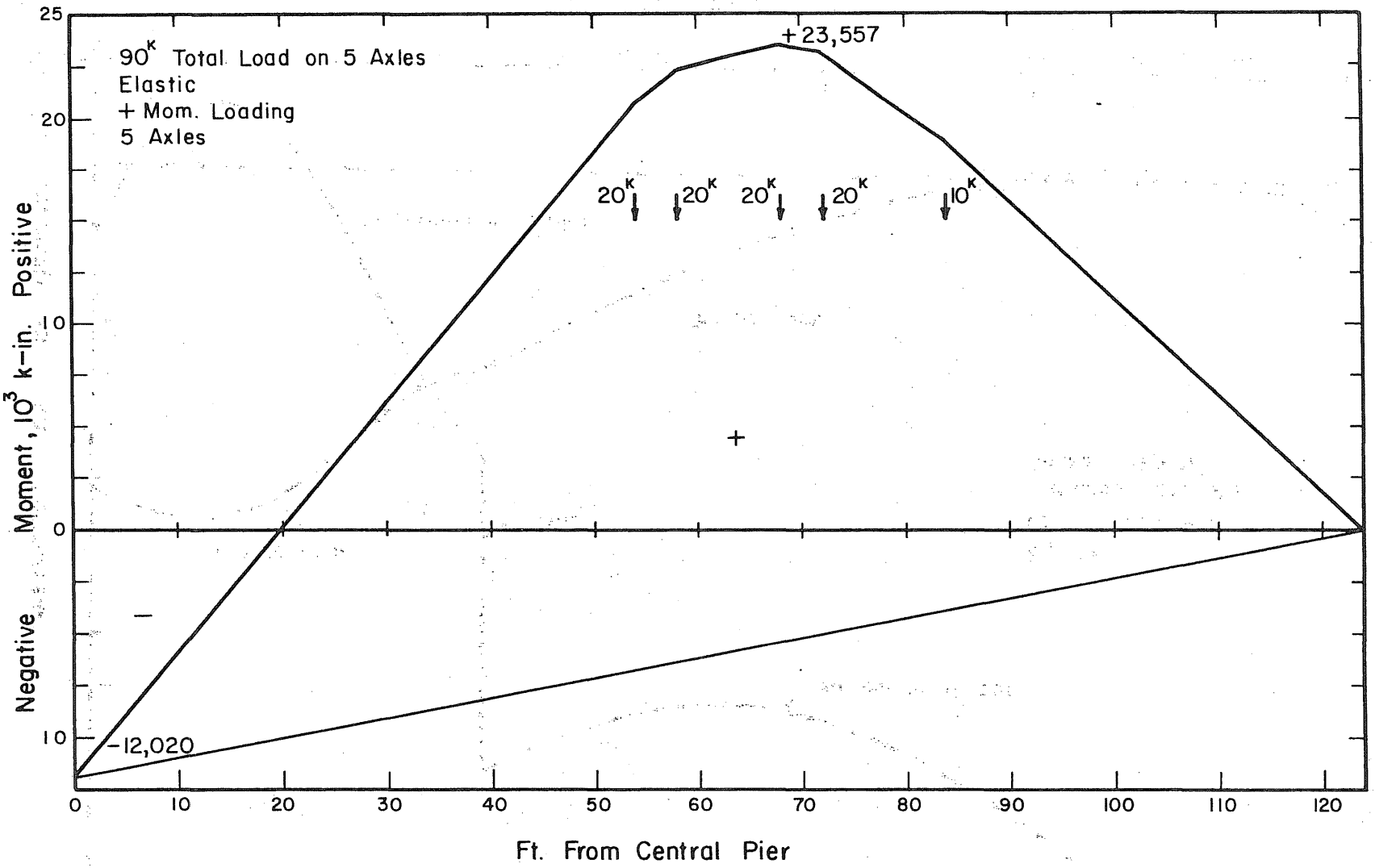

FIG. 7.4 ELASTIC BENDING MOMENT DIAGRAM FOR 5-AXLE VEHICLE POSITIONED FOR MAXIMUM POSITIVE MOMENT

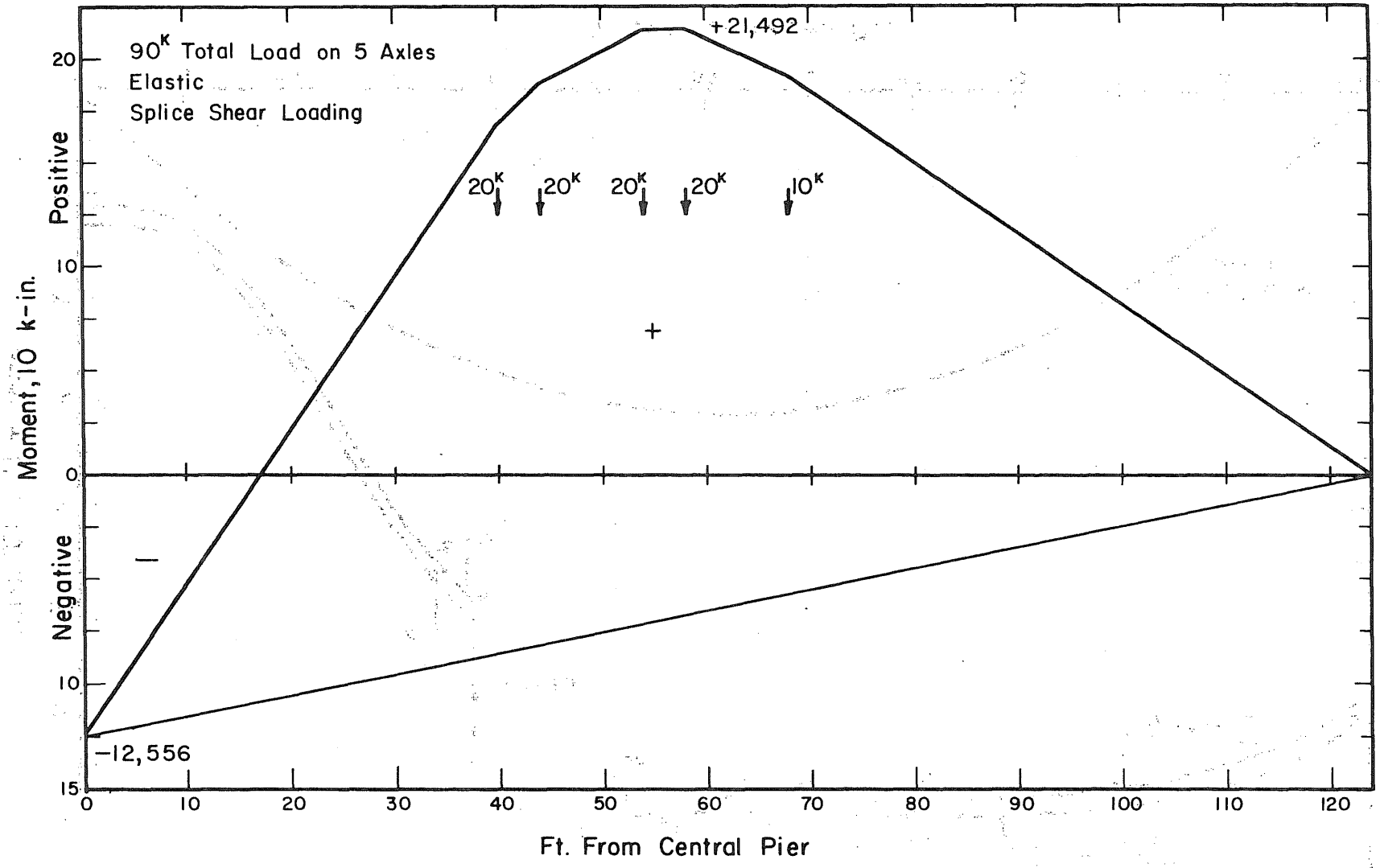

FIG. 7.5 ELASTIC BENDING MOMENT DIAGRAM FOR 5-AXLE VEHICLE POSITIONED FOR MAXIMUM SPLICE SHEAR

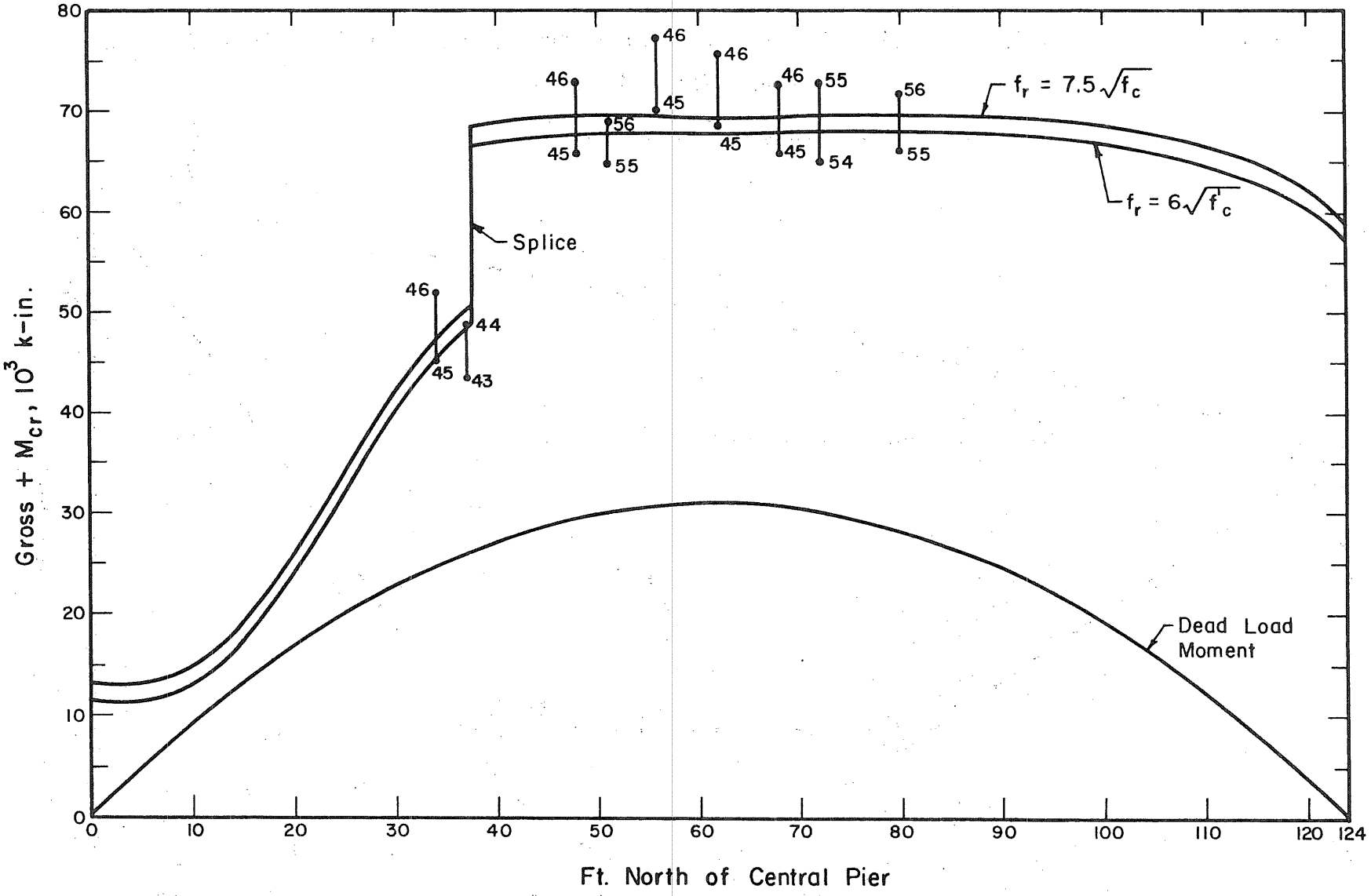

FIG. 7.6 MEASURED AND COMPUTED POSITIVE CRACKING MOMENTS, NORTH SPAN

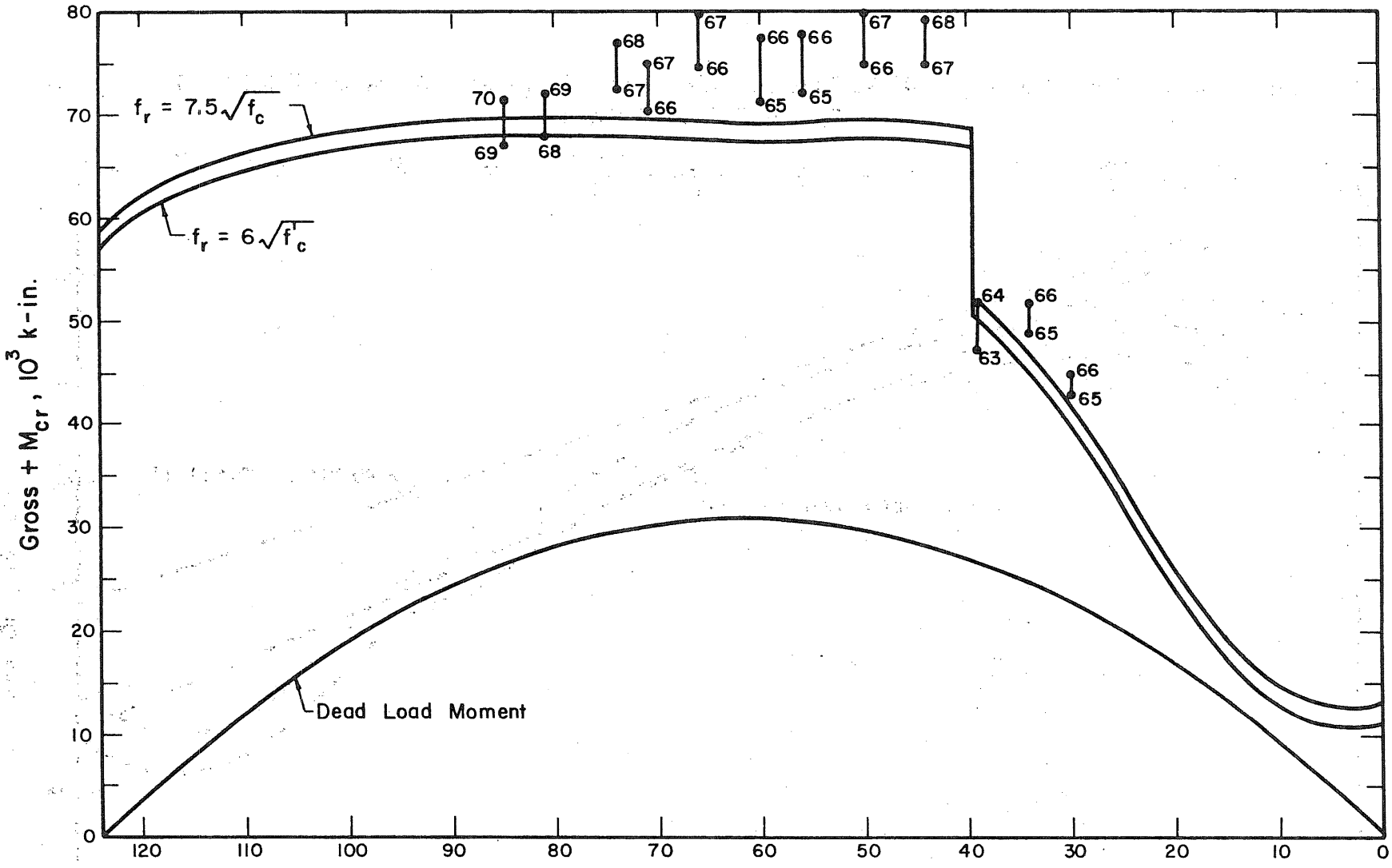

FIG. 7.7 MEASURED AND COMPUTED POSITIVE CRACKING MOMENTS, SOUTH SPAN

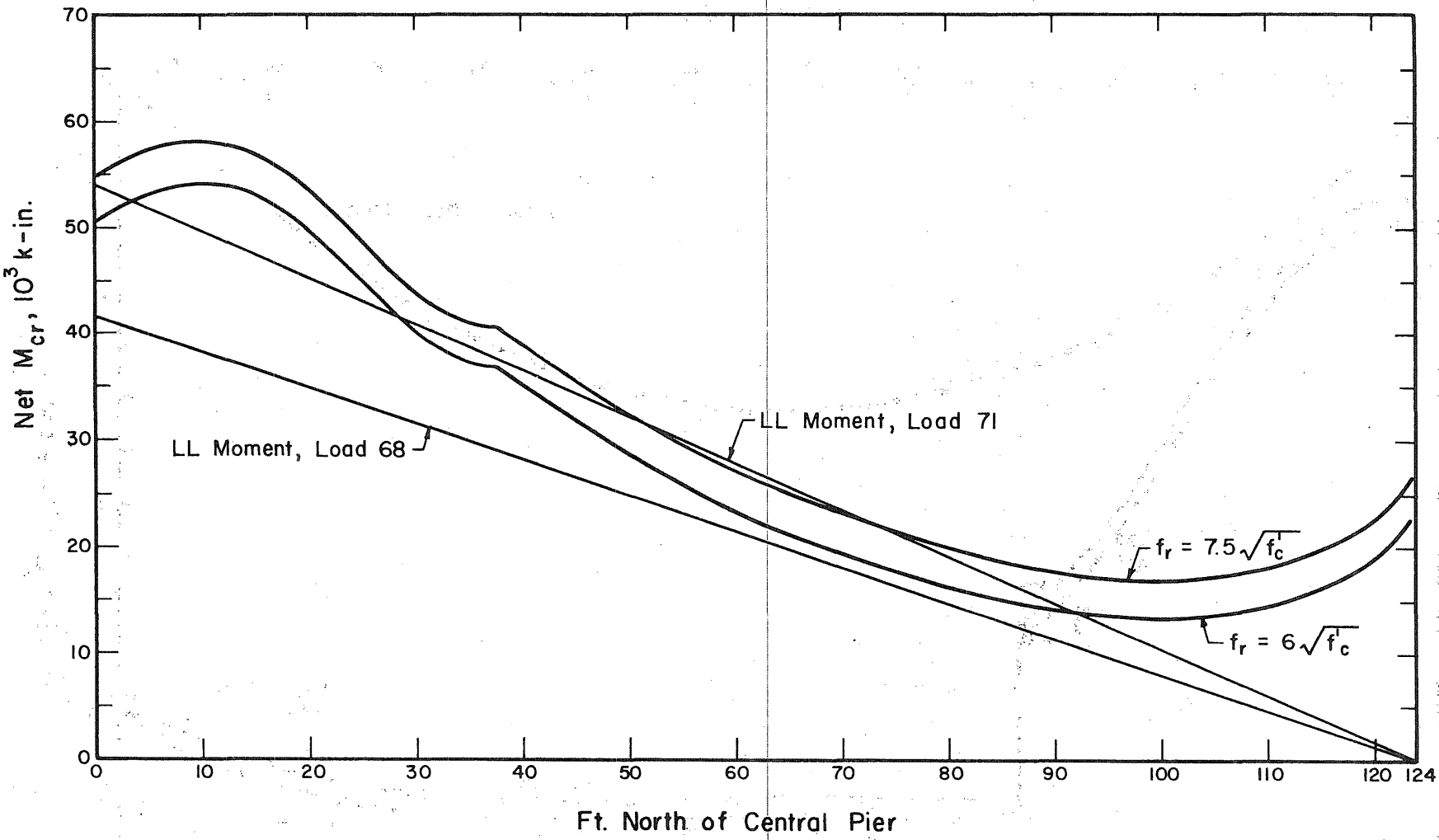

FIG. 7.8 LIVE LOAD NEGATIVE MOMENTS AND COMPUTED CRACKING MOMENTS IN NORTH SPAN, SOUTH SPAN OVERLOAD TEST

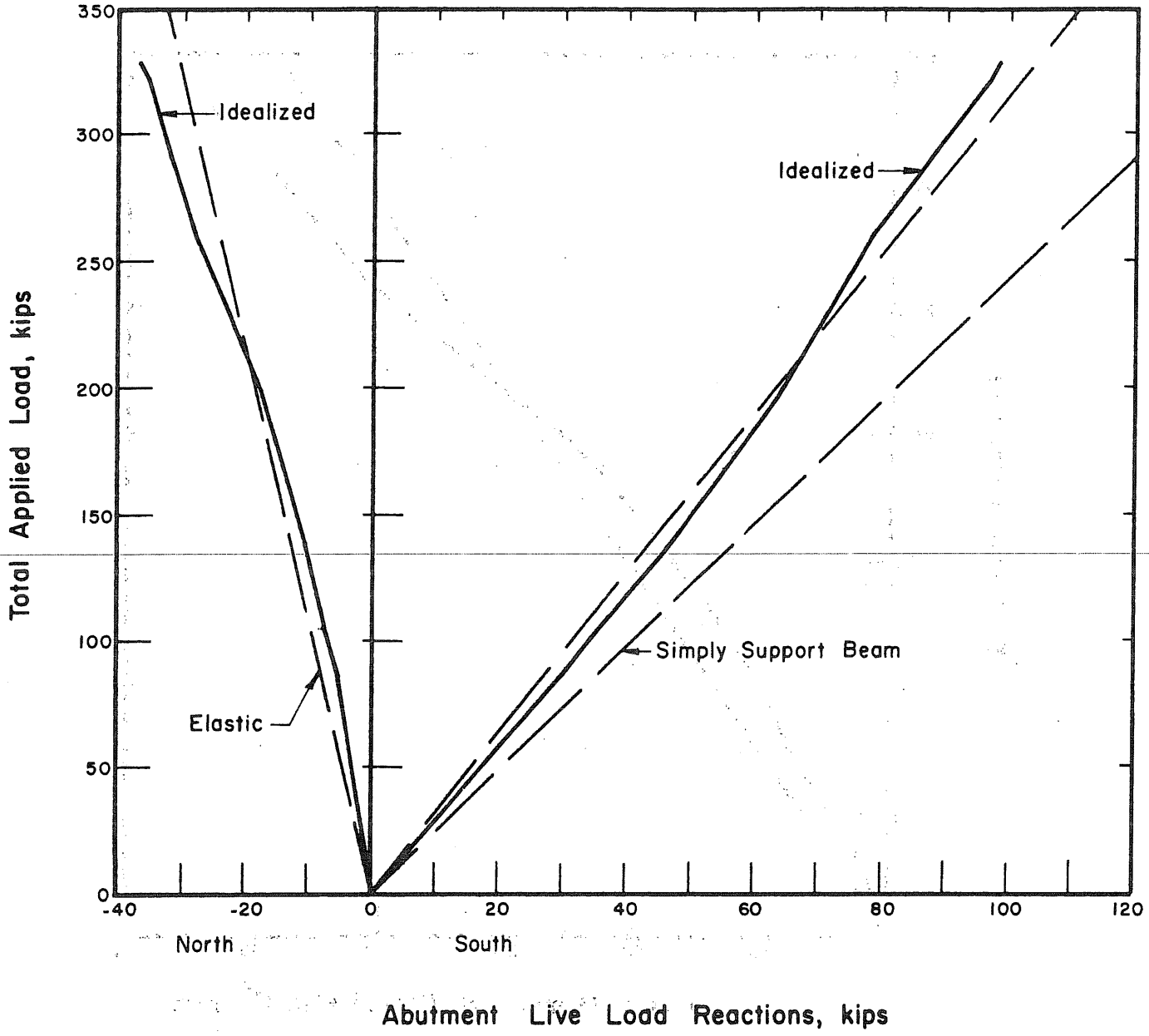

FIG. 7.9 LOAD-IDEALIZED ABUTMENT REACTION CURVES, SOUTH SPAN OVERLOAD TEST

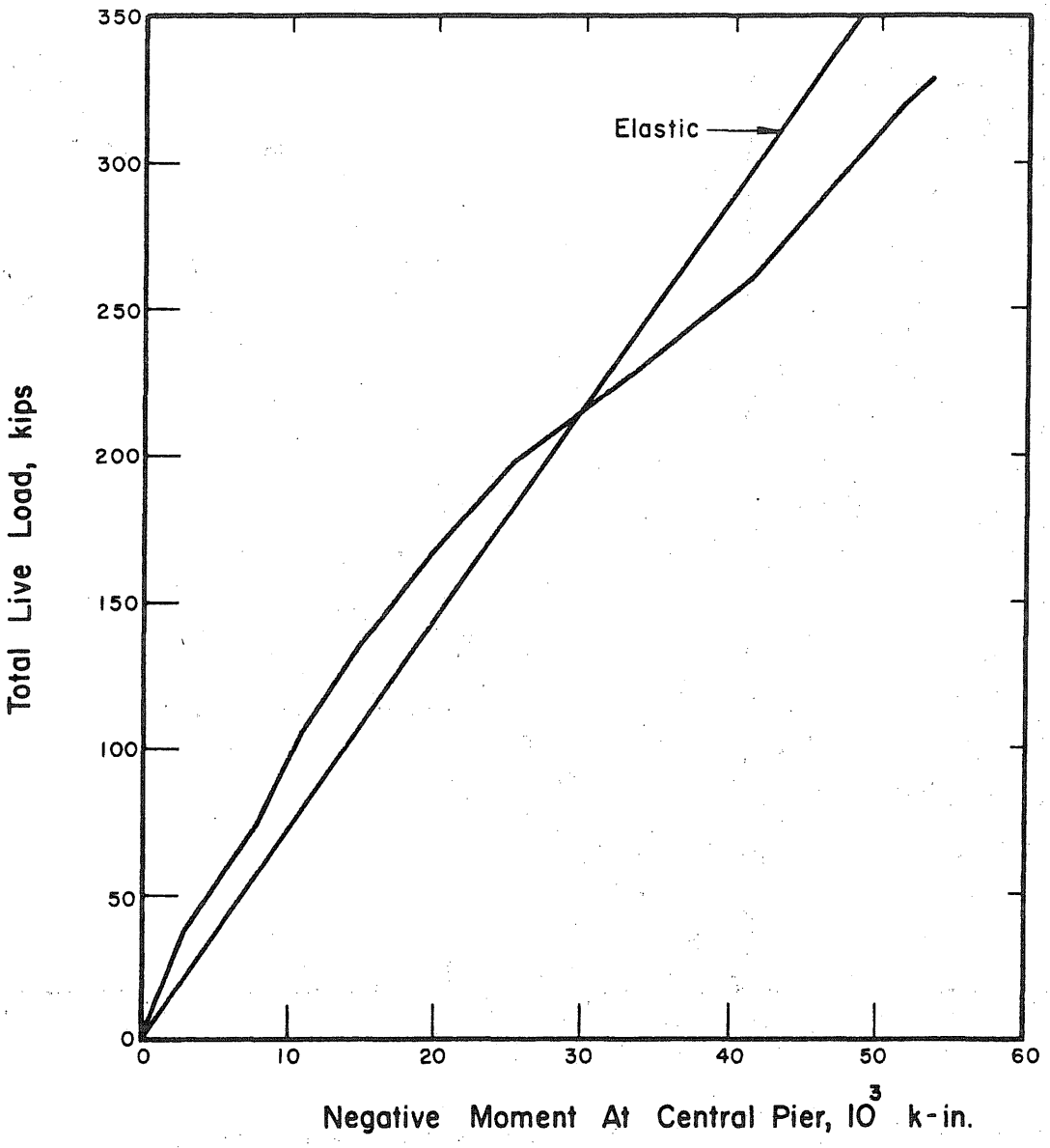

FIG. 7.10 LOAD-NEGATIVE MOMENT CURVE FROM IDEALIZED REACTIONS, SOUTH SPAN OVERLOAD TEST

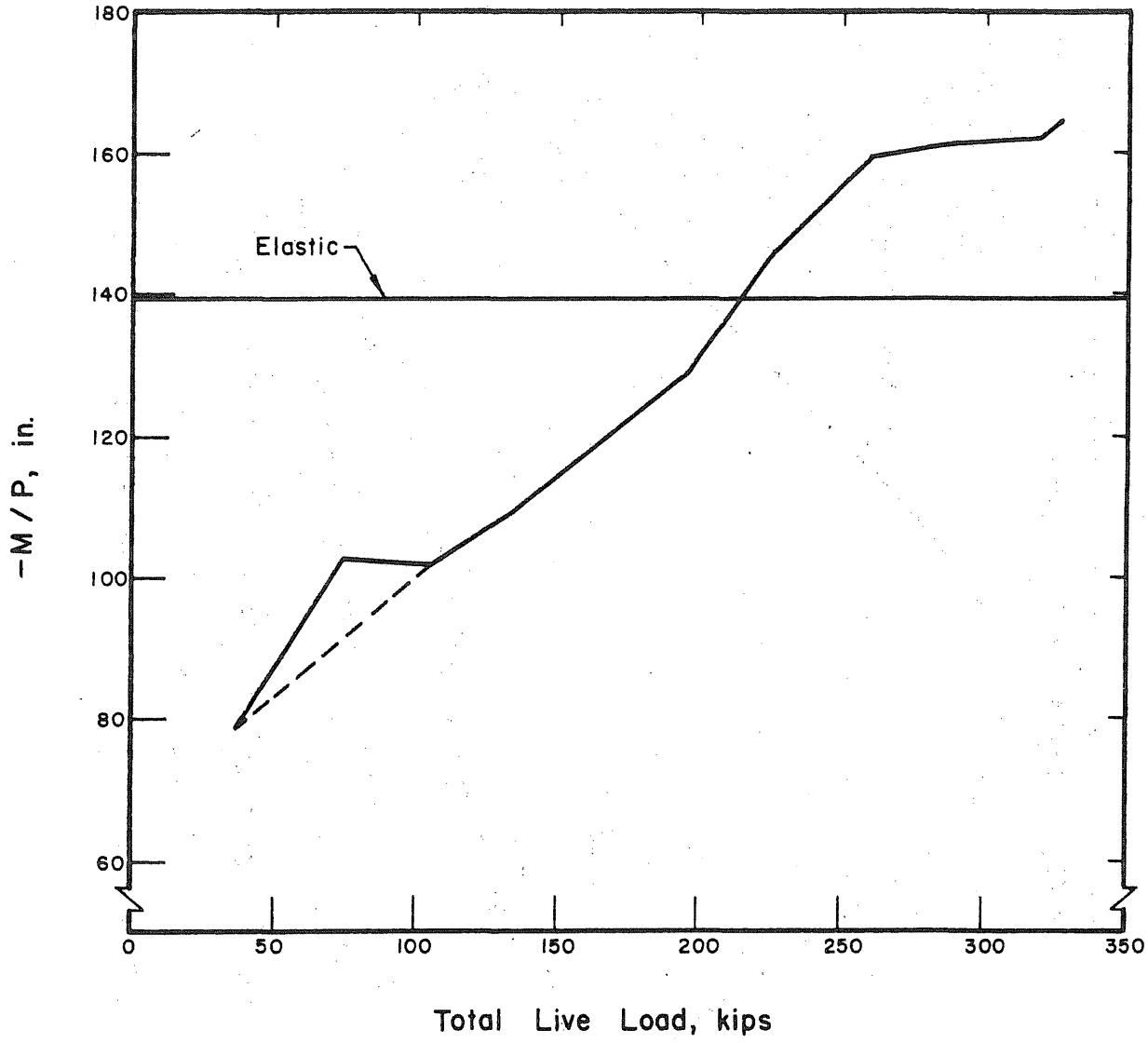

FIG. 7.11 LOAD-NEGATIVE MOMENT COEFFICIENT FROM IDEALIZED REACTIONS, SOUTH SPAN OVERLOAD TEST

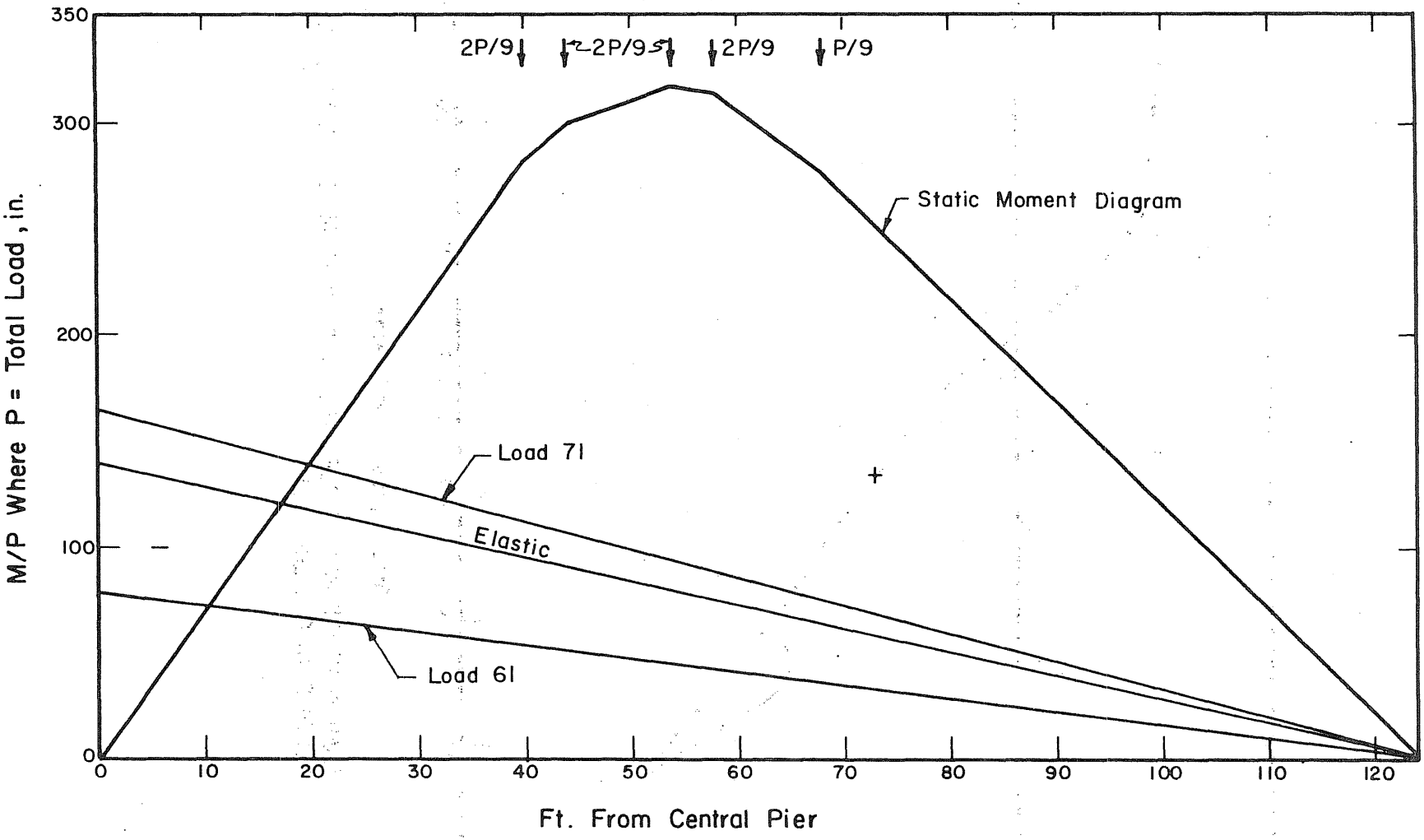

FIG. 7.12 SOUTH SPAN LIVE LOAD MOMENT DIAGRAMS FOR FINAL TEST

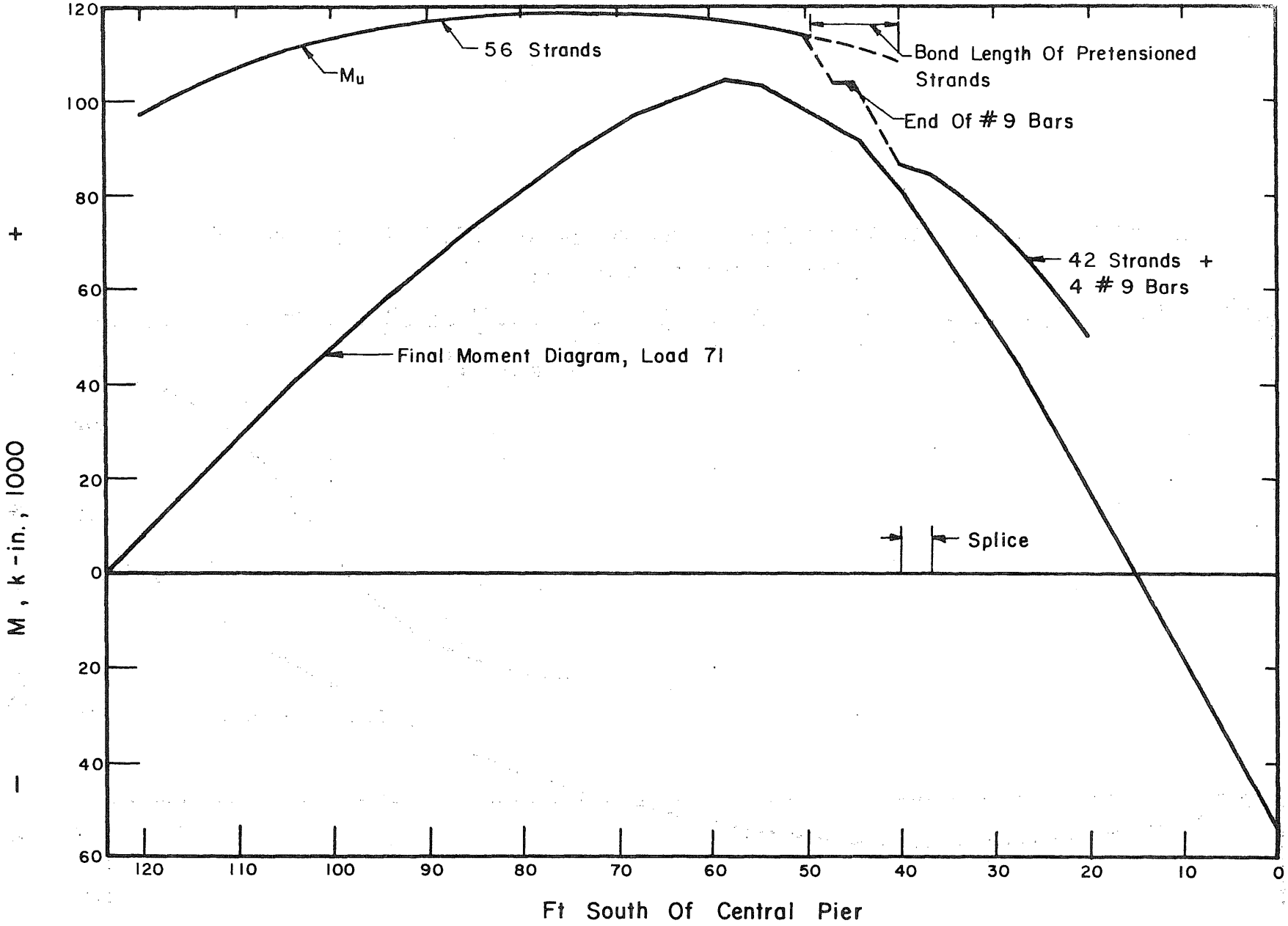

FIG. 7.13 APPLIED MOMENT AND MOMENT CAPACITY DIAGRAMS FOR SOUTH SPAN, LOAD 71

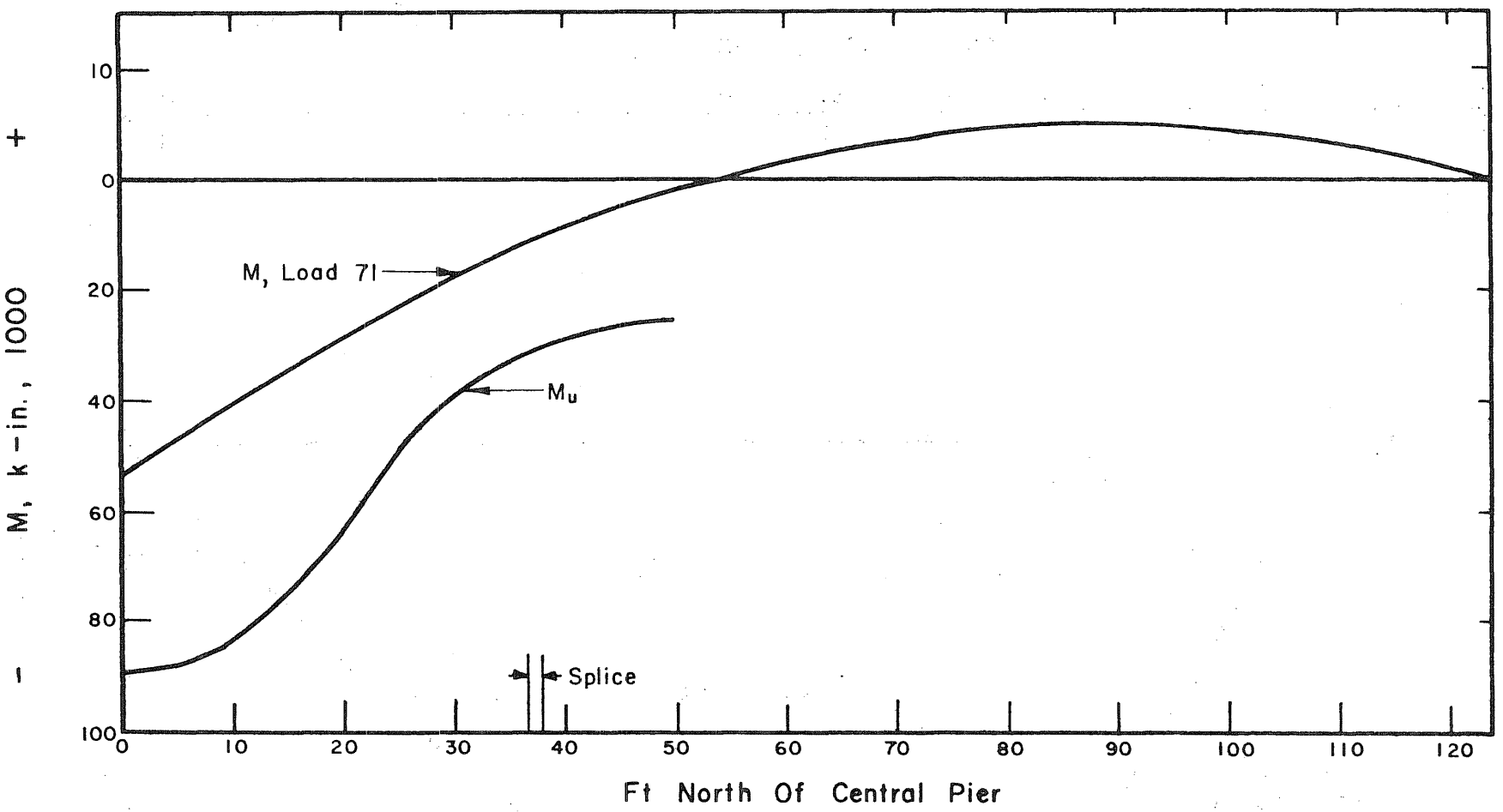

FIG. 7.14 VARIATION OF APPLIED MOMENT AND NEGATIVE MOMENT CAPACITY IN NORTH SPAN, LOAD 71

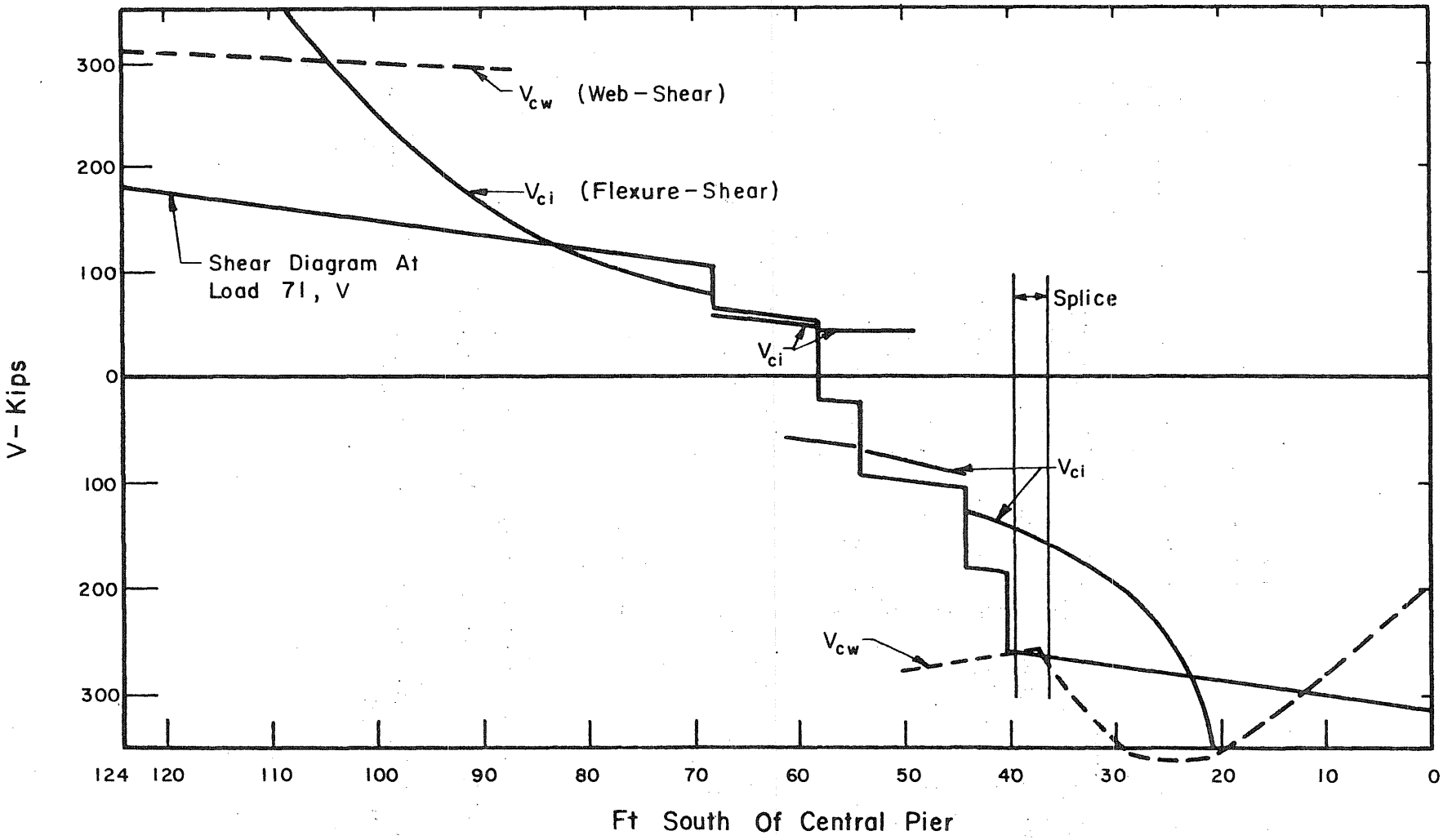

FIG. 7.15 VARIATION IN APPLIED SHEAR AND CONCRETE SHEAR CAPACITY IN SOUTH SPAN, LOAD 71

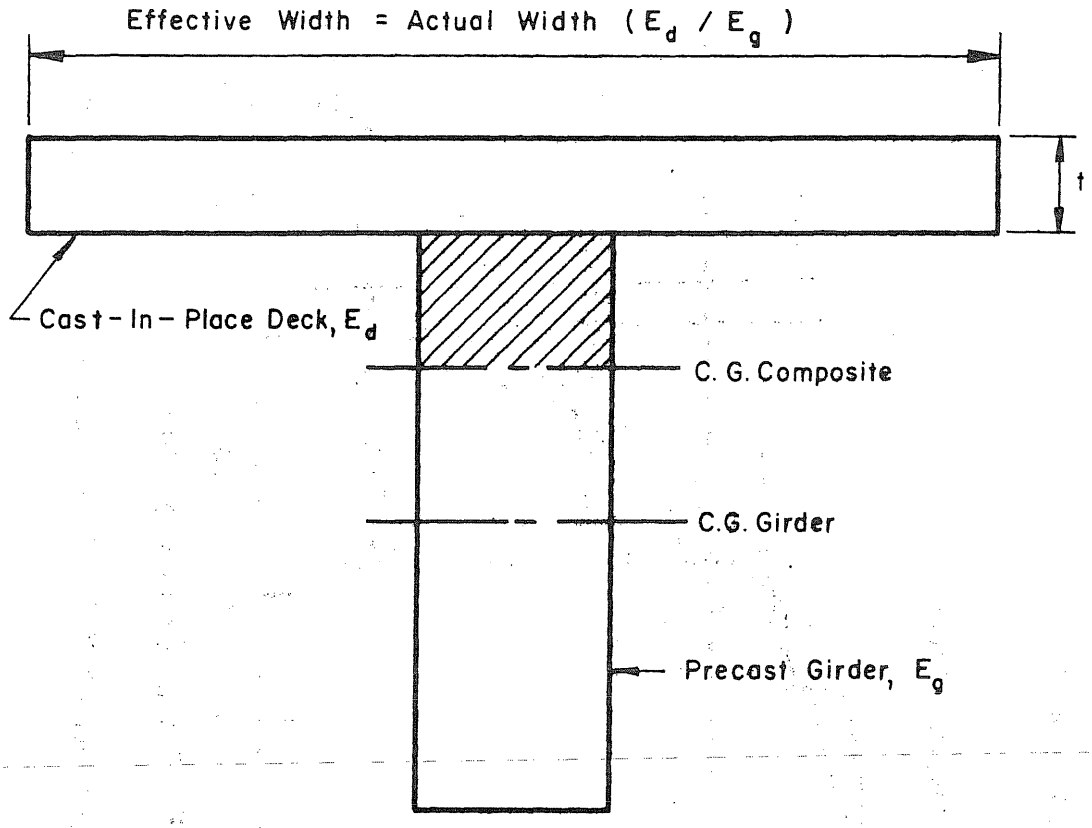

Q_g = 1^{st} Moment Of Shaded Area About C.G. Girder

Q_c = 1^{st} Moment Of Shaded Area Plus Deck Area About C.G. Composite

FIG. 7.16 SCHEMATIC REPRESENTATION OF AREAS CONSIDERED IN FIRST MOMENT COMPUTATIONS

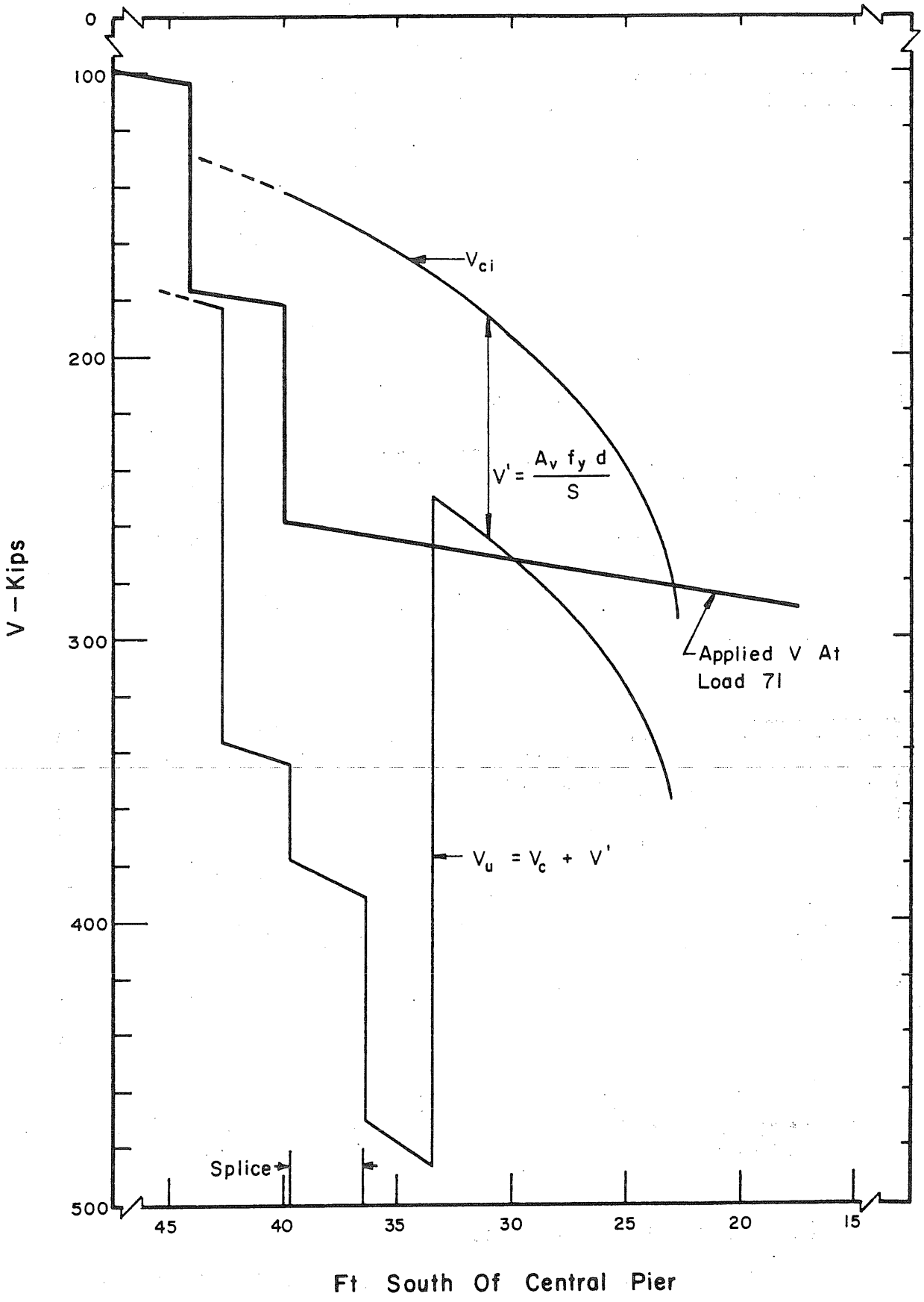

FIG. 7.17 VARIATION IN APPLIED SHEAR AND SHEAR STRENGTH NEAR SOUTH SPLICE

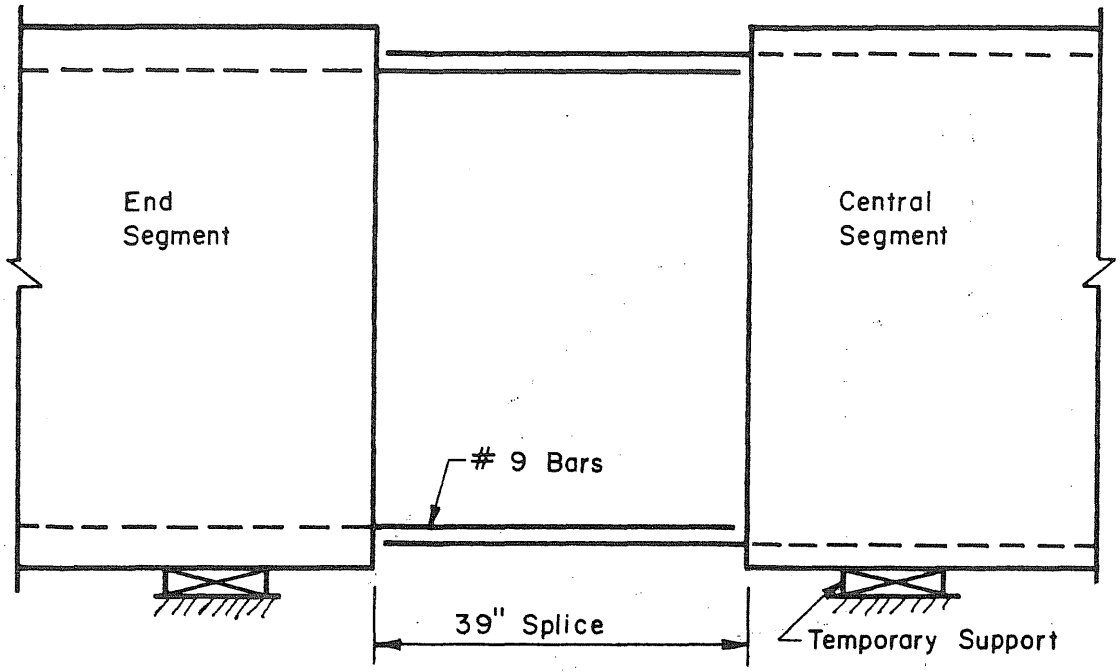

(a) As-Built Lap Splice

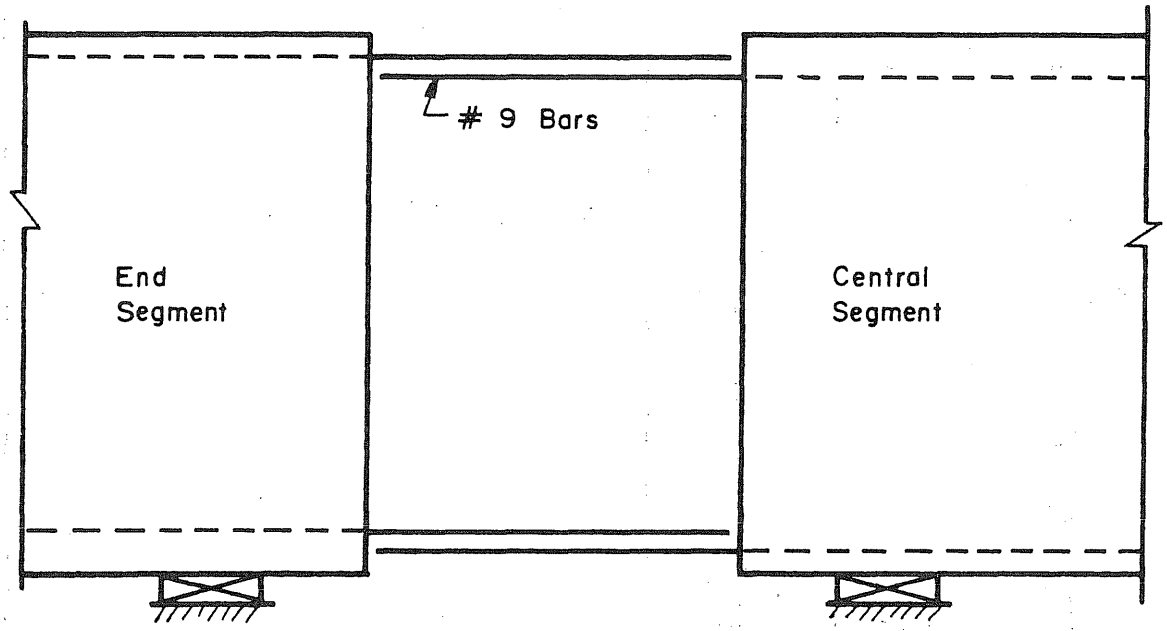

(b) Suggested Lap Splice Detail

FIG. 7.18 SUGGESTED CHANGE IN BAR ARRANGEMENT AT LAP-SPLICED JOINT